



# **Catalytic Route for the Synthesis of Cyclic Organic Carbonates from Renewable Polyols**

Thesis submitted in accordance with the requirements of the University of Liverpool for the degree of Doctor of Philosophy

by

**Nadiah Mohamad Noh**

February 2017



# ACKNOWLEDGEMENTS

In the name of God, the Most Merciful and the Most Loving,

Firstly, I would like to express my gratitude to my supervisor, Professor Lopez-Sanchez for allowing me to join his research group. His guidance and immense knowledge has helped in the time of my research here in Liverpool which I am truly grateful. I would also like to thank Professor Greeves for his organic chemistry knowledge and helping me in interpreting those complicated NMRs. And special thanks to Dr Davies for helping me in my research, for his patience in teaching me, providing continuous guidance and even becoming my 'walking dictionary'.

I would like to thank all the current members of the group, Monica, Ali, Joel, Azam, Aldo, Annarita, Liqaa, Romen, David, Javier, Hammed and Edgar for providing support and help, for those crazy conversations we had in the office and in labs. I wish you all the best!

I would like to thank Ka Aznida for those late nights binging on takeaway food and giving me advices about life in general. I would like to thank \*awesomest liv girls\* for making my stay here in Liverpool a memorable one. I would also like to thank two of my best friends, Syazwina and Farisa for their support, motivation and advices. I can't wait to be an auntie soon!

Last but not least, I would like to thank my parents, Mamih and Ayah for their continuous support throughout my PhD years and telling me to persevere till the end! To my siblings, Nabil, Nabilah and auntie Malou for those late night skypes and being there for me. And also big thanks to my 3141 family for their endless support. I would like to dedicate this thesis to kaka, it has been 5 years since you have gone and I miss you so much!

"So verily, with the hardship, there is relief. Verily, with the hardship, there is relief. So when you have finished (from your occupation), then stand up for Allah's worship. And to your Lord (Alone) turn all your intentions and hopes and your invocations" (Quran, 94:5-8)

# ABSTRACT

In this project, two platform molecules, glycerol and sorbitol, were selected to produce cyclic organic carbonates as they are cheaply available alcohols that can be derived from biomass in the biorefinery.

The reaction of glycerol with carbon dioxide is the most challenging route to produce glycerol carbonate due to CO<sub>2</sub> being the most stable form of carbon. The key for producing high yield of carbonate is in choosing the best dehydrating agent as the reaction with carbon dioxide produce water as by-product. This is a very attractive reaction as it utilises two readily available raw materials. The direct carbonylation reaction is an important process for carbon dioxide sequestration and glycerol valorisation.

In these studies, different dehydrating agents were tested and 2-cyanopyridine is the best dehydrating agent. High yield of glycerol carbonate can be achieved at a short period of time. Conventional hydrothermal and microwave methods were investigated in the synthesis of the lanthana and ceria catalysts and we have found that catalysts synthesised by microwave method have higher activity compare to hydrothermal method. Different catalyst characterisation techniques were used to investigate the structure and relate it to the activity of the catalyst.

Urea as a carbonate source is being utilised to produce glycerol carbonate. Lanthanum oxide and cerium oxide were tested and the activity of the catalysts was compare in producing glycerol carbonate. Microwave heating was also investigated in the synthesis of glycerol carbonate from urea and the yield of glycerol carbonate is higher than using conventional heating. This is the first reported synthesis of glycerol carbonate *via* microwave heating.

Lastly, in the synthesis of sorbitol carbonate, two types of synthesis were investigated, enzymatic synthesis and chemical synthesis. Sorbitol carbonate is considered a novel compound and has not been commercially available. IR, QTOF and NMR were being used to characterise the sample being produced.

## Contents

1	INTRODUCTION.....	2
1.1	Sustainability and Green Chemistry .....	2
1.1.1	Oil consumption is an environmental problem .....	4
1.1.2	Alternative sources of energy/Renewable energy .....	6
1.1.3	The significance of biomass.....	7
1.2	Organic Carbonates .....	9
1.3	Synthesis of organic carbonates.....	11
1.3.1	Phosgenation method.....	11
1.3.2	Reaction with CO .....	12
1.3.3	Transesterification reactions.....	13
1.3.4	Carbonate formation with urea .....	14
1.3.5	Reaction with CO <sub>2</sub> .....	15
1.4	Advantages of catalysis.....	18
1.4.1	Heterogeneous catalysis.....	20
1.4.2	Lanthanides .....	22
1.5	Glycerol .....	24
1.6	Glycerol carbonate.....	27
1.6.1	Synthesis of glycerol carbonate .....	29
1.7	Enzymatic catalysis .....	46
1.7.1	Lipases.....	49
1.7.2	Enzymatic catalysed synthesis of glycerol carbonate .....	51
1.8	Microwave chemistry .....	52
1.9	Sorbitol.....	55
1.9.1	Synthesis of sorbitol carbonate.....	56
1.10	Objective and thesis organisation.....	57
2	EXPERIMENTAL .....	60
2.1	Chemicals and solvents – Source and purity .....	60
2.2	Catalyst preparation .....	62
2.2.1	Hydrothermal method.....	62
2.2.2	Microwave method .....	63

2.2.3	Hydrothermal synthesis of lanthanum oxide (Chapter 3 and Chapter 4)	63
2.2.4	Modified hydrothermal synthesis of lanthanum oxide using microwave (Chapter 4).....	65
2.2.5	Copper supported on lanthanum oxide by impregnation (Chapter 3 and Chapter 4).....	66
2.2.6	One pot copper impregnation of lanthanum hydroxide (Chapter 4) ..	66
2.2.7	One pot microwave preparation of copper supported on lanthanum oxide with early copper incorporation (Chapter 4) .....	66
2.2.8	Hydrothermal synthesis of lanthanum oxide (Chapter 5 and Chapter 6)	67
2.2.9	Modified hydrothermal synthesis of lanthanum oxide using microwave heating (Chapter 5 and Chapter 6) .....	67
2.2.10	Hydrothermal synthesis of cerium oxide (Chapter 5 and Chapter 6).	68
2.2.11	Modified hydrothermal synthesis of cerium oxide using microwave (Chapter 5 and Chapter 6) .....	68
2.2.12	Copper supported on CeO <sub>2</sub> or La <sub>2</sub> O <sub>3</sub> by impregnation (Chapter 6) .....	68
2.3	Catalyst characterisation.....	69
2.3.1	X-ray diffraction (XRD).....	69
2.3.2	BET analysis .....	71
2.3.3	Transmission Electron Microscopy (TEM).....	74
2.3.4	Temperature Programmed Desorption (CO <sub>2</sub> -TPD) .....	76
2.3.5	H <sub>2</sub> -Temperature Programmed Reduction (H <sub>2</sub> -TPR).....	77
2.3.6	Ultraviolet-Visible Spectroscopy (UV-Vis).....	78
2.3.7	Thermogravimetric analysis (TGA).....	79
2.4	Catalytic reaction.....	80
2.4.1	Direct carbonylation of glycerol with CO <sub>2</sub> using molecular sieves as dehydrating agent (Chapter 3) .....	80
2.4.2	Direct carbonylation of glycerol with CO <sub>2</sub> using trimethyl orthoformate as dehydrating agent (Chapter 3) .....	81
2.4.3	Direct carbonylation of glycerol with CO <sub>2</sub> using acetonitrile as dehydrating agent (Chapter 3) .....	81
2.4.4	Direct carbonylation of glycerol with CO <sub>2</sub> using acetonitrile as dehydrating agent (Chapter 4) .....	81
2.4.5	Direct carbonylation of glycerol with CO <sub>2</sub> using 2-cyanopyridine as dehydrating agent (Chapter 5) .....	82

2.4.6	Reaction of glycerol and urea using conventional heating (Chapter 6)	83
2.4.7	Reaction of glycerol and urea using microwave heating (Chapter 6).	83
2.4.8	Chemical reactions in the synthesis of sorbitol carbonate (Chapter 7)	83
2.4.9	Enzymatic reactions in the synthesis of sorbitol carbonate .....	84
2.5	Product analysis .....	86
2.5.1	Gas chromatography (GC).....	86
2.5.2	High performance liquid chromatography (HPLC).....	89
2.5.3	Quadrupole Time of Flight Liquid Chromatography Mass Spectroscopy (Q-TOF LC/MS) .....	90
2.5.4	Fourier Transform Infrared Spectroscopy (FTIR).....	90
2.5.5	Nuclear Magnetic Resonance (NMR) .....	91
3	DIRECT SYNTHESIS OF GLYCEROL CARBONATE FROM GLYCEROL AND CARBON DIOXIDE CATALYSE BY COPPER SUPPORTED ON LANTHANUM OXIDE USING DIFFERENT DEHYDRATING AGENTS.....	93
3.1	Introduction .....	93
3.2	Results and Discussion.....	95
3.2.1	Catalyst characterisation.....	95
3.2.2	Catalytic reaction.....	121
3.2.3	Conclusion.....	130
4	ENHANCE ROUTE OF MICROWAVE SYNTHESIS OF COPPER SUPPORTED ON LANTHANUM OXIDE IN THE DIRECT CARBONYLATION OF GLYCEROL CARBONATE FROM CARBON DIOXIDE.....	133
4.1	Introduction .....	133
4.2	Results & Discussion.....	133
4.2.1	Catalyst characterisation.....	135
4.2.2	Catalytic reaction.....	144
4.3	Conclusion.....	150
5	DIRECT SYNTHESIS OF GLYCEROL CARBONATE FROM GLYCEROL AND CARBON DIOXIDE CATALYSE BY RARE EARTH METAL OXIDES USING 2-CYANOPYRIDINE AS DEHYDRATING AGENT.....	152
5.1	Introduction .....	152
5.2	Results & Discussion.....	152
5.2.1	Catalyst characterisation.....	152
5.2.2	Catalytic reaction.....	162

5.3	Conclusion.....	170
6	SYNTHESIS OF GLYCEROL CARBONATE FROM UREA OVER RARE EARTH METAL OXIDES AS A SOLID BASE CATALYST .....	172
6.1	Introduction .....	172
6.2	Results and Discussion.....	172
6.2.1	Catalyst characterisation.....	172
6.2.2	Catalytic reaction.....	173
6.2.3	Conclusion.....	189
7	NEW ROUTE IN THE SYNTHESIS OF SORBITOL CARBONATE .....	191
7.1	Introduction .....	191
7.2	Results & Discussion .....	193
7.2.1	Enzymatic reactions of sorbitol carbonate.....	193
7.2.2	Chemical reactions of sorbitol carbonate .....	198
7.3	Conclusion.....	204
8	CONCLUSION AND FUTURE WORK .....	206
9	APPENDIX.....	210
9.1	CHAPTER 3 .....	210
9.2	CHAPTER 5 .....	212
9.3	CHAPTER 6 .....	214
9.4	CHAPTER 7 .....	215
10	References .....	220

Figure 1-1: Global energy consumption of different sources in 2015. <sup>14</sup> .....	5
Figure 1-2: The 12-platform molecules that are the building block of producing renewable chemicals as suggested by Werpy and Peterson <sup>35</sup> .....	9
Figure 1-3: Classification of organic carbonates <sup>36</sup> .....	10
Figure 1-4: CO oxidation on metal surface <sup>93</sup> .....	21
Figure 1-5: Energy diagram of heterogeneous catalytic reaction <sup>93</sup> .....	22
Figure 1-6: The structure of glycerol .....	24
Figure 1-7: The conversion of glycerol into different functionalised compounds <sup>115,116</sup> .....	27
Figure 1-8: Applications of glycerol carbonate <sup>118</sup> .....	29
Figure 1-9: High pressure reactor in the presence of molecular sieves. T=180C, P=30 MPa, 72 h. <sup>77</sup> .....	42
Figure 1-10: Formation of carbonate and nitrile hydration catalyse by CeO <sub>2</sub> <sup>158</sup> .....	44
Figure 1-11: Lock and key model for enzyme binding <sup>166</sup> .....	49



Figure 1-12: Induced-fit model for enzyme binding <sup>166</sup> .....	49
Figure 1-13: Differences between conventional and microwave heating <sup>195</sup> .....	53
Figure 1-14: Ionic conduction and dipolar polarisation due to microwave heating <sup>195</sup> .....	53
Figure 1-15: The structure of sorbitol.....	55
Figure 2-1: The oven used to synthesise catalyst using conventional heating.....	64
Figure 2-2: Carbolite furnace.....	64
Figure 2-3: CEM Discover SP used to synthesise the catalyst.....	65
Figure 2-4: Bragg's law representation in a diagram <sup>217</sup> .....	70
Figure 2-5: Different types adsorption isotherm classified by Brunauer. <sup>224</sup> .....	72
Figure 2-6: Micromeritics Autochem II 2920 to determine basic strength.....	77
Figure 2-7: 50 mL stainless-steel autoclave equipped with a thermocouple and overhead stirrer.....	80
Figure 2-8: General autoclave vessel.....	82
Figure 2-9: Gas chromatography.....	86
Figure 2-10: High liquid gas chromatography.....	89
Figure 2-11: Pelkin-Elmer 100 series spectrometer.....	91
Figure 3-1: XRD patterns of the calcination product of dried powder of $\text{La}_2\text{O}_3$ at different temperature of 500°C, 700°C and 900°C.....	96
Figure 3-2: XRD patterns of $\text{La}_2\text{O}_3$ after degassing at 120°C under vacuum.....	98
Figure 3-3: XRD patterns of 2.3wt% $\text{Cu}/\text{La}_2\text{O}_3$ reproductions after hydrogen reduction (catalyst A-D). Catalyst E -was reduced catalyst with copper (blank).....	99
Figure 3-4: XRD patterns of $\text{Cu}/\text{La}_2\text{O}_3$ catalysts with different copper loadings...	101
Figure 3-5: XRD patterns of 2.3 wt% $\text{Cu}/\text{La}_2\text{O}_3$ with peak prediction of several phases of copper.....	102
Figure 3-6: Crystal structure of lithium lanthanum carbonate. Lanthanum is shown in pink, oxygen is shown in blue, carbon is shown in red and lithium is shown in green.....	<b>Error! Bookmark not defined.</b>
Figure 3-7: Thermogravimetric analysis of precursor.....	104
Figure 3-8: The graph of surface area of $\text{La}_2\text{O}_3$ against temperature.....	106
Figure 3-9: TEM images of $\text{La}_2\text{O}_3$ prepared by hydrothermal method.....	107
Figure 3-10: TEM images of 2.3 wt% $\text{CuLa}_2\text{O}_3$ .....	108
Figure 3-11: TEM images of 6.9 wt% $\text{CuLa}_2\text{O}_3$ .....	109
Figure 3-12: TEM images of 13.9 wt% $\text{CuLa}_2\text{O}_3$ .....	110
Figure 3-13: EDX elemental mapping of 2.3 wt% $\text{Cu}/\text{La}_2\text{O}_3$ .....	112
Figure 3-14: Individual EDX elemental mapping of 2.3 wt% $\text{Cu}/\text{La}_2\text{O}_3$ .....	113
Figure 3-15: EDX elemental mapping of 6.9 wt% $\text{Cu}/\text{La}_2\text{O}_3$ .....	113
Figure 3-16: Individual EDX elemental mapping of 6.9 wt% $\text{Cu}/\text{La}_2\text{O}_3$ .....	114
Figure 3-17: EDX elemental mapping of 13.9 wt% $\text{Cu}/\text{La}_2\text{O}_3$ .....	114
Figure 3-18: Individual EDX elemental mapping of 13.9 wt% $\text{Cu}/\text{La}_2\text{O}_3$ .....	115
Figure 3-19: Temperature-programmed reduction profiles of $\text{CuO}/\text{La}_2\text{O}_3$ at different copper loadings.....	116
Figure 3-20: UV-VIS of $\text{La}_2\text{O}_3$ and $\text{Cu}/\text{La}_2\text{O}_3$ catalysts.....	118

Figure 3-21: Temperature-programmed desorption profiles of Cu/La <sub>2</sub> O <sub>3</sub> at different copper loadings .....	119
Figure 3-22: Adsorbed CO <sub>2</sub> on the catalyst surface characterized by IR <sup>274,275</sup> .....	120
Figure 3-23: <sup>1</sup> H NMR spectra of the reaction mixture at 150°C reaction .....	123
Figure 3-24: <sup>13</sup> C NMR spectra of reaction at 150°C reaction .....	123
Figure 3-25: GC chromatogram at 1 h during reaction.....	125
Figure 3-26: GC chromatogram at 2 h during reaction.....	125
Figure 3-27: GC chromatogram at 4 h during reaction.....	126
Figure 3-28: GC chromatogram at 6 h during reaction.....	126
Figure 3-29: GC chromatogram at 8 h during reaction.....	126
Figure 3-30: Time online analysis for 2.3 wt% Cu/La <sub>2</sub> O <sub>3</sub> at 150°C, P=7 MPa CO <sub>2</sub>	128
Figure 4-1: Different preparation methods for copper supported on lanthanum oxide.....	135
Figure 4-2: XRD patterns of La <sub>2</sub> O <sub>3</sub> synthesise by HT and MW-16 method .....	136
Figure 4-3: XRD patterns of 2.3 wt% Cu/La <sub>2</sub> O <sub>3</sub> prepared by five different methods: HT, MW-16, MW-3, HT-pre and MW-pre.....	138
Figure 4-4: Thermogravimetric analysis of synthesized La(OH) <sub>3</sub> at different preparation methods.....	140
Figure 4-5: Temperature-programmed reduction profiles of 2.3 wt% Cu/La <sub>2</sub> O <sub>3</sub> prepared by different methods .....	142
Figure 4-6: Temperature-programmed desorption profiles of 2.3 wt% Cu/La <sub>2</sub> O <sub>3</sub> at different preparation method.....	144
Figure 4-7: Conversion of glycerol for catalysts prepared by different methods. Reaction conditions: 2.3 g glycerol, 5 mL acetonitrile, 0.11 g catalyst, temperature: 150°C, pressure: 6.2 MPa, time: 24 h .....	145
Figure 4-8: Yield of glycerol carbonate for catalysts prepared by different methods. Reaction conditions: 2.3 g glycerol, 5 mL acetonitrile, 0.11 g catalyst, temperature: 150°C, pressure: 6.2 MPa, time: 24 h .....	147
Figure 4-9: Yield of acetin for catalysts prepared by different methods. Reaction conditions: 2.3 g glycerol, 5 mL acetonitrile, 0.11 g catalyst, temperature: 150°C, pressure: 6.2 MPa, time: 24 h.....	148
Figure 4-10: XRD patterns of ammonium bicarbonate.....	149
Figure 5-1: XRD patterns of La <sub>2</sub> O <sub>3</sub> synthesise by hydrothermal and microwave method calcined at two different temperatures.....	154
Figure 5-2: XRD patterns of CeO <sub>2</sub> synthesise by hydrothermal and microwave method calcined at two different temperatures.....	155
Figure 5-3: Temperature-programmed desorption profiles of La <sub>2</sub> O <sub>3</sub> prepared by hydrothermal and microwave method calcined at two different temperatures...	158
Figure 5-4: Temperature-programmed desorption profiles of CeO <sub>2</sub> prepared by hydrothermal and microwave method calcined at two different temperatures...	160
Figure 5-5: Adsorbed CO <sub>2</sub> on the catalyst surface characterized by FTIR <sup>296</sup> .....	161
Figure 5-6: Effect of pressure on the carbonylation of glycerol with CO <sub>2</sub> catalysed by CeO <sub>2</sub> Reaction conditions: 0.92 g glycerol, 3.27 g 2-cyanopyridine, 0.34 g CeO <sub>2</sub> , temperature: 150°C, time: 5 h .....	164

Figure 5-7: Effect of reaction time on the carbonylation of glycerol and CO <sub>2</sub> catalysed by CeO <sub>2</sub> . Reaction conditions: 0.92 g glycerol, 3.27 g 2-cyanopyridine, 0.34 g CeO <sub>2</sub> , temperature: 150°C, pressure: 4.2 MPa .....	165
Figure 5-8: Effect of catalyst amount on the carbonylation of glycerol and CO <sub>2</sub> . Reaction conditions: 0.92 g glycerol, 3.27 g 2-cyanopyridine, temperature: 150°C, pressure: 3.1 MPa, time: 8 h .....	166
Figure 5-9: Effect of calcination temperature of catalyst on the carbonylation of glycerol and CO <sub>2</sub> . Reaction conditions: 0.92 g glycerol, 3.27 g 2-cyanopyridine, 0.34 g CeO <sub>2</sub> , temperature: 150°C, pressure: 4.2 MPa, time: 5 h .....	167
Figure 6-1: Time online analysis for blank reaction. Reaction conditions: glycerol/urea molar ratio: 1:1.5, temperature 150°C, catalyst 0.25 g, time: 4 h, under N <sub>2</sub> bubbling .....	178
Figure 6-2: Time online analysis for zeolite Y. Reaction conditions: glycerol/urea molar ratio: 1:1.5, temperature 150°C, catalyst 0.25 g, time: 4 h, under N <sub>2</sub> bubbling .....	179
Figure 6-3: Time online analysis for HT CeO <sub>2</sub> 400°C. Reaction conditions: glycerol/urea molar ratio: 1:1.5, temperature 150°C, catalyst 0.25 g, time: 4 h, under N <sub>2</sub> bubbling .....	180
Figure 6-4: Time online analysis for HT CuCeO <sub>2</sub> 400°C. Reaction conditions: glycerol/urea molar ratio: 1:1.5, temperature 150°C, catalyst 0.25 g, time: 4 h, under N <sub>2</sub> bubbling .....	181
Figure 6-5: Time online analysis for HT La <sub>2</sub> O <sub>3</sub> 700°C. Reaction conditions: glycerol/urea molar ratio: 1:1.5, temperature 150°C, catalyst 0.25 g, time: 4 h, under N <sub>2</sub> bubbling .....	182
Figure 6-6: Time online analysis for HT CuLa <sub>2</sub> O <sub>3</sub> 700°C. Reaction conditions: glycerol/urea molar ratio: 1:1.5, temperature 150°C, catalyst 0.25 g, time: 4 h, under N <sub>2</sub> bubbling .....	182
Figure 6-7: Reaction conditions: glycerol/urea molar ratio: 1:1.5, temperature 150°C, catalyst 0.25 g, time: 2 h, under N <sub>2</sub> bubbling, microwave heating (MW)...	186
Figure 7-1: Conversion of sorbitol into high value added products <sup>35</sup> .....	192
Figure 7-2: FTIR spectra of reaction samples at different ratio of solvent in the presence of Lipase B .....	194
Figure 7-3: <sup>1</sup> H NMR spectroscopy of the reaction with 20:80 ratio of DMSO:t-BuOH after 24 h in the presence of Lipase B .....	195
Figure 7-4: FTIR spectra of reaction samples at different ratio of solvent in the presence of Novozyme 435 .....	196
Figure 7-5: FTIR spectra of reaction sample for solvent free reaction in the presence of Novozyme 435 .....	197
Figure 7-6: FTIR spectra of reaction sample for solvent free reaction with silica gel in the presence of Novozyme 435 .....	198
Figure 7-7: FTIR spectra of reaction sample for sorbitol/CDI reaction at 1:1 ratio .....	200
Figure 7-8: <sup>1</sup> H NMR spectroscopy of the reaction sample for sorbitol/CDI at 1:1 ratio .....	200

Figure 7-9: FTIR spectra of reaction sample for sorbitol/CDI reaction at 1:4 ratio .....	202
Figure 7-10: $^1\text{H}$ NMR spectroscopy of the reaction sample for sorbitol/CDI at 1:4 ratio .....	202
Figure 7-11: $^{13}\text{C}$ NMR spectroscopy of the reaction sample for sorbitol/CDI at 1:4 ratio .....	203
Figure 9-1: Calibration of glycerol .....	210
Figure 9-2: Calibration of glycerol carbonate .....	210
Figure 9-3: Calibration curve of monoacetin .....	211
Figure 9-4: Calibration curve of diacetin .....	211
Figure 9-5: Calibration curve of triacetin .....	212
Figure 9-6: Calibration curve of glycerol .....	212
Figure 9-7: Calibration curve of glycerol carbonate .....	213
Figure 9-8: Calibration curve of 2-cyanopyridine .....	213
Figure 9-9: Calibration curve of 2-picolinamide .....	214
Figure 9-10: Calibration curve of glycerol .....	214
Figure 9-11: Calibration curve of glycerol carbonate .....	215
Figure 9-12: IR of sorbitol .....	215
Figure 9-13: IR of DMC .....	216
Figure 9-14: $^1\text{H}$ NMR of sorbitol .....	216
Figure 9-15: $^{13}\text{C}$ NMR of sorbitol .....	217
Figure 9-16: $^1\text{H}$ NMR of sorbitol/CDI at 1:2 ratio .....	218
Figure 9-17: $^{13}\text{C}$ NMR of sorbitol/ CDI at 1:2 ratio .....	218
Figure 9-18: The HPLC chromatogram of tris sorbitol carbonate heated at 100°C for 4 h .....	219
Figure 9-19: The HPLC chromatogram of tris sorbitol carbonate heated at 100°C for 24 h .....	219
Figure 9-20: TIC chromatogram in negative mode using HILIC column .....	219
Figure 9-21: Mass spectrum [M-1] at t=1.45 min for mono sorbitol carbonate from Figure 9-20 .....	220
Scheme 1-1: Phosgenation reaction to produce organic carbonates. $T=70^\circ\text{C}^{36}$ .....	11
Scheme 1-2: Oxidative carbonylation of methanol to produce dimethyl carbonate from CO. $T=100^\circ\text{C}$ , $P=6\text{ MPa}$ , 8 h. <sup>56</sup> .....	12
Scheme 1-3: Transesterification of propylene carbonate with methanol. $T=150^\circ\text{C}$ , 4 h. <sup>57,61</sup> .....	13
Scheme 1-4: Transesterification reaction of DMC with ethanol. $T=60^\circ\text{C}^{49}$ .....	14
Scheme 1-5: Transesterification reaction of urea with ethylene glycol to produce EC. $T=150^\circ\text{C}$ , 3 h <sup>67</sup> .....	15
Scheme 1-6: Transesterification reaction of urea with methanol producing DMC. $T=170^\circ\text{C}$ , 4 h <sup>68</sup> .....	15
Scheme 1-7: Decomposition of urea forming isocyanate species and ammonia <sup>69</sup> ..	15
Scheme 1-8: Synthesis of DMC from methanol and $\text{CO}_2$ . $T=180^\circ\text{C}$ , $P=30\text{ MPa}$ , 70 h <sup>38,77</sup> .....	17

Scheme 1-9: Synthesis of ethylene carbonate from ethylene oxide. T=100°C, P=4 MPa, 4 h <sup>80</sup> .....	18
Scheme 1-10: General mechanism for transesterification of methyl esters <sup>107</sup> .....	25
Scheme 1-11: Acid-induced dehydration of glycerol to acrolein, T=360°C, P=25 MPa <sup>111</sup> .....	26
Scheme 1-12: 2-step process in the production of epichlorohydrin with glycerol as the starting material <sup>112</sup> .....	26
Scheme 1-13: Synthesis of glycerol carbonate from phosgene. T=30°C, 6 h <sup>136</sup> .....	30
Scheme 1-14: Synthesis of glycerol carbonate from dimethyl carbonate. T=75°C, 30 min, molar ratio of 2 <sup>138</sup> .....	31
Scheme 1-15: Synthesis of glycerol carbonate from ethylene carbonate. T=50°C, 5 h, molar ratio of 2 <sup>140</sup> .....	31
Scheme 1-16: Synthesis of glycerol carbonate from urea. T=150°C, 4 h, molar ratio=1.5 <sup>141</sup> .....	32
Scheme 1-17: Acid-base properties <sup>140</sup> .....	33
Scheme 1-18: Reaction mechanism in the formation of carbonate from urea <sup>150</sup> .....	35
Scheme 1-19: Reaction mechanism in the formation of glycerol carbonate from tin-glycerol complex. T=180°C, P=5 MPa, 15 h <sup>135</sup> .....	36
Scheme 1-20: Formation of zwitterionic adducts to form glycerol carbonate. T=100°C, P=2.5 MPa, 1 h <sup>153</sup> .....	38
Scheme 1-21: Activation of glycerol and CO <sub>2</sub> by ZnO and La <sub>2</sub> O <sub>2</sub> CO <sub>3</sub> respectively. T=170°C, P=7.0 MPa, 12 h <sup>154</sup> .....	39
Scheme 1-22: Reaction mechanism in the direct carbonylation of glycerol in the presence of acetonitrile. T=150°C, P=7.0 MPa, 12 h <sup>155</sup> .....	40
Scheme 1-23: Reaction of methanol and CO <sub>2</sub> in the presence of orthoesters. T=180°C, P=30 MPa, 24 h <sup>38</sup> .....	43
Scheme 1-24: Reaction mechanism of between methanol and CO <sub>2</sub> in the presence of acetonitrile as dehydrating agent. T= 150°C, P=0.5 MPa, 4 h. <sup>158</sup> .....	44
Scheme 1-25: Reaction mechanism between acetamide and benzamide with methanol. T=150°C, P=1 MPa. <sup>158,162</sup> .....	45
Scheme 1-26: Reaction mechanism between methanol and CO <sub>2</sub> in the presence of 2-cyanopyridine as dehydrating agent. T=120°C, P=5 MPa, 12 h <sup>163</sup> .....	45
Scheme 1-27: Enzymatic reaction catalysed by lipase.....	51
Scheme 1-28: Synthesis of sorbitol tricarboxylate with glycerol as starting material <sup>208</sup> .....	57
Scheme 3-1: Synthesis of glycerol carbonate via different chemical.....	93
Scheme 3-2: Reaction scheme of the precursor undergoing different heat treatment .....	103
Scheme 3-3: Direct carbonylation of glycerol carbonate from glycerol and CO <sub>2</sub> ..	121
Scheme 3-4: Reaction of glycerol with CO <sub>2</sub> and trimethyl orthoester .....	124
Scheme 3-5: Reaction between glycerol and acetic acid .....	129
Scheme 4-1: Formation of ammonium bicarbonate from ammonia and carbonic acid .....	149

Scheme 5-1: Reaction of glycerol with CO <sub>2</sub> to produce glycerol carbonate using 2-cyanopyridine as dehydrating agent.....	162
Scheme 5-2: Plausible reaction mechanism of carbonylation of glycerol with CO <sub>2</sub> .....	170
Scheme 6-1: Possible reaction pathways that have been reported by Hammond <i>et al</i> <sup>141</sup> .....	173
Scheme 6-2: Reaction scheme of glycerol and urea and its possible products. ....	188
Scheme 7-1: Synthesis of sorbitol carbonate.....	193
Table 1: E factors across chemical industry <sup>7</sup> .....	3
Table 2: DMC yield in the presence of different types of nitrile <sup>163</sup> .....	46
Table 3: Classification of pores by IUPAC <sup>221</sup> .....	71
Table 4: Retention times and calibration curve obtained for standards used in direct carbonylation reaction of glycerol with CO <sub>2</sub> .....	87
Table 5: Retention times and calibration curve obtained for standards used in direct carbonylation reaction of glycerol with CO <sub>2</sub> .....	88
Table 6: Retention times and calibration curve obtained for standards used in direct carbonylation reaction of glycerol with CO <sub>2</sub> .....	90
Table 7: Lattice parameters and particle size of La <sub>2</sub> O <sub>3</sub> at different calcination temperature .....	97
Table 8: Lattice parameters and particle size of 2.3 wt% Cu/La <sub>2</sub> O <sub>3</sub> .....	100
Table 9: Lattice parameters and particle size of 2.3 wt% Cu/La <sub>2</sub> O <sub>3</sub> and 13.9 wt% Cu/La <sub>2</sub> O <sub>3</sub> .....	101
Table 10: Textural properties of Cu/La <sub>2</sub> O <sub>3</sub> and bare support La <sub>2</sub> O <sub>3</sub> .....	105
Table 11: Basic sites distribution calculated on the basis of CO <sub>2</sub> -TPD profiles.....	121
Table 12: Catalytic performance of 2.3 wt% Cu/La <sub>2</sub> O <sub>3</sub> in the synthesis of glycerol carbonate .....	127
Table 13: Catalytic performance of Cu/La <sub>2</sub> O <sub>3</sub> at different loadings in the synthesis of glycerol carbonate from glycerol and CO <sub>2</sub> .....	130
Table 14: Abbreviations for catalysts preparation of 2.3 wt% Cu/La <sub>2</sub> O <sub>3</sub> .....	134
Table 15: Lattice parameters and particle size of La <sub>2</sub> O <sub>3</sub> for HT and MW-16 .....	136
Table 16: Lattice parameters and particle size of 2.3 wt% Cu/La <sub>2</sub> O <sub>3</sub> for different preparation methods.....	138
Table 17: Cu wt% analysed by EDX.....	142
Table 18: Lattice parameters and particle size of La <sub>2</sub> O <sub>3</sub> synthesised by hydrothermal method at different calcination temperature .....	154
Table 19: Lattice parameters and particle size of CeO <sub>2</sub> synthesised by hydrothermal method at different calcination temperature .....	155
Table 20: Textural properties of CeO <sub>2</sub> and La <sub>2</sub> O <sub>3</sub> .....	157
Table 21: Basic sites distribution calculated on the basis of CO <sub>2</sub> -TPD profiles.....	159
Table 22: Basic sites distribution calculated on the basis of CO <sub>2</sub> -TPD profiles.....	160
Table 23: The effect of preparation method of the catalyst on the carbonylation reaction.....	168
Table 24: Catalytic activity of prepared catalysts for glycerol carbonylation .....	169

Table 25: Glycerol carbonate synthesis from urea over various catalyst.....	174
Table 26: Catalytic performance of the catalyst .....	177
Table 27: Catalytic performance for the synthesis of glycerol carbonate at different reaction temperature .....	183
Table 28: Catalytic performance for the synthesis of glycerol carbonate using conventional and microwave heating.....	186
Table 29: C-H-N analysis of the synthesised tris sorbitol carbonate.....	203

Equation 1.....	3
Equation 2.....	18
Equation 3.....	18
Equation 4.....	18
Equation 5.....	19
Equation 6.....	19
Equation 7.....	19
Equation 8.....	19
Equation 9.....	54
Equation 10.....	69
Equation 11.....	71
Equation 12.....	74
Equation 13.....	74
Equation 14.....	74
Equation 15.....	74
Equation 16.....	75
Equation 17.....	75
Equation 18.....	78
Equation 19.....	129





# **CHAPTER 1**

## **INTRODUCTION**

# 1 INTRODUCTION

## 1.1 Sustainability and Green Chemistry

Sustainability can be defined as a dynamic equilibrium in the process of interaction between a population and the carrying capacity of its environment such that the population develops to express its full potential without producing irreversible, adverse effects on the carrying capacity of the environment upon which it depends.<sup>1</sup> The concept of sustainability has created much interest from numerous disciplines such as economics, engineering, environmental studies and the physical sciences.<sup>2</sup> This requires advancement in science and technology to tackle any environmental related problems. Therefore there must be a balance in economic development and resource consumption along with environmental impact in attaining sustainability.<sup>3</sup> Sustainability must be achieved as a result of deteriorating environmental conditions due to increasing global development. Numerous problems have arisen such as bioaccumulation and persistence of organic compounds, ozone depletion as well as climate change.<sup>4</sup>

The term Green Chemistry was coined by Paul Anastas and John Warner.<sup>5</sup> He laid out 12 fundamental principles of Green Chemistry that can be applied especially in chemistry and chemical engineering. The aim of Green Chemistry is the design of chemical products and processes that reduce or eliminate the use and generation of substances hazardous to human health and the environment.<sup>5</sup> Research & development (R&D) is crucial at the very start of every new production line to produce high-quality materials that are environmentally safer. Academic research has a big and important role in improving and perfecting the whole system continuously. The principle of Green Chemistry is a powerful tool to ensure the benefit of the environment, economy and social welfare. There are many ways to study Green Chemistry to quantify its performance using metrics such as atom economy or E-factor. Atom economy is one of the common Green Chemistry metrics. Atom economy can be defined as the incorporation of all atoms in the starting material to produce desired products which can be quantified using the equation shown in Equation 1.<sup>6</sup>

$$\% \text{ Atom economy} = \frac{\text{molecular mass of desired product}}{\text{Molecular mass of all reactants}} \times 100\% \quad \text{Equation 1}$$

Another metric that is commonly used is the E-factor which was introduced by Roger A. Sheldon. E-factor can be defined as the amount of waste being generated in a reaction.<sup>7</sup> It can be calculated by the amount of waste generated per mass of product in which the ideal E-factor is zero. Table 1 shows the chemical industry performances based on E-factor. Pharmaceuticals and fine chemicals industries have the highest E-factor due to multi-step syntheses and heavy usage of stoichiometric reagents instead of catalysts.<sup>7</sup> Other metrics such as carbon efficiency, reaction mass efficiency or EcoScale are some of the metrics used in Green Chemistry.

**Table 1: E factors across chemical industry<sup>7</sup>**

Industry segment	Product tonnage	E-factor (kg waste/kg product)
<b>Oil refining</b>	10 <sup>6</sup> -10 <sup>8</sup>	<0.1
<b>Bulk chemicals</b>	10 <sup>4</sup> -10 <sup>6</sup>	<1-5
<b>Fine chemicals</b>	10 <sup>2</sup> -10 <sup>4</sup>	5-50
<b>Pharmaceuticals</b>	10-10 <sup>3</sup>	25-100

There are a number of ways academia, industry and government can work together and be able to contribute to the development of sustainability.<sup>8</sup> Firstly, academic research has the ability to design cleaner technologies with the knowledge and skills they acquire before developing new chemical processes and products. Next, chemical industry can benefit from academic research by using new chemicals and processes that were invented on lab scale before scaling up to industrial scale. Furthermore, both have the ability to educate the public on the impact, stress and consequences they are putting on the ecosystem as a whole, especially students, on the importance of sustainable development thus assisting them on mastering the skills and knowledge to further improving the technologies.<sup>8</sup> Lastly, government can collaborate with industry and academia to

promote greener technologies by provide funding for research and education as well as setting up legislation on the impacts of sustainable development.<sup>8</sup>

#### **1.1.1 Oil consumption is an environmental problem**

Global oil consumption has increased in recent years due to increase in human population and consumption. The world consumes 30 billion barrels of oil per year.<sup>9</sup> The petrochemical industry is a multi-billion dollar industry, which comprises of production, distribution, refining and marketing. Petrochemicals have significantly contributed to the development of society in both economic aspects and improvement of the standard of living due to its continuous improvement in technologies.<sup>10</sup> There are numerous advantages in using petroleum feedstocks over other energy resources. Petroleum consist of hydrocarbons which is relatively cheap, better in performance than coal in terms of producing less CO<sub>2</sub> emission due to number of hydrogen it contains, therefore, giving higher yields, and easily accessible which can be converted into value-added products.<sup>11</sup> Most of the commodities such as gasoline, naphtha or lubricant are made from petroleum.

The chemical industry produces synthetic materials such as polyester, plastic and solvents which use petroleum-based substances as starting materials. This is because it contains the basic petroleum compounds, which every industry needs that can be designed, produced and manipulated accordingly.<sup>12</sup> This produces products that can improve our lives immensely and upon which we can depend such as household products.<sup>12</sup> Petroleum is also used as an energy resource and the world's energy consumption has been steadily increasing. Energy consumption grew more than 50 fold from 0.2 billion toe to 11.4 billion toe between 1850 to 2005.<sup>13</sup> Figure 1-1 shows the global energy consumption of different energy sources in 2015 in which oil dominates the world energy consumption followed by coal.<sup>14</sup> Petroleum is a non-renewable resource that requires millions of years to regenerate from dead organisms such as zooplankton which undergoes intense heat and pressure under sedimentary rocks; this resource is rapidly depleting as chemical industries use a huge amount of petroleum resources.

Excessive consumption of petrochemicals has resulted in extensive damage to the environment which can affect the environmental stability, such as global temperature. It has been making headlines for the past few years for causing

climate change due to the release of greenhouse gases especially carbon dioxide. For example, extreme weather conditions of cold spells and hot weather events, thereby disrupting the natural weather cycle.<sup>15</sup> The refining sector of the petroleum industry contributes to the vast emission of volatile organic compounds (VOCs) such as benzene, dioxin, chlorocarbons or methylene chloride mainly from its production processes. Other sources contributing to the production of VOCs are motor vehicle exhausts, solvent usage and other industrial processes such as electronic manufacturing and equipment spraying.<sup>16</sup> VOCs have carcinogenic properties and are toxic to both plants and animals.<sup>17</sup> Air qualities must be monitored constantly, as air quality has the ability to change the atmospheric composition and affecting the ozone layer. This contributes to the global greenhouse effect as well as other air pollutants such as sulphur dioxide, carbon monoxide and nitrogen dioxide that can harm human health especially children and the elderly.<sup>18</sup>

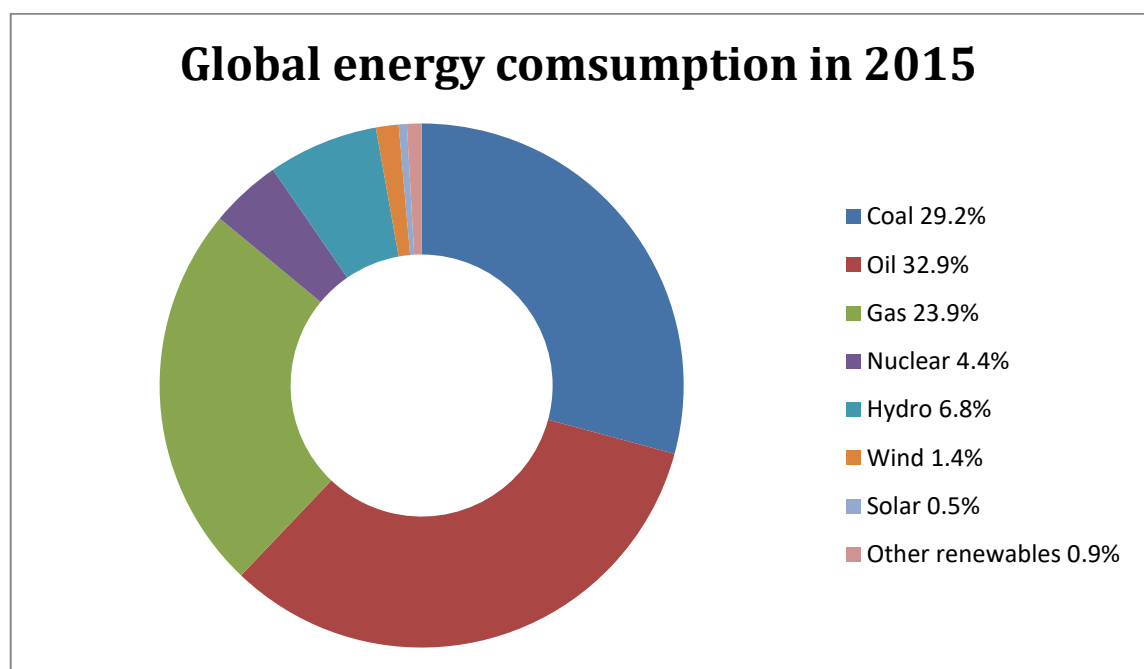


**Figure 1-1: Global energy consumption of different sources in 2015.**<sup>14</sup>

### 1.1.2 Alternative sources of energy/Renewable energy

There is the need to find alternative sources of energy such as hydroelectricity or solar power, thus shifting energy consumption to a more reliable, environmentally friendly and renewable resources. This can significantly reduce all of the problems mentioned above and thus can improve the country's own energy security. Chemical reactions/syntheses generate large quantities of waste which can be toxic.<sup>19</sup> For example, hazardous chemicals such as dimethylbutyryl chloride and methyl iodide were used in the multistep synthesis of simvastatin, a drug which was used to treat high cholesterol producing huge amounts of toxic by-products which could harm the environment if not treated properly.<sup>20,21</sup> Previously expensive and highly toxic reagents such as chromate or permanganate were used as stoichiometric oxygen donor in the selective oxidation reaction of primary alcohols to aldehydes.<sup>20,22</sup>

Principle 7 aforementioned of Green Chemistry that can be applied is that the raw material/feedstock should be renewable rather than depleting whenever technically and economically practicable. The goal for sustainability to be achieved will result in resources and energy being utilised efficiently and will contribute to the stabilisation of the economy and has the ability to generate revenue.<sup>23</sup> The challenge is to find the best alternative renewable resources that can sustain for a long period of time without affecting the environment and also resources that are suitable for the country's need depending on the geographical location and climate.<sup>24</sup>

Renewable resources such as biomass are predicted to be the next future feedstock. Biomass is renewable, widely available, sustainable and environmental-friendly renewable resource for the growing global population. EU regulations require 20% of the energy supplies must come from alternative and renewable resources in 2020.<sup>25</sup> The usage of biomass as the world future feedstock as the potential resources that could cater the growing consumption of energy from the increasing human population looks promising. Scientists are interested in similar

functional and active chemicals or compounds that are obtained from petroleum-derived sources, which can be obtained or extracted from biomass.

There was a study conducted by University of Florida on the usage of fossil fuels and renewable energy in 2012 and 2040 across four different countries.<sup>26</sup> For example in United States of America, the energy source heavily depended on fossil fuels in which 38% comes from coal and 30% from natural gas whereas only 3% comes from wind and 7% from hydroelectric. However they predicted an increase in renewable energy consumption in 2040. Wind energy contributes 44% of the energy source in United States followed by 25% of nuclear energy, 18% of solar energy, 9% of hydroelectric and 3% from biomass.<sup>26</sup>

### 1.1.3 The significance of biomass

Biomass can be defined as sources that is derived from organic materials of plants and living organisms.<sup>27</sup> Biofuel can be made from a range of biomass such as oil-seed rape, vegetable oil, plant and animal waste, algae or plant cell walls which can be obtained by esterification or fermentation process.<sup>28</sup> Some considered biomass as carbon neutral as they emit the same amount of carbon when burnt as their origination crop absorbed from the air while growing.<sup>25</sup> The use of biomass is associated with the competition with food supply for example sugar beet, sugarcane, corn or vegetable oils as resources and this will compete with the world supply food chain as well as competition for land. These are generally known as first generation biomass. As a consequence the price of global food supply would increase, this is a matter of concern for an increasing global population as it can affect food supply in some parts of the world.<sup>25</sup>

Therefore, second-generation biomass or lignocellulosic biomass, for example, wood, energy crops such as willow, poplar and straw is a potential solution to these problems. Energy crops are expected to produce 400 million dry tons in United States by 2030 and 155 million dry tons of agricultural residues from corn stover can be used for energy production.<sup>29</sup> Second generation biomass are harder to extract due to the presence of lignocellulose however the carbon can then be converted to energy *via* biological or thermochemical processes as they are

difficult to extract.<sup>30</sup> In addition, second-generation feedstocks grow as fast as any other tree or plantations, and the energy crop can be planted even in a poor quality land. Also one of the main compounds present is cellulose, is indigestible by humans, making it an ideal candidate for fuel production.<sup>31</sup>

In order to acquire chemicals of interest, careful selection of methods is very important, to obtain the maximum yield of biomass conversion and to prevent unwanted side reactions that would destroy the process. Therefore, the concept of bio-refinery is similar to the petrochemical refinery. It integrates biomass conversion mainly using three conversion techniques; they are thermo-chemical conversion, physico-chemical conversion and bio-chemical conversion.<sup>32</sup> These processes help to produce energy, fuel and chemical products to ensure the security of a country's resources as well as sustaining the chemical industry's lifespan. A bio-refinery manipulates biomass from different components and intermediates to produce high-quality products. Products that are derived from biomass can be generally divided into two:

- 1) High value, low volume products such as cosmetics or nutraceuticals, also known as specialty products.<sup>33</sup>
- 2) Low value, high volume products, commodity products, such as biofuel that can be used as a transport fuel as well as to generate heat and electricity.<sup>33</sup>

Biomass can be transformed into producing desired molecules with the use of catalyst in the process that could have a huge impact in terms of selectivity and efficiency of biomass conversion. Werpy and Petersen have systematically screened 300 possible building block chemicals and managed to put together 12 platform molecules shown in Figure 1-2, that are the building blocks for any chemical reaction which can be converted into value added products.<sup>34,35</sup>



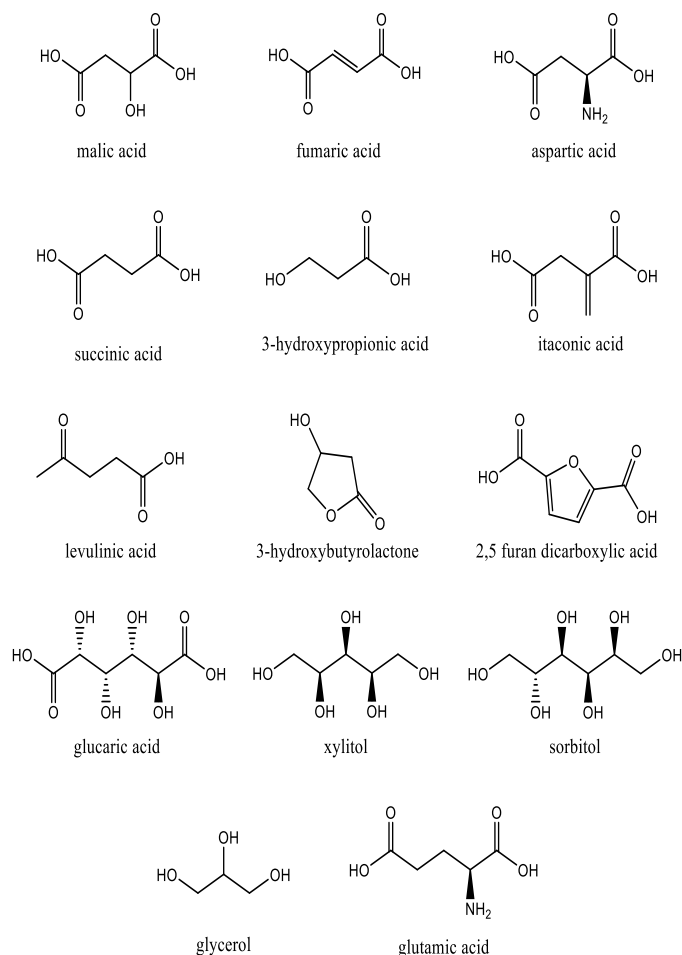


**Figure 1-2: The 12-platform molecules that are the building block of producing renewable chemicals as suggested by Werpy and Peterson<sup>35</sup>**

## 1.2 Organic Carbonates

Organic carbonates or carbonic esters are typically formed by diesterification of carbonic acid, which is unstable at room temperature, with hydroxyl compounds and the type of organic carbonate varies according to the initial substrate used.<sup>36</sup> Organic carbonates (Figure 1-3, a) can be divided into two different types.<sup>36</sup> They are acyclic carbonates, such as dimethyl carbonate (Figure 1-3, b) or diethyl carbonate and cyclic carbonates, such as propylene carbonate (Figure 1-3, c) or propylene carbonate.

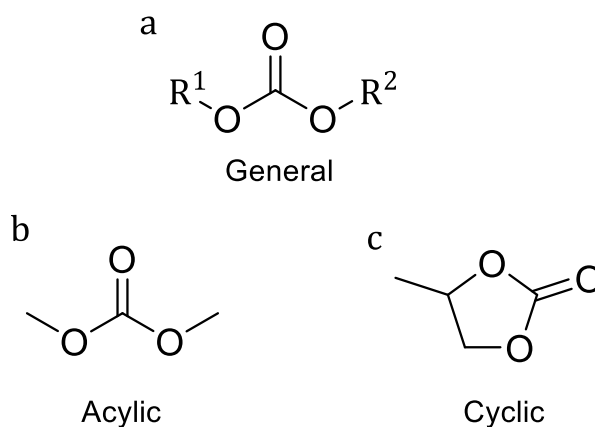


**Figure 1-3: Classification of organic carbonates<sup>36</sup>**

Organic carbonates for example dimethyl have a wide range of applications in which it can reach up to 599 kilo tons by the end of 2023 in its usage according to transparency market research and are useful in different industrial sectors.<sup>37</sup> Cyclic organic carbonates are utilised as intermediates in organic synthesis to produce fine chemicals for medicines and agricultural chemicals.<sup>38</sup> The organic carbonate monomer, such as ethylene carbonate, undergoes ring opening polymerisation to produce polymers such as poly(ethylene oxide-co-ethylene carbonate, poly(cyclohexene carbonate) and poly(propylene carbonate), which produce materials such as engineering plastics for the production of electronics.<sup>38,39</sup> Polymers synthesised from organic carbonates are known for their strength, durability, heat resistance, biodegradability, lightness, high electrical insulation and colour.

Organic carbonates can also be used as organic solvents, as they are excellent aprotic polar solvents, having a broad solvency power, which can be used to replace toxic and VOCs that are sometimes used during chemical reactions.<sup>38</sup> They possess low toxicity and suitable boiling points (90°C-250°C).<sup>38</sup> Organic carbonates can also be used as electrolyte solvents for lithium ion batteries as a result of their high dielectric constant.<sup>40</sup> Organic carbonates are also used as fuel additives, to replace methyl tert-butyl ether as it improves the octane number. Organic carbonates are being utilised as an alternative solvent to numerous toxic chemical reagents that are currently being used in factories and industries worldwide, for example, dimethyl carbonate can be used as a methylating reagent to replace methyl halides and dimethylsulfate as conventional methylating agents that can

cause serious damage to the environment.<sup>41,42,43,44,45,46,47</sup> The excellent physical properties of organic carbonates are crucial as they offer safe and clean alternative solvent compare to using toxic solvents such as phosgene, pyridine and toluene.<sup>36</sup>

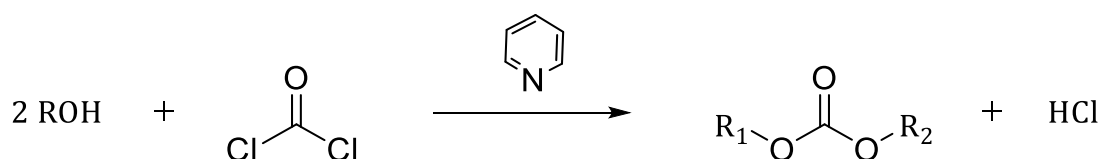
### 1.3 Synthesis of organic carbonates

There are many ways to synthesise organic carbonates. These methods can be generally categorised into four methods:

- 1) Phosgenation method.<sup>36</sup>
- 2) Reaction with carbon monoxide.<sup>48</sup>
- 3) Reaction with carbon dioxide.<sup>38</sup>
- 4) Transesterification method.<sup>49</sup>
- 5) Carbonate formation with urea.<sup>50,51</sup>

#### 1.3.1 Phosgenation method

One of the first methods for the synthesis of organic carbonates was used by Shaikh *et al.* This was the phosgenation method shown in Scheme 1-1.<sup>36</sup>



**Scheme 1-1: Phosgenation reaction to produce organic carbonates. T=70°C<sup>36</sup>**

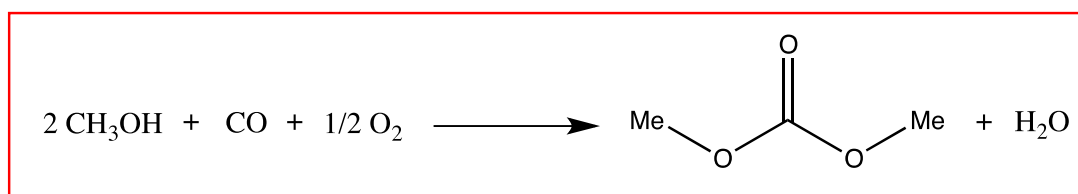
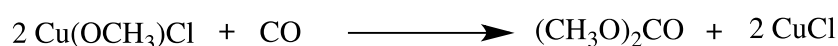
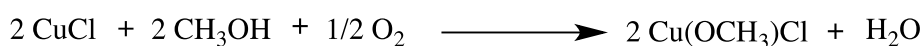
Phosgene is toxic and highly corrosive.<sup>52</sup> Phosgene reacts with the mixture of hydroxyl compounds dissolved in an anhydrous solvent such as toluene and excess pyridine. Then excess pyridine must be neutralised with a mild acidic solution such as HCl as it is highly flammable with low flash point which can be cogenerated.<sup>36,52</sup> These compounds also readily react with hydroxyl compounds such as methanol or

polyols under mild reaction conditions at 70°C. The by-product salts of the reaction can be washed with water and be removed after the reaction. This reaction produces a low yield of carbonates, if organic base is absent during the reaction and left with unreacted chlorocarbonates at a high temperature of 150°C.<sup>36</sup> However, the reaction is not environmentally friendly due to production of by-product HCl which is corrosive.<sup>53</sup>

### 1.3.2 Reaction with CO

Another route for producing organic carbonates is by oxidative carbonylation of methanol catalysed by either copper or palladium complexes.<sup>54,55</sup> The reaction first shown by Rebora and co-workers was carried out in the presence of carbon monoxide in a redox system using cuprous chloride as a catalyst allowing for the oxidation and reduction of cupric methoxy chloride to take place shown in Scheme 1-2 producing dimethyl carbonate (DMC).<sup>56</sup> The reaction produced a very high conversion of DMC giving a yield of 96% at P=6 MPa, T=100°C for 8 h. However, the reaction uses carbon monoxide which is toxic and must be handled with proper care. The reaction also requires pressure which is costly.

#### Catalytic mechanism



**Scheme 1-2: Oxidative carbonylation of methanol to produce dimethyl carbonate from CO. T=100°C, P=6 MPa, 8 h.<sup>56</sup>**

### 1.3.3 Transesterification reactions

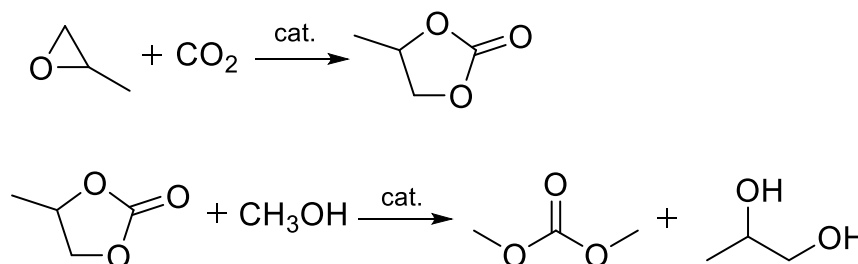
Transesterification reactions of organic carbonates can be categorised into two types of reaction:

- 1) Transesterification of cyclic carbonates.<sup>57</sup>
- 2) Transesterification of acyclic carbonates.<sup>58</sup>

There are numerous research papers describing the use of catalysts to improve the conversion and selectivity of the reactions.<sup>57</sup>

#### 1.3.3.1 Transesterification of cyclic carbonates

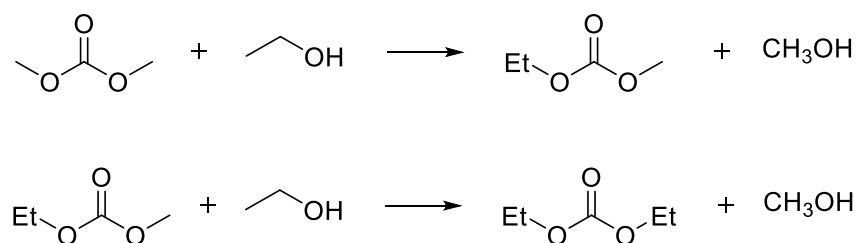
Transesterification of cyclic carbonates with alcohols produce linear organic carbonates, such as DMC.<sup>57</sup> Scheme 1-3 shows the transesterification reaction of propylene carbonate with methanol producing DMC firstly reported by Bhanage *et al.*<sup>57</sup> This reaction is a two-step process. Initially, the cyclic carbonate, propylene carbonate, is synthesised by direct conversion of CO<sub>2</sub> with an epoxide, propylene oxide. Few solid base catalysts were tested in the reaction such as MgO and ZnO.<sup>57</sup> In the second step the propylene carbonate is transesterified with methanol at 150°C for 4 h producing a yield of 66.1% DMC.<sup>57</sup> The by-product, propylene glycol can be recycled back as propylene glycol can be used as a feedstock to produce cyclic carbonates and as antifreeze in the automotive industry.<sup>59,60</sup> The atom economy for the transesterification of propylene carbonate with methanol is 54%.



**Scheme 1-3: Transesterification of propylene carbonate with methanol. T=150°C, 4 h.<sup>57,61</sup>**

### 1.3.3.2 Transesterification of acyclic carbonates

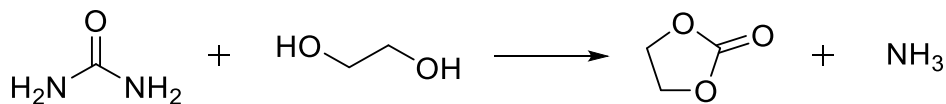
The transesterification of DMC into diethyl carbonate (DEC) is a two-step reaction synthesised by Keller *et al*; shown in Scheme 1-4.<sup>49</sup> Initially the transesterification of DMC with ethanol at 60°C produced ethyl methyl carbonate (EMC). EMC then reacts further with ethanol forming DEC.<sup>49</sup> There are numerous catalysts such as Mg–Al hydrotalcite, a solid base, which catalyses this reaction.<sup>62,63,64,65</sup> The by-product of this reaction is an alcohol which also can be recycled and used as starting reagent in the production of DMC, thus it is economical.<sup>49</sup>



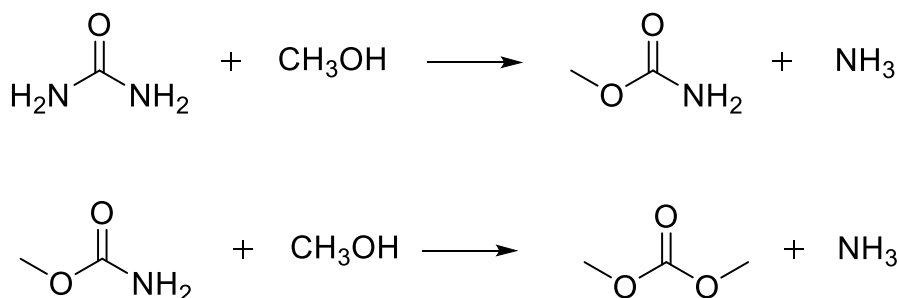
**Scheme 1-4: Transesterification reaction of DMC with ethanol. T=60°C<sup>49</sup>**

### 1.3.4 Carbonate formation with urea

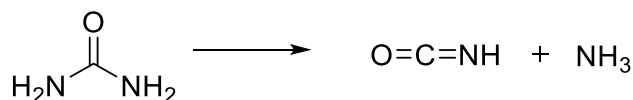
The reaction between urea and alcohols, or diols, is attractive since urea is considered as an activated form of carbon dioxide, and urea is relatively cheap and possesses low toxicity levels.<sup>66</sup> The reaction between urea and ethylene glycol, Scheme 1-5, was performed by Li *et al* under mild reaction conditions at 150°C for 3 h giving high yields of 93% ethylene carbonate.<sup>67</sup> Ethylene carbonate can also be used as a raw feedstock in the production of DMC thus lowering the cost of production of DMC.<sup>67</sup> Joe *et al* reported the reaction of urea and methanol at 170°C produced methyl carbamate (MC) as an intermediate, Scheme 1-6. MC reacts further with methanol to produce DMC and ammonia as by-product.<sup>68</sup> Chun *et al* proposed that the key to urea alcoholysis is the decomposition of urea to give isocyanate species shown in Scheme 1-7, these species will react with alcohol, for example, methanol forming DMC.<sup>69</sup>



**Scheme 1-5: Transesterification reaction of urea with ethylene glycol to produce EC.**  
**T=150°C, 3 h<sup>67</sup>**



**Scheme 1-6: Transesterification reaction of urea with methanol producing DMC.** T=170°C, 4 h<sup>68</sup>



**Scheme 1-7: Decomposition of urea forming isocyanate species and ammonia<sup>69</sup>**

### 1.3.5 Reaction with CO<sub>2</sub>

The usage of raw materials is also a crucial factor to determine the ‘greenness’ of a process, for example, exploiting carbon dioxide as a renewable feedstock is an attractive proposition.<sup>70</sup> Carbon dioxide is one of the primary greenhouse gases and is considered one of the major contributors to global warming. The alarming increase of CO<sub>2</sub> emission has encouraged researchers to exploit and transform chemically formed carbon dioxide, attracting a great interest as an alternative feedstock.<sup>71</sup> The main advantages for using CO<sub>2</sub> are its high abundance, low

toxicity, high atom and economical efficiencies and being a non-flammable C1 building block.<sup>72</sup> Carbon dioxide is a highly thermodynamically stable compound and inert in nature, requiring different methods to chemically transform it:

- By using high energy starting materials such as hydrogen and organometallics.<sup>73</sup>
- Choosing low energy synthetic targets such as organic carbonates.<sup>73</sup>
- Removing products in the forward reaction, and thereby forcing the equilibrium to the right as it is being continuously removed.<sup>73</sup>
- Supplying energy i.e. light or energy.<sup>73</sup>

High temperature and high pressure, such as 200°C and 14 MPa are often required for activation which restricts its application.<sup>72,74</sup> Therefore, the need to find methods to develop CO<sub>2</sub> activation under milder conditions is a promising research goal.<sup>75</sup>

As an alternative to using phosgene and carbon monoxide for the synthesis of organic carbonates, carbon dioxide can be utilised in the formation of organic carbonates. Organic carbonates can be produced by oxidative carbonylation by CO<sub>2</sub> producing two types of organic carbonates, linear organic carbonates (LOCs) and cyclic carbonates.<sup>73</sup>

#### 1.3.5.1 Synthesis of linear organic carbonates

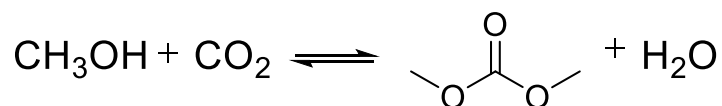
The simplest method for forming LOCs such as DMC and DEC is the reaction of alcohol with CO<sub>2</sub>.<sup>76</sup> Scheme 1-8 shows the synthesis of DMC from methanol at 180°C and 30 MPa for 70 h using molecular sieves as dehydrating agent and was reported by Choi *et al.*<sup>38,77</sup> Unfortunately there is a thermodynamic limitation in performing this reaction as the equilibrium lies on the reactant side, resulting in low yields and conversions between the range of 0.5% to 4%.<sup>38,72,78</sup> The Gibbs free energy,  $\Delta G$ , of the reaction is 23.92 kJ/mol.<sup>79</sup> There are three ways to overcome this problem of thermodynamic restrictions:

- Removing water continuously on the right hand side of the equation by using appropriate drying agents such as orthoesters.



- Increasing the pressure of CO<sub>2</sub> thus increasing the concentration of CO<sub>2</sub> to shift the equilibrium to the product side.
- Development of an effective catalyst to accelerate the reaction.<sup>38,72,77</sup>

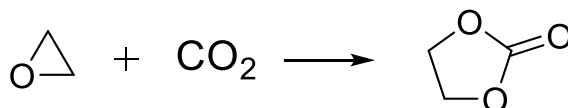
It will give a positive impact on the reaction and can lead to negative  $\Delta G$  for the reaction.<sup>72</sup>



**Scheme 1-8: Synthesis of DMC from methanol and CO<sub>2</sub>. T=180°C, P=30 MPa, 70 h<sup>38,77</sup>**

### 1.3.5.2 Synthesis of cyclic organic carbonates

The coupling reaction between CO<sub>2</sub> and ethylene oxide, the simplest epoxide, produces the five-membered ring carbonate, ethylene carbonate as shown in Scheme 1-9.<sup>80</sup> The high energy of the oxirane as a starting material readily produces carbonates with high yield of 97% and selectivity of 99% using bi-functional metal-salen complexes which was reported by Miao *et al.*<sup>81</sup> The reaction requires high temperature and pressure, 100°C and of 4 MPa respectively.<sup>81</sup> This reaction is 100% atom economical, all starting materials are incorporated into the final product.<sup>81,82</sup> Previously, these reactions required high temperatures 100-200°C and the pressure of 7-10 MPa, however catalysts such as bi-functional cobalt salen complex or metal organic framework Cr-MIL-101 have been tested to overcome these high conditions as well as thermodynamic limitations.<sup>81,83</sup> The importance of having mild reaction conditions is to decrease energy usage, thus reducing capital input. More importantly, mild conditions utilise the full potential of a catalyst in chemical reactions, enabling them to speed up a reaction and improve the product yield drastically.<sup>84</sup>



**Scheme 1-9: Synthesis of ethylene carbonate from ethylene oxide. T=100°C, P=4 MPa, 4 h<sup>80</sup>**

There are numerous reports on using catalysts in the production of carbonates via CO<sub>2</sub> route such as Et<sub>4</sub>NBr, phthalocyanine, MgO and SmOCl.<sup>38</sup>

## 1.4 Advantages of catalysis

Catalysis can be defined as the increase in rate of chemical reaction using substance i.e. catalyst that is not consumed in the chemical process until the chemical system attained equilibrium. The chemical reaction must be thermodynamically feasible for a catalytic reaction to take place which can be associated with changes in Gibbs free energy; G. Equation 2 relates Gibbs free energy with enthalpy, H and entropy, S in which  $\Delta G < 0$  for a chemical reaction to take place. The catalyst does not change chemical equilibrium and only the kinetics of the reaction.

$$\Delta G = \Delta H - T\Delta S \quad \text{Equation 2}$$

Therefore increasing rate of chemical reaction is to increase its rate coefficient, k. Equation 3 relates k with steric factor, P, collision frequency, Z, activation energy, E, gas constant, R and T the absolute temperature according to collision theory.

$$k = PZ e^{(-E/RT)} \quad \text{Equation 3}$$

Rate coefficient and Gibbs free energy can be related using absolute rate theory equation shown in Equation 4 where **k** is Boltzmann constant, Planck constant, h and Gibbs free energy of activation denoted by  $\Delta G^\ddagger$ . Therefore catalyst decreases activation energy of reaction which affects the enthalpy and entropy of activation.

$$k = \frac{kT}{h} e^{(-\Delta G^\ddagger/RT)} \quad \text{Equation 4}$$

Catalytic cycle comprises of reactant, catalyst i.e. active sites, reaction intermediate and product. There are three components present in a typical solid catalyst: catalytic agent, support and promoters or inhibitors. The performance of catalyst can be measured using several key performance indicators such as conversion, activity, selectivity and lifetime. Conversion can be described as the amount of reactant, X, being converted into product shown in Equation 5. Activity of a catalyst can be defined as the rate for conversion of reactants to products under defined conditions and one of the ways to measure activity is using turnover frequency (TOF) shown in Equation 6. Another performance indicator is selectivity which can be defined the amount of desired product being formed from the initial reactant and can be expressed in Equation 7 in which  $s_a$  is the moles of desired product and moles of undesired product denoted by  $s_b$ . Lastly turnover number or TON can be described as the number of reactions that a catalyst can perform before it starts to lose its activity or decay. TON and TOF can be expressed in an equation shown in Equation 8

$$\text{Conversion} = \frac{X_{\text{in}} - X_{\text{out}}}{X_{\text{in}}} \times 100\% \quad \text{Equation 5}$$

$$\text{TOF} = \frac{\text{mol of product}}{\text{Active sites} \times \text{time}} \quad \text{Equation 6}$$

$$\text{Selectivity} = \frac{s_a}{s_a + s_b} \times 100\% \quad \text{Equation 7}$$

$$\text{TON} = \text{TOF} \times \text{lifetime of catalyst} \quad \text{Equation 8}$$

Catalysts have been used in a wide range of application ranging from petrochemical industries, food industries, pharmaceutical, and cosmetics.<sup>85</sup> An ideal catalytic reaction is when catalyst would speed up chemical reaction and having selectivity of 100%, this would have lower reaction times thus increasing productivity and decrease overall capital input as it lowers the activation energy.

Lower catalyst loadings and decreased temperatures are also advantageous.<sup>86</sup> For a catalytic reaction to proceed at a desired rate with higher yield, it should lower the production of unwanted by-products and minimise side reactions. The catalyst should be able to be reused several times without losing its activity either due to poisoning after the first usage. The catalysts must have no uncontrollable hazards and have good resistance to poisons. It must possess high thermal stability as most reactions occur at high temperature hence the possibility of inactivity and degradation will be lowered and most importantly the catalyst should be easily separated at the end of the reaction. This is the reason why heterogeneous catalyst favours over the usage of homogenous catalyst as purification steps are reduced, decreasing the production of waste. There are three combinations in heterogeneous catalyst-reactant phase: liquid/gas, solid/liquid and solid/gas. There is also another important class of catalysis made of polypeptide chains specifically folded for substrate recognition called enzymes.<sup>87</sup> They can be either homogeneous or heterogeneous catalyst depending on their properties.

#### 1.4.1 Heterogeneous catalysis

Heterogeneous catalysis is defined as having the reactants, products and catalysts in different phases.<sup>86</sup> Hence, the substrate and catalyst are separated by a phase boundary for example in the catalytic oxidation of CO on the surface of noble metals for automotive exhaust.<sup>88</sup> Catalysis provides an alternative, low energy, pathway for the reaction to take place, as it lowers the activation energy and thus accelerates the forward and reverse reaction without changing the thermodynamics of the reaction in which the standard enthalpy and standard entropy of the reaction remains the same.<sup>89</sup> Heterogeneous catalysts are mostly inorganic solids, for example, metal oxides, metal sulphides, mixed oxides.<sup>86</sup> They also can be organic materials such as enzymes.<sup>86,90</sup>

Heterogeneous catalysis is associated with the surface adsorption phenomenon.<sup>91</sup> Adsorption is a spontaneous process in which Gibbs free energy is negative. Scheele and Fontana describe adsorption science by carrying out several experiments on the uptake of gases by charcoal and clays in the late 1700s.<sup>91</sup> Heterogeneous catalysis can be described as having active sites on the surface of

the catalyst in which the surface of the catalyst has unsaturated bonds due to termination of bulk structure and expose atoms to surface irregularities. Hence the surface possesses surface energy as a consequence of the presence of free bonds enabling reactions to take place with incoming molecules, this is the driving force for catalyst reactivity.<sup>92</sup> Figure 1-4 illustrates a simple example of the catalytic cycle of CO oxidation on a metal surface.

A solid heterogeneous catalytic reaction goes through the following steps:

1. Diffusion of the reactant (liquid or gas) from the surrounding to the catalyst surface.
2. The reactants bind to the surface of the catalyst. This process is called adsorption; or chemical adsorption.
3. The reactants diffuse on the surface of the catalyst.
4. Then the reactants may dissociate on the surface.
5. Reaction of the adsorbed species on the surface of catalyst and usually the rate determining step.
6. Desorption of the product from the catalyst surface.<sup>93</sup>

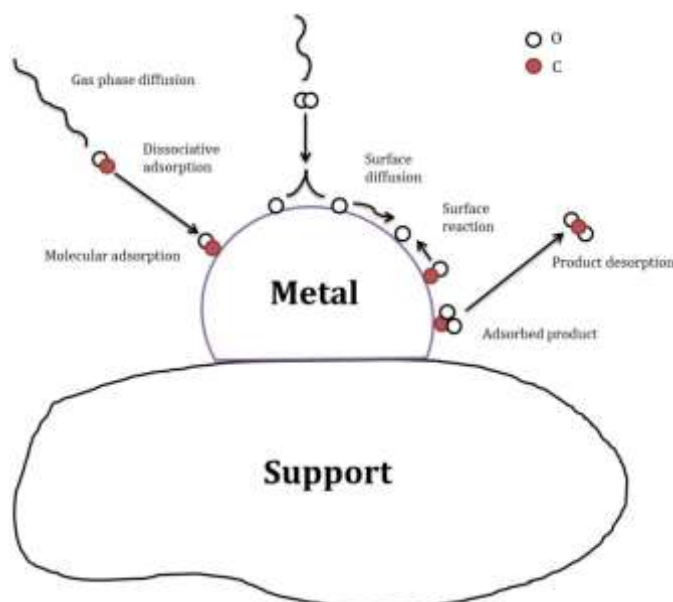


**Figure 1-4: CO oxidation on metal surface<sup>93</sup>**

The process can be depicted using an energy diagram, Figure 1-5. In a non-catalysed gas phase reaction, high energy is required to break and make new bonds and produce high energy gas phase intermediates which can be denoted by  $\Delta E_g$ . Heterogeneous catalyst can stabilise the intermediate by bonding thus lowering its energy.<sup>93</sup>

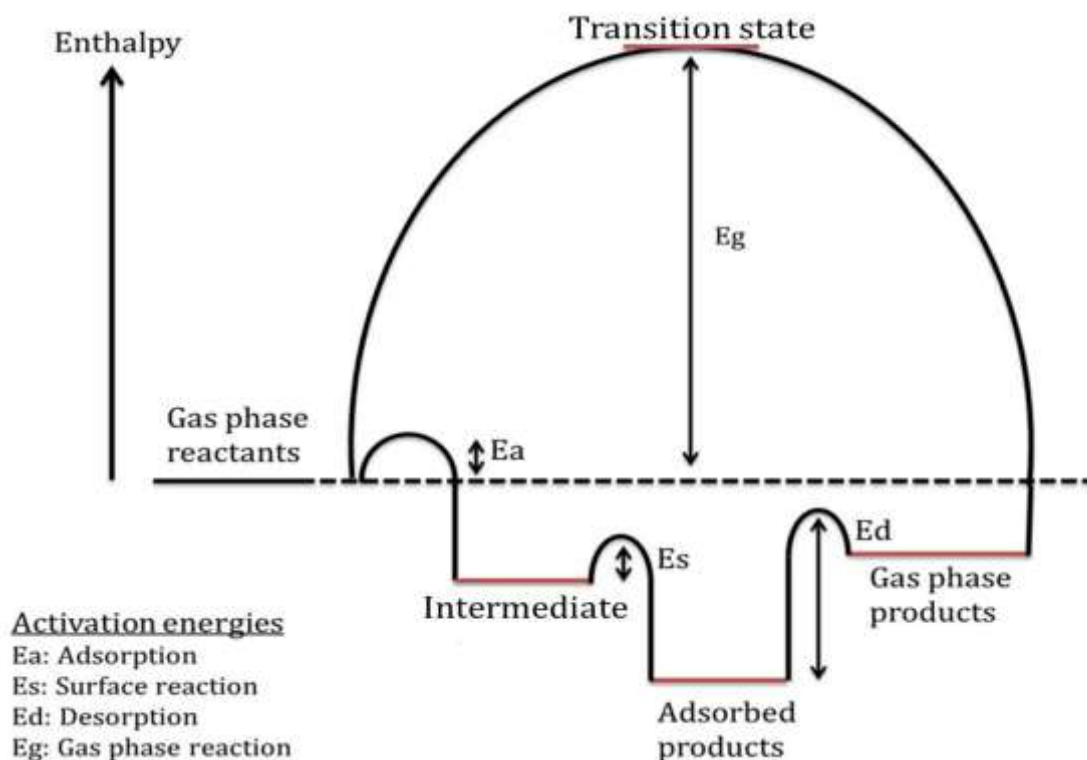


Figure 1-5: Energy diagram of heterogeneous catalytic reaction<sup>93</sup>

#### 1.4.2 Lanthanides

Lanthanides, or rare earth metals, consist of 14 elements which also called f-block elements. These metals commonly have a stable oxidation state of +3 and can also adopt +2 and +4 oxidation states. Previously lanthanides were little used due to difficulty in processing and purifying the materials, however; recent progress in reducing the cost of extracting lanthanides has been advantageous.<sup>94</sup> This has enabled the discovery of many useful chemical properties allowing for the development of these metals in current technologies. Some of the lanthanides metals form an oxide coating when exposed to air by reacting with oxygen. Lanthanides are silvery white metals with high melting and boiling points. They

are strong reducing agent and reacts with  $H_2$  in an exothermic reaction. In this work, two rare earth metals in their oxide form are utilised in the synthesis of carbonates: cerium oxide and lanthanum oxide.

Cerium oxide or ceria ( $CeO_2$ ) is a pale yellow-white material that adopts a cubic fluorite crystal structure which has a wide range of applications and is an interesting material due to its ability to store or release oxygen under redox conditions.<sup>95</sup> It is widely used as catalytic support due to its stability as well high oxygen ion conductivity.<sup>96</sup>  $CeO_2$  is also being applied in electrochemistry as an electrolyte material and in the solid oxide fuel cell (SOFC) due to its high ionic conductivity.<sup>97</sup> Lanthanum oxide ( $La_2O_3$ ) is a white solid having hexagonal crystal structure and is well-known to be a hygroscopic material which can change to lanthanum hydroxide or lanthanum carbonate over time.  $La_2O_3$  is being used in the production of ceramics as well as a semi-conductor material for the production of photoelectrochemical (PEC) cell.<sup>98,99</sup>  $La_2O_3$  is also being used as a catalyst in the degradation of 1,4-butanediol, production of syngas from  $CO_2$  and synthesis of glycerol carbonate from urea.<sup>100,101</sup> There are several methods for producing rare earth oxides such as hydrothermal synthesis or electrochemical deposition that produce structures such as nanorods, nanocubes or nanowires.<sup>102</sup>

There are numerous literatures that investigated the reactivity of ceria and lanthana. Wu *et al* have reported that ceria modified  $MnO_x/TiO_2$  catalysts prepared by sol-gel method was an effective catalyst in the NO reduction with  $NH_3$  at low temperature.<sup>103</sup> 84% NO conversion was reported after doping the catalyst was doped with ceria from 39% at 80°C where 0.07 ratio of Ce to Ti gave the highest conversion compare to 0.2.  $Ce(0.07)MnTi$  has the highest BET surface area of 80  $m^2/g$  compared to the rest of the ratio with pore volume of  $18.10 \times 10^{-2} cm^3/g$ .<sup>103</sup> The increase in doping of ceria shifts the main reduction peak to higher temperature which causes the reduction in activity. However the introduction of Ce improves the oxygen storage capacity thus improves the redox activity of the reaction which indicates that there must be an appropriate amount of Ce to achieve the optimum reactivity.<sup>103</sup>

Transalkylation of propylene carbonate with methanol producing dimethyl carbonate catalysed by gold nanoparticles supported on ceria was reported by Juarez *et al*. They have reported a conversion of 63% using 0.5 wt%  $Au/CeO_2$  with

a yield of 35% and selectivity of 55% to dimethyl carbonate.<sup>104</sup> The catalyst can be used up to four reactions with no leaching of Au from the catalyst. The activity of the catalyst can be linked to oxygen vacancies on the support as well as the presence of positively charged gold species which can interact strongly with CO due to oxygen vacancies in the lattice.<sup>104</sup>

The oxidation of CO was investigated by Zhang *et al* which were catalysed by Au/La<sub>2</sub>O<sub>3</sub>-TiO<sub>2</sub> nanotubes to observe the activity of the catalyst on the reaction. The catalyst was calcined at 300°C with 4.18 wt% Au and 1.62 wt% La gave the highest activity in which CO was fully converted at 30°C. The introduction of lanthanum improves the synergistic effect between the gold species and the support. It also increased the thermal stability of the catalyst as well as improving the reactivity of surface oxygen species of the catalyst.<sup>105</sup> Lanthanum also improves the adsorption of CO onto the Ti<sup>4+</sup> site due to surface oxygen vacancies.<sup>105</sup>

## 1.5 Glycerol

Glycerol is a viscous colourless liquid with a very sweet taste and is classed as a simple polyol with three hydroxyl groups Figure 1-6, which makes it very soluble in water.

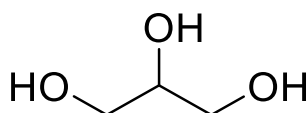
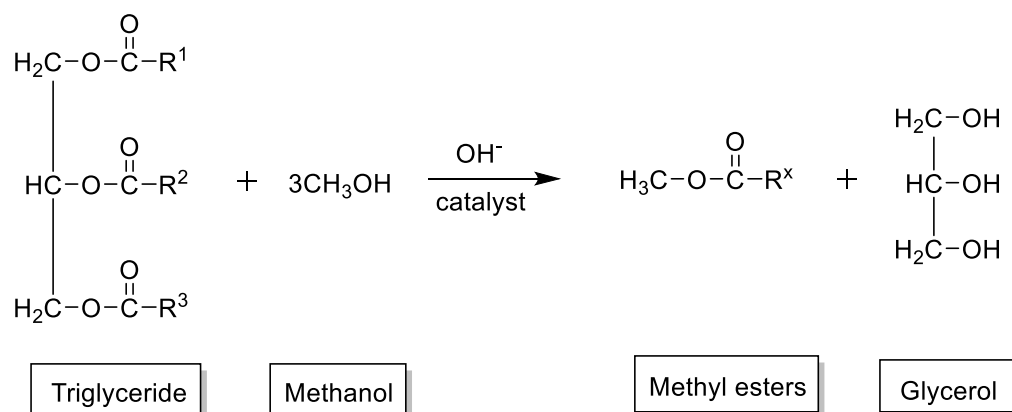


Figure 1-6: The structure of glycerol

Glycerol is produced by saponification and hydrolysis reactions in oleochemical plants that manufacture household and personal care products using plants and animal fats.<sup>106</sup> Predominantly glycerol is produced in the production of biodiesel, which can be manufactured by the transesterification of oil extracted from seeds and recovered waste vegetable/cooking oils as well as animal fats such as tallow. The production of biodiesel can be catalysed by NaOH to produce methyl esters, Scheme 1-10.<sup>107,108</sup> The by-product of the reaction is glycerol, a valuable chemical

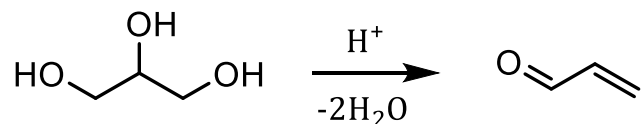


waste. The production of biodiesel, especially in the EU, has increased from 6 Mt to 12 Mt in 2010; this will lead to the surplus production of crude glycerol. For every 10 kg of biodiesel being produced, 1 kg of crude glycerol is formed.<sup>109</sup>



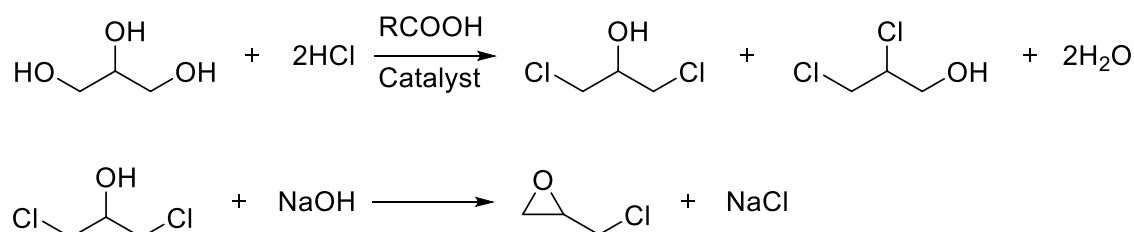
**Scheme 1-10: General mechanism for transesterification of methyl esters<sup>107</sup>**

The huge amount of undesired glycerol produced from biodiesel production has reduced significantly the prices of crude glycerol, whereas purified glycerol is valued much higher at \$0.60-\$0.90/lb compared to the price of crude glycerol which has fallen to \$0.05/lb.<sup>110</sup> This can benefit chemical industries providing cheap feedstock as well as eliminating the disposal costs of glycerol and decreasing the environmental impact of its production. The main question here is how the industries, especially the bio-refineries, can utilise huge amounts of waste glycerol. Glycerol has numerous applications in food as a sweetener in candies, in pharmaceuticals as a lubricant or in skincare, antifreeze, and for extraction of botanical plants and, most importantly, as a chemical intermediate to produce valuable chemicals, such as acrolein or glycerol carbonate.<sup>106</sup> Acrolein can produce acrylic acid esters, superabsorbent polymers and detergents by catalytic dehydration of glycerol using sub- and supercritical water as the reaction media at 360°C and 25 MPa giving a selectivity of 75% acrolein shown in Scheme 1-11.<sup>111</sup>



**Scheme 1-11: Acid-induced dehydration of glycerol to acrolein, T=360°C, P=25 MPa<sup>111</sup>**

There are also examples where glycerol is used as a chemical intermediate in the production of valuable chemicals, such as propylene glycol or conversion to epichlorohydrin.<sup>112</sup> Previously the conventional method to produce epichlorohydrin required multiple steps from propylene and chlorine thus producing a huge amount of unwanted and toxic hydrogen chloride, glycerol was then reacted with hydrogen chloride and catalysed by carboxylic acids.<sup>112</sup> Scheme 1-12 shows the production of epichlorohydrin with glycerol as its starting material at 90°C, 0.5 MPa for 4 h with a yield of 95%.<sup>112,113</sup>



**Scheme 1-12: 2-step process in the production of epichlorohydrin with glycerol as the starting material<sup>112</sup>**

There are numerous research groups looking into applications of crude glycerol as crude glycerol does not have a certain purity for it to be applied in pharmacy or cosmetics, providing applications as a low-cost feedstock.<sup>114</sup> Therefore to functionalised fully crude glycerol with its derivatives is by increasing the additional usage of crude glycerol using a different mode of processes that undergoes a catalytic transformation for example oxidations or hydrogenation.<sup>115</sup> This will lead to the transformation of high value-added products from a highly functionalised molecule. For example in Figure 1-7 below shows glycerol as a

platform chemical to manufacture functionalised chemicals.<sup>116</sup> On the other hand, glycerol could also be directly burned as fuel.

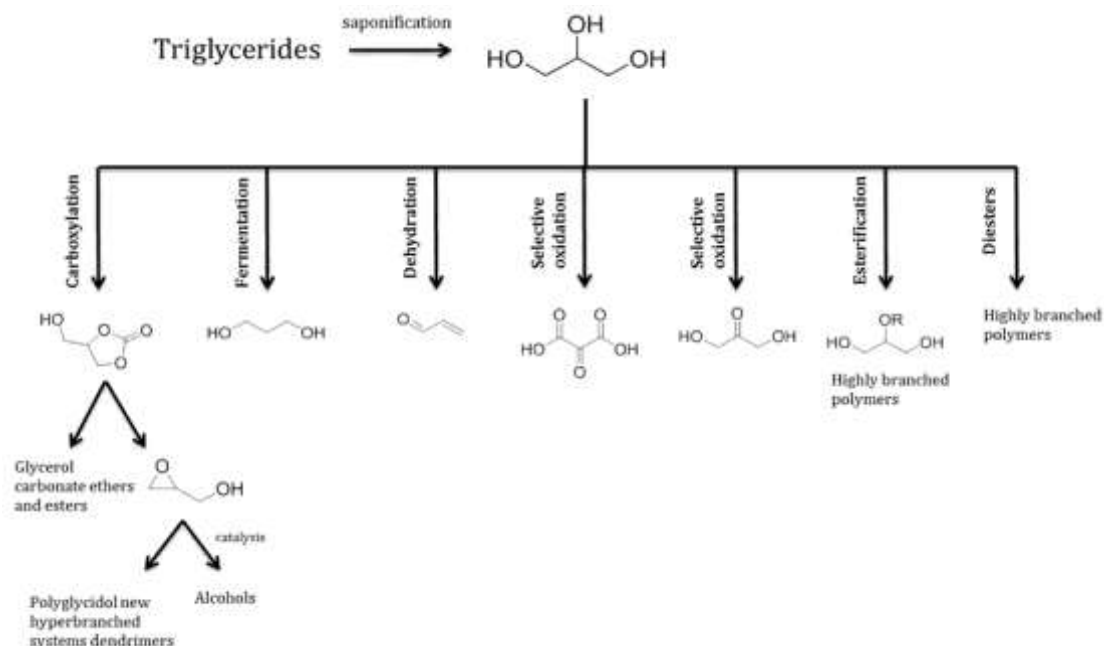


**Figure 1-7: The conversion of glycerol into different functionalised compounds**<sup>115,116</sup>

## 1.6 Glycerol carbonate

Glycerol carbonate is one of the products produced from glycerol. This cyclic carbonate has many important usages in both direct and indirect applications.<sup>117</sup> Glycerol carbonate can be employed as a carrier in pharmaceutical preparations, solid laundry detergent compositions, beauty/personal care, and wetting agent for cosmetics as well as chemical intermediates to synthesise polymers such as polyesters, polycarbonates, hyperbranched polyglycerol, polyurethanes, and non-isocyanate polyurethanes (NIPUs).<sup>118,119,120,121</sup> The use of glycerol carbonate as potential green chemical derivatives is very attractive, thus the development of synthetic procedures to yield glycerol carbonate at its maximum is desirable.<sup>122</sup>

The physical properties of glycerol carbonate are: (a) it is biodegradable, (b) has a low evaporation rate, (c) it is safe to handle (d) it is a non-flammable, water soluble, non-toxic and a slightly viscous compound of 85.4 mPa at room temperature.<sup>123,124,125</sup> Glycerol carbonate can be used in the component in a gas separation membrane as well as a precursor in biomedical applications such as

targeted drug delivery and tissue engineering.<sup>126,127</sup> Recently glycerol carbonate has been employed as a green solvent due to its high boiling point of 354°C for pre-treatment of sugarcane bagasse effectively removing lignin from the bagasse by 84% compared to using another carbonate, ethylene carbonate, which was only 54%.<sup>128</sup> The yield of glucan digestibility was reported to be as high as 90% and glucose yield of 80% when using glycerol carbonate as the solvent compared to ethylene carbonate which only gives 16% glucan digestibility and 15% glucose yield.<sup>128</sup> Glycerol carbonate can replace ionic liquids as it has been used widely as a solvent and catalyst in organic synthesis, for example in the transesterification of linear and cyclic organic carbonates giving high yield and selectivity of carbonates.<sup>129</sup> Ionic liquids are highly polar and non-coordinating materials which are suitable for catalytic reactions and their properties such as volatility or miscibility can be modified to suit specific chemical reactions.<sup>130</sup> There are concern in the usage of ionic liquids specially toxicological properties and biodegradability, as well as high cost thus making these less desirable compared to glycerol carbonate.<sup>130</sup>

The favourable properties and range of chemicals produced from glycerol carbonate are due to the fact that glycerol carbonate has several reactive sites that undergo electrophilic and nucleophilic attack on its 3-carbon atom on dioxolane ring and pendant hydroxyl moiety respectively in which glycerol carbonate can act as an intermediate or reactant by reacting with aromatic amines, alcohols, thiols and carboxylic acid producing useful compounds that are used in surfactants, plasticizer, cross-linking agents and curing agent.<sup>118,131</sup> Figure 1-8 shows some application of glycerol carbonate.

Currently there is no account on the global market for glycerol carbonate as the chemical has been introduced recently in the chemical industry. However there is an article published by Global Market Insight Inc. on November 9<sup>th</sup> 2016 in which the global market for dimethyl carbonates is estimated to worth USD 738.3 million by 2024 due to increase in production of polycarbonate industries as well as automotive and electronics industries. Therefore glycerol carbonate could potentially surpass the current market for dimethyl carbonate as it is more environmentally friendly compound with numerous potential applications which were mentioned above.

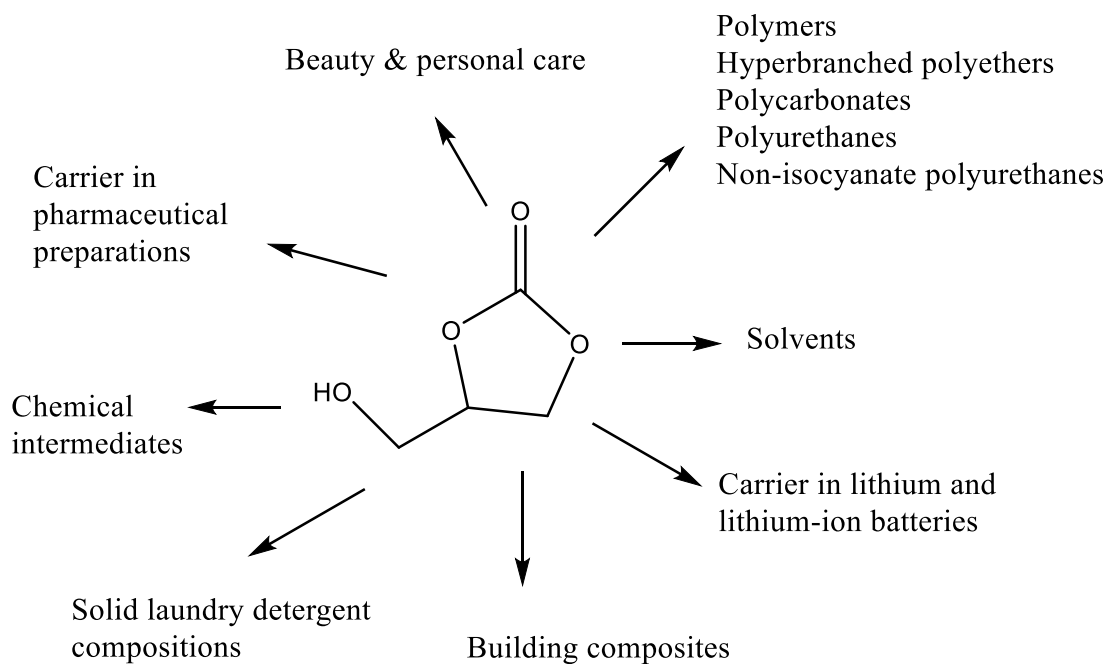


**Figure 1-8: Applications of glycerol carbonate<sup>118</sup>**

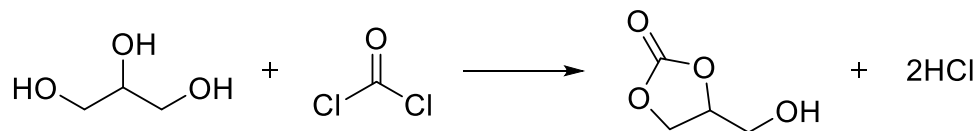
### 1.6.1 Synthesis of glycerol carbonate

The synthetic routes in the production of glycerol carbonate can be classified into four categories:<sup>132</sup>

- 1) The reaction of glycerol with phosgene.<sup>133</sup>
- 2) The transesterification with other carbonates.<sup>134</sup>
- 3) Direct carbonylation with CO<sub>2</sub>.<sup>135</sup>
- 4) The glycerolysis of urea.<sup>132</sup>

#### 1.6.1.1 Phosgenation method

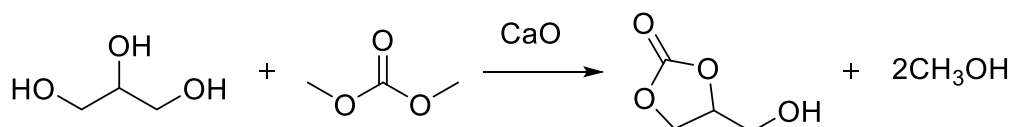
The first reported reaction of glycerol carbonate was with liquid phosgene which is toxic. The reaction produced high yields of glycerol carbonate at mild reaction conditions i.e. 30°C for 6 h without the use of a catalyst. Unfortunately, this reaction generated toxic waste, HCl shown in Scheme 1-13.<sup>136</sup> The atom economy for this reaction is 62%.



**Scheme 1-13: Synthesis of glycerol carbonate from phosgene. T=30°C, 6 h<sup>136</sup>**

#### 1.6.1.2 Transesterification with acyclic carbonates

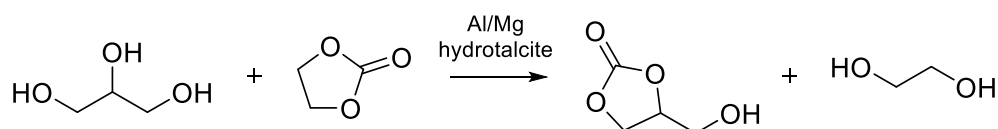
Transesterification of glycerol to glycerol carbonate using acyclic carbonates have been studied extensively as it is a simple and environmentally benign reaction. Glycerol carbonate can be prepared from two types of carbonate source: alkylene carbonate or dialkyl carbonate under mild reaction conditions. A wide range of heterogeneous catalysts has been reported to produce high yields of glycerol carbonate. Heterogeneous base catalysts favour transesterification of glycerol to glycerol carbonate over heterogeneous acid catalysts due to the hydrophobic surface of the resins slows down the diffusion of hydrophilic reactants in this case glycerol thus limits mass transport of the carbonate source.<sup>137</sup> Catalysts such as CaO, MgO, mixed oxides, hydrotalcite, and basic zeolites have been employed in the transesterification reaction. A yield of 94% and 99.7% selectivity to glycerol carbonate was achieved by Simanjuntak *et al* when utilising CaO as catalyst at 75°C for 30 min with dimethyl carbonate/glycerol molar ratio=2 shown in Scheme 1-14 and the atom economy of the reaction is 65%.<sup>138</sup> The basic strength of the heterogeneous catalyst must be strong enough to abstract a proton from the primary hydroxyl group of glycerol.<sup>134</sup> This can be easily achieved by homogenous catalysts producing glyceroxide anion as there are no mass transport limitations from the bulk solution to the active sites.<sup>134</sup> However recycling of the catalyst reduced the activity significantly as the basic catalyst converted into calcium carbonate, a low strength basic catalyst.<sup>139</sup> The reaction produced methanol which could be recycled and used to synthesise dimethyl carbonate.



**Scheme 1-14: Synthesis of glycerol carbonate from dimethyl carbonate. T=75°C, 30 min, molar ratio of 2<sup>138</sup>**

### 1.6.1.3 Transesterification of cyclic carbonates

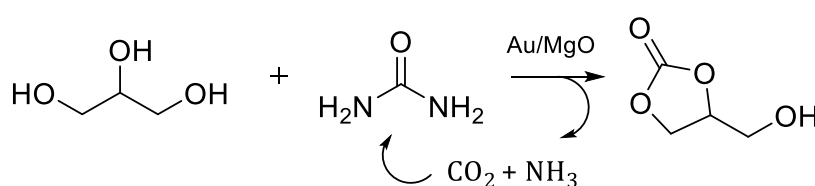
Alkylene carbonates such as ethylene carbonate have been used as a carbonate source and its physical properties make it an attractive choice in the transesterification reaction shown in Scheme 1-15. Hydrotalcites have been used as catalyst instead of an alkaline base for example sodium bicarbonate due to the required additional neutralisation step which produces excess salts at the end of the reaction.<sup>140</sup> Al/Mg hydrotalcite is an active catalyst in the transesterification of glycerol and ethylene carbonate which was reported by Climent *et al.*<sup>140</sup> The reaction was performed under inert atmosphere for 5 h at 50°C using 7 wt% of catalyst and molar ratio of 2. The conversion of glycerol was 85% with glycerol carbonate yield of 82% where the atom economy is 66%. This is due to the strength of basic sites of Al/Mg hydrotalcite. The strength of the basic sites is comparable to MgO which has similar activity but the selectivity to glycerol carbonate is lower for MgO than Al/Mg hydrotalcite. MgO is likely to produce glycidol as one of the by-products of the reaction.<sup>140</sup> The reaction can be improved by substituting Mg with Li or Ca. This increases the basicity as the density of negative charge on the oxygen increases due to more electropositive ions. There was an increase in conversion by 4% and glycerol carbonate yield was 87%. The reactions were operated at a lower temperature of 35°C using only 0.5 wt% of the catalyst under 1 h and no glycidol was being observed in the reaction.



**Scheme 1-15: Synthesis of glycerol carbonate from ethylene carbonate. T=50°C, 5 h, molar ratio of 2<sup>140</sup>**

#### 1.6.1.4 Glycerolysis of urea

Another alternative route to produce glycerol carbonate is by transcarbonation of glycerol with urea. Urea is an attractive carbonate source which is inexpensive and readily available. Urea can be considered as an activated form of CO<sub>2</sub> and as indirect route for carbon dioxide utilisation.<sup>141</sup> The overall reaction is a very simple process that operates without the usage of solvent producing high conversion and yield under moderate reaction conditions in which the atom economy is 78%.<sup>141</sup> The by-product of the reaction is ammonia which can be recycled and reacts with CO<sub>2</sub> to produce urea especially in industrial process using Bosch-Meiser urea process, Scheme 1-16.<sup>141,142</sup> Ammonia can be removed easily in two ways either by flowing through dry nitrogen into the reaction mixture and under vacuum, this will shift the equilibrium to the product side.<sup>140,141</sup>



**Scheme 1-16: Synthesis of glycerol carbonate from urea. T=150°C, 4 h, molar ratio=1.5<sup>141</sup>**

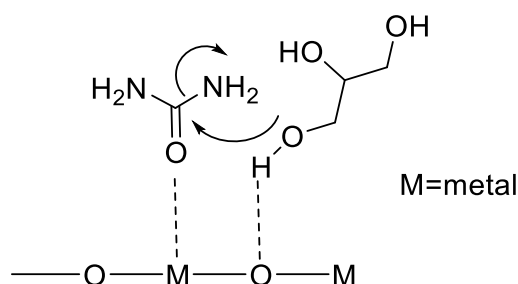
Woo *et al* have reported using ZnSO<sub>4</sub> as a homogeneous catalyst in the synthesis of glycerol carbonate from urea producing a high yield of 86% at 140°C for 2 h with a reduced pressure of 40 mbar.<sup>143</sup>

Co<sub>3</sub>O<sub>4</sub> nanoparticles highly dispersed on ZnO microparticles have been used as a catalyst by using dry nanodispersion process shows higher catalytic activity compared to Co<sub>3</sub>O<sub>4</sub>/ZnO catalyst being preheated at 500°C.<sup>144</sup> Dry nanodispersion process showed high catalytic activity as the process creates new reactive surface with high dispersion of Co<sub>3</sub>O<sub>4</sub>. Glycerol carbonate yield was reported to reach up to 69% with 97% selectivity.<sup>144</sup>

Climent *et al* reported ZnO as catalyst in the carbonylation with urea. They proposed that the carbonyl group can be activated by Lewis acid then subsequent



nucleophilic attack from the hydroxyl group of glycerol absorbed on the Lewis basic site occurs shown on Scheme 1-17.<sup>140</sup>



**Scheme 1-17: Acid-base properties<sup>140</sup>**

By introducing hydrotalcite compounds into ZnO, the basicity of the catalyst was increased while maintaining the strength of Lewis acid sites, the glycerol carbonate yield increased from 60% to 72% and the selectivity increased from 75% to 88%. The activity decreased by introducing Li into the hydrotalcite thus increasing its basicity. Therefore there must be a balance in the strength of acid-basic properties as strong Lewis acid or basic sites stimulate polymerisation reaction.<sup>140</sup>

Gold nanoparticles have been used in the synthesis of glycerol carbonate supported on different types of metal oxide and MgO was the most active and was prepared by impregnation method.<sup>141</sup> Hammond *et al* have reported 80% conversion of glycerol and yield of 56% glycerol carbonate was achieved using 2.5 wt% Au/MgO at 150°C with glycerol/urea molar ratio = 1.5 for 4 h. Gallium and zinc were also being used in the reaction due to their ability to act as a Lewis acid but gold showed the highest activity.<sup>141</sup>

La<sub>2</sub>O<sub>3</sub> has been tested by Wang *et al* in the carbonylation of glycerol with urea and showed high activity compared to other rare earth oxide such as CeO<sub>2</sub>, Y<sub>2</sub>O<sub>3</sub>, Pr<sub>2</sub>O<sub>3</sub>, Nd<sub>2</sub>O<sub>3</sub>, Sm<sub>2</sub>O<sub>3</sub>, Eu<sub>2</sub>O<sub>3</sub>.<sup>101</sup> La<sub>2</sub>O<sub>3</sub> catalysts were treated at different calcination temperatures from 400°C to 800°C which affected its texture and basicity. La<sub>2</sub>O<sub>3</sub> that undergoes heat treatment at 600°C exhibited high catalytic activity. This is due to the presence of high amounts of La<sub>2</sub>O<sub>2</sub>CO<sub>3</sub> phase in La<sub>2</sub>O<sub>3</sub>-600°C compared to the other La<sub>2</sub>O<sub>3</sub> catalysts being used. This was demonstrated by CO<sub>2</sub>-TPD and XRD

analysis. Commercial  $\text{La}_2\text{O}_3$  showed decreased activity due to the catalyst having strong basic sites thus blocking the active sites which indicate a strong interaction between the reactants and the catalyst with no indication on the presence of  $\text{La}_2\text{O}_2\text{CO}_3$  phase. Therefore  $\text{La}_2\text{O}_2\text{CO}_3$  has the ability to influence the content of strong basic sites.<sup>101</sup> The yield of glycerol carbonate was 91% having a selectivity of 98% when using  $\text{La}_2\text{O}_3$ -600°C.

The performance of  $\text{LaCl}_3$  was investigated in the carbonylation of glycerol with urea producing glycerol carbonate. Wang *et al* have reported that they achieved 95% glycerol conversion with 99% selectivity to glycerol carbonate at 150°C for 3 h. They reported that 2,3 dihydroxypropyl carbamate forms a coordination complex with  $\text{LaCl}_3$  where three molecules of 2,3 dihydroxypropyl carbamate interact with  $\text{La}^{3+}$ .<sup>145</sup>

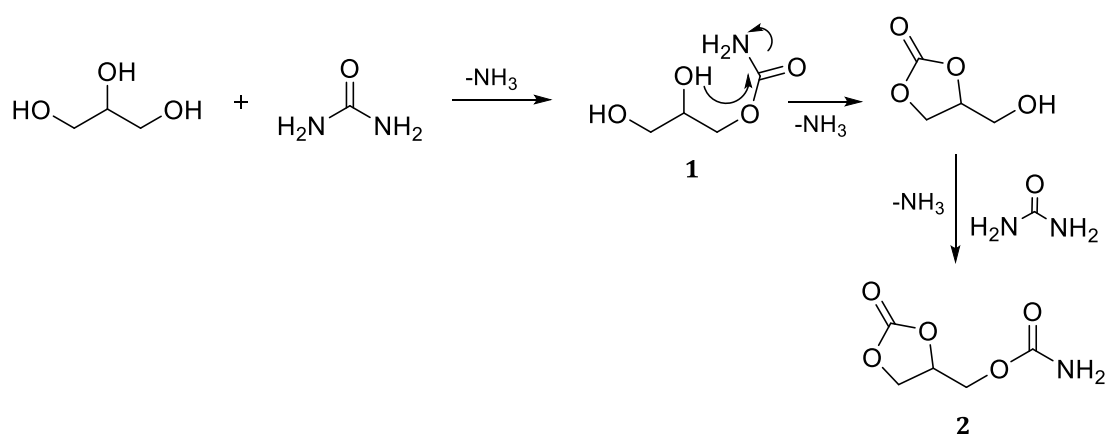
The performance of lanthanum based mixed oxides were studied by Zhang *et al* and they have found that  $\text{La}_2\text{CuO}_4$  shows the highest activity in the synthesis of glycerol carbonate. The introduction of Fe into the mixed oxides which was calcined at 950°C improved the overall activity with the glycerol conversion of 49% and selectivity of 82% to glycerol carbonate at 150°C for 4 h.<sup>146</sup>

Supported Au-Pd nanoparticles on MgO synthesised by sol immobilisation technique have shown to be an active catalyst in the synthesis of glycerol carbonate compare to using Au/MgO and Pd/MgO.<sup>147</sup> Rahim *et al* have reported that the bimetallic nanoparticles have achieved a conversion of 87% with a glycerol carbonate yield of 67% for 4 h at 150°C with continuous flow of nitrogen.<sup>147</sup> The high activity is due to the high dispersion of the active metals and the synergistic effect of combining the two metals together.<sup>147</sup>

MCM-41 or  $\text{SiO}_2$  is well-known material with high surface area and has been used as an efficient catalyst to produce glycerol carbonate. Transition metals such as Cu, Ni and Zn have been loaded on MCM-41 by impregnation method and Zn gave the highest activity at 145°C for 5 h reaction. This effect can be attributed to the balance of acid and basic sites as well as the high dispersion of the metal onto the mesoporous framework of the support giving 75% conversion and 98% selectivity.<sup>148</sup>  $\text{WO}_3$  supported on  $\text{TiO}_2$  catalysts was tested to the carbonylation reaction, 15 wt% loading of  $\text{WO}_3$  gave the highest activity.<sup>149</sup> The highly dispersed

catalyst was calcined at 500°C giving 73% conversion of glycerol and 100% selectivity at 140°C for 4 h under reduced pressure. The high activity is due to the presence of many acid sites at 15 wt%. Above 15 wt% the acid sites started to decrease due to aggregation of WO<sub>3</sub>. The activity of the catalyst was reduced slowly after several usages. The activity reduced to 66.2% after the third cycle.<sup>149</sup>

Scheme 1-18 shows the reaction mechanism between glycerol and urea. The reaction takes place in two consecutive steps. The first step is the nucleophilic attack of the hydroxyl group on the electrophilic carbon of the carbonyl group producing glycerol carbamate (**1**) releasing one molecule of ammonia.<sup>150</sup> The secondary hydroxyl group of glycerol carbamate then attacks the carbamate releasing a second molecule of ammonia thus forming five-membered ring carbonate. Further reaction between urea and glycerol carbonate will generate compound **2**.



**Scheme 1-18: Reaction mechanism in the formation of carbonate from urea<sup>150</sup>**

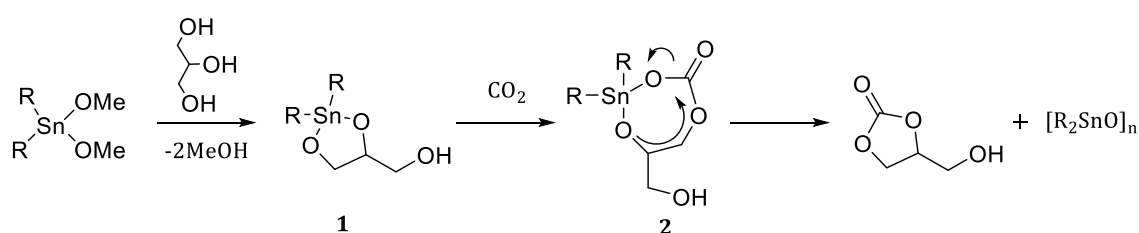
#### 1.6.1.5 Direct carbonylation with carbon dioxide

In direct carbonylation with CO<sub>2</sub> with glycerol, two cheap raw materials are converted into value-added chemicals producing water as by-product with atom utilisation of 87% which is higher than other method of producing glycerol carbonate.<sup>5,132</sup> This is a very attractive reaction as CO<sub>2</sub> is a non-toxic, non-flammable and inexpensive source of carbon.<sup>72</sup> However the carbonylation of

glycerol to glycerol carbonate reaction is thermodynamically limited due to the formation of water but this can be overcome by using suitable dehydrating agents such as molecular sieves which can be regenerated by heat or orthoesters to remove water.<sup>38</sup> Another way is by pressurising CO<sub>2</sub> therefore shifting the equilibrium to the product side and developing effective catalysts for the reaction.<sup>38,72,74</sup>

The direct insertion of CO<sub>2</sub> to glycerol has only been reported in less than 20 journals indicating that the reaction is quite challenging. The first reported reaction for synthesising glycerol carbonate from glycerol and CO<sub>2</sub> using Amberlyst and zeolite in supercritical CO<sub>2</sub> was by Vieville *et al*, but no product was formed. However by adding ethylene carbonate, the yield of glycerol carbonate was 32% and suggesting that CO<sub>2</sub> alone is not a carbonate source for the reaction.<sup>151</sup>

Aresta *et al* reported that tin complexes mainly Bu<sub>2</sub>Sn(OCH<sub>3</sub>)<sub>2</sub> have the ability to catalyse the direct carbonylation of glycerol into glycerol carbonate under solvent free conditions.<sup>135</sup> Tin complexes were used as a homogenous catalyst with tin-glycerol complex as intermediate. The reaction was performed at 180°C at 5 MPa CO<sub>2</sub> for 15 h giving a yield of 6% glycerol carbonate. They proposed a reaction mechanism where the tin catalyst reacts with glycerol producing tin-glycerol complex (**1**) releasing methanol. CO<sub>2</sub> inserts into complex **1** at high temperature followed by elimination of Sn catalyst and producing five-membered ring glycerol carbonate shown in Scheme 1-19.<sup>135</sup>

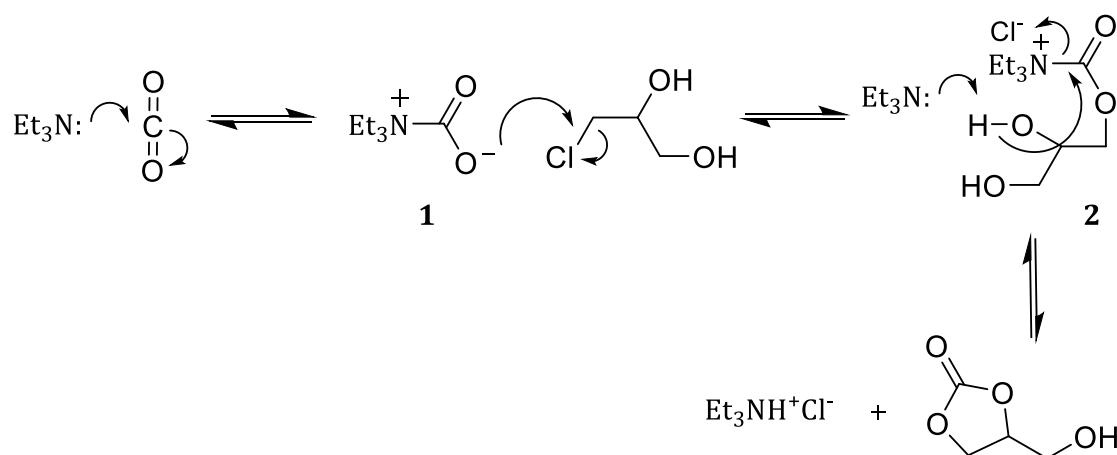


**Scheme 1-19: Reaction mechanism in the formation of glycerol carbonate from tin-glycerol complex. T=180°C, P=5 MPa, 15 h<sup>135</sup>**

Methanol was used as a solvent to assist dibutyltin(IV)oxide in catalysing the direct carbonylation reaction. A yield of 35% of glycerol carbonate was achieved under 4 h at 80°C and 3.5 MPa CO<sub>2</sub>. George *et al* reported that dimethyl carbonate was not present in the reaction.<sup>152</sup> The reaction conditions were significantly lowered compared what was being reported by Aresta *et al* and they reported that the reaction is 100% selective. Methanol acts as a solvent to increase the solubility of CO<sub>2</sub> into glycerol hence the reaction mixture dissolved homogenously. According to their findings, methanol activated the catalyst forming tin-methanol complex and it followed the same reaction pathway reported by Aresta *et al*.<sup>152</sup>

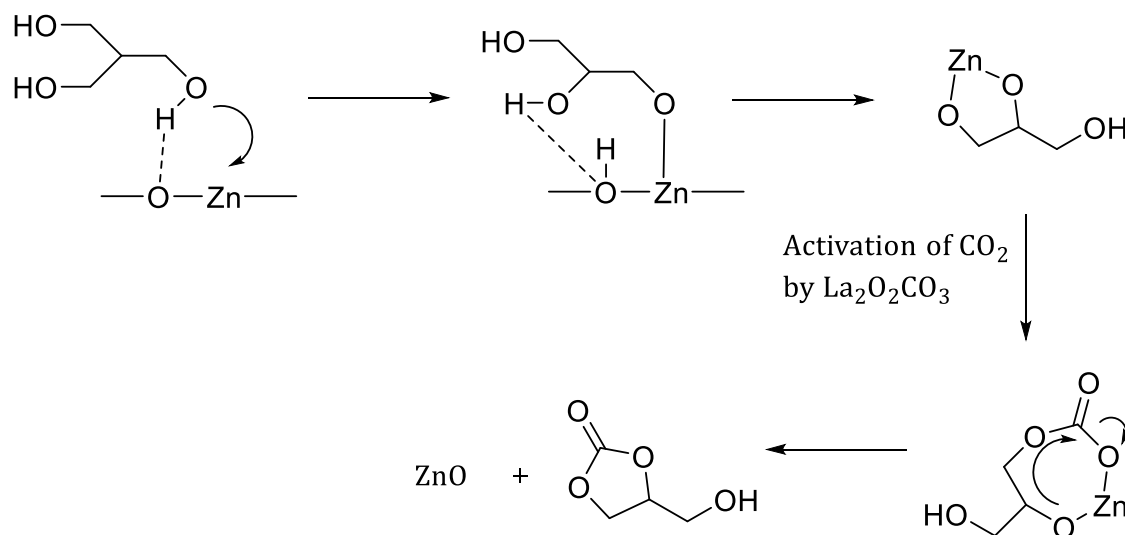
Tetra (ethylene glycol) dimethyl ether (TEGDME) was employed as solvent in the direct carbonylation of glycerol with CeO<sub>2</sub>/Al<sub>2</sub>O<sub>3</sub> as heterogeneous catalyst. Glycerol carbonate was only observed when the temperature was 180°C with a pressure of 5 MPa of CO<sub>2</sub> for 15 h. The reported yield was 2.5% which was lower than using tin catalysts.<sup>132</sup>

Another approach was to employ triethylamine for CO<sub>2</sub> activation as well as solvent giving a high yield of glycerol carbonate from a glycerol derivative, 3-chloro-1,2-propanediol with an atom economy of 46%.<sup>153</sup> They reported 100% conversion of 3-chloro-1,2-propanediol with 90% glycerol carbonate yield under 1 h with a pressure of 2.5 MPa of CO<sub>2</sub> at 100°C.<sup>153</sup> Zwitterionic adduct (**1**) is formed from the activation of CO<sub>2</sub> by triethylamine and undergoes nucleophilic attack on the electrophilic carbon bonded with chlorine to form intermediate (**2**). Five-membered ring carbonate is formed by the abstraction of hydrogen by triethylamine to produce alkoxide ion which then has the ability to attack carbonyl carbon and releasing triethylamine hydrochloride.<sup>153</sup> Intermediate (**2**) undergoes nucleophilic attack to form glycerol carbonate shown in Scheme 1-20. It also can undergo nucleophilic attack to form the compound glycidol.



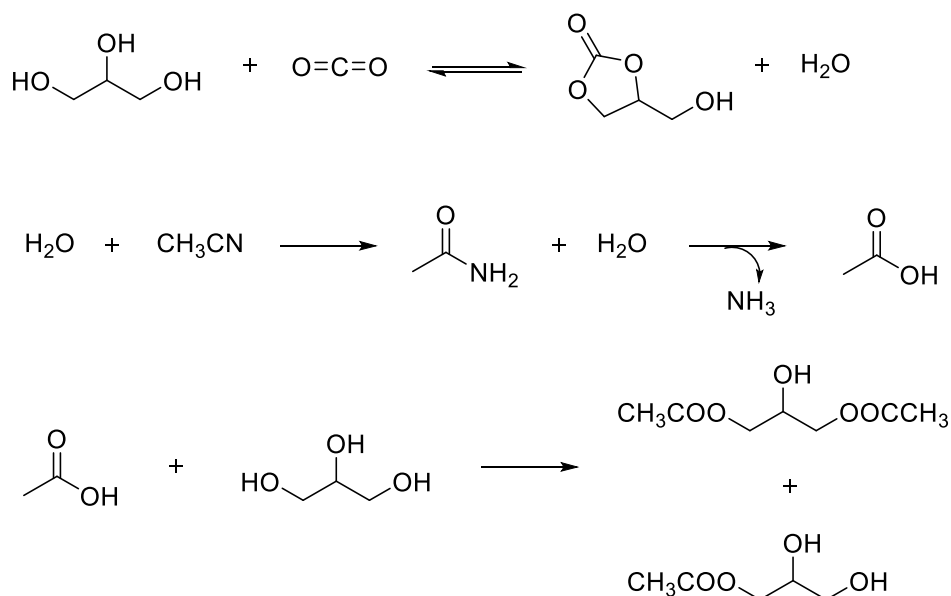
**Scheme 1-20: Formation of zwitterionic adducts to form glycerol carbonate. T=100°C, P=2.5 MPa, 1 h<sup>153</sup>**

Li *et al* have reported using La-Zn oxides in the synthesis of glycerol carbonate from CO<sub>2</sub>.<sup>154</sup> La-Zn mixed oxides were subjected to different calcination temperatures and the temperature of 500°C resulted in the formation of La<sub>2</sub>O<sub>2</sub>CO<sub>3</sub> improved the overall activity.<sup>154</sup> This is due to the amount of medium basic sites present on the catalyst in which CO<sub>2</sub> adsorption takes place and is activated. Medium basic sites also provide active sites for acetonitrile hydrolysis.<sup>154</sup> Increasing the amount of La content would increase the basic sites but that would result in the decrease of ZnO and ZnO has the ability to activate glycerol to form zinc glycerolate, which was confirmed by FTIR. However, this can be balanced by electron transfer from zinc ions to lanthanum ions due to the formation of La<sub>2</sub>O<sub>2</sub>CO<sub>3</sub>. This improves the activation of glycerol and promotes the dispersion of ZnO.<sup>154</sup> Recently, acetonitrile has been utilised as the dehydrating agent and the yield of glycerol carbonate increased drastically to 15% with the glycerol conversion of 30%. The hydrolysis of acetonitrile leads to the formation of monoacetin and diacetin which lowered the selectivity of glycerol carbonate. The reaction was performed at 170°C at a pressure of 7.0 MPa for 12 h. Scheme 1-21 shows the activation of glycerol and CO<sub>2</sub> by ZnO and La<sub>2</sub>O<sub>2</sub>CO<sub>3</sub> respectively.<sup>154</sup>



**Scheme 1-21: Activation of glycerol and CO<sub>2</sub> by ZnO and La<sub>2</sub>O<sub>2</sub>CO<sub>3</sub> respectively. T=170°C, P=7.0 MPa, 12 h<sup>154</sup>**

Another reaction that utilised acetonitrile in the direct synthesis of glycerol carbonate was employing Cu/La<sub>2</sub>O<sub>3</sub> as heterogeneous catalyst which was reported by Zhang *et al.*<sup>155</sup> The physical and chemical properties of Cu/La<sub>2</sub>O<sub>3</sub> were investigated to evaluate its performance. The support was prepared by hydrothermal method with impregnation of metal salts into the support. Different Cu loadings were tested at 150°C with a pressure of 7.0 MPa for 12 h and 2.3 wt% Cu/La<sub>2</sub>O<sub>3</sub> gave the best result.<sup>155</sup> At higher loadings of copper, the performance decreased due to basic sites being covered by copper particles. The basic sites of the La<sub>2</sub>O<sub>3</sub> were tested by CO<sub>2</sub>-TPD and medium basic sites were responsible for the overall catalytic performance of the catalyst which caused by bidentate carbonates adsorbed on La<sup>3+</sup>-O<sup>2-</sup> pairs and it was the site for glycerol adsorption which will then be dissociated.<sup>155</sup> They reported that CO<sub>2</sub> was being activated by copper metal forming a Cu-O-CO-L complex. Scheme 1-22 shows the reaction mechanism of direct carbonylation of glycerol in the presence of acetonitrile. Acetonitrile is being hydrolysed to form acetamide and further reacts with water to form acetic acid. Esterification reaction occurs between glycerol and acetic acid forming monoacetin and diacetin. The two by-products are used in making smokeless powder, explosives and food additives.<sup>155</sup>



**Scheme 1-22: Reaction mechanism in the direct carbonylation of glycerol in the presence of acetonitrile. T=150°C, P=7.0 MPa, 12 h<sup>155</sup>**

Acetonitrile was also employed as a dehydrating agent in the direct carbonylation reaction with La modified Zn-Al hydrotalcite as the catalyst.<sup>156</sup> Halogen anions were incorporated into the mixed oxides which improved the surface area as there is an increase in the amount of open porous networks after it undergoes heat treatment. This increased the amount of exposed active sites and Br<sup>-</sup> anions have the highest surface area compared to Cl<sup>-</sup> and F<sup>-</sup>.<sup>156</sup> The formation of La<sub>2</sub>O<sub>2</sub>CO<sub>3</sub> improved the basicity of the catalyst; however, the introduction of halogen anions decreased the amount of basic sites and did not affect the surface area of the catalyst. Li *et al* have reported that halogen anions have an effect in the catalytic activities not the amount of medium basic sites present in the catalyst as glycerol can be activated by halogen anions and improve the catalytic activities.<sup>156,157</sup> Cl<sup>-</sup> anions have the highest catalytic performance with conversion of 36% and glycerol carbonate yield of 16% at 170°C with a pressure of 7.0 MPa for 12 h.<sup>156</sup>



#### 1.6.1.5.1 Dehydration methods

Direct synthesis of organic carbonates from CO<sub>2</sub> and alcohol is highly desirable as the only by-product of the reaction is water. However water has the ability to hydrolyse the carbonate, thus shifting the equilibrium towards the opposite side.<sup>158</sup> Therefore, there is a need to find effective dehydrating agents thus breaking the thermodynamic limitations and generating high yield of carbonates. There are two types of dehydrating system being reported in the literature: non-reactive dehydration system and reactive dehydration system

Non-reactive dehydration system uses non-reactive materials that can absorb water without reacting with the substrates and can be divided into three: gas phase systems, membrane separation systems and inorganic absorbents.<sup>158</sup> For example, molecular sieves 3Å have been used to absorb water without producing any by-products and molecular sieves are easily recyclable. Methanol was used as a substrate and the yield of dimethyl carbonate obtained was 50% after 72 h at 180°C and 30 MPa.<sup>77</sup> However, the reaction requires complex setup shown on Figure 1-9. In this system, molecular sieves are placed in a different reactor at room temperature and a circulation pump was used to pump the heated reaction mixture into the dehydrating reactor. No DMC was observed when molecular sieves were not used in the reaction which indicates the reaction is thermodynamically controlled.<sup>77</sup> The catalyst being employed in this reaction was dibutyltin dimethoxide.

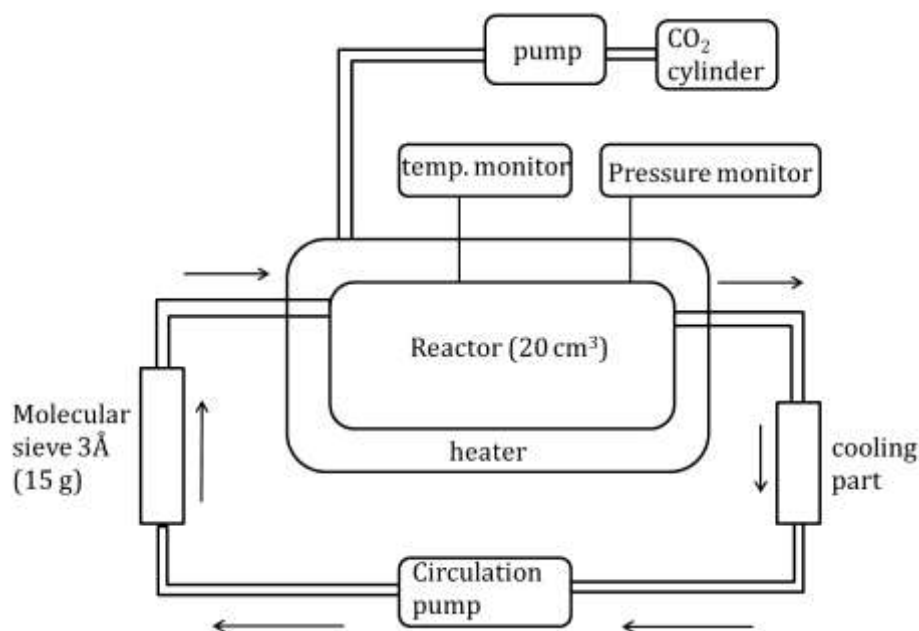
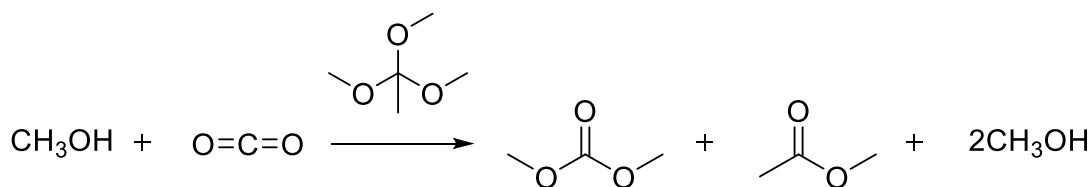


**Figure 1-9: High pressure reactor in the presence of molecular sieves. T=180C, P=30 MPa, 72 h.<sup>77</sup>**

However, dehydration using molecular sieves in a one pot system can be quite challenging as the mechanism of dehydration is by physical adsorption at high pressure and temperature. Therefore reactive dehydration system is used in the direct reaction with carbon dioxide.<sup>158</sup> Reactive dehydration can be divided into two: non-catalytic reactive dehydration systems and catalytic reactive dehydration systems.

Orthoesters can be used as non-catalytic reactive dehydration system. Orthoesters contains three alkoxy groups attached to one carbon which can be used in hydrolysis, Johnson-Claisen rearrangement as well as a protecting group.<sup>159,160</sup> It has been reported that orthoesters produce the highest yield of dimethyl carbonate from methanol and carbon dioxide. In this reaction, trimethyl orthoacetate was used as the dehydrating agent in which it reacts with water to produce two molecules of methanol and one molecule of methyl acetate shown in Scheme 1-23.<sup>38</sup> The atom economy of the reaction is 46%.



**Scheme 1-23: Reaction of methanol and CO<sub>2</sub> in the presence of orthoesters. T=180°C, P=30 MPa, 24 h<sup>38</sup>**

Another way of removing water is by dehydrating the substrate methanol into its dehydrating derivatives such as dimethyl ether and trimethyl orthoester and the dehydrating derivatives were reacted with carbon dioxide producing DMC.<sup>161</sup> The reaction produced 20% yield of dimethyl carbonate with 93% selectivity at 180°C, 30 MPa in the presence of dimethyltin dimethoxide catalyst.<sup>161</sup> However this reaction is not sustainable as orthoesters are generally expensive and regenerating orthoesters from ester and alcohols is difficult.<sup>38</sup>

Therefore, catalytically reactive dehydration systems are attractive as it gives high carbonate yield which has been studied extensively by Honda *et al.*<sup>158</sup> In this reaction the catalyst, CeO<sub>2</sub> has the ability to catalyse both the formation of carbonates from the alcohol and hydration of dehydration reagents which is illustrated in Figure 1-10.<sup>158</sup> Acetonitrile was used as dehydration reagent in direct carbonylation of methanol and the yield produced was 8.9% with selectivity of 65% at pressure of 0.5 MPa. Scheme 1-24 shows direct carbonylation of methanol using acetonitrile as the dehydrating agent at 150°C for 48 h. The low selectivity of the reaction is due to the reaction of water with acetonitrile producing acetamide. The amide then reacts with methanol to produce methyl acetate and ammonia. Ammonia then reacts with dimethyl carbonate producing methyl carbamate.<sup>158</sup>

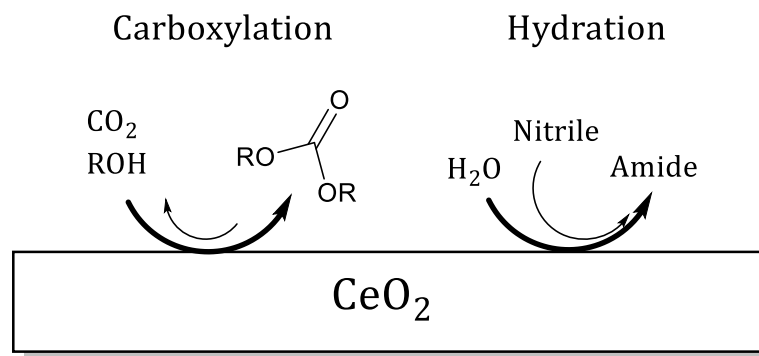
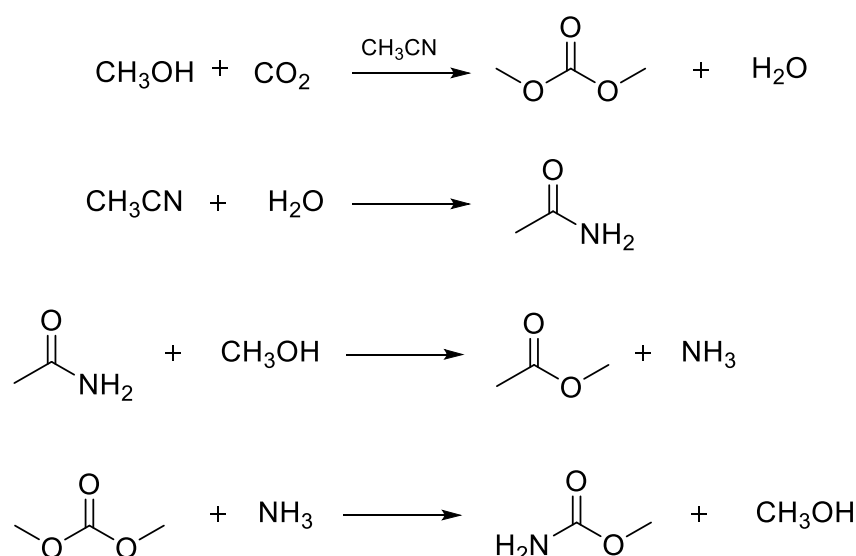


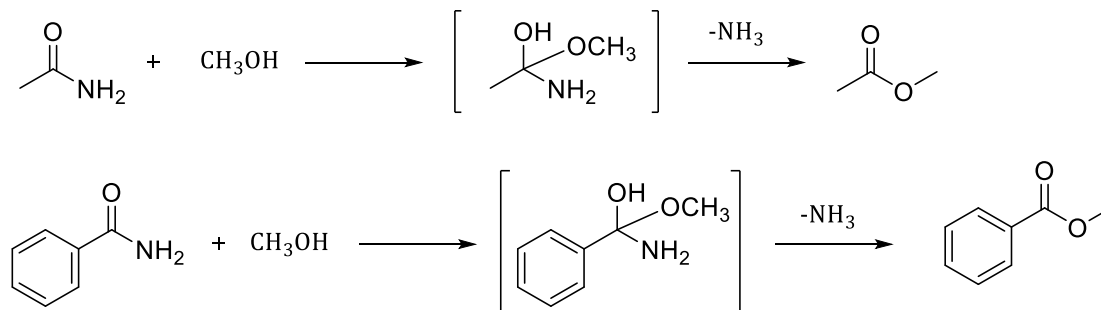
**Figure 1-10: Formation of carbonate and nitrile hydration catalyse by  $\text{CeO}_2$** <sup>158</sup>



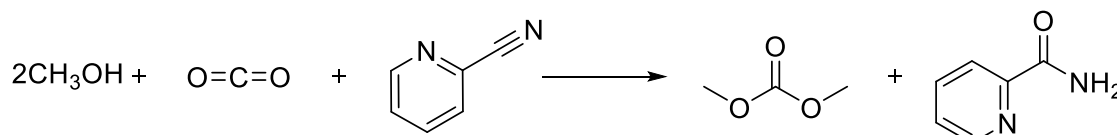
**Scheme 1-24: Reaction mechanism of between methanol and  $\text{CO}_2$  in the presence of acetonitrile as dehydrating agent. T= 150°C, P=0.5 MPa, 4 h.**<sup>158</sup>

However, the yield and selectivity of dimethyl carbonate improves when acetonitrile is replaced with benzonitrile by 47% and 78% respectively at 150°C with a pressure of 1 MPa.<sup>162</sup> This is due to hydration of benzonitrile producing benzamide. The resonance between the amide and the phenyl ring in benzamide makes it more stable than acetamide in Scheme 1-25.<sup>162</sup> Although the reaction was left longer, dimethyl carbonate yield did not increase which is due to deactivation of the catalyst,  $\text{CeO}_2$ , by benzamide and it was demonstrated by FTIR and TG-DTA that benzamide poisons the catalyst by adsorbing onto it.<sup>158,162</sup> Therefore in order to solve the problem of adsorption of the by-product onto the catalyst, the same

group used 2-cyanopyridine as dehydrating agent to increase the yield of dimethyl carbonate.<sup>163</sup> The reaction produced 2-picolinamide due to 2-cyanopyridine hydration shown on Scheme 1-26.



**Scheme 1-25: Reaction mechanism between acetamide and benzamide with methanol.**  
**T=150°C, P=1 MPa.**<sup>158,162</sup>

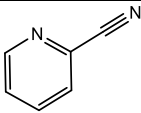
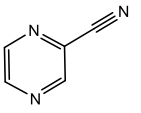
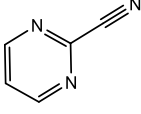
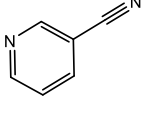
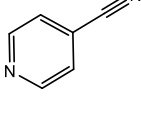
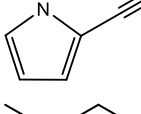
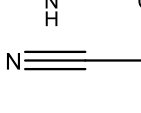
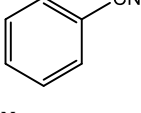
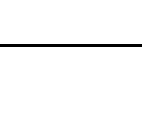


**Scheme 1-26: Reaction mechanism between methanol and CO<sub>2</sub> in the presence of 2-cyanopyridine as dehydrating agent.** T=120°C, P=5 MPa, 12 h<sup>163</sup>

The group reported that they attained 94% yield of dimethyl carbonate at 120°C with 1% methyl carbamate as by-product and almost all 2-cyanopyridine was converted into 2-picolinamide after 12 h reaction. Various nitriles have also been tested which can be shown on Table 2. 2-cyanopyridine and pyrazine-2-carbonitrile gave the highest yield of dimethyl carbonate. This is because 2-picolinamide does not adsorb strongly on the surface of the catalyst which was confirmed by FTIR and TG-DTA. The weak adsorption of 2-picolinamide is due to the weak interaction of between -NH<sub>2</sub> groups and Ce atoms on the catalyst as there is intramolecular hydrogen bonding between H atoms in the amide group and N atoms of the pyridine rings.<sup>163</sup> CeO<sub>2</sub> was recycled and regenerated and it still maintained its catalytic performance as the fresh catalyst without changing its physical properties.<sup>163</sup> The presence of 6-membered nitrogen heteroaromatic ring

and its position have an effect in the amount of dimethyl carbonate produced shown on Table 2.

**Table 2: DMC yield in the presence of different types of nitrile<sup>163</sup>**

Entry	Nitrile	Yield of product %			
		DMC	Methyl carbamate	Amide	Ester
1		94.0	0.99	94.6	1.18
2		91.2	0.18	86.9	0.26
3		38.6	0.41	44.1	0.69
4		2.06	n.d	3.06	<0.1
5		4.10	n.d	2.72	0.20
6		2.94	n.d	4.74	n.d
7		n.d	n.d	<0.1	<0.1
8		0.38	<0.1	0.48	<0.1
9		0.76	<0.1	0.74	<0.1
10	None	0.32	-	-	-

## 1.7 Enzymatic catalysis

Enzymes are class as macromolecules made from a long repeated chain of amino acids called polypeptides chains or polypeptide backbone.<sup>164</sup> The presence of these

peptide bonds and side chains from the amino acids caused these chains to specifically fold into higher ordered secondary, tertiary and quaternary structures. Folding is due to different types of bonding present in the peptide chains: hydrogen bonds, ionic bonds, hydrophobic interaction and Van der Waals attraction which results in enzymes having a 3-D structure.<sup>164,165</sup> The nature of the folding gives the enzymes the ability to specifically bind to a substrate molecule enabling specific selective enzymatic reactions to take place.<sup>166</sup> These polypeptide bonding forms internal cavities or pockets or clefts found on the surface of the protein at different sizes forming the active sites of the enzyme.<sup>167</sup> The formation of active site is due to the folding of tertiary structures of the amino acid. However not all the enzyme structure comprises of the active site only a small portion of the structure.<sup>168</sup> The rest of the enzyme provides support to the active sites by giving correct orientation by providing framework to support the structure. The specificity of the enzyme is due to the amino acids that reside in the active site which provides binding to the incoming substrate molecule.<sup>168</sup>

Enzymes are known for their reaction specificity and can only catalyse one particular reaction. There are five distinct types of enzyme specificity:

- Bond specificity: Enzymes act upon a substrate that has same type of bond and a similar structure. For example the enzyme amylase catalyses  $\alpha$  1-4 glycosidic bond in starch or glycogen.<sup>169</sup>
- Structural or group specificity: The enzyme has the ability to catalyse the structure surrounding the substrate as well as the bond on the structure for example the carboxyl group of aromatic amino acids can be catalyse by Chymotrypsin an endopeptidase via the peptide bonds of the amino acids.<sup>169</sup>
- Absolute substrate specificity: This type of enzyme can only catalyse one substrate. For instance, the enzyme Maltase can catalyse maltose or the substrate lactose is catalysed by Lactase.<sup>169</sup>
- Stereochemical specificity: The enzyme can catalyse the substrate with the right optical configuration. For example D amino acids can only be catalysed by D amino acid oxidase.<sup>169</sup>

- Dual specificity: In dual specificity, the enzyme catalysed only on substrate at two different reactions or the enzyme can catalyse two substrates in one reaction.<sup>169,170</sup>

Enzymes accelerate chemical reactions without itself being chemically changed, similar to chemical catalysis by providing an alternative pathway by stabilising the transition state thus lowering its energy compared to the uncatalysed reaction.<sup>166</sup> Enzymes are known to catalyse a specific single chemical reaction or similar reactions which is an advantage due to its active site.<sup>171</sup> For example carbonic anhydrase catalyses the hydration of CO<sub>2</sub> in the respiration cycle.<sup>171</sup> Another example is the degradation of H<sub>2</sub>O<sub>2</sub> by the enzyme catalase into oxygen and water, this is because H<sub>2</sub>O<sub>2</sub> can damage important cells in the body such as RNA, DNA, lipids and proteins.<sup>172</sup>

Most enzymes require cofactors to facilitate chemical transformation. These cofactors are usually non-protein compounds example metals or small organic molecules.<sup>166</sup>

As mentioned earlier the active site is a very important component in catalysis. There are two models in which the enzyme binds to the substrate.<sup>166</sup> The lock and key model proposed by Emil Fischer in which the substrate has the same shape to the active site and fits it perfectly shown in Figure 1-11. Danied E. Koshland suggested the induced fit model, Figure 1-12, where enzymes can change shape to accommodate the incoming substrate therefore binding to it forming transition state.<sup>166</sup> The substrate binds to the enzymes mostly by Van der Waals forces as well as other interactions such as electrostatic interaction, hydrogen bonds and hydrophobic interactions.<sup>166</sup>



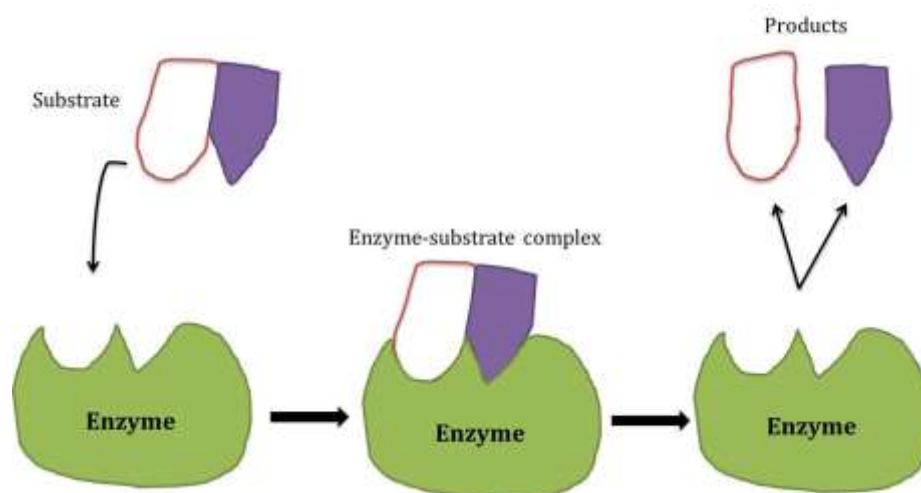


**Figure 1-11: Lock and key model for enzyme binding<sup>166</sup>**

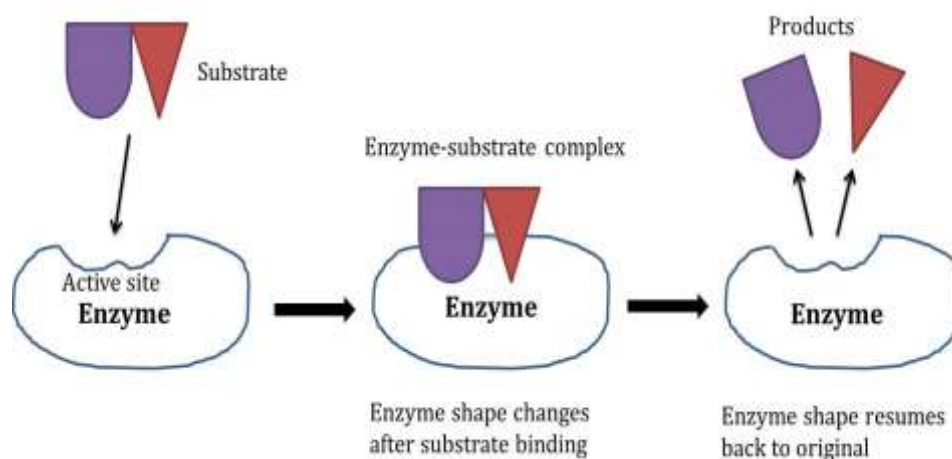


**Figure 1-12: Induced-fit model for enzyme binding<sup>166</sup>**

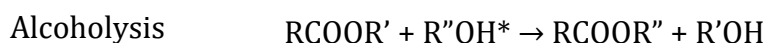
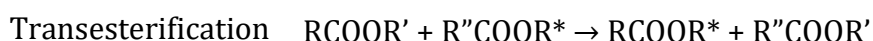
### 1.7.1 Lipases

Lipases is a hydrolase, a class of enzyme, produced from microbes have an advantage over plants and animals as the lipase production can be controlled according to the microbes' growth medium and cultivation conditions producing high yield which is economically attractive.<sup>173</sup> Lipases have gained considerable attention as industrial biocatalysts due to their attractive properties for example high stability towards temperatures and solvent, broad substrate tolerance and easy handling. Lipases produce a wide range of products containing chemo-, regio-

and enantioselective transformations for example lipase can differentiate between the enantiomer of Aspartame in a racemic mixture in which the S-isomer is bitter whereas R-isomer tastes sweet.<sup>173,174</sup> Lipases or triacylglycerol hydrolases are extensively used in chemical reactions such as hydrolysis and the effects of non-aqueous media on the reaction has been studied.<sup>175</sup> Most enzymes denature once removed from their optimum environment, hence numerous methods have been explored to stabilise enzymes.<sup>176</sup>

There are several methods to increase the stability and activity of lipases such as non-covalent interaction with surfactants, entrapment in water in oil microemulsions, reverse micelles, immobilisation on appropriate insoluble supports, utilisation of lyophilised enzyme powders suspended in organic solvents and protein engineering.<sup>177,178,179</sup> This can improve many reactions that are performed in organic media as free enzymes are more susceptible to denaturing due to low pH, temperature and chemical stability in organic solvents compared to water rich media.<sup>173,180,181</sup>

As previously mentioned, one of the ways to increase enzyme stability and reusability is through immobilisation onto a commercially available solid support such as methylated silica, phenyl-Sepharose, polypropylene particles or nitrocellulose membranes.<sup>173,182</sup> Immobilisation allows reusability of enzymes which is economical as enzymes are expensive. Ease of separation and purification which is an advantage in big chemical reactors for industries.<sup>183</sup> Lipases can catalyse a wide range of reaction such as hydrolysis, esterification, transesterification, alcoholysis and acidolysis shown in Scheme 1-27.<sup>183</sup>



#### Scheme 1-27: Enzymatic reaction catalysed by lipase.

### 1.7.2 Enzymatic catalysed synthesis of glycerol carbonate

The first enzymatic synthesis of glycerol carbonate was transesterification of glycerol with DMC using lipase by Kim *et al.*<sup>184</sup> They screened several lipases and immobilised lipase B from *Candida antarctica* gave the highest activity giving 100% yield at 60°C.<sup>184</sup> However, the reaction took 30 h to obtain full conversion. Virendra *et al* reported using ultrasound irradiation for the synthesis of glycerol carbonate and it reduced the reaction time to 4 h giving high conversion. Mild reaction conditions and high efficiency can be achieved using ultrasonic irradiation compared to conventional methods.<sup>185</sup>

The use of solvent plays an important role in the synthesis of glycerol carbonate. Glycerol has low solubility in dimethyl carbonate and this will affect the activity of the enzyme as insoluble glycerol forms a coating around the surface.<sup>186</sup> A number of solvents have been tested such as THF, tert-butanol, acetonitrile, hexane, toluene and xylene however only THF, tert-butanol and acetonitrile gave conversion of glycerol carbonate due to their hydrophilicity.<sup>186</sup> Studies have shown that THF is considered moderately toxic and corrosive to the eyes as well as producing tumours in rats.<sup>187</sup> To carry out a solvent-free reaction is an attractive way to synthesise glycerol carbonate from enzymes using DMC as both the solvent and reactant without the need to purify the reaction mixture.<sup>188,189</sup> DMC has been classified environmentally benign.<sup>190</sup>

However glycerol is not soluble in DMC and has the tendency to form two phases.<sup>188</sup> To overcome this, Lee *et al* used a different approach by adsorbing

glycerol onto silica with a 1:1 ratio of glycerol to silica producing over than 90% conversion of glycerol carbonate.<sup>188</sup> The conversion of glycerol carbonate was maintained when silica gel was recycled for four times.<sup>188</sup> Furthermore, enzyme activity was not affected in the presence of silica gel.

The activity of the *Aspergillus niger* lipase immobilized onto magnetic nanoparticles has been investigated extensively by Tudorache *et al* and found high stability and recyclability.<sup>191</sup> They achieved 45% glycerol conversion after 6 h reaction time under solvent free conditions.

## 1.8 Microwave chemistry

Microwave irradiation is considered an alternative green technology over conventional heating. Recently, microwave irradiation has been used in chemical synthesis due to their efficient and rapid heating over conventional thermal activation. There are several advantages in using microwave heating: faster reaction due to selective absorption of microwave energy by polar molecules, high yield as well as high purity of products with less formation of side products.<sup>192,193</sup>

Microwave irradiation is based on the principles of electromagnetic radiation absorption where molecules absorb radiation and undergo excitation. There are two effects that cause heating in microwave irradiation: dipolar polarisation and ionic conduction.<sup>194</sup> Microwave radiation shown in Figure 1-13 causes the dipoles or ions to align with the applied field. Continuous oscillation of electric field caused the polar molecules to try to attempt to align itself and rotate producing localised heating known as dielectric heating shown in Figure 1-14.<sup>193,194</sup> No heating occurs when the dipole realign rapidly with the electric field or there is no time for it to realign itself.<sup>194</sup>

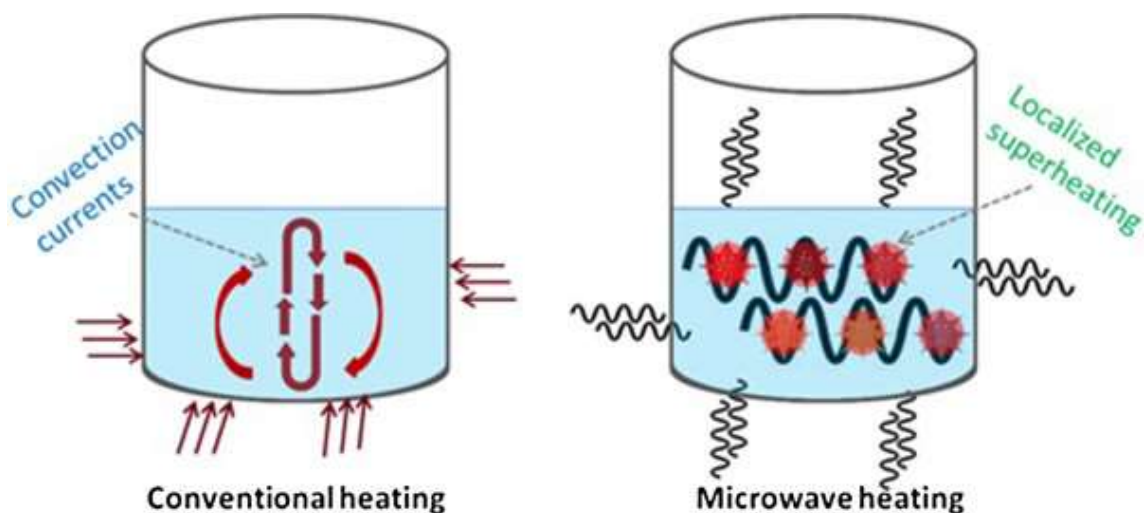


Figure 1-13: Differences between conventional and microwave heating<sup>195</sup>

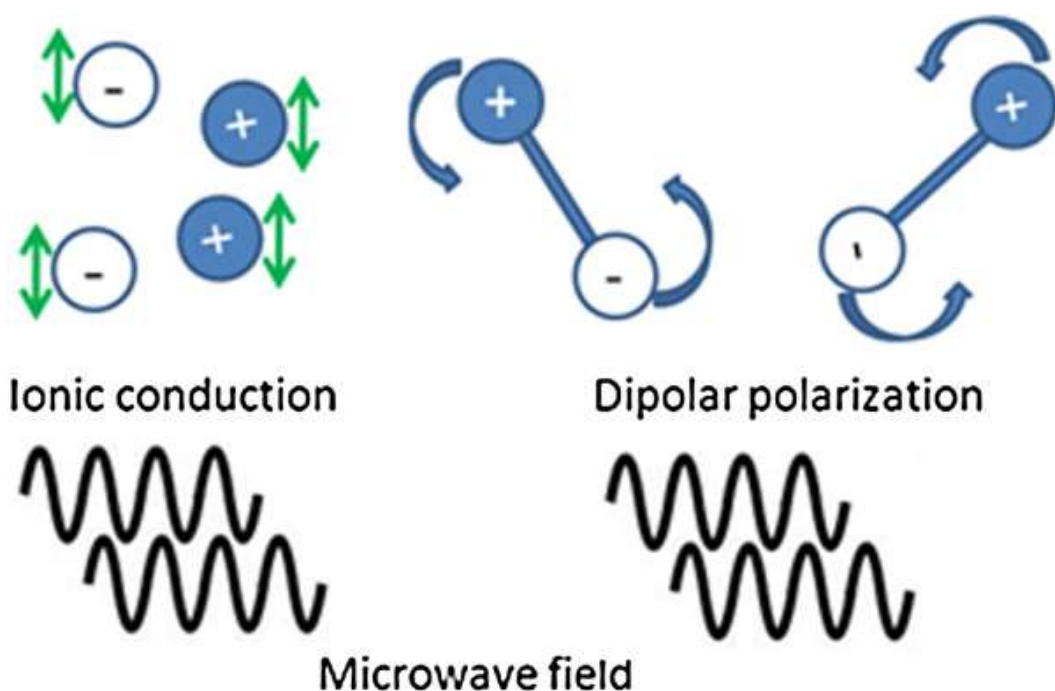


Figure 1-14: Ionic conduction and dipolar polarisation due to microwave heating<sup>195</sup>

Polar molecules such as water or acetone have high dielectric constants and this property enables the molecules to convert electromagnetic energy into thermal energy.<sup>193</sup> These polar molecules have dipole moment in which the dipole moments are free to rotate. This can be determined by an equation shown in Equation 9 in which  $\tan\delta$  is the dielectric loss tangent,  $\epsilon'$  is the relative permittivity which measures the ability of a molecule to be polarised by electric field and  $\epsilon''$  is

dielectric loss where it measures the ability of a medium to convert dielectric energy into heat.<sup>196</sup> This value can be determined at a given frequency and temperature. Solvents such as hexane or toluene do not heat under microwave irradiation due to having low dielectric constant.<sup>193,196</sup>

$$\tan\delta = \varepsilon'/\varepsilon''^{196}$$

**Equation 9**

The polar molecules have dipole moment in which the dipole moments are rotated freely and can have orientation depending on their neighbouring molecules. However the orientation of the dipoles can be changed according to the direction of the applied field which is known as dipolar polarisation. This can produce energy between the transitions state. Rotational spectroscopy can be used to measure the changes in orientation between the rotational and vibrational energy that occur simultaneously.

Recently microwave assisted synthesis of heterogeneous catalyst has got a lot of interest due to its rapid and efficient heating. Studies have shown that microwave assisted synthesis produced smaller and more uniform particles during nucleation due to selective activation of precursors.<sup>197</sup> Metal catalysts such as titanium oxide supported on activated carbon and palladium nanoparticles deposited on carbon nanotubes have been synthesised using microwave for the photocatalytic reactions.<sup>197</sup> Synthesis of titanium oxide on activated carbon prepared by microwave heating showed a higher photodegradation activity of isopropanol producing acetone and carbon dioxide than conventional method which is six fold slower.<sup>197</sup> Scanning electron microscopy (SEM) has shown that a thin uniform layer of titanium oxide forms on the surface of activated carbon produced by microwave heating which can be linked to the titanium oxide growth on activated carbon surface due to heat conduction from the solution.<sup>197</sup> Synthesis of nanocatalysts have also been reported using microwave irradiation. Metal oxides such as iron oxide nanoparticles can form different 3D structures which can be used in hydrogenation reaction and exhibits high catalytic activity. Microwave heating can effectively produce gold nanoparticles at different shaped by changing the concentration of the reducing agent.<sup>198</sup> Microwave heating can reduce the

aging time of metal oxide supports which takes longer in the normal hydrothermal method.

Microwave assisted reactions have been used in converting biomass at a faster rate and convert into gas products such as H<sub>2</sub>, CH<sub>4</sub>, CO and CO<sub>2</sub>.<sup>199</sup> Recently, Romano *et al* used microwave heating to convert furfural to furfuryl alcohol using cyclopentyl-methyl ether as green solvent using copper supported on titanium oxide. They reported to have achieved 100% conversion and 99% selectivity at 125°C for 3 h at a pressure of 1 MPa of hydrogen.<sup>200</sup>

## 1.9 Sorbitol

Sorbitol, also known as D-glucitol is a well-known polyol with 6 OH groups shown on Figure 1-15. Sorbitol is naturally found in food products especially in fruits.

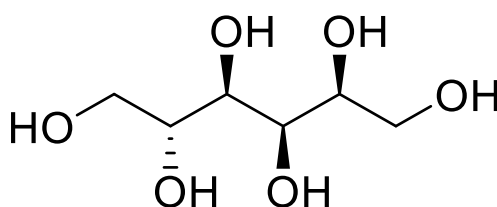


Figure 1-15: The structure of sorbitol

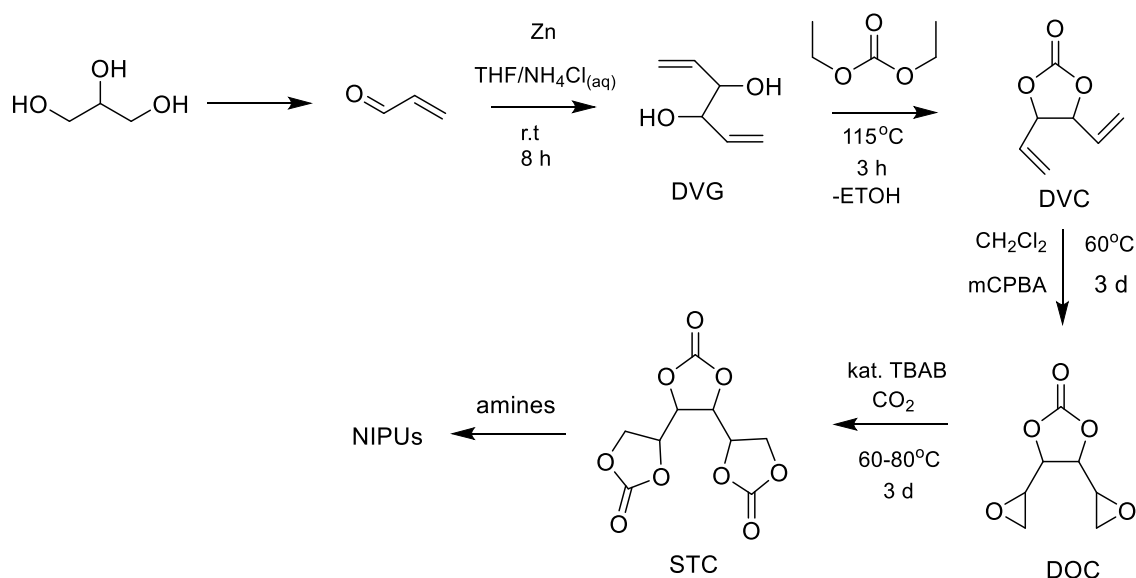
Sorbitol can be produced by chemical conversion of biomass-derived saccharides for example, in the reduction of glucose where the aldehyde is being converted into a hydroxyl group by using catalyst.<sup>201</sup> Sorbitol can also be produced directly by conversion of cellulose using aqueous phase hydrolysis-hydrogenation process using nickel catalyst giving reasonably good yields.<sup>202</sup> Almeida *et al* have successfully convert cellulose to sorbitol in a one-pot reaction. 81% yield of sorbitol was achieved in 5 h reaction at 150°C using bifunctional catalyst, 3% RuNPs/A15 at a pressure of 4 MPa.<sup>203</sup> Sorbitol is mainly used in food products for example as a cryoprotectant additive in the manufacture of surimi and it is also

used as a nutritive sweetener. Sorbitol is widely used in medical and pharmaceutical industries, such as the differentiation of pathogenic strands of *E. coli* as some strands are incapable of fermenting sorbitol.<sup>204</sup> It is also being commercialised in the use of toothpaste and mouthwash. Sorbitol is categorised as one of the potential platform molecules, which can synthesise useful chemical compounds such as glycerol, sorbitan, isosorbide and L-sorbose where the reaction conditions of sorbitol can be optimised with good catalytic systems to achieve high selectivity of products.<sup>205</sup> Sorbitol can be used in the production of fuel for example in the transformation to hexane, an important constituent in gasoline, by aqueous-phase reforming of sorbitol with the help of hydrogen and also by utilising bifunctional catalytic system of tungstated oxides with Pt/ZrO<sub>2</sub>, to transform sorbitol into biofuels in a very environmentally benign medium, which is water.<sup>206,207</sup>

With the successful conversion of glycerol into glycerol carbonate, the attention can be shifted towards sorbitol or any other polyols with similar structures such as mannitol that can be carbonated. By using the knowledge we have on glycerol carbonate, similar reactions could be performed with sorbitol due to the number of OH groups that are present on its chain. These OH groups could be possibly carbonated and therefore able to capture and sequester more carbon dioxide. Sorbitol carbonate could be a novel feedstock in producing polycarbonates which is sought after materials from chemical industries to produce commodities such as engineering plastics.

### 1.9.1 Synthesis of sorbitol carbonate





**Scheme 1-28: Synthesis of sorbitol tricarcarbonate with glycerol as starting material<sup>208</sup>**

Recently, Schmidt *et al* have synthesised sorbitol tri carbonate to produce non-isocyanate polyhydroxyurethane (NIPU) via glycerol as the starting material shown in scheme 1.31.<sup>208</sup> Glycerol undergoes dehydration to produce acrolein which is being covered extensively using different supports and catalysts especially acidic catalysts.<sup>209</sup> Acrolein dimerized to produce divinyl ethylene glycol (DVG) by McMurry coupling reaction catalysed by Zinc. Transesterification occurs between DVG and diethyl carbonate at 115°C for 3 h to produce divinyl ethylene carbonate (DVC) which will then undergoes oxidation reaction to produce diepoxy carbonate (DOC). DOC will then be converted into sorbitol tricarcarbonate via epoxy-mediated CO<sub>2</sub>.<sup>208</sup>

This reaction is not sustainable in terms of green chemistry due to several reaction steps require producing sorbitol tri carbonate which leads to additional reagents and generating waste.<sup>5</sup> Therefore in this project, several routes have investigated in synthesising sorbitol carbonate directly from sorbitol.

## 1.10 Objective and thesis organisation

In this project two platform molecules glycerol and sorbitol will be utilised to produce organic carbonates. The objective of this project is to produce renewable organic carbonates from platform molecules. Current literature has focused on the conversion of glycerol into glycerol carbonate, this will be one of the model reactions used within this thesis.<sup>136</sup>

Chapter 1 provides the introduction to green chemistry and sustainability and general background on heterogeneous catalysis. Introduction to the synthesis of organic carbonates. The synthesis of glycerol carbonates using catalysis is discussed. A brief introduction to sorbitol as the potential feedstock for producing organic carbonates.

Chapter 2 is the experimental part of the thesis describing the methods used in synthesizing the catalyst. Methods describing the synthesis of glycerol carbonate. All characterisation techniques used to characterise the catalysts were explained in detail. All product analysis techniques also were explained in detail.

Chapter 3 discuss the direct synthesis of glycerol carbonate from glycerol and carbon dioxide with different dehydrating agent using copper supported on lanthanum oxide with different loadings synthesised.

Chapter 4 focus on the synthesis of 2.3 wt% Cu/La<sub>2</sub>O<sub>3</sub> using microwave heating and using it to produce glycerol carbonate from CO<sub>2</sub>

Chapter 5 discuss the activity of two rare earth metal oxides in the direct carbonylation of glycerol carbonate using 2-cyanopyridine as a dehydrating agent

Chapter 6 explains the synthesis of glycerol carbonate from urea catalyse by cerium oxide and lanthanum oxide

Chapter 7 explains the synthesis of sorbitol carbonate via chemical and enzymatic routes.

Chapter 8 draws the conclusions and future work regarding the synthesis of organic carbonate from renewable resources

# CHAPTER 2

# EXPERIMENTAL

## 2 EXPERIMENTAL

### 2.1 Chemicals and solvents – Source and purity

Sigma Aldrich	Acetonitrile, HPLC
	Acetin
	Ammonium hydroxide solution, 28.0-30.0% NH <sub>3</sub> basis
	<i>Candida Antartica</i> immobilized on Immobead 150 recombinant from

	yeast named Lipase B
	Cerium (III) nitrate hexahydrate, 99.999%
	Cerium (IV) oxide, powder, 99.995%
	Copper (II)nitrate trihydrate, 99-104%
	Diethylene glycol methyl ether, ≥99.0%
	Dichloromethane
	Dimethyl carbonate, anhydrous, ≥99%
	D-Sorbitol, >99%
	Ethanol
	Glycerol, anhydrous
	Lanthanum (III) carbonate, 99.9%
	Lanthanum (III) hydroxide, 99.9%
	Lanthanum (III) nitrate hexahydrate, 99.999%
	Lanthanum (III) oxide, 99.999%
	Lipase acrylic resin from <i>Candida Antarctica</i>
	Magnesium oxide, 99.995%
	Methanol, HPLC
	Molecular sieves 4Å
	Molecular sieves 5Å
	Molecular sieves 13X
	N,N-Dimethylformamide, anhydrous,

	99.8%
	Picolinamide, 98%
	Silica gel
	<i>t</i> -BuOH
	Urea pellets, ≥99.5%
	4-(hydroxymethyl)-1,3-dioxolan-2-one
	1,1'-Carbonyldiimidazole
	2-Pyridinecarbonitrile
Alfa Aesar	Cetyltrimethylammonium bromide (CTAB), 98%
BOC industrial backup	CO <sub>2</sub> gas withdrawal N4.5, 99.995%
	H <sub>2</sub> gas, 99.99%
	N <sub>2</sub> gas 99.99%
Fischer Scientific	Dimethyl sulfoxide
	Sodium hydroxide, pellets
Acros Organic	Glycerol carbonate

## 2.2 Catalyst preparation

### 2.2.1 Hydrothermal method

Hydrothermal synthesis is a widely used technique to synthesise mixed oxides used in catalytic reactions as it is a simple reaction that can produce different structures of materials. Hydrothermal synthesis requires high pressure above 1 atm and high-temperature water above 100°C conditions for crystal growth that is insoluble at room temperature.<sup>210</sup> Water itself is a very important reaction medium

as it is able to control crystal growth, morphology, particle size and size distribution.<sup>211</sup> For this reason, hydrothermal synthesis has been used in industry to produce magnetic oxides, chalcogenides, oxides, etc.<sup>212</sup>

### 2.2.2 Microwave method

Synthesising mixed oxides using microwave irradiation method is a promising technique. The method has been recently studied as it is a fast process that provides rapid and selective heating.<sup>213</sup> Microwave depends on dielectric constant as a source of heating which converts electromagnetic energy into thermal energy.<sup>193</sup> Microwave heating has been used to synthesise solid supports such as alumina, silica and zeolites and can generate better crystallinity.<sup>193</sup>

### 2.2.3 Hydrothermal synthesis of lanthanum oxide (Chapter 3 and Chapter 4)

Lanthanum oxide synthesis was carried out according to Zhang *et al* using the hydrothermal method.<sup>155</sup> 0.01 mol of  $\text{La}(\text{NO}_3)_3 \cdot 6\text{H}_2\text{O}$  was dissolved in 40 mL of deionised water with 0.003 mol of Cetyltrimethylammonium bromide (CTAB) at 70°C with stirring. CTAB has the ability to reduce the surface energy of the incoming particles by providing a surface in which the particles can adsorb to and prevent agglomeration of particles.<sup>214</sup> The precipitate was formed by adding 20 mL of NaOH solution with a concentration of 1 mol/L into the mixture and was stirred for 6 h. 25% Ammonium hydroxide solution was added to the solution until the pH reached 10 and the solution was transferred to a 30 mL Teflon-lined autoclave. The precipitate was treated hydrothermally at 100°C for 48 h using a General Purpose Oven (Genlab, Model number PRO/50) shown in Figure 2-1. After the reaction, the precipitate was washed thoroughly with ethanol and deionised water until the pH was neutral. The support,  $\text{La}(\text{OH})_3$  was dried in the oven for 24 h at 110°C and calcined in air using Carbolite tube furnace shown in Figure 2-2 at 700°C for 3 h at the heating rate of 10°C/min producing white solid,  $\text{La}_2\text{O}_3$ .<sup>155</sup>



**Figure 2-1: The oven used to synthesise catalyst using conventional heating**

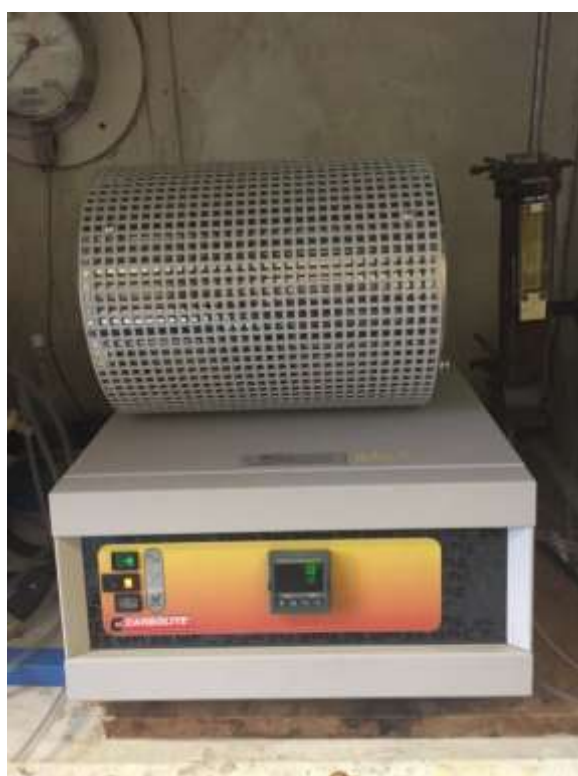


**Figure 2-2: Carbolite furnace**



#### 2.2.4 Modified hydrothermal synthesis of lanthanum oxide using microwave (Chapter 4)

Zhang's hydrothermal synthesis was modified slightly for the microwave synthesis. 0.01 mol of  $\text{La}(\text{NO}_3)_3 \cdot 6\text{H}_2\text{O}$  was dissolved in 20 mL deionised water with 0.003 mol of CTAB at 70°C with stirring. Then 20 mL of NaOH solution (1 mol/L) was added dropwise and the precipitate was transferred to a 35 mL microwave vessel. The precipitate was treated in the microwave (CEM Discover SP) with heating power of 200 W at 70°C for 2 h with constant stirring shown in Figure 2-3. 25% ammonium hydroxide solution was added to increase the pH to 10 and was treated again in the microwave for 16 h at 100°C with stirring. After the reaction, the precipitate was washed with deionised water and ethanol until the pH reached 7. The support was dried in the oven for 24 h at 110°C and was calcined in air using a Carbolite tube furnace at 700°C for 3 h at the heating rate of 10°C/min producing white solid.



Figure 2-3: CEM Discover SP used to synthesise the catalyst

### **2.2.5 Copper supported on lanthanum oxide by impregnation (Chapter 3 and Chapter 4)**

Cu/La<sub>2</sub>O<sub>3</sub> catalysts were prepared by impregnation method. Cu(NO<sub>3</sub>)<sub>2</sub>·3H<sub>2</sub>O (0.110 g, 2.3 wt%) was dissolved in 40 mL ethanol. La<sub>2</sub>O<sub>3</sub> (1.0 g) support was added to the solution and stirred for 24 h at room temperature. The solution was heated to 60°C to remove ethanol and dried further in the oven overnight at 110°C. The catalyst was calcined in air using Carbolite tube furnace at 300°C for 3 h and was reduced at 450°C under hydrogen atmosphere for 2 h at a flow rate of 10 mL/min; both heat treatments were at the heating rate of 10 °C/min producing dark blue solid.<sup>155</sup>

### **2.2.6 One pot copper impregnation of lanthanum hydroxide (Chapter 4)**

Instead of immediate calcination after hydrothermal step, Cu(NO<sub>3</sub>)<sub>2</sub>·3H<sub>2</sub>O was dissolved in 40 mL ethanol and La(OH)<sub>3</sub> was added to the solution and stirred for 24 h at room temperature, heated to 60°C to remove ethanol and dried further in the oven overnight at 110°C. The catalyst was calcined at 700°C for 3 h and was reduced to 450°C under hydrogen atmosphere at a flow rate of 10 mL/min to obtain 2.3 wt% Cu/La<sub>2</sub>O<sub>3</sub>. Both heat treatments were at the heating rate of 10°C/min producing dark blue solid. This reduced the preparation time by one calcination step.

### **2.2.7 One pot microwave preparation of copper supported on lanthanum oxide with early copper incorporation (Chapter 4)**

0.005 mol La(NO<sub>3</sub>)<sub>3</sub>·6H<sub>2</sub>O, 0.0007 mol Cu(NO<sub>3</sub>)<sub>2</sub>·3H<sub>2</sub>O and 0.5 g CTAB were dissolved in 20 mL deionised water and was heated to 70°C. 10 mL of NaOH solution (1 mol/L) was added dropwise and the precipitate was transferred to a 35 mL microwave vessel. The precipitate was treated in the microwave (CEM Discover SP) with a heating power of 200 W at a temperature of 70°C for 2 h with constant stirring. 25% ammonium hydroxide solution was added to increase the pH to 10

and was treated again in the microwave for 16 h at 100°C with stirring. After the reaction, the precipitate was washed with deionised water and ethanol until the pH reached 7. The catalyst was dried for 24 h at 110°C and was calcined using Carbolite tube furnace at 700°C for 3 h and reduced to 450°C under hydrogen atmosphere at a flow rate of 10 mL/min to obtain 2.3 wt% Cu/La<sub>2</sub>O<sub>3</sub>. Both the heating treatments were at 10°C/min

#### **2.2.8 Hydrothermal synthesis of lanthanum oxide (Chapter 5 and Chapter 6)**

The synthesis of La<sub>2</sub>O<sub>3</sub> was carried out according to Liu *et al.* 0.3 mol/L La(NO<sub>3</sub>)<sub>3</sub>·6H<sub>2</sub>O solution (20 mL) was added to 6 mol/L NaOH (40 mL) solution and was stirred for 20 min at room temperature. The mixture was transferred to 30 mL Teflon-lined autoclave and was treated hydrothermally for 24 h at 120°C. Then the precipitate was washed with deionized water and was dried at 60°C for 24 h. The catalyst was calcined using Carbolite tube furnace at 400°C/700°C for 5 h at a heating rate of 10°C/min.<sup>215</sup>

#### **2.2.9 Modified hydrothermal synthesis of lanthanum oxide using microwave heating (Chapter 5 and Chapter 6)**

Liu's hydrothermal synthesis of La<sub>2</sub>O<sub>3</sub> was modified slightly for microwave synthesis.<sup>215</sup> The synthesis method was used as follows: 0.3 mol/L of La(NO<sub>3</sub>)<sub>3</sub>·6H<sub>2</sub>O (20 mL) was added to 6 mol/L NaOH (40 mL) solution and was stirred for 20 min producing precipitate. The precipitate solution was transferred to a 35 mL microwave vessel and treated in the microwave (CEM Discover SP) with heating power of 200 W at temperature of 120°C for 12 h with constant stirring. The resulting precursor was washed with deionized water and was dried at 60°C for 24 h. The catalyst was calcined using Carbolite tube furnace at 400°C/700°C for 5 h at a heating rate of 10°C/min.

#### 2.2.10 Hydrothermal synthesis of cerium oxide (Chapter 5 and Chapter 6)

The synthesis of cerium oxide was carried out according to Liu *et al.* 0.3 mol/L  $\text{Ce}(\text{NO}_3)_3 \cdot 6\text{H}_2\text{O}$  solution (20 mL) was added to 6 mol/L NaOH (40 mL) solution and was stirred for 20 min at room temperature.<sup>215</sup> The mixture was transferred to 30 mL Teflon-lined autoclave and was treated hydrothermally for 24 h at 120°C. Then the precipitate was washed with deionised water and was dried at 60°C for 24 h. The catalyst was calcined in air using Carbolite tube furnace at 400°C/700°C for 5 h producing yellow solid at a heating rate of 10°C/min.<sup>215</sup>

#### 2.2.11 Modified hydrothermal synthesis of cerium oxide using microwave (Chapter 5 and Chapter 6)

Liu's hydrothermal synthesis of cerium oxide was modified slightly for microwave synthesis.<sup>215</sup> The synthesis method was as follows: 0.3 mol/L of  $\text{Ce}(\text{NO}_3)_3 \cdot 6\text{H}_2\text{O}$  (20 mL) was added to 6 mol/L NaOH (40 mL) solution and was stirred for 20 min producing a precipitate. The precipitate was transferred to a 35 mL microwave vessel and treated in the microwave (CEM Discover SP) with a heating power of 200 W at 120°C for 12 h with constant stirring. The resulting precursor was washed with deionised water and was dried at 60°C for 24 h in the oven. The catalyst was calcined in air using Carbolite tube furnace at 400°C/700°C at a heating rate of 10°C/min for 5 h producing yellow solid.

#### 2.2.12 Copper supported on $\text{CeO}_2$ or $\text{La}_2\text{O}_3$ by impregnation (Chapter 6)

Cu support catalysts were prepared by impregnation method. Certain amount of  $\text{Cu}(\text{NO}_3)_2 \cdot 3\text{H}_2\text{O}$  was dissolved in 40 mL ethanol depending on the weight % of copper.  $\text{CeO}_2$  or  $\text{La}_2\text{O}_3$  (1.0 g) support was added to the solution and stirred for 24 h at room temperature. The solution was heated to 60°C to remove ethanol and dried further in oven overnight at 110°C. The catalyst was calcined using Carbolite tube furnace at 300°C for 3 h and was reduced at 450°C under hydrogen

atmosphere for 2 h at a flow rate of 10 mL/min; both heat treatments were at the heating rate of 10 °C/min.

## 2.3 Catalyst characterisation

The different instrumental techniques used to characterise the catalysts mainly to identify the structure of the catalyst, surface area, size of the catalyst, basicity of the catalyst, reduction behaviour of the active metals and chemical states of the metal which are described here.

### 2.3.1 X-ray diffraction (XRD)

#### 2.3.1.1 Theory

XRD is an analytical technique which provides valuable information on the properties of the crystalline samples as each crystalline solid has its own unique fingerprint of x-ray intensity.<sup>216</sup> It is mostly used to identify bulk structure of the crystalline solids, crystalline phase composition and to determine the particle size of the crystalline solids as x-ray wavelengths are the same size as the atom and the spacings between lattice planes in the crystal.<sup>216</sup> XRD is based on the principle of diffraction. Equation 10 shows the Bragg equation used to measure d-spacings of the crystalline material.

$$2d\sin\theta = n\lambda \qquad \text{Equation 10}$$

In this equation,  $n$  is the order of reflection,  $\lambda$  is the incident x-ray wavelength,  $d$  is the lattice planar spacing and  $\theta$  is the diffraction angle. Figure 2-4 shows the schematic diagram of Bragg's law.<sup>217</sup>

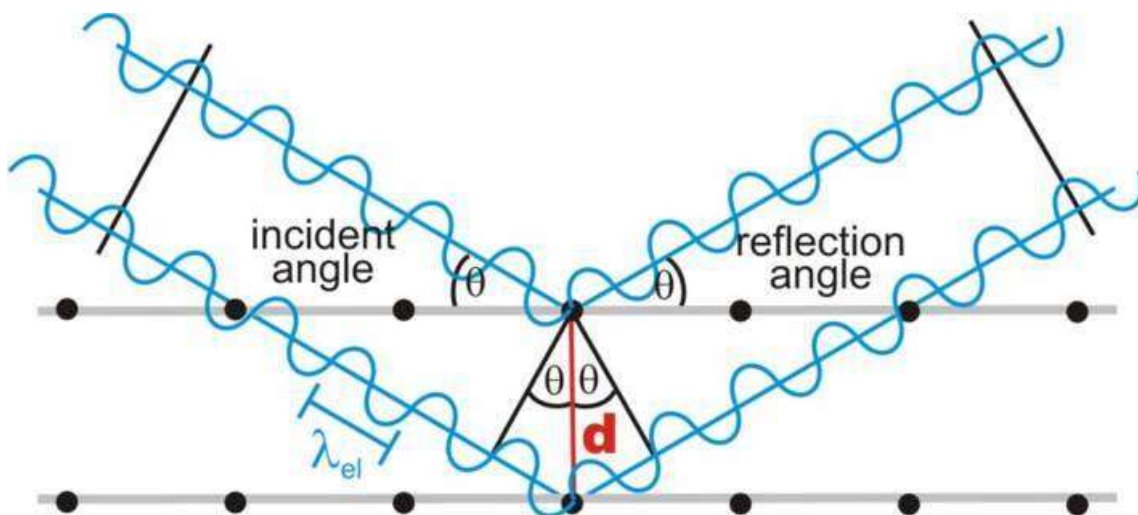


Figure 2-4: Bragg's law representation in a diagram<sup>217</sup>

Although XRD is a powerful technique, it has some limitations on its usage. The determination of the size of large crystalline structures is more accurate than the size of small crystalline structures. The XRD samples must be known prior to analysis as overlapping peaks can be difficult to characterise. The amount of different phase in the catalyst could not be quantified.

### 2.3.1.2 Experimental

The X-ray diffraction (XRD) patterns were recorded on a Panalytical X'Pert PRO HTS X-ray diffractometer using Cu-K $\alpha$  radiation ( $\lambda = 0.154$  nm) over the range of 10-80° 2 $\theta$  for approximately 60 minutes to determine crystal phases of the prepared catalysts. The samples were crushed into fine powders with enough amounts to be put in the device and analysed by the detector. Subsequently, the XRD data can be searched and matched with the standard reference patterns, the International Centre for Diffraction Data database. XRD data also can display the level of crystallinity whether the solid samples are amorphous or crystalline. Six different types of crystal systems also can be derived from the XRD patterns. Crystallite size of the catalyst can be calculated from XRD data using the Scherrer equation. Equation 11 shows the Scherrer equation where  $k$  is a constant which is

always 0.9,  $\beta$  is the full width at half maximum (FWHM) usually in radian,  $\theta$  is the diffraction angle and  $\lambda$  is the wavelength of the incident X-rays.

$$L = \frac{k\lambda}{\beta \cos \theta} \quad \text{Equation 11}$$

### 2.3.2 BET analysis

#### 2.3.2.1 Theory

Surface area is crucial in heterogeneous catalysis as the active sites are present on the surface and it generally influences the overall catalytic reactivity. Surface area is associated with porosity, morphology of the particle, particle size and surface texture.<sup>218</sup> These characteristics are important as reactants can easily access the active sites without having mass transport limitations.<sup>219</sup> High surface area is highly desirable as it can be achieved by producing small particles or by creating highly porous materials.<sup>220</sup> Pores can be classified into 3 types by International Union of Pure and Applied Chemistry (IUPAC) shown in Table 3.<sup>221</sup> The pore size can be affected by the presence of active components or metals on the surface and during the preparation of the catalyst.<sup>219</sup>

**Table 3: Classification of pores by IUPAC<sup>221</sup>**

	Diameter nm
<b>Micropores</b>	< 2
<b>Mesopores</b>	2-50
<b>Macropores</b>	> 50

The surface area of the catalyst can be measured by adsorption of an inert gas such as nitrogen or argon. Adsorption is a phenomenon where gas molecules or adsorbate can attach itself to the surface of the catalyst also known as adsorbent

due to unbalanced molecular forces on the surface. Adsorption can be classified into two types depending on the interaction:

- Chemical adsorption or chemisorption, where there is a significant change in the electronic arrangement within the molecule usually at high temperature with a high enthalpy of adsorption of 40-800 kJ/mol. The process is selective where adsorption occurs on the selective adsorbent, and it is usually used to measure the surface area and dispersion of active metals. Chemisorption only forms a monolayer adsorption.<sup>222</sup>
- Physical adsorption or physisorption, where weak Van der Waals forces are present between the catalyst and the adsorbed molecules. It usually occurs at low temperature with a low enthalpy of adsorption of 8-20 kJ/mol. Physisorption tends to form a multilayer adsorption with an increase in pressure. This condition enables the measurement of pore size distribution, pore volume, specific surface area and total surface area of the catalyst.<sup>222</sup>

An adsorption isotherm is the measurement of the amount of gas adsorbed over a wide range of relative pressures at constant temperature. This information can tell us whether the adsorbent is porous or non-porous material and the types of pores present in the catalyst.<sup>223</sup> From the information Brunauer classified the adsorption isotherm into six types shown in Figure 2-5.<sup>223,224</sup>

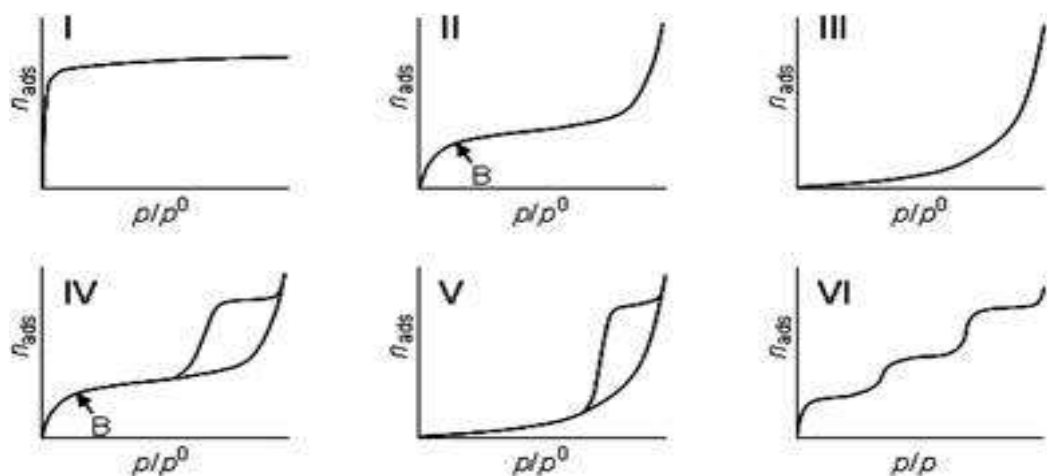


**Figure 2-5: Different types adsorption isotherm classified by Brunauer.**<sup>224</sup>



- Type I isotherm is generally adsorption in small pores or microporous materials. The plateau indicates that the micropores are completely filled with adsorbate with no further adsorption. It is sometimes called the Langmuir isotherm.
- Type II isotherm is for adsorption on macroporous materials. Rapid adsorption of gas occurs until it reaches point B where monolayer coverage is completed by adsorbate. Multilayer coverage starts to form with an increase in pressure.
- Type III isotherm adsorption has little information surrounding it. This adsorption has a stronger adsorbate with adsorbate interaction than adsorbate with adsorbent.
- Type IV isotherm is similar to type II isotherm where monolayer formation forms at first. Then at higher pressure before it reached saturation level, the adsorbate fills the tiny capillary pores and condensed.<sup>224</sup>
- Type V isotherm adsorption occurs at high pressure after it undergoes capillary condensation and has the same adsorption as type III isotherm where adsorbate-adsorbate interaction is stronger than adsorbate-adsorbent interaction.<sup>225</sup>

The surface area of catalysts and pore volume can be measured approximately by Brunauer-Emmett-Teller (BET) method. It is also used to explain multilayer adsorption. Stephen Brunauer, P.H. Emmet and Edward Teller developed the BET method in 1938 while working with ammonia catalysts. Nitrogen is commonly used as the adsorbate gas for surface area measurement.<sup>226</sup> Equation 12 shows the BET equation where  $p$  is the partial pressure;  $p_0$  is the saturated pressure at the temperature being used in the experiment,  $v$  is the volume of gas adsorbed,  $v_m$  is gas adsorbed at monolayer coverage and  $C$  is the BET constant.  $C$  indicates the degree in which the adsorbate and adsorbent interact. It also indicate the energy of adsorption in the first layer.<sup>226</sup> BET equation uses a linear plot to determine the monolayer coverage where  $p/v(p_0-p)$  is plotted against  $p/p_0$ . Equation 13 is used to determine the monolayer coverage,  $v_m$ , from the slope ( $s$ ) and intercept ( $i$ ) of the BET equation.<sup>226</sup>

$$\frac{p/v (p_0-p)}{(p/p_0)} = 1/v_m C + C-1/v_m C$$

$$s = C-1/v_m C$$

$$i = 1/v_m C$$

**Equation 12**

$$v_m = 1/s+i$$

**Equation 13**

Then total surface area ( $S_A$ ) can be calculated where  $v_m$  is the gas adsorbed at monolayer,  $N_A$  is the Avogadro's number,  $v_v$  molar volume of gas and  $A$  is the cross sectional area of nitrogen molecule,  $16.2 \text{ \AA}^2$  shown on Equation 14. Therefore specific surface area ( $S_{SA}$ ) can be calculated shown on Equation 15 where  $w$  is the weight of the catalyst.<sup>226</sup>

$$S_A = v_m N_A A / v_v$$

**Equation 14**

$$S_{SA} = S_A / w$$

**Equation 15**

### **2.3.2.2 Experimental**

The specific surface area and total pore volume of the catalysts were determined through low-temperature  $N_2$  adsorption-desorption at liquid nitrogen temperature  $-196^\circ\text{C}$  using a Quantachrome Nova 4200E analyzer. The samples (100 mg) were degassed overnight at  $120^\circ\text{C}$  under vacuum prior to analysis to remove any adsorbed impurities present on the surface. The surface area was calculated using the multipoint BET method.

### **2.3.3 Transmission Electron Microscopy (TEM)**

#### **2.3.3.1 Theory**

TEM was first developed by two German scientists, Max Knoll and Ernst Ruska in 1931. TEM is an analytical technique which uses a focused beam of high-energy electrons instead of using a light source as used in a conventional microscope, and

it works by the same principle as a light microscope.<sup>227</sup> TEM produces high resolution and magnification imaging down to an atomic level which displays the crystallographic information such as the structure of the sample, features, chemical composition and morphology of the solid sample. It is used in numerous fields such as medical, metallurgy and nanotechnology due to its detail and high-quality analysis of solid samples.<sup>228</sup>

Equation 16 shows the maximum resolution that can be achieved by conventional microscopy, which uses light as a source of illumination.  $d$  represents the maximum resolution,  $\lambda$  is the wavelength of light or photons,  $n$  is the refractive index between the solid samples and objective front lens,  $\theta$  is the maximal half-angle of the cone of light that can enter or exit lens which also equates to numerical aperture, NA.<sup>228</sup>

$$d = \lambda / 2n \sin \theta \approx \lambda / 2NA \quad \text{Equation 16}$$

The reason why TEM has the ability to produce better resolution is due to de Broglie wavelength of electrons. Equation 17 shows the de Broglie equation where  $h$  is the Planck's constant,  $E$  is the energy of accelerated electron,  $c$  is the speed of light and  $m_0$  is the rest mass of electron.<sup>229</sup>

$$\lambda_e = h / \sqrt{2m_0E (1 + E/2m_0C^2)} \quad \text{Equation 17}$$

### 2.3.3.2 Experimental

Transmission electron microscopy (TEM) observations of the catalyst were carried out by using a Jeol 2100 at an acceleration voltage of 200 kV. This is to determine the sizes and shapes of the supported particles. Before analysis, a small sample of the catalyst was added in ethanol and was put in the ultrasonic bath. One drop of the suspension was placed in the carbon grid.

### 2.3.4 Temperature Programmed Desorption (CO<sub>2</sub>-TPD)

#### 2.3.4.1 Theory

There are many ways to study the interaction between adsorbate and adsorbent which will then characterise the surface reactivity. Titration can be used to determine the surface reaction using indicators however this only applies for colourless catalysts and also the possibility that the indicator will react with a non-acidic or basic surface.<sup>230</sup> The most widely used technique is temperature-programmed desorption which is used to characterise the basicity and acidity of solid samples with an increase in temperature.<sup>231</sup> Ammonia gas is being used as probe molecule to determine acidic sites whereas carbon dioxide gas is used to determine basic sites.<sup>232</sup> The study of acidic or basic sites on the surface of the catalyst provides a deeper understanding of the types of interaction the catalyst undergoes and can predict possible mechanism between the adsorbate and adsorbent.

In CO<sub>2</sub>-TPD, desorption peaks reflect the amount of basic sites present on the catalyst and desorption temperature relates the bond strength of CO<sub>2</sub> with the adsorbent.<sup>233</sup>

#### 2.3.4.2 Experimental

Temperature programmed desorption of CO<sub>2</sub> (TPD-CO<sub>2</sub>) was carried out on Micromeritics Autochem 2920 equipped with a thermal conductivity detector (TCD) to determine the basic properties of the catalysts shown in Figure 2-6. 100 mg of sample was packed in a quartz U-tube reactor, pre-treated at 650°C in flowing He for 30 min to remove any impurities that might present on the surface of the catalyst such as water and then cooled to 50°C. The adsorption of CO<sub>2</sub> was performed at 50°C for 30 min followed by helium purge to remove the physisorbed CO<sub>2</sub>. The desorption process of CO<sub>2</sub> was performed at a heating rate of 10°C/min from 50°C to 750°C in a flow of helium at 30 mL/min. The peak area of the desorbed CO<sub>2</sub> was measured by integrating the peaks and calibrating the mass signal of standard CO<sub>2</sub>/He gases.



**Figure 2-6: Micromeritics Autochem II 2920 to determine basic strength**

### **2.3.5 H<sub>2</sub>-Temperature Programmed Reduction (H<sub>2</sub>-TPR)**

#### **2.3.5.1 Theory**

Temperature programmed reduction (TPR) is an effective technique to characterise reducible materials present on the surface of the catalyst and to identify oxidation states of metals with an increase in temperature and continuous flow of reducing gas mixtures.<sup>234</sup> TPR is also used to measure the gas evolved and taken up by the sample.

TPR data is used to investigate the strength of metal-support interaction. A higher reduction peak temperature indicates stronger metal-support interaction.<sup>235</sup> It also can show the presence of metals and multiple peaks of hydrogen consumption indicate different oxidation states of the metal present on the surface of the catalyst.

### 2.3.5.2 Experimental

The catalysts were characterised by H<sub>2</sub> temperature programmed reduction (H<sub>2</sub>-TPR) on Micromeritics Autochem 2920 equipped with a thermal conductivity detector (TCD). Each sample (100 mg) was pre-treated in helium gas at 500°C for 30 min at the rate of 30 ml/min to remove adsorbed water and was cooled. TPR was performed using 5% H<sub>2</sub>/N<sub>2</sub> with a flow rate of 30 ml/min at a heating rate of 10°C/min from 50°C to 800°C.

### 2.3.6 Ultraviolet-Visible Spectroscopy (UV-Vis)

#### 2.3.6.1 Theory

Ultraviolet light has the energy of 630 kJ/mol and wavelength of  $1.9 \times 10^{-7}$  m. UV-Vis spectroscopy measures absorption in the Ultraviolet region used to identify the presence of a functional group called chromophores. The interaction between ultraviolet radiation and matter caused electronic transitions.

Absorption of UV-vis is measured using Beer-Lambert law. Beer-Lambert law states that the concentration of absorbing molecules is proportional to the absorbance of the solution and it is independent of the intensity of radiation. Equation 18 shows the Beer-Lambert equation where  $I$  is the intensity of transmitted radiation,  $I_0$  is the intensity of incident radiation,  $l$  is the path length,  $c$  is the concentration of absorbing species and  $\epsilon$  is molar absorption coefficient.

$$\log_{10} I_0/I = \epsilon lc \quad \text{Equation 18}$$

### **2.3.6.2 Experimental**

The diffuse reflectance UV-VIS spectroscopy measurements were recorded on a Shimadzu UV-2550 equipped with diffuse reflectance accessory using BaSO<sub>4</sub> as a reference for the spectra in the range of 200-800 nm at room temperature.

### **2.3.7 Thermogravimetric analysis (TGA)**

#### **2.3.7.1 Theory**

In this technique, the mass of the substance is monitored with increase in temperature in a controlled environment. The substance can either undergo loss in mass or gain in mass. It is used to determine volatile material, moisture content and thermal stability.

#### **2.3.7.2 Experimental**

The thermal stability of the catalyst was determined by TGA using TA Instruments Q5000 equipment under air. The sample was placed in aluminium pan and heater from room temperature to 550°C at a heating rate of 10°C/min.

## 2.4 Catalytic reaction

### 2.4.1 Direct carbonylation of glycerol with CO<sub>2</sub> using molecular sieves as dehydrating agent (Chapter 3)

The glycerol carbonate synthesis using molecular sieves as the dehydrating agent was carried out in a 50 mL stainless-steel autoclave equipped with a thermocouple and overhead stirrer shown in Figure 2-7. Glycerol (2.3 g, 25 mmol), Cu/La<sub>2</sub>O<sub>3</sub> (0.11 g, 2.3 wt%) and 13X molecular sieves (1.0 g) were placed in the autoclave and CO<sub>2</sub> was purged into the autoclave to remove any air present. The autoclave was pressurised with CO<sub>2</sub> with an initial pressure of 4.0 MPa and the autoclave was heated to 150°C with a final pressure of 5.2 MPa for 16 h. After the reaction, the reactor was cooled to room temperature, and CO<sub>2</sub> was depressurised slowly. The reaction mixture was dissolved in methanol to separate the solid and liquid by centrifugation. The products were analysed by GC and <sup>1</sup>H NMR and <sup>13</sup>C NMR.



**Figure 2-7:** 50 mL stainless-steel autoclave equipped with a thermocouple and overhead stirrer



#### **2.4.2 Direct carbonylation of glycerol with CO<sub>2</sub> using trimethyl orthoformate as dehydrating agent (Chapter 3)**

The glycerol carbonate synthesis was carried out in 50 mL autoclave system equipped with a thermocouple and overhead stirrer. Glycerol (2.3 g, 25 mmol), Cu/La<sub>2</sub>O<sub>3</sub> (0.11 g, 2.3 wt%) was dissolved in 5 mL trimethyl orthoformate. CO<sub>2</sub> was introduced into the autoclave with an initial pressure of 4.5 MPa at room temperature, and the autoclave was heated to 150°C where the final pressure reached 7.0 MPa for 16 h. After the reaction, the autoclave was cooled down to room temperature, and CO<sub>2</sub> was depressurised slowly. The products were analysed by GC to obtain the conversion of glycerol and yield of glycerol carbonate.

#### **2.4.3 Direct carbonylation of glycerol with CO<sub>2</sub> using acetonitrile as dehydrating agent (Chapter 3)**

The glycerol carbonate synthesis was carried out in 50 mL stainless-steel autoclave system equipped with a thermocouple and overhead stirrer. Glycerol (2.3 g, 25 mmol), Cu/La<sub>2</sub>O<sub>3</sub> (0.11 g, x wt%), x was the loading amount of copper, was dissolved in 5 mL acetonitrile. CO<sub>2</sub> was introduced into the autoclave with an initial pressure of 4.6 MPa at room temperature and the autoclave was heated to 150°C where the final pressure reached 7.3 MPa for 16 h. After the reaction, the autoclave was cooled down and CO<sub>2</sub> depressurised. The product was analysed by GC to obtain conversion of glycerol and yield of glycerol carbonate.

#### **2.4.4 Direct carbonylation of glycerol with CO<sub>2</sub> using acetonitrile as dehydrating agent (Chapter 4)**

The glycerol carbonate synthesis was carried out in a general autoclave vessel shown in Figure 2-8. Glycerol (2.3 g, 25 mmol), 2.3 wt% Cu/La<sub>2</sub>O<sub>3</sub> (0.11 g) was dissolved in 5 mL acetonitrile. The vessel was purged 3 times with CO<sub>2</sub> to remove

air from the system. The vessel was charged with CO<sub>2</sub> to 4.8 MPa and the autoclave vessel was heated to 150°C for 24 h. The final pressure of the autoclave vessel was 6.2 MPa. The reaction products were analysed by GC to obtain conversion of glycerol and yield of glycerol carbonate.



**Figure 2-8: General autoclave vessel**

#### **2.4.5 Direct carbonylation of glycerol with CO<sub>2</sub> using 2-cyanopyridine as dehydrating agent (Chapter 5)**

The glycerol carbonate synthesis was carried out in 50 mL stainless-steel autoclave system with a thermocouple and overhead stirrer shown in Figure 2-7. Glycerol (0.92 g, 10 mmol), CeO<sub>2</sub> (0.34 g, 2mmol), 2-cyanopyridine (3.27 g, 30 mmol) was dissolved in 10 mL DMF. CO<sub>2</sub> was introduced into the autoclave with an initial pressure of 2.4 MPa and was heated to 150°C where the final pressure reached 3.1 MPa for 5 h. After the reaction, the autoclave was cooled down to room temperature, and CO<sub>2</sub> was depressurised and a certain amount of diethylene glycol monomethyl ether (DEGME) was added to the reaction mixture as an internal

standard. The products were analysed using GC to obtain the conversion of glycerol and yield of glycerol carbonate.

#### **2.4.6 Reaction of glycerol and urea using conventional heating (Chapter 6)**

In a typical catalytic test, glycerol (10 g, 108 mmol) was dried under a flow of nitrogen (60 ml/min) for 20 min at 150°C in a 3 neck 100 mL round-bottomed flask. Then urea (9.77 g, 162 mmol) was added, and once solubilised, catalyst (0.25 g) was added. The system was under flow of nitrogen to remove ammonia being formed and to shift the thermodynamic equilibrium. Reaction samples were taken every hour for 4 h. The product was analysed by HPLC to obtain conversion of glycerol and yield of glycerol carbonate.

#### **2.4.7 Reaction of glycerol and urea using microwave heating (Chapter 6)**

Glycerol (10 g, 108 mmol) was dried under a flow of nitrogen (60 ml/min) for 20 min at 150°C using microwave heating (200 W, high stirring). Urea (9.77 g, 162 mmol) was added and once solubilised the catalyst (0.25g) was added. 5 sets of reaction were tested: 30 min, 1 h, 2h, 3h and 4h. The product was analysed by HPLC to obtain conversion of glycerol and yield of glycerol carbonate.

#### **2.4.8 Chemical reactions in the synthesis of sorbitol carbonate (Chapter 7)**

##### **2.4.8.1 Synthesis of sorbitol carbonate from sorbitol and 1'-Carbonyldiimidazole (CDI)**

Sorbitol (1.09 g, 6 mmol) and CDI (3.89 g, 24 mmol) were dissolved in DMSO (10 mL) and was heated to 40°C. A flow of N<sub>2</sub> gas (100 ml/min) was passed through the reaction mixture to remove DMSO and the reaction was left stirring for 24 h.

After reaction work-up, the reaction product was analysed by IR,  $^1\text{H}$  NMR,  $^{13}\text{C}$  NMR and HPLC.

#### 2.4.9 Enzymatic reactions in the synthesis of sorbitol carbonate

Two types of enzyme were used in the enzymatic reaction:

- *Candida Antartica* immobilised on Immobead 150 recombinant from yeast named Lipase B. 2000 u/g
- Lipase acrylic resin from *Candida Antartica* (Novozyme 435). 5000 u/g

##### 2.4.9.1 Reaction of sorbitol and DMC in t-Butanol and DMSO (80:20)

Sorbitol (1.09 g, 6 mmol) and DMC (0.54 g, 6 mmol) were dissolved in a solvent mix of DMSO (2 mL) and *t*-BuOH (8 mL) in a 50 mL round bottomed flask and was heated to 40°C for 24 h with stirring. Then molecular sieves 4Å (2 g) and the enzyme (0.3 g) were also added to the mixture. Samples were taken at 0 h, 5 h and 24 h. After the reaction, the molecular sieves and the enzyme were removed by filtration. The final product was characterised using HPLC, FTIR, NMR and mass spectrometry.

##### 2.4.9.2 Reaction of sorbitol and DMC in t-Butanol and DMSO (20:80)

The reaction followed the same method as described in 2.4.9.1. Sorbitol and DMC were dissolved in a solvent mix of DMSO (8 mL) and *t*-BuOH (2 mL) with molecular sieves 4Å (2 g) and the enzyme (0.3 g) were added to the mixture. Samples were taken at 0 h, 5 h and 24 h. After reaction work-up, the reaction product was analysed.

#### 2.4.9.3 Reaction of sorbitol and DMC in *t*-Butanol and DMSO (50:50)

The reaction followed the same method as described in 2.4.9.1. Sorbitol and DMC were dissolved in a solvent mix of DMSO (5 mL) and *t*-BuOH (5 mL) with molecular sieves 4Å (2 g) and the enzyme (0.3 g) were added to the mixture. Samples were taken at 0 h, 5 h and 24 h. After reaction work-up, the reaction product was analysed.

#### 2.4.9.4 Solvent free reaction of sorbitol and DMC

Sorbitol (1.09 g, 6 mmol) and DMC (5.40 g, 60 mmol) were heated to 40°C for 24 h in a 50 mL round bottomed flask with stirring. Then molecular sieves 4Å (2 g) and the enzyme (0.3 g) were added. Samples were taken at 0 h, 5 h and 24 h. After reaction work-up, the reaction product was analysed.

#### 2.4.9.5 Solvent free reaction of sorbitol and DMC with silica gel act as a support

Sorbitol (1.09 g, 6 mmol) was heated to 110°C for 10 min, then silica (0.36 g, 6 mmol) was added into the hot sorbitol and was stirred for 10 min in 50 mL round bottomed flask. DMC (5.41 g, 60 mmol) and molecular sieves 4Å (2 g) were then added when the temperature was lowered to 60°C. The enzyme (0.3 g) was then added to the reaction mixture. Samples were taken at 0 h, 5 h and 24 h. After reaction work-up, the reaction product was analysed.

## 2.5 Product analysis

The reaction mixtures were determined and quantified using gas chromatography (GC), high-performance liquid chromatography (HPLC), nuclear magnetic resonance (NMR) and infrared spectroscopy (IR).

### 2.5.1 Gas chromatography (GC)

#### 2.5.1.1 Experimental

The products were analysed quantitatively using an Agilent series 7890A model with a Supelcowax 10 capillary column (30 m x 0.32 mm x 0.25  $\mu$ m) equipped with an auto sampler and flame ionisation detector (FID) shown in Figure 2-9. Internal and external calibration methods were used to quantify the products being formed and reactants being consumed which were identified using standard samples and obtained from Sigma-Aldrich.



Figure 2-9: Gas chromatography

### 2.5.1.2 Product concentration determination

#### 2.5.1.2.1 Synthesis of glycerol carbonate from CO<sub>2</sub> using acetonitrile as dehydrating agent

GC method: The initial temperature of the column was 50°C. The column temperature was ramped to 60°C at a heating ramp rate of 20°C/min and ramping the temperature to 270°C and was held for 3 min. The inlet port was held at 290°C with a pressure of 8.8 psi and a split ratio of 20:1. The flow of the column was 2 ml/min with average velocity of 33.98 cm/s. The carrier gas was nitrogen. The total run was 6.66 min.

External standard method was used to calibrate reaction products for this reaction. Four standards of known concentration were injected into the GC and 1 µL of sample was injected into the GC four times. The calibration plots showed a linear response for each chemical shown in Table 4. The calibration profiles of the products can be found in the appendix.

**Table 4: Retention times and calibration curve obtained for standards used in direct carbonylation reaction of glycerol with CO<sub>2</sub>**

<b>Chemical</b>	<b>Retention times (min)</b>	<b>Equation</b>	<b>R<sup>2</sup></b>
Glycerol	4.71	$y=0.0013x + 0.1$	0.99907
<b>Glycerol carbonate</b>	<b>2.94</b>	<b><math>y=0.0022x + 0.0173</math></b>	<b>0.9991</b>
Triacetin	4.12	$y=0.0014x + 0.00627$	0.9653
<b>Diacetin</b>	<b>4.45</b>	<b><math>y=0.0011x + 0.0688</math></b>	<b>0.9734</b>
Monoacetin	4.58	$y=0.0036x + 0.076$	0.9709
<b>Methanol</b>	<b>1.78</b>	-	-

#### 2.5.1.2.2 Synthesis of glycerol carbonate from CO<sub>2</sub> using 2-cyanopyridine as dehydrating agent

GC method: The initial temperature of the column was 50°C. The column temperature was ramped to 100°C at a heating ramp rate of 20°C/min and held for 2 min. The ramping then increased to 160°C and at a heating ramp rate of 10°C/min and held for 2 min. The temperature of the column was raised again to 200°C at heating ramp rate of 10°C/min and held for 1 min. Finally ramping the column temperature to 220°C at a heating ramp rate of 50°C/min and held for 1 min. The inlet port was held at 290°C with a pressure of 15.179 psi and a split ratio of 5:1. The flow of the column was 4 ml/min with average velocity of 57.04 cm/s. The carrier gas was nitrogen. The total run was 26.4 min.

Internal standard method was used to calibrate reaction products for this reaction. Five standards of known concentration were injected into the GC and 1 µL of sample was injected into the GC four times. The calibration plots showed a linear response for each chemical shown in Table 5. The calibration profiles of the products can be found in the appendix.

**Table 5: Retention times and calibration curve obtained for standards used in direct carbonylation reaction of glycerol with CO<sub>2</sub>**

Chemical	Retention times (min)	Equation	R <sup>2</sup>
Glycerol	20.67	y=16.501x + 0.7666	0.9999
Glycerol carbonate	25.81	y=26.866x - 0.1586	0.9998
Diethylene glycol monomethyl ether	5.19	-	-
2-cyanopyridine	9.80	y=6.5691x - 1.6126	0.997



2-picolinamide	21.38	$y=6.0239 + 0.4965$	0.9994
DMF	3.37		

## 2.5.2 High performance liquid chromatography (HPLC)

### 2.5.2.1 Experimental

The products were analysed using Agilent 1200 series equipped with an inline degasser, quaternary pump, an auto sampler, RID and Varian Metacarb 67H column (300 x 6.5 mm) shown in Figure 2-10. The mobile phase solution is sulphuric acid (2.8 mM) with a flow rate of 0.8 mL/min. The total run time was 30 min.



Figure 2-10: High liquid gas chromatography

### 2.5.2.2 Product concentration determination in the synthesis of glycerol carbonate from glycerol and urea

External standard method was used to calibrate reaction products for this reaction. Four standards of known concentration were injected into the HPLC and 1  $\mu\text{L}$  of sample was injected into the HPLC four times. The calibration plots showed a linear response for each chemical shown in Table 6. The calibration profiles of the products can be found in the appendix.

**Table 6: Retention times and calibration curve obtained for standards used in direct carbonylation reaction of glycerol with  $\text{CO}_2$**

<b>Chemical</b>	<b>Retention times (min)</b>	<b>Equation</b>	<b><math>R^2</math></b>
<b>Glycerol</b>	7.30	$y=7\text{E-}06x - 0.2388$	0.9998
<b>Glycerol carbonate</b>	10.00	$y=7\text{E-}06x + 0.2299$	0.9999

### 2.5.3 Quadrupole Time of Flight Liquid Chromatography Mass Spectroscopy (Q-TOF LC/MS)

#### 2.5.3.1 Experimental

The Q-ToF data was obtained on an Agilent XX system equipped with a Thermo Scientific Accucore-150-amide HILIC column (mm) 100 x 2.1 and quadrapolar time of flight detector Agilent 6530b Accurate Mass QTOF LC/MS. The mobile phase was 0.1% formic acid in nanopure water and 0.1% formic acid in acetonitrile using a gradient to 85% acetonitrile with a flow rate of 0.400 mL/min for 15 min.

### 2.5.4 Fourier Transform Infrared Spectroscopy (FTIR)

#### 2.5.4.1 Experimental

FTIR analysis was performed on a Perkin-Elmer 100 series Spectrometer to determine functional groups in the sample products shown in Figure 2-11. FT-IR spectra with a resolution of  $4\text{cm}^{-1}$ , 10 scans per analysis, and in the range of 4000-650  $\text{cm}^{-1}$  were taken after background spectrum was collected, then placing a

droplet in the sampling plate at room temperature and same parameters were used as for background. All samples were analysed without any pretreatment.



**Figure 2-11: Pelkin-Elmer 100 series spectrometer**

## **2.5.5 Nuclear Magnetic Resonance (NMR)**

### **2.5.5.1 Experimental**

$^1\text{H}$  NMR and  $^{13}\text{C}$  NMR spectra were recorded at 400.61 MHz on a Bruker Avance III HD 400 against a TMS internal standard at ambient temperature using standard power-gated decoupling program with 30° pulse angle and 2 s interpulse delay. Chemical shifts ( $\delta$ ) are given in parts per million (ppm), and coupling constants ( $J$ ) are given in Hertz (Hz). The external standard used for NMR analysis was DMSO.

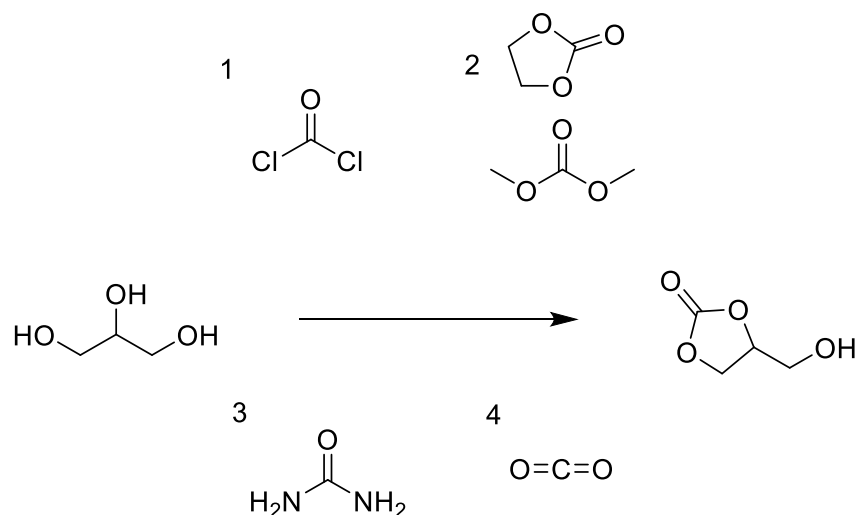
# **CHAPTER 3**

## **DIRECT SYNTHESIS OF GLYCEROL CARBONATE FROM GLYCEROL AND CARBON DIOXIDE CATALYSED BY COPPER SUPPORTED ON LANTHANUM OXIDE USING DIFFERENT DEHYDRATING AGENTS**

### 3 DIRECT SYNTHESIS OF GLYCEROL CARBONATE FROM GLYCEROL AND CARBON DIOXIDE CATALYSE BY COPPER SUPPORTED ON LANTHANUM OXIDE USING DIFFERENT DEHYDRATING AGENTS

#### 3.1 Introduction

There are four main methods that have been reported in the literature for the synthesis of glycerol carbonate using different carbonyl sources either by direct synthetic routes or indirect synthetic routes. The synthesis of glycerol carbonate can be summarised in Scheme 3-1.



**Scheme 3-1: Synthesis of glycerol carbonate via different chemical**

The first reported attempt for synthesising glycerol carbonate from glycerol and carbon dioxide used Amberlyst and zeolites with supercritical carbon dioxide, but no product was formed. However, when adding ethylene carbonate, the yield of glycerol carbonate reached 32% and they concluded that carbon dioxide alone was

not a carbonate source for the reaction.<sup>151</sup> Tin complexes were used as a homogeneous catalyst by Aresta *et al* through the tin-glycerol complex as an intermediate giving a 6% yield and the yield was reported to increase to 35% with the addition of methanol.<sup>135,152</sup>  $\text{CeO}_2/\text{Al}_2\text{O}_3$  and  $\text{CeO}_2/\text{NbO}_5$  were used as a catalyst with tetraethylene glycol dimethyl ether (TEGDME) as a solvent was employed in the carbonylation of glycerol to glycerol carbonate giving a very low yield of 2.5%.<sup>132</sup> Another method was by employing triethylamine as  $\text{CO}_2$  activation as well as a solvent giving a high yield of glycerol carbonate through a glycerol derivative, 3-chloro-1,2-propanediol.<sup>153</sup> Recently lanthanides based catalysts have been employed in direct carbonylation of glycerol with  $\text{CO}_2$ . The yield of glycerol carbonate was increased to 15% when using La-Zn mixed oxides due to the formation of the  $\text{La}_2\text{O}_2\text{CO}_3$  phase which is responsible for the presence of medium basic sites where  $\text{CO}_2$  adsorption takes place.<sup>154</sup> La modified Zn-Al hydrotalcite with halogen anions shows high catalytic activities due to large surface area of the catalyst by incorporation of halogen anions. The highest glycerol carbonate yield being achieved in the reaction was 16% with the presence of  $\text{Cl}^-$  anions. However, the catalyst basicity decreases due to the formation of LaOF and LaOCl phases in the catalyst.<sup>156</sup> Zhang *et al* employed copper supported on  $\text{La}_2\text{O}_3$  as heterogeneous catalyst and the glycerol carbonate yield reached 14%. They proposed that Cu metal has the ability to activate  $\text{CO}_2$  by inserting itself into Cu/ $\text{La}_2\text{O}_3$  bond forming a ligand complex.<sup>155</sup>  $\text{CeO}_2$  catalysts prepared by hydrothermal synthesis gave the highest yield of glycerol carbonate compared to precipitation and citrate sol-gel method and the preparation methods produced three different kinds of morphologies. The high yield and conversion can be contributed to the redox properties of nanorods  $\text{CeO}_2$ , acid-base properties as well as its high surface area.<sup>215</sup>

In this work, the performances of different dehydrating agents were investigated in the direct synthesis of glycerol carbonate. Copper supported on lanthanum based heterogeneous catalysts were tested and examined in detail on its catalytic performance as well as its role in  $\text{CO}_2$  activation. The effects of copper loading were also being investigated as well as the relationship between the catalytic performances.

## 3.2 Results and Discussion

### 3.2.1 Catalyst characterisation

#### 3.2.1.1 Structural characterisation studies

The samples were characterised using XRD to identify any crystallographic phases present on the materials.  $\text{La}_2\text{O}_3$  (ICDD 05-0602) can be obtained by thermal decomposition of  $\text{La}(\text{OH})_3$  (ICDD 36-1481).<sup>236</sup>  $\text{La}_2\text{O}_3$  is known to be very sensitive and reacts readily with  $\text{CO}_2$  and  $\text{H}_2\text{O}$  in ambient air producing bulk hydroxyl, carbonate and mixed phases; the system undergoes phase changes during heat treatment and under vacuum.<sup>237,238,239</sup> The  $\text{La}(\text{OH})_3$  phase has the tendency to adsorb moisture in air at the surface of the powder and  $\text{La}(\text{OH})_3$  reacts with  $\text{CO}_2$  from the atmosphere to form the carbonate species by a process called carbonation.<sup>236,238</sup> Removal of carbonates needs heating as they are known to be inert to reaction.<sup>239</sup> A higher temperature is then required to obtain pure  $\text{La}_2\text{O}_3$  if the carbonate phase,  $\text{La}_2\text{O}_2\text{CO}_3$  (ICDD 48-1113), are present in the precursor,  $\text{La}(\text{OH})_3$ .<sup>236</sup> The principle diffraction peaks for  $\text{La}(\text{OH})_3$  are at  $15.6^\circ$ ,  $27.2^\circ$  and  $27.9^\circ$  which corresponds to 100, 110 and 101 planes respectively. The amount of hydroxide and carbonate phases varies in every preparation due to different atmospheric conditions in every preparation. According to Wang *et al*, the carbonate phases decomposed at  $350^\circ\text{C}$  whereas the hydroxyl phases decomposed at  $700^\circ\text{C}$ .<sup>240</sup> However, Klingenberg *et al* reported quite the opposite results in which the hydroxyl phases decomposed at  $350^\circ\text{C}$  and carbonate phases decomposed at  $700^\circ\text{C}$ .<sup>237</sup>

Figure 3-1 shows the XRD patterns of  $\text{La}_2\text{O}_3$  after calcination at different temperatures. The carbonate phase,  $\text{La}_2\text{O}_2\text{CO}_3$ , can be observed appearing at  $500^\circ\text{C}$  but is lost at  $700^\circ\text{C}$  and  $900^\circ\text{C}$ .  $\text{La}_2\text{O}_2\text{CO}_3$  diffraction peaks can be observed at  $10.9^\circ$ ,  $22.2^\circ$ ,  $25.8^\circ$ ,  $30.3^\circ$ ,  $33.6^\circ$  and  $44.5^\circ$  which correspond to 002, 004, 101, 103, 006 and 106 planes respectively. Table 7 shows the lattice parameters and the particle

sizes of  $\text{La}_2\text{O}_3$  calcined at three different temperatures. The crystallite size of  $\text{La}_2\text{O}_3$  can be calculated using Scherrer's equation from the XRD data. The average crystallite size of  $\text{La}_2\text{O}_3$  at  $500^\circ\text{C}$  is 4.8 nm. The average crystallite size of  $\text{La}_2\text{O}_3$  at  $700^\circ\text{C}$  is 9.2 nm. It can be observed that the calcination product after heat treatment at  $900^\circ\text{C}$  consists of pure  $\text{La}_2\text{O}_3$ .  $\text{La}_2\text{O}_3$  diffraction peaks can be observed at  $26.1^\circ$ ,  $29.1^\circ$ ,  $29.9^\circ$ ,  $39.5^\circ$ ,  $46.0^\circ$ ,  $53.6^\circ$  and  $55.8^\circ$ , which correspond to 100, 022, 011, 012, 110, 200 and 201 planes respectively. The average crystallite size of  $\text{La}_2\text{O}_3$  at  $900^\circ\text{C}$  is 14.8 nm. Pure  $\text{La}_2\text{O}_3$  can be obtained when the calcination temperature reached  $750^\circ\text{C}$ .<sup>240</sup> Both  $\text{La}_2\text{O}_2\text{CO}_3$  and  $\text{La}_2\text{O}_3$  are having a hexagonal crystal structure which has been reported by Wang *et al.*<sup>240</sup> The diffraction peaks of  $\text{La}_2\text{O}_3$  become narrowed as an increase in calcination temperature from an amorphous structure to crystalline structure. This indicates crystallite growth of  $\text{La}_2\text{O}_3$  and gradual bulk sintering of the oxides, which in accordance to BET results shown in Table 10.

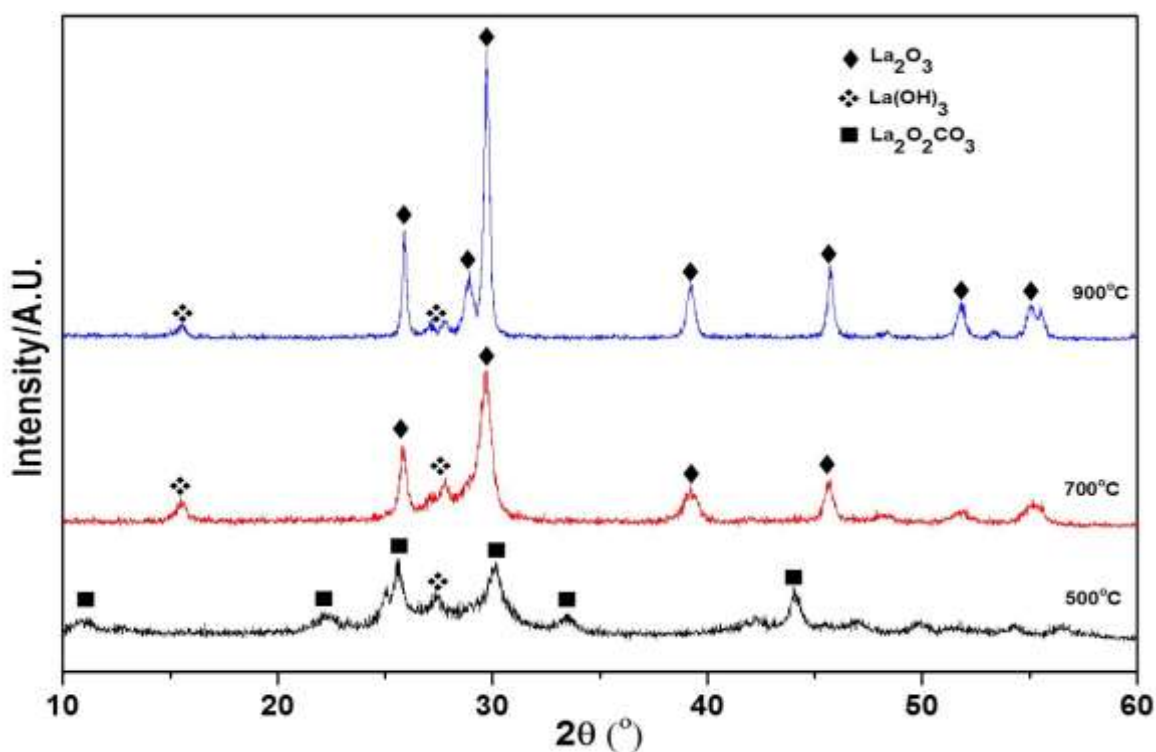


Figure 3-1: XRD patterns of the calcination product of dried powder of  $\text{La}_2\text{O}_3$  at different temperature of  $500^\circ\text{C}$ ,  $700^\circ\text{C}$  and  $900^\circ\text{C}$



**Table 7: Lattice parameters and particle size of La<sub>2</sub>O<sub>3</sub> at different calcination temperature**

Catalyst	Lattice parameters	Particle size
<b>La<sub>2</sub>O<sub>3</sub>-500°C</b>	a=4.0 Å	4.8 nm
	b=4.0 Å	
	c=16.3 Å	
<b>La<sub>2</sub>O<sub>3</sub>-700°C</b>	a=3.9 Å	9.2 nm
	b=3.9 Å	
	c=6.1 Å	
<b>La<sub>2</sub>O<sub>3</sub>-900°C</b>	a=3.9 Å	14.8 nm
	b=3.9 Å	
	c=6.1 Å	

The high reactivity of these materials is due to strong basicity of the oxide which brings about hydroxylation and carbonation.<sup>239</sup> The system is very dynamic and La<sub>2</sub>O<sub>3</sub> readily reacts with H<sub>2</sub>O producing La(OH)<sub>3</sub> via an intermediate LaOOH.<sup>241</sup> Figure 3-2 shows how the diffraction peaks of La(OH)<sub>3</sub> can be seen at the temperature of 900°C and disappear when the powder was degassed under vacuum to remove water present. This indicates that hydroxylation is a reversible process therefore heating the material can restore back to pure oxide phase but this caused an increase in crystallite size due to sintering.<sup>239</sup> Proper care must be taken into account during heat treatment and storage as exposure to atmospheric air which leads to bulk hydroxylation and carbonation.<sup>237</sup> Therefore in order to prevent carbonation to take place, the material must be placed and stored in a CO<sub>2</sub>-free protective gas atmosphere such as in argon.<sup>242</sup>

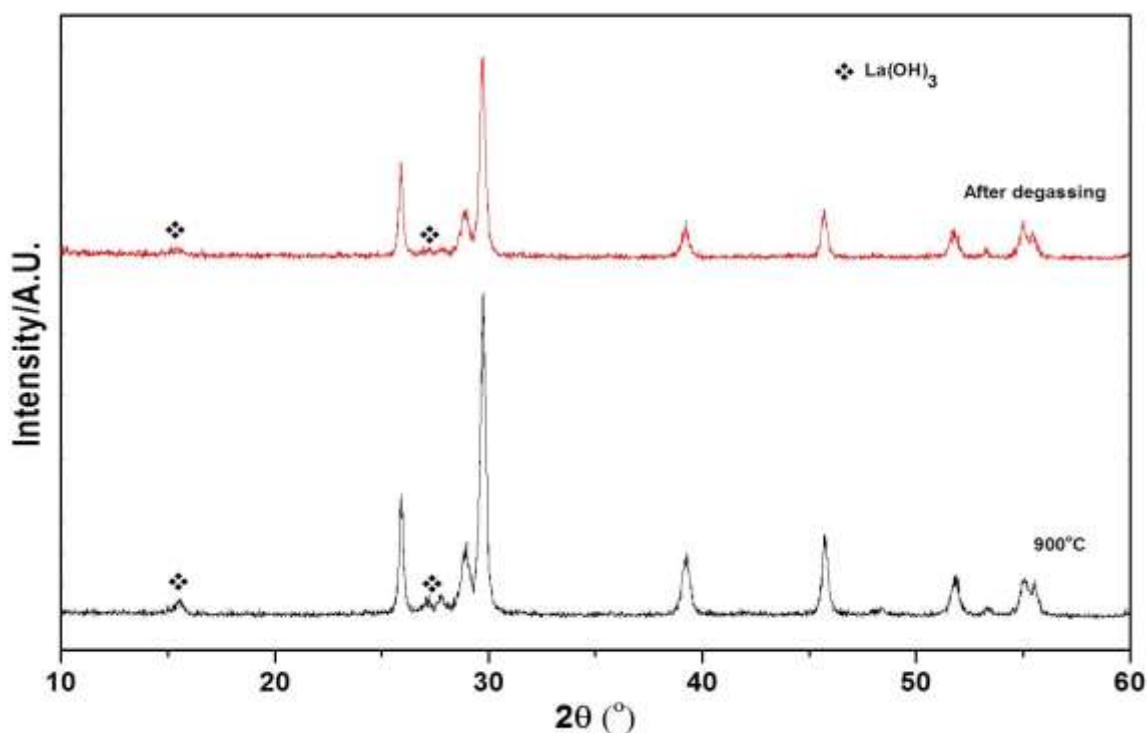
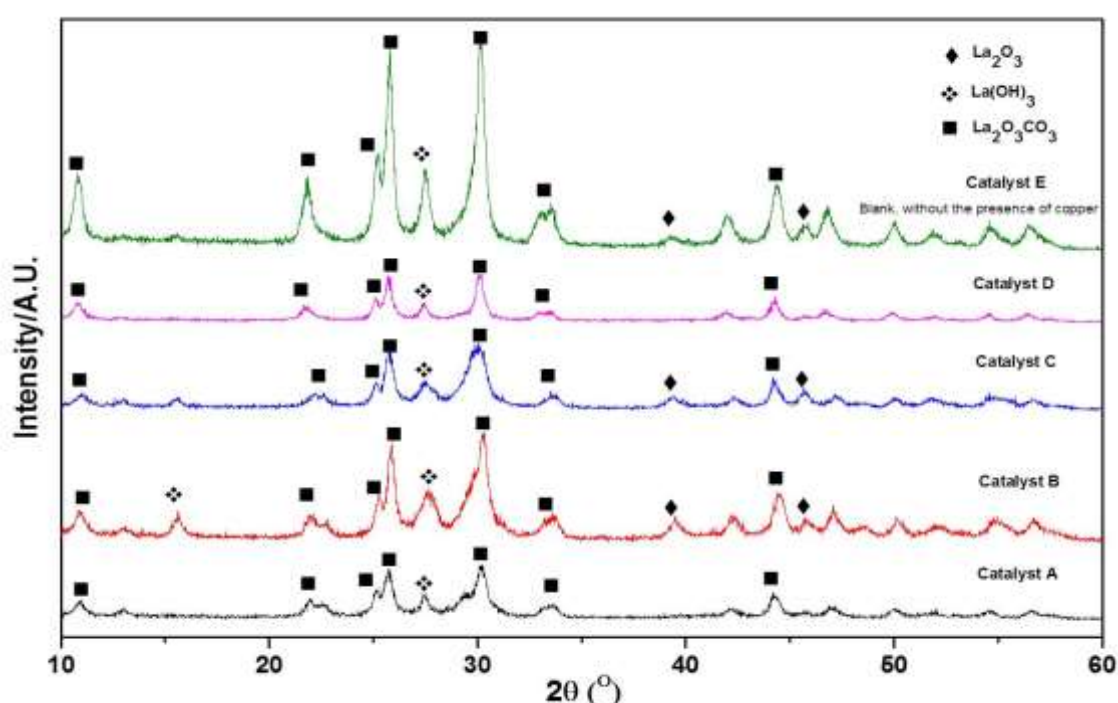


Figure 3-2: XRD patterns of  $\text{La}_2\text{O}_3$  after degassing at  $120^\circ\text{C}$  under vacuum

Metal impregnation is widely used to generate metal supported catalysts. The impregnation of metals into  $\text{La}_2\text{O}_3$  would chemically change the structural arrangements of the support as  $\text{La}_2\text{O}_3$  is highly reactive to water.<sup>241</sup> Impregnation of the aqueous solution of copper nitrate into the support followed by calcination at  $300^\circ\text{C}$  and reduction at  $450^\circ\text{C}$  generated two recognisable phases,  $\text{La}(\text{OH})_3$  phase and  $\text{La}_2\text{O}_2\text{CO}_3$  phase. The most dominant phase that can be observed on Figure 3-3 is the  $\text{La}_2\text{O}_2\text{CO}_3$  phase. This implies that impregnation step can generate further carbonation of the catalysts. It has also being reported that the amount of carbonate present is higher during impregnation as compared to leaving the oxide in air for some time.<sup>243</sup> The nucleation of carbonate phase is therefore associated with the wetting treatment rather than the drying treatment.<sup>243,244</sup> The effect also being observed with rhodium metal being supported on lanthana, however, this effect was not observed on samaria and ytterbia supports.<sup>244</sup> The formation of carbonates reduced the crystallinity of the powder which is caused by the interaction of hydroxide and oxide with  $\text{CO}_2$  due to its basic nature which was mentioned previously and the crystallinity can be observed on the XRD data.<sup>245,246</sup> In spite of the reports and evidences obtained, Zhang *et al* did not report these

findings in their catalysts; only the presence of  $\text{La}(\text{OH})_3$  phase which is due to interaction of  $\text{La}_2\text{O}_3$  with water during impregnation process and subsequent reduction step.<sup>155</sup> Four reproductions doped with 2.3 wt% copper were performed and Figure 3-3 shows that the catalysts are reproducible (catalyst A-D). Catalyst E is the bare support without copper that has undergone the same heat treatment as the other catalysts. The  $\text{La}_2\text{O}_3$  peaks shift slightly to the right with the impregnation of copper into the support. Copper metal is expected to be in the prepared catalyst as the catalyst undergoes the heat treatment under hydrogen atmosphere at 450°C for 2 h with a flow rate of 10 mL/min. The copper metal loading is measured using EDX analysis.  $\text{CuO}$  and  $\text{Cu}_2\text{O}$  reflections could not be observed in the XRD patterns of the catalyst.



**Figure 3-3: XRD patterns of 2.3wt% Cu/ $\text{La}_2\text{O}_3$  reproductions after hydrogen reduction (catalyst A-D). Catalyst E -was reduced catalyst with copper (blank)**

Table 8 displays the lattice parameters of 2.3 wt% Cu/ $\text{La}_2\text{O}_3$  as well as its particle sizes. 2.3 wt% Cu/ $\text{La}_2\text{O}_3$  catalysts have the same lattice parameters as  $\text{La}_2\text{O}_3$ -500°C. This is due to the catalyst undergoing impregnation process and heat treatment at 450°C under hydrogen atmosphere which leads to the formation of carbonate phase which was mentioned earlier. The particle sizes are higher than  $\text{La}_2\text{O}_3$ -700°C

which can be attributed to three heat treatments explained in experimental section, Chapter 2.

**Table 8: Lattice parameters and particle size of 2.3 wt% Cu/La<sub>2</sub>O<sub>3</sub>**

Catalyst	Lattice parameters	Particle size
<b>Catalyst A</b>	a=4.0 Å	12.8 nm
	b=4.0 Å	
	c=16.2 Å	
<b>Catalyst B</b>	a=3.9 Å	11.8 nm
	b=3.9 Å	
	c=16.3 Å	
<b>Catalyst C</b>	a=3.9 Å	12.6 nm
	b=3.9 Å	
	c=16.1 Å	
<b>Catalyst D</b>	a=4.0 Å	12.1 nm
	b=4.0 Å	
	c=15.9 Å	
<b>Catalyst E</b>	a=4.0 Å	11.9 nm
	b=4.0 Å	
	c=16.2 Å	

Zhang *et al* reported that they observed diffraction peaks of copper above 6.9 wt% Cu/La<sub>2</sub>O<sub>3</sub>. However diffraction peaks of copper metal were not observed on the XRD patterns shown in **Error! Reference source not found.** until the amount of copper loading was 13.9 wt% Cu/La<sub>2</sub>O<sub>3</sub>. This could be due to copper particles being highly dispersed and too small to be detected or copper particles could be

intercalated within the framework of the support. The size of the crystallite copper was 9.0 nm calculated from the peak at  $2\theta=43.1^\circ$  using Scherrer formula shown in **Error! Reference source not found..** The increase in loading for Cu/La<sub>2</sub>O<sub>3</sub> does not change the lattice parameters of the catalyst and its particle size which can be shown in Table 9.

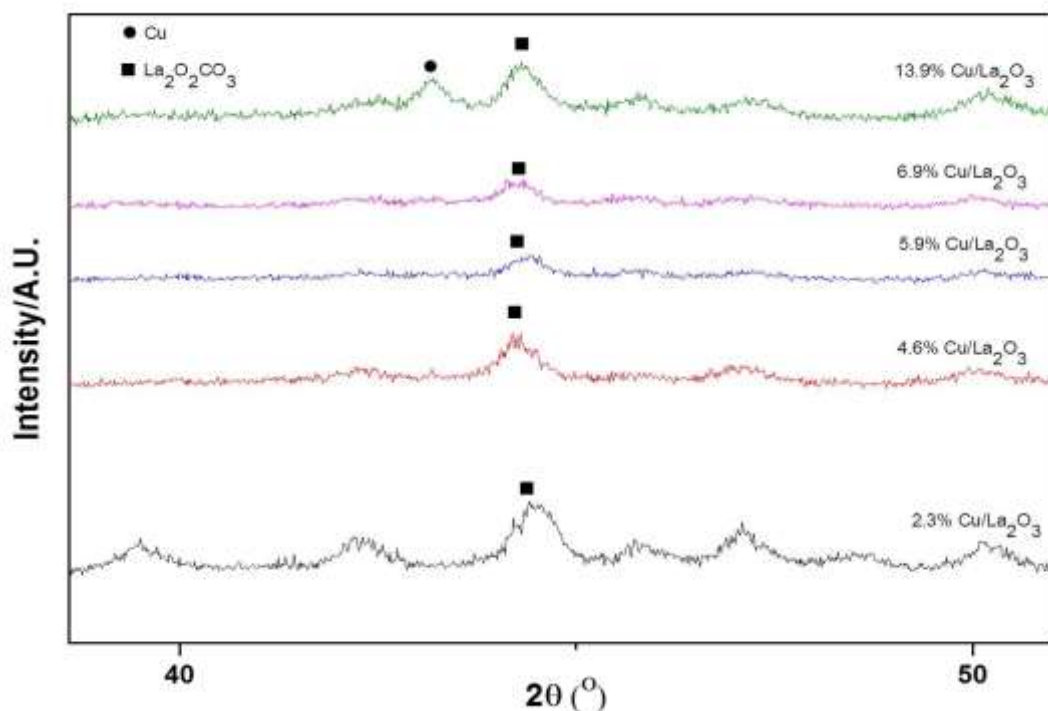


Figure 3-4: XRD patterns of Cu/La<sub>2</sub>O<sub>3</sub> catalysts with different copper loadings

Table 9: Lattice parameters and particle size of 2.3 wt% Cu/La<sub>2</sub>O<sub>3</sub> and 13.9 wt% Cu/La<sub>2</sub>O<sub>3</sub>

Catalyst	Lattice parameters	Particle size
2.3 wt% Cu/La <sub>2</sub> O <sub>3</sub>	a=4.0 Å	12.0 nm
	b=4.0 Å	
	c=16.0 Å	
13.9 wt% Cu/La <sub>2</sub> O <sub>3</sub>	a=3.9 Å	11.8 nm
	b=3.9 Å	
	c=15.9 Å	

Figure 3-5 shows the XRD patterns of reduced 2.3 wt% Cu/La<sub>2</sub>O<sub>3</sub> with peak prediction of several copper phases. There are four possible states of copper that can exist in the material according to their oxidation states. There are Cu<sub>2</sub>O (ICDD 00-001-1142), CuO (ICDD 00-002-1040) and Cu (ICDD 01-085-1326) which corresponds to +1, +2 and 0 oxidation state respectively. The last possible phase is CuLa<sub>2</sub>O<sub>4</sub> (ICDD 01-079-0351) that could appear in the XRD patterns. However all these phases of copper in any oxidation states are not present in the XRD patterns. The most intense reflections for all the copper phases are in the region of 30-45° 2θ. Cu/La<sub>2</sub>O<sub>3</sub> does not show any strong reflection in this region.

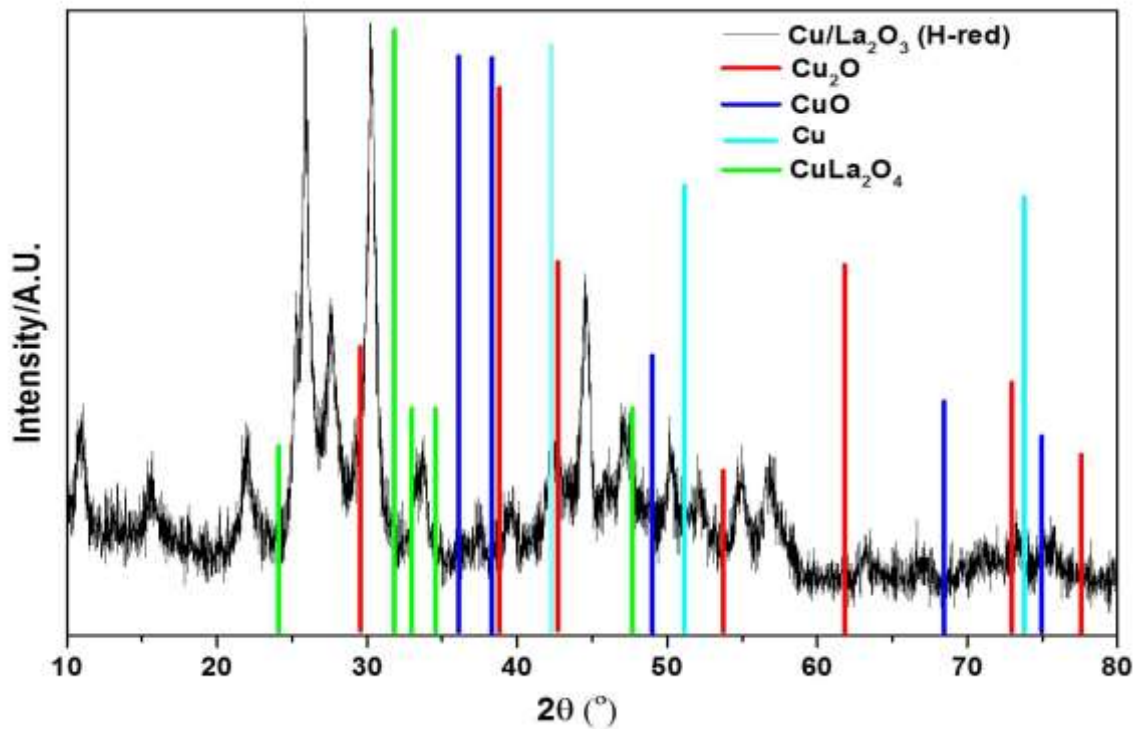
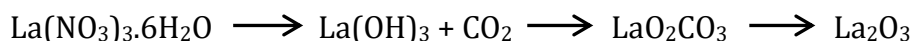


Figure 3-5: XRD patterns of 2.3 wt% Cu/La<sub>2</sub>O<sub>3</sub> with peak prediction of several phases of copper

### 3.2.1.2 Thermogravimetric analysis (TGA)

Scheme 3-2 shows the general reaction scheme of the catalyst at different calcination temperatures. TGA analysis was performed on the thermal decomposition of  $\text{La}_2\text{O}_2\text{CO}_3$  shown in Figure 3-6 in which there is three significant weight losses at three temperature intervals. The first weight loss was 3.11% due to the loss of surface absorptive water below 200°C. The second weight loss step was 12% at 350°C. This corresponds to the decomposition of precursor and the formation of  $\text{La}_2\text{O}_2\text{CO}_3$  by the reaction between  $\text{CO}_2$  and  $\text{La}(\text{OH})_3$  which also being reported in the literature.<sup>247</sup> The last step of thermal decomposition of  $\text{La}_2\text{O}_2\text{CO}_3$  is at 550°C with a weight loss of 9%. This is when  $\text{La}_2\text{O}_2\text{CO}_3$  is being transformed into  $\text{La}_2\text{O}_3$  with a subsequent release of  $\text{CO}_2$  from the carbonate.<sup>248</sup> This change in phase can also be monitored using temperature-dependent X-ray diffraction (HT-XRD).<sup>242</sup> Alternatively, IR spectroscopy can be used to detect different absorption bands of the samples.



**Scheme 3-2: Reaction scheme of the precursor undergoing different heat treatment**

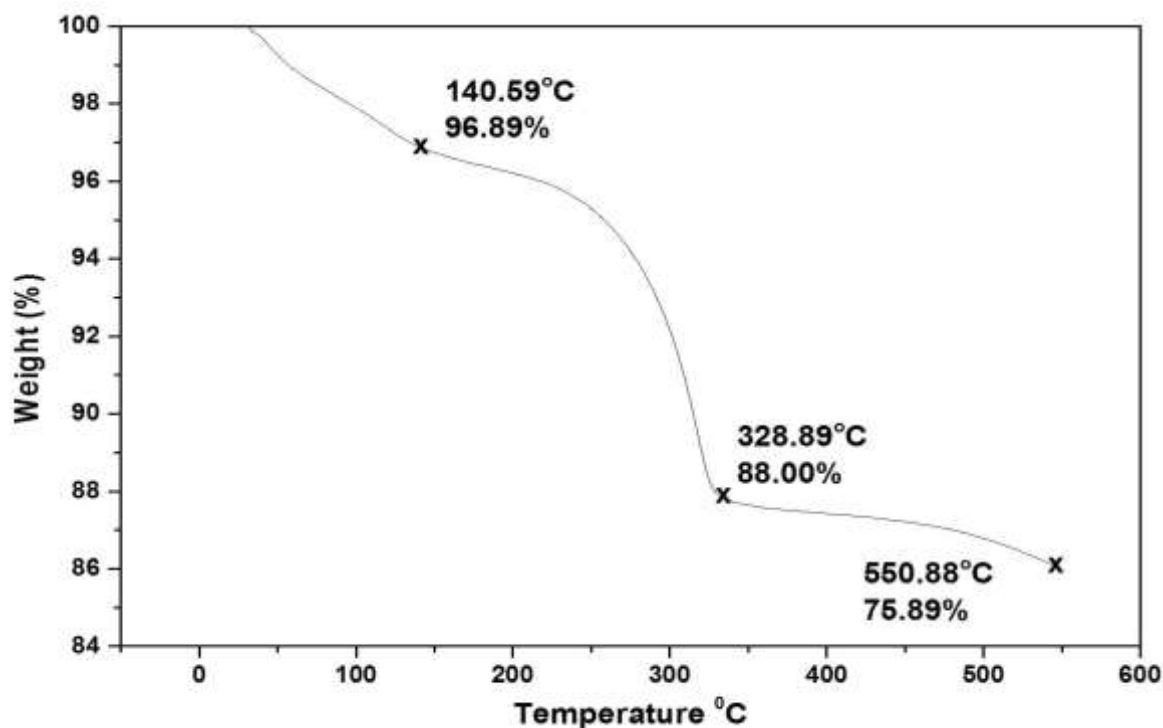


Figure 3-6: Thermogravimetric analysis of precursor

### 3.2.1.3 Characterisation of N<sub>2</sub> adsorption

La<sub>2</sub>O<sub>3</sub> has a perovskite structure and is known to be a very stable mixed oxide but with a low surface area. There are many ways to increase surface area of La<sub>2</sub>O<sub>3</sub> and several attempts have been made such as using saturated fatty acids in the presence of ethylenediamine or by templating the support with high surface area material such as polystyrene beads (PS) to obtain larger dispersion of copper metal loadings and more basic sites for gas adsorption.<sup>249,250</sup> In this case, polystyrene beads were used as a template to increase surface area of the catalyst.

BET surface areas and pore volumes of Cu/La<sub>2</sub>O<sub>3</sub> at different Cu loadings and bare La<sub>2</sub>O<sub>3</sub> calcined at different temperature were determined and summarised in Table



10. As calcination temperature increased, the surface area decreased. This can be observed with  $\text{La}_2\text{O}_3$  undergoes heat treatment at  $900^\circ\text{C}$  (entry 9) and having a surface area of  $2 \text{ m}^2 \text{ g}^{-1}$  with a crystalline structure from narrowed diffraction peaks, which can be observed from the XRD patterns in Figure 3-1.  $\text{La}_2\text{O}_3$  after heat treatment at  $500^\circ\text{C}$  (entry 7) has a high surface area of  $50 \text{ m}^2 \text{ g}^{-1}$ , which gives rise to an amorphous structure that can be shown on the XRD patterns. Pore volume decreased as well. Similarly, Klingenberg *et al* reported similar results, in which pure  $\text{La}_2\text{O}_3$  shows low surface area compared to the other catalyst with different phases due to increase in crystallinity and gradual bulk sintering.<sup>237</sup> The surface area of the catalyst against temperature can be summarised in Figure 3-7. Templating  $\text{La}_2\text{O}_3$  with polystyrene beads (entry 6) did not increase the surface area and the pore volume significantly decreased after calcining at  $700^\circ\text{C}$ . Removing the PS templates by calcination in air caused the internal pores of  $\text{La}_2\text{O}_3$  to collapse.

BET surface areas of  $\text{Cu}/\text{La}_2\text{O}_3$  and the bare support,  $\text{La}_2\text{O}_3$  at  $700^\circ\text{C}$  (entry 8) were determined and were as high as  $31 \text{ m}^2 \text{ g}^{-1}$ . Zhang reported that the surface area to be around  $20 \text{ m}^2 \text{ g}^{-1}$ .<sup>155</sup> The impregnation of Cu into the support did not reduce the surface area of the support until it reached 6.9 wt%, where the surface area decrease from 31 to  $28 \text{ m}^2 \text{ g}^{-1}$ . Pore volume significantly decreased once the Cu loading reached 13.9 wt%. The error for BET analysis measurement is 2%.

**Table 10: Textural properties of  $\text{Cu}/\text{La}_2\text{O}_3$  and bare support  $\text{La}_2\text{O}_3$**

Entry	Catalysts	Surface area ( $\text{m}^2 \text{ g}^{-1}$ )	Pore Volume ( $\text{cm}^3 \text{ g}^{-1}$ )
1	2.3% $\text{Cu}/\text{La}_2\text{O}_3$	31	0.13
2	4.6% $\text{Cu}/\text{La}_2\text{O}_3$	31	0.13
3	5.9% $\text{Cu}/\text{La}_2\text{O}_3$	31	0.16
4	6.9% $\text{Cu}/\text{La}_2\text{O}_3$	28	0.14
5	13.9% $\text{Cu}/\text{La}_2\text{O}_3$	25	0.09

6	La <sub>2</sub> O <sub>3</sub> (PS)	30	0.05
7	La <sub>2</sub> O <sub>3</sub> 500°C	50	0.30
8	La <sub>2</sub> O <sub>3</sub> 700°C	32	0.19
9	La <sub>2</sub> O <sub>3</sub> 900°C	2	0.10

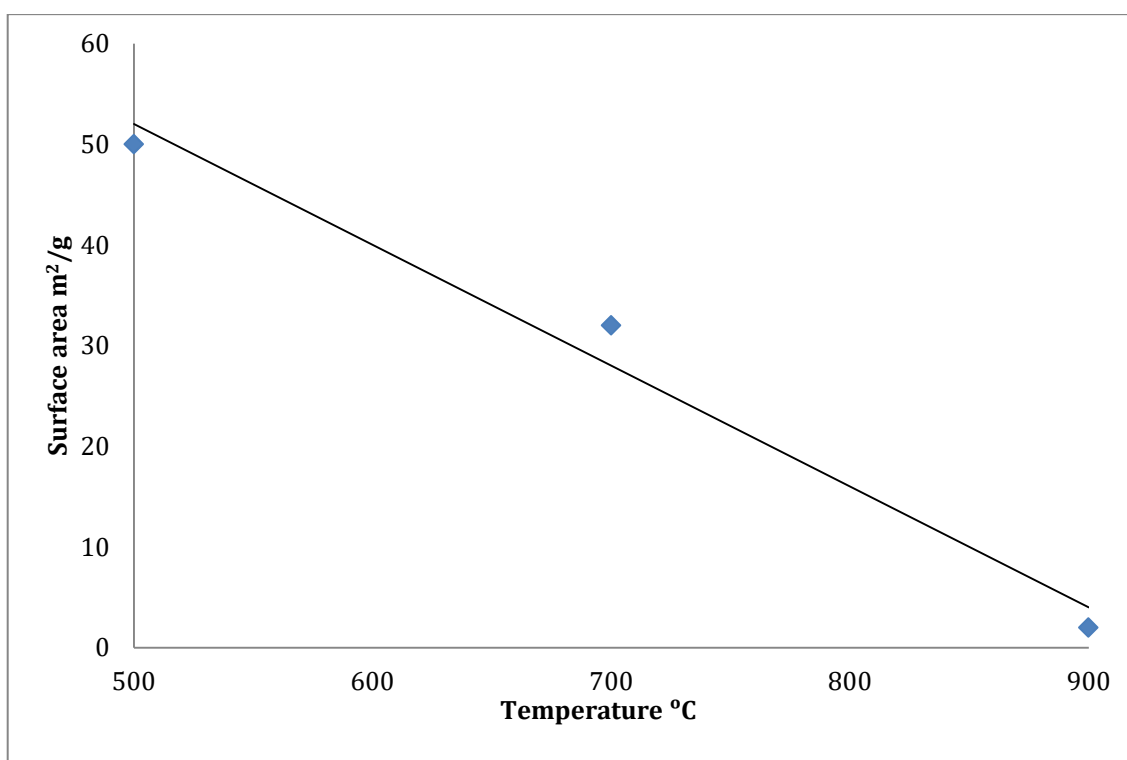
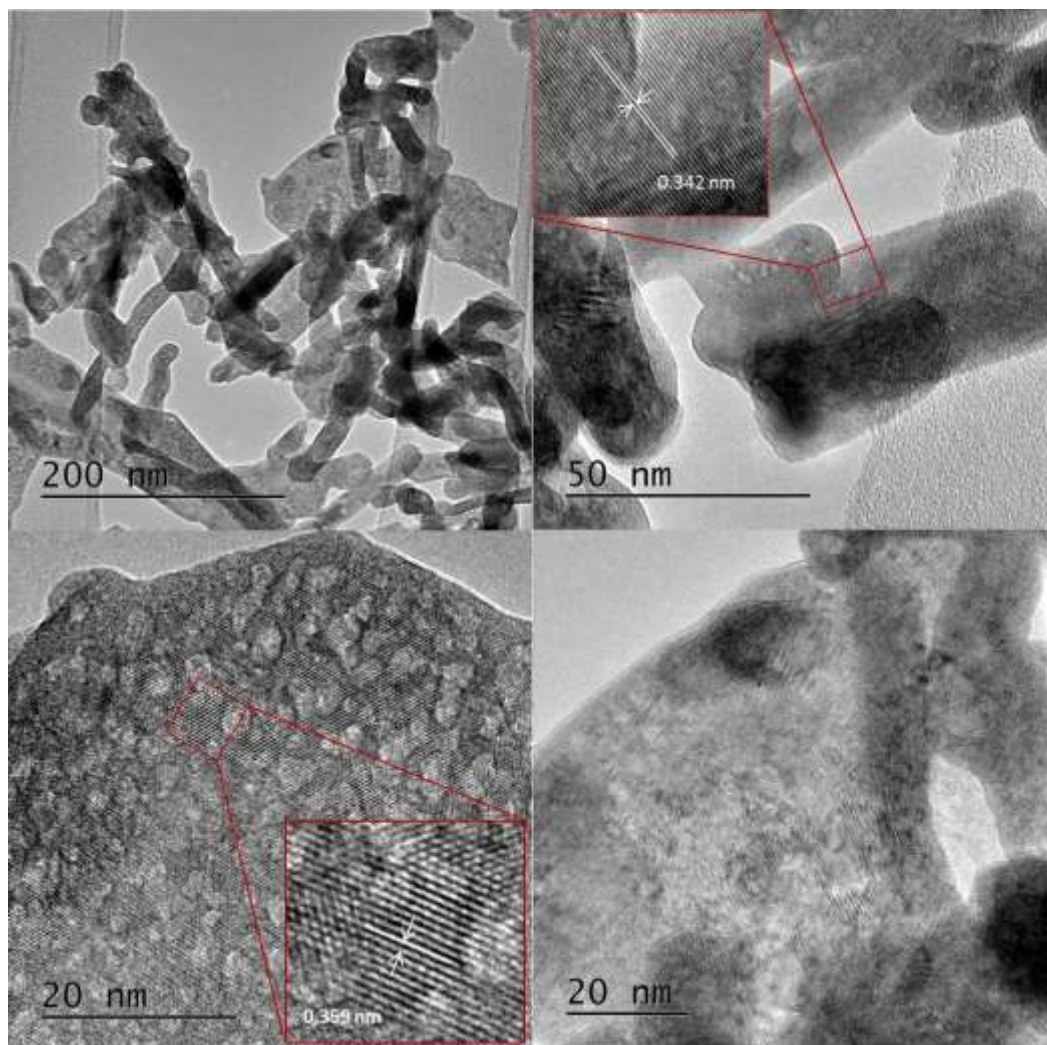


Figure 3-7: The graph of surface area of La<sub>2</sub>O<sub>3</sub> against temperature

#### 3.2.1.4 Morphology of the catalysts-TEM

The morphology of synthesised La<sub>2</sub>O<sub>3</sub> was observed using transmission electron microscopy (TEM) shown in Figure 3-8. The La<sub>2</sub>O<sub>3</sub> support has irregular shape and size rod-like structure with an interplanar spacing of 0.35 nm along the rod and was also reported by Zhang *et al*, which was due to self-assembly process of

$\text{La}^{3+}$ .<sup>155,251</sup> Others have reported observing spherical nanoparticles, nanotubes, nanowires, nanocubes and 3D bundles of  $\text{La}_2\text{O}_3$  which can be attributed to different preparation method.<sup>236,240,252,253,254</sup> The advantage of using CTAB as a templating agent in synthesising the catalyst is the ability to stimulate preferential growth even at low concentration and prevents agglomeration of particles at high concentration.<sup>255</sup> Thus producing desired nano-rod structures.



**Figure 3-8: TEM images of  $\text{La}_2\text{O}_3$  prepared by hydrothermal method**

The formation of nano-rod structures were triggered by anisotropic growth of the nanoparticles with the help of NaOH that acts as soft template and mineralizer which stimulates nucleation and growth of nano-rods.<sup>256,257</sup> These nano-rods grew anisotropically in such a way that it promotes self-assembly of nano-rods forming aggregations and 3D structures of nano-rods by weak intermolecular interactions.<sup>257</sup> As mentioned earlier, the  $\text{La}_2\text{O}_3$  exhibited hexagonal crystal

structure which favours anisotropic growth producing crystal along the 101 planes.<sup>258</sup> It has been identified that 101 plane of  $\text{La}_2\text{O}_3$  possessed lowest plane energy thus having high growth rate accelerating the formation of nano-rods.<sup>259</sup> Figure 3-9 shows the TEM images of 2.3 wt%  $\text{Cu}/\text{La}_2\text{O}_3$ . Cu particles could not be detected due to either high dispersion, or even intercalated within the framework.

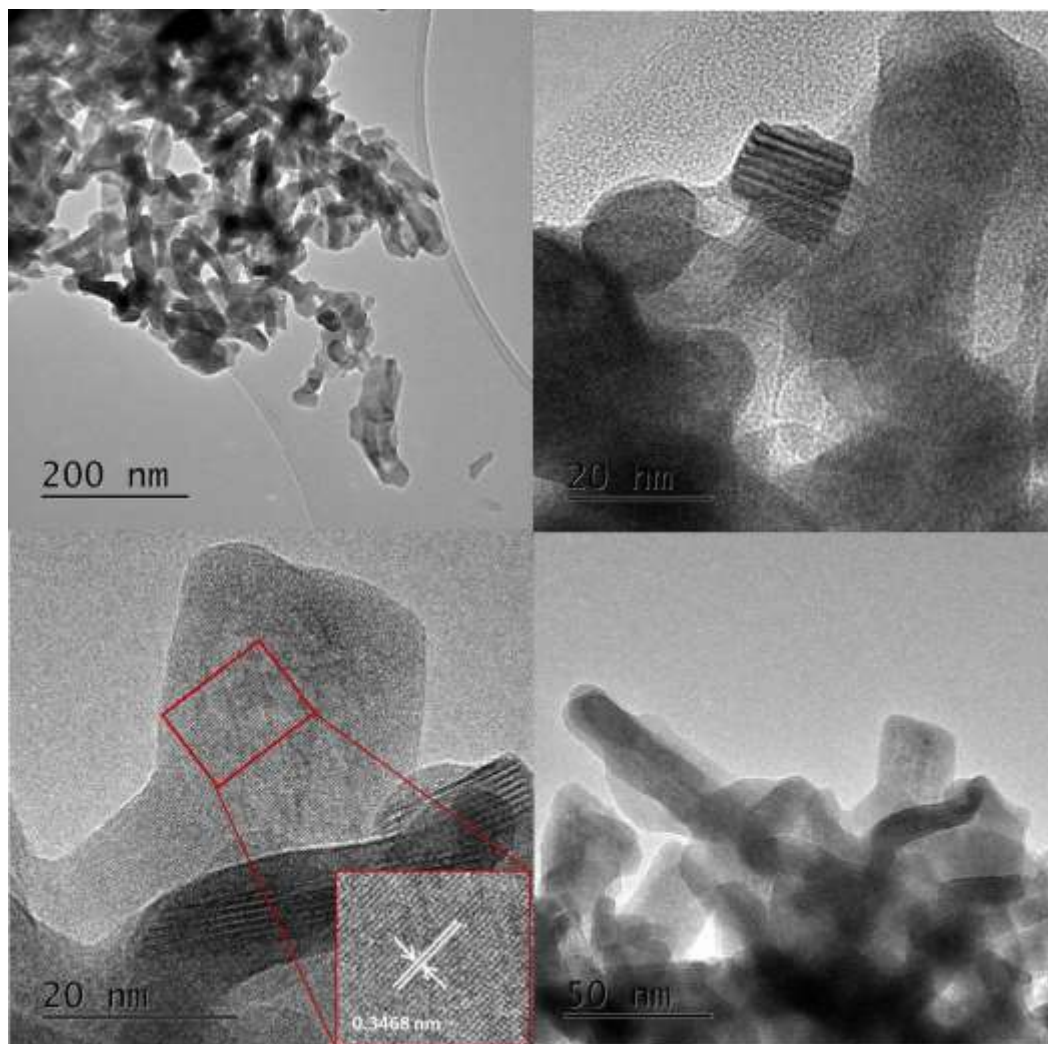
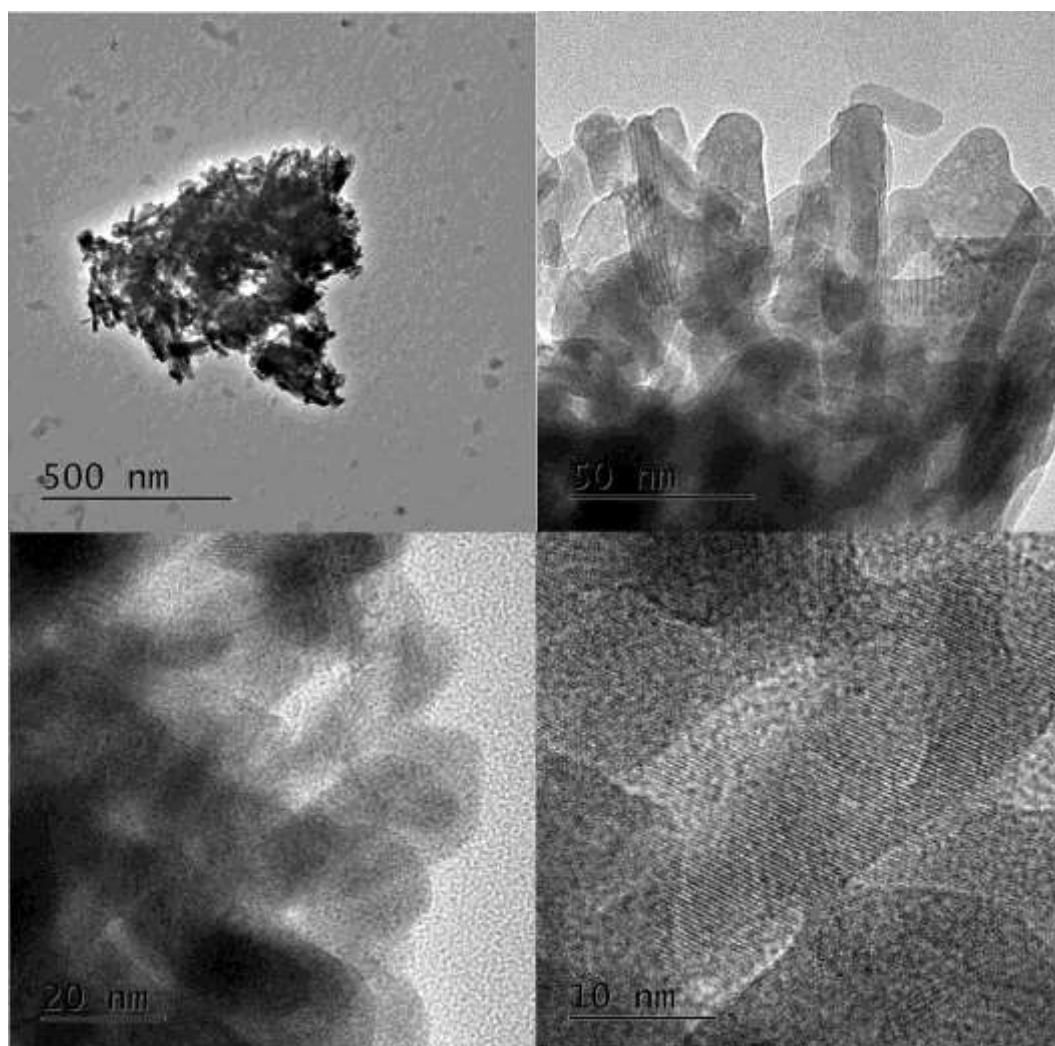


Figure 3-9: TEM images of 2.3 wt%  $\text{CuLa}_2\text{O}_3$

The Cu particles were not detectable even when the loading is as high as 6.9 wt% shown in Figure 3-10 even though Zhang *et al* reported the presence of Cu particles in their TEM analysis at lower Cu loadings.<sup>155</sup> This result can be confirmed by EDX analysis to determine elemental composition in section 3.2.1.5.



**Figure 3-10: TEM images of 6.9 wt%  $\text{CuLa}_2\text{O}_3$**

Cu particles can be seen clearly in Figure 3-11 with 13.9 wt% loading of Cu metals onto the support. This can be seen as large dark spots deposited on the surface of the support. However, the deposition of Cu is not uniformly distributed in the  $\text{La}_2\text{O}_3$  matrix. The average size of the copper particles could not estimate due to deposition of large particles of Cu on the surface of the support.

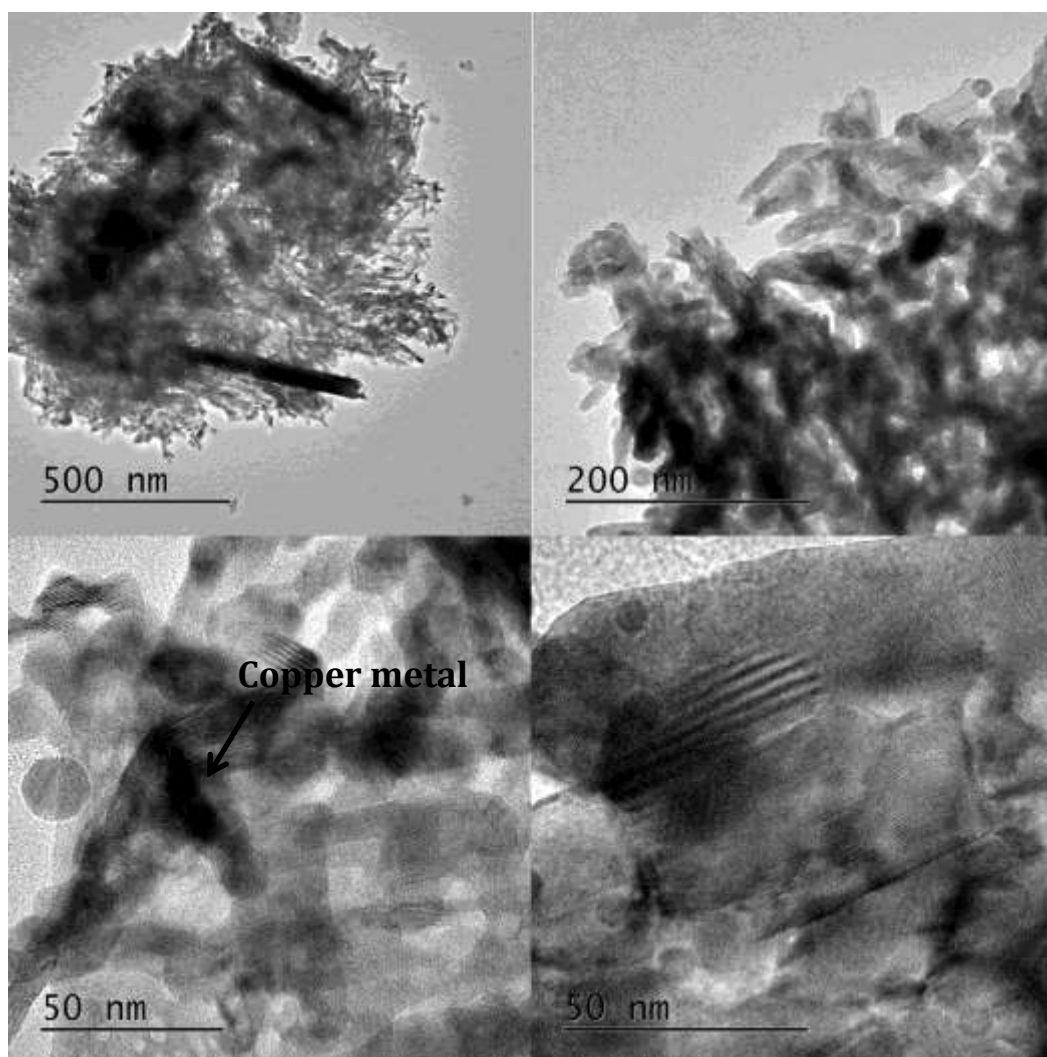


**Figure 3-11: TEM images of 13.9 wt%  $\text{CuLa}_2\text{O}_3$**



### 3.2.1.5 Elemental analysis-EDX analysis

Cu/La<sub>2</sub>O<sub>3</sub> catalysts at different loadings were subjected to Energy-dispersive X-ray Spectroscopy or EDX analysis to determine the Cu loading. Individual elemental mapping of 2.3 wt% Cu/La<sub>2</sub>O<sub>3</sub> shows highly dispersed uniform Cu distribution particles (green colour) which could not be seen in the TEM images in the lanthanum matrix shown in Figure 3-12. The EDX calculations were measured at several points over the sample and the real weight loading was 2.65 wt%. This is suggested copper is incorporated into the La<sub>2</sub>O<sub>3</sub> lattice or copper could be highly dispersed on the external surface.

Keshavaraja *et al* also reported that transition metals such as Mn or Cu were incorporated into the perovskite oxide, in this case, is ZrO<sub>2</sub> lattice.<sup>260</sup> This effect stabilised the oxides with the incorporation of metals.<sup>260</sup> Another evidence that suggested the incorporation of metal into the oxide which shifts the 2 $\theta$  value of the peaks to a higher value in the XRD shown in **Error! Reference source not found..** As previously mentioned La<sub>2</sub>O<sub>3</sub> is known to have a low surface area which is confirmed by BET analysis and the low surface area of La<sub>2</sub>O<sub>3</sub> means that 2.3 wt% Cu should be visible in XRD as Cu should begin to form clusters on the surface. This also suggests that copper is incorporated within the framework of the support.

There were few reports describing the effect of heat treatment on the behaviour of Cu particles which driving it from the bulk to the surface of the support at lower Cu content.<sup>261,262</sup> The heat treatment of Cu catalysts (300°C calcination, 450°C reduction) were not high enough to observe copper atoms on the surface from the bulk thus forming copper clusters.<sup>261</sup>

Figure 3-14 shows an elemental mapping of 6.9 wt% Cu/La<sub>2</sub>O<sub>3</sub>. The real weight loading of Cu was 7.02 wt%. The distribution of Cu particles were not equal and clusters of Cu can be observed. However, the diffraction peaks of Cu could not be seen in 6.9 wt% Cu/La<sub>2</sub>O<sub>3</sub>. This results also agrees with the XRD data in which only La<sub>2</sub>O<sub>2</sub>CO<sub>3</sub> phase was observed.

Several Cu clusters could be seen clearly on the elemental mapping of 13.9 wt% Cu/La<sub>2</sub>O<sub>3</sub> shown in Figure 3-16. Large particles of Cu formed due to increase in Cu loadings thus it aggregates forming clusters of Cu particles.<sup>262</sup> The result agrees

with the XRD data in which a Cu diffraction peak could be observed at about  $2\theta=43.5^\circ$  in **Error! Reference source not found..** A report being published that copper peaks could only be observed on the XRD when the copper loading reached more than 15% with  $\text{CeO}_2$  as the support.<sup>261</sup> The actual weight loading of Cu was 10.84 wt% which is relatively low compared to the original weight loading. This difference is caused by the irregular dispersion of Cu on the support.

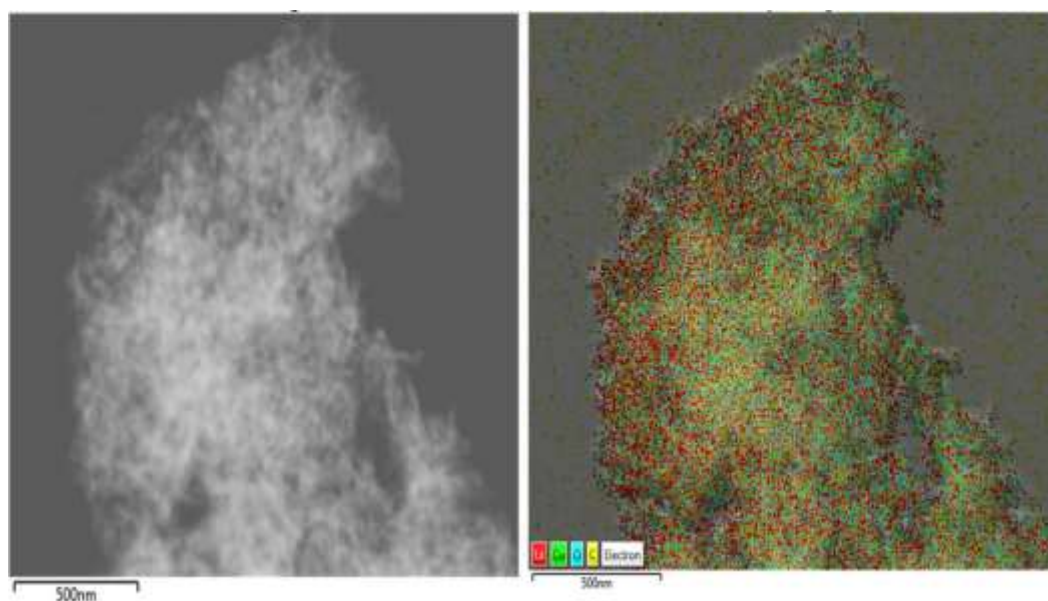


**Figure 3-12: EDX elemental mapping of 2.3 wt% Cu/ $\text{La}_2\text{O}_3$**



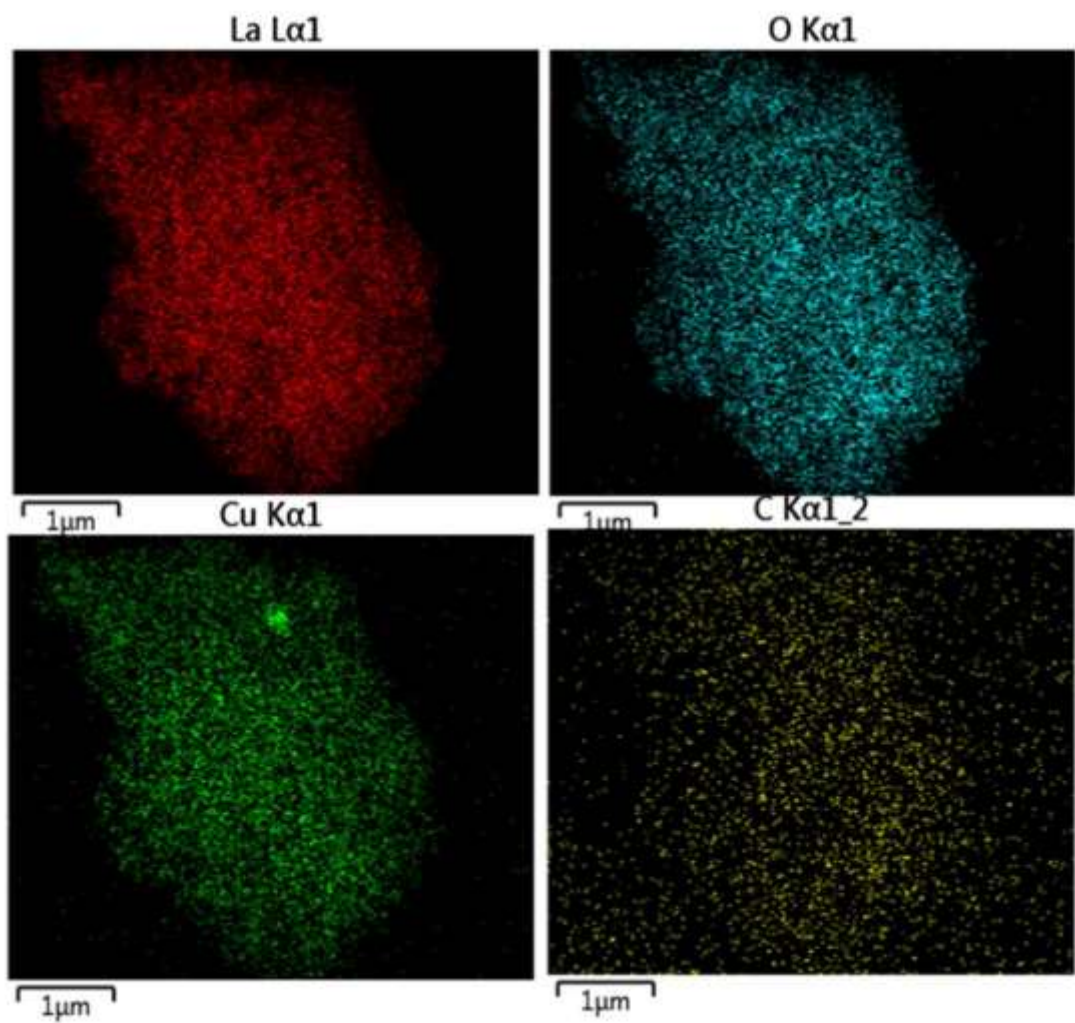


**Figure 3-13: Individual EDX elemental mapping of 2.3 wt% Cu/La<sub>2</sub>O<sub>3</sub>**

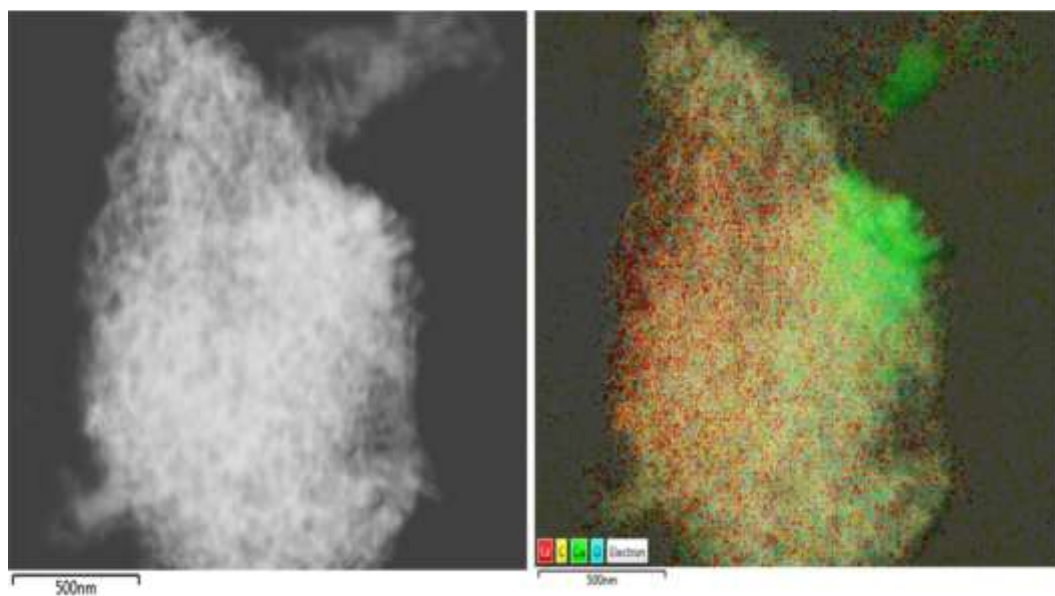


**Figure 3-14: EDX elemental mapping of 6.9 wt% Cu/La<sub>2</sub>O<sub>3</sub>**

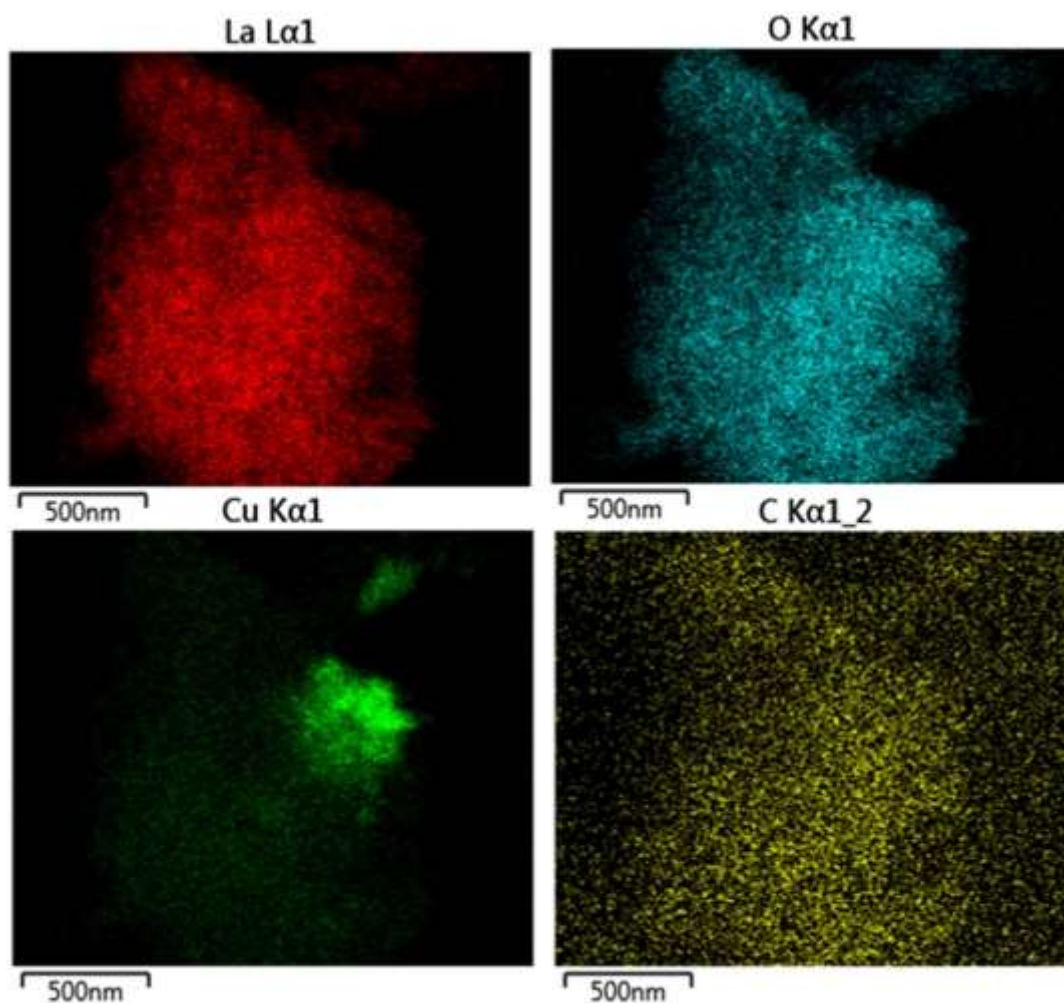


Figure 3-15: Individual EDX elemental mapping of 6.9 wt% Cu/La<sub>2</sub>O<sub>3</sub>

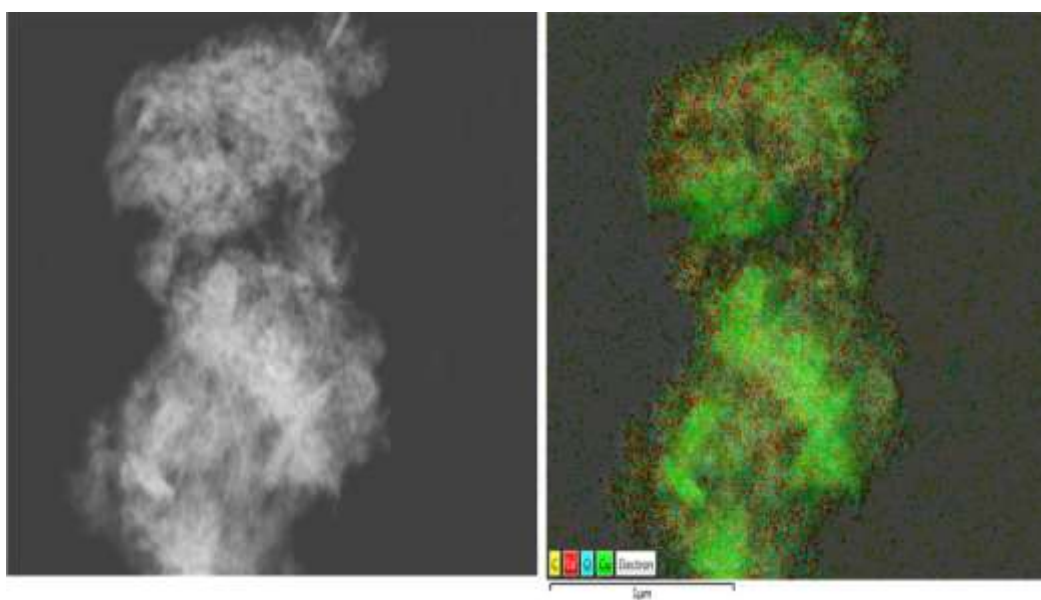


Figure 3-16: EDX elemental mapping of 13.9 wt% Cu/La<sub>2</sub>O<sub>3</sub>

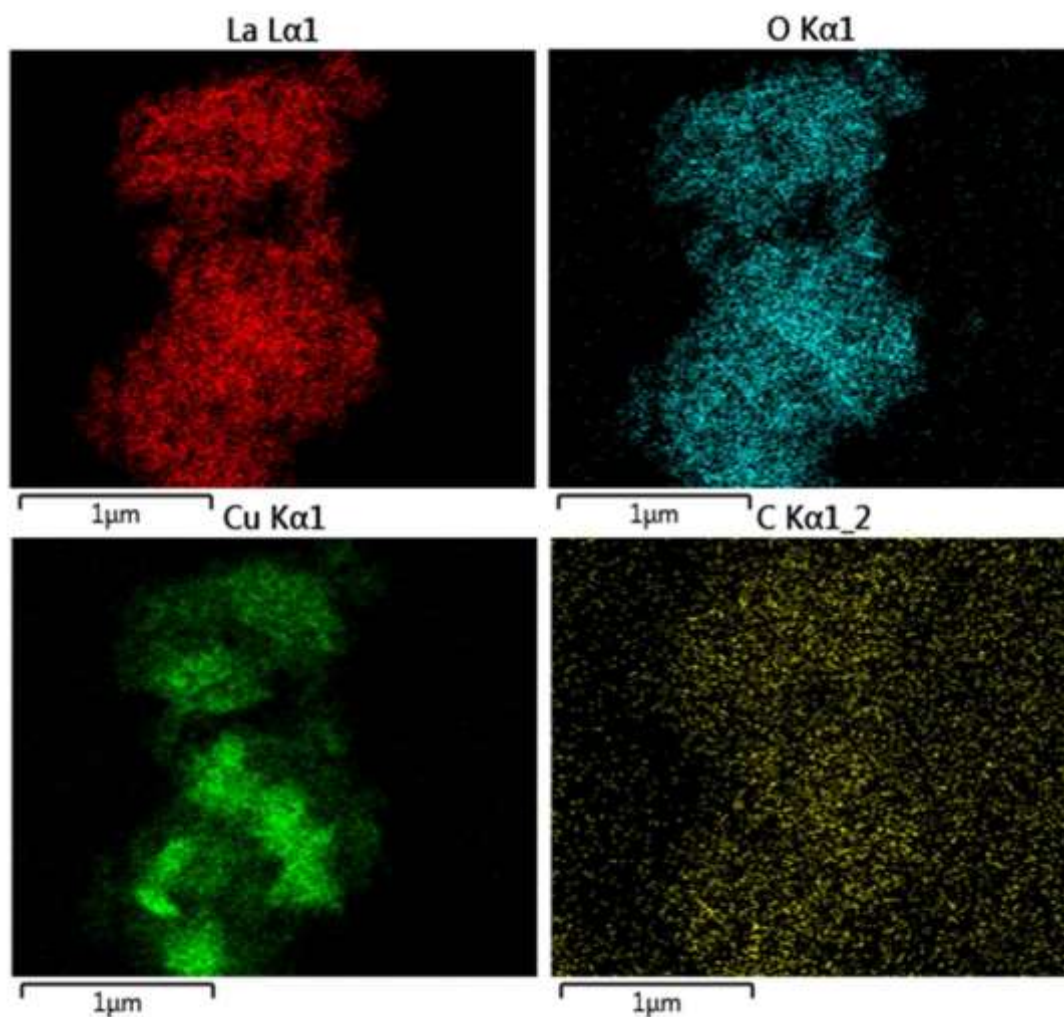


Figure 3-17: Individual EDX elemental mapping of 13.9 wt% Cu/La<sub>2</sub>O<sub>3</sub>

#### 3.2.1.6 Reduction profiles characterized by H<sub>2</sub>-TPR

H<sub>2</sub>-TPR analysis was performed on the catalyst that had not been exposed to hydrogen atmosphere. This technique used to investigate the redox properties of the CuO and the ease of reduction to copper metal as well as to examine the interaction between CuO particles and La<sub>2</sub>O<sub>3</sub> to observe the reduction behaviour of these two phases. Figure 3-18 shows the H<sub>2</sub>-TPR of CuO at different loadings onto the support. Each sample exhibits two major peaks occurring at 120°C-200°C and at higher temperatures in the range of 500°C-650°C. The later can be attributed to the decomposition of carbonate species and this result agrees with the XRD data in Figure 3-1 in which the carbonate phases were not present when the heat treatment reached 700°C. According to Zhang *et al* data, the peak at high reduction



temperature of 400°C-500°C is attributed to strongly bound CuO particles interacting with the support.<sup>155</sup> The reduction peak of La<sub>2</sub>O<sub>3</sub> is above 700°C.<sup>155</sup>

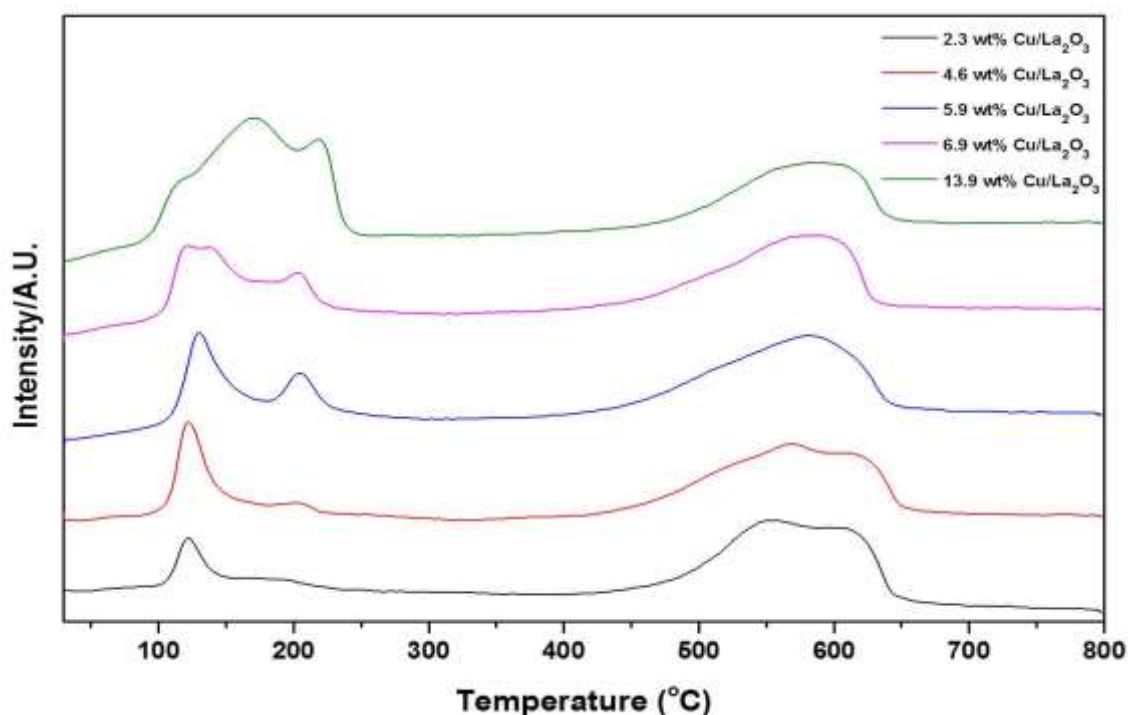


**Figure 3-18: Temperature-programmed reduction profiles of CuO/La<sub>2</sub>O<sub>3</sub> at different copper loadings**

The complete reduction of bare CuO without support to metallic Cu is at about 385°C.<sup>263</sup> From the literature, the incorporation of Cu species on the support reduced the reduction temperature of the Cu catalyst.<sup>263</sup> There were two characteristic peaks at around 125°C and 200°C that were obtained from the reduction profile at lower reduction region and it slowly appeared as the Cu loading increased. This indicates that at least two different Cu species present on the support, La<sub>2</sub>O<sub>3</sub>, interacting weakly and strongly with the support.<sup>264</sup> The lowest reduction peak roughly at 125°C can be attributed to highly dispersed CuO species with the smallest particle size predominantly occurring when the copper loading was 2.3 wt%.<sup>252</sup> The ease of reduction could possibly be due to one-step reduction of CuO species to Cu<sup>0</sup>.<sup>265</sup> This also implies that there is a weak metal support interaction at a lower metal loading of highly dispersed copper species.<sup>266</sup> The high reduction temperature peak at about 200°C can be ascribed to bulk CuO species

with largest particle size.<sup>252,265,267,268</sup> The peak can be observed appearing when the weight loading is 4.6 wt%.

As copper loading increased, peak broadening occurs and shifted toward higher temperature region which is due to increase in crystallinity of CuO species as well as stronger interaction.<sup>264,267</sup> The shifting of reduction peaks are more prominent when the loading is 13.9 wt% copper. There is an overlap of reduction peaks between 170°C and 220°C which caused by the reduction of bulk CuO species and Cu<sup>2+</sup> ions having strong metal-support interaction respectively by chemically interacting with the surface of the support.<sup>265,266</sup> The presence of Cu<sup>2+</sup> ions are mostly found when the copper precursors are prepared by impregnation method compared to other preparative routes.<sup>266</sup>

#### **3.2.1.7 Absorption measurement using UV-VIS**

The solid UV-VIS spectra of La<sub>2</sub>O<sub>3</sub> and Cu/La<sub>2</sub>O<sub>3</sub> at different loadings are presented in Figure 3-19. La<sub>2</sub>O<sub>3</sub> shows a strong absorption band at 230 nm, which can be attributed to low energy oxygen to metal charge transfer band.<sup>269</sup> Electronic transition from 5d orbital to 4f orbital of La<sup>3+</sup> is also related to sharp absorption band at around 200 nm.<sup>270</sup> Large absorption band in the range of 580-600 nm is associated to electron d-d transitions of Cu<sup>2+</sup> ions in distorted octahedral surrounding by oxygen in CuO particles.<sup>267,271</sup> Large broad absorption band between 300-350 nm at 13.9 wt% Cu/La<sub>2</sub>O<sub>3</sub> can be assigned to the presence of small copper clusters in a highly dispersed state which can be confirmed by TPR results.<sup>267</sup>

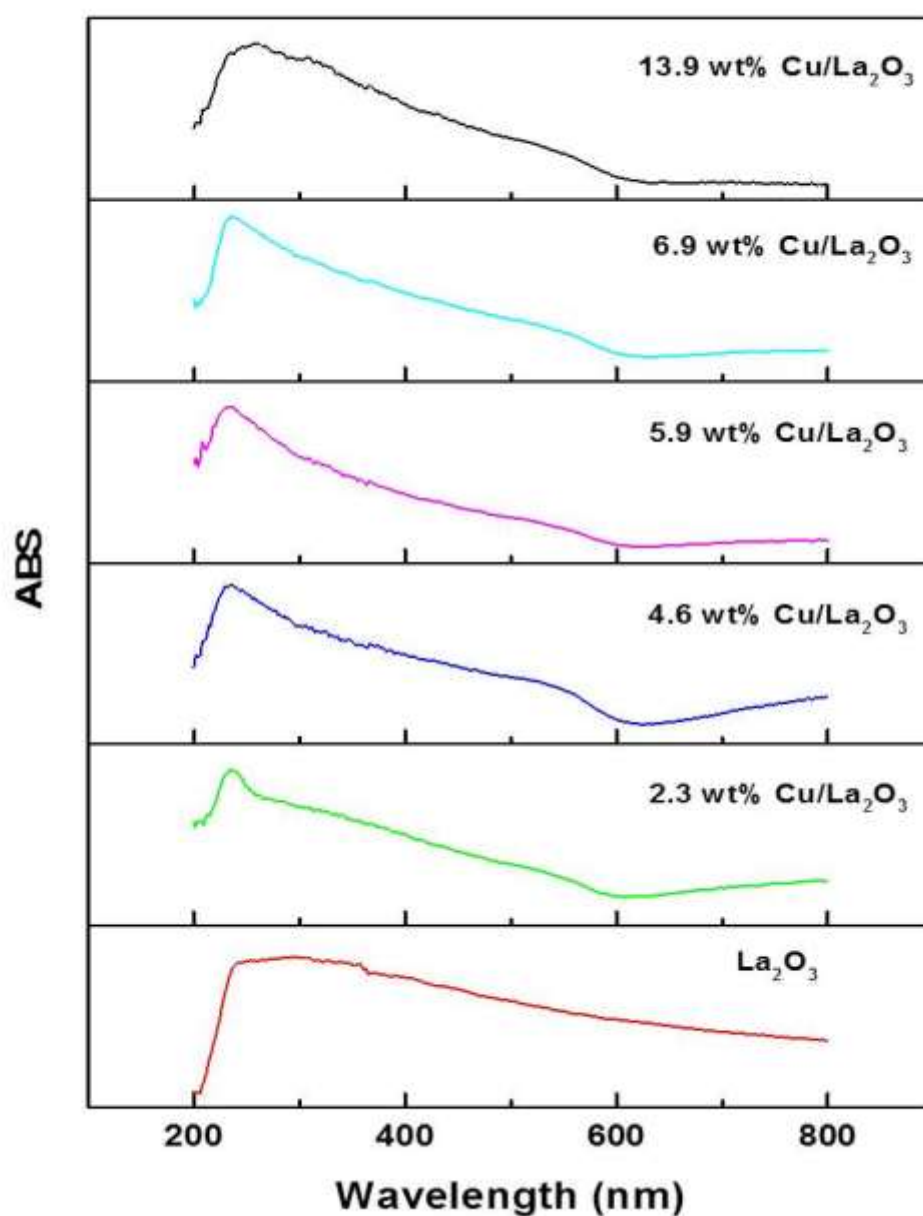
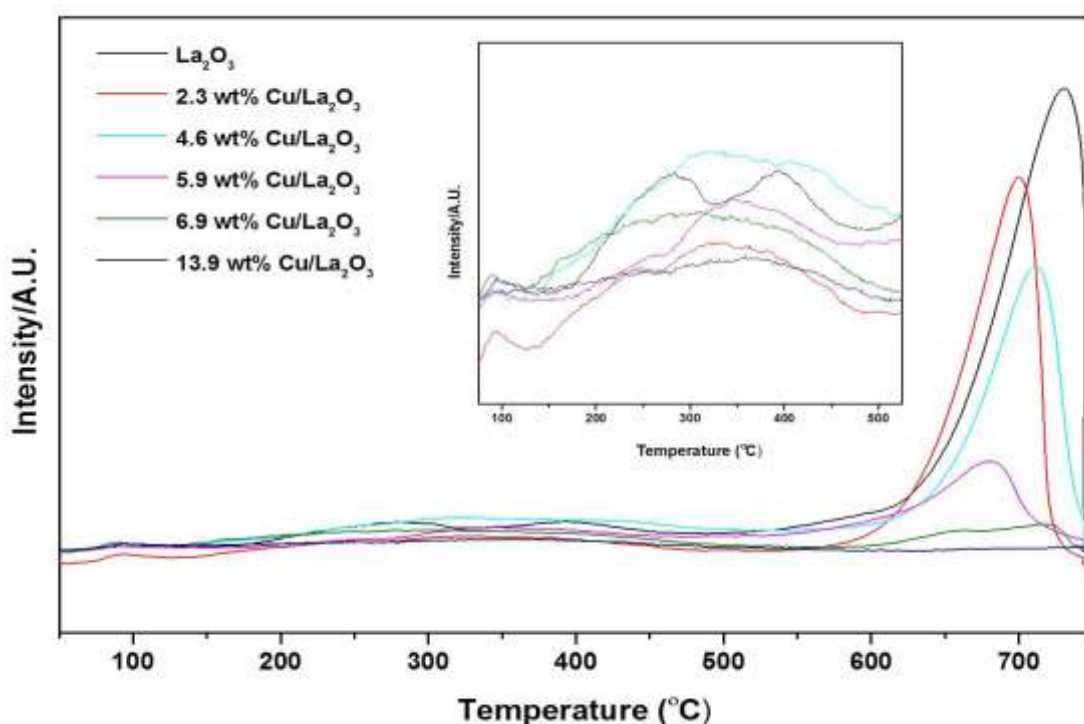


Figure 3-19: UV-VIS of  $\text{La}_2\text{O}_3$  and  $\text{Cu/La}_2\text{O}_3$  catalysts

#### 3.2.1.8 Basicity measurement by $\text{CO}_2$ -TPD

Figure 3-20 shows the  $\text{CO}_2$ -TPD profiles of  $\text{Cu/La}_2\text{O}_3$  at different Cu loadings to determine and quantify the basicity of the catalysts at different desorption temperatures which indicate the presence of different types of basic sites of different strength on the surface of the catalyst.<sup>155</sup> The desorption of  $\text{CO}_2$  produced

the desorption peaks which can be roughly divided into three regions: weak basic sites (50°C-150°C), medium basic sites (150°C-550°C) and strong basic sites (above 550°C). Few reports in the literature have reported that strong basic sites appear in the range of 400°C-500°C, however, the desorption temperature of strong basic sites for the synthesised catalysts were reasonably high.<sup>101,154</sup> The peaks were not related to decomposition of carbonate species because the decomposition happened during pre-treatment of the analysis at 650°C. La<sub>2</sub>O<sub>3</sub> and 2.3 wt% Cu/La<sub>2</sub>O<sub>3</sub> have two desorption peaks in the medium basic sites region, which indicates two types of adsorption taking place. These two peaks were not observed in the other catalysts.



**Figure 3-20: Temperature-programmed desorption profiles of Cu/La<sub>2</sub>O<sub>3</sub> at different copper loadings**

The weak basic sites were ascribed to OH<sup>-</sup> groups on the surface of the catalyst; medium basic sites could be assigned to bidentate carbonate adsorbed on metal-oxygen (La-O<sup>2-</sup>) pairs and strong basic sites were related to unidentate carbonate adsorbed on isolated O<sup>2-</sup> ions.<sup>101,155,252,272</sup>

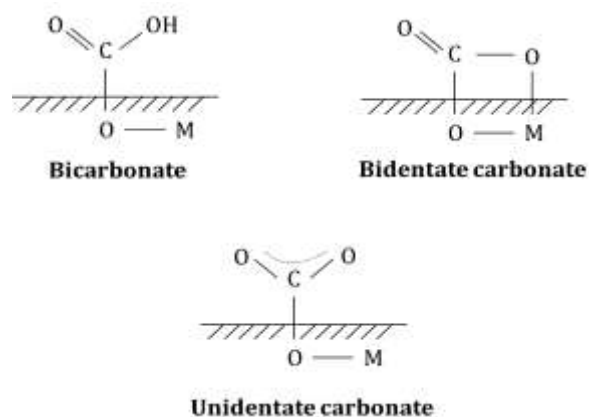


**Figure 3-21: Adsorbed CO<sub>2</sub> on the catalyst surface characterized by IR<sup>273,274</sup>**

One of the ways to characterise CO<sub>2</sub> adsorption is by using in situ FTIR. There were reports being published in the study of adsorption of CO<sub>2</sub> on the surface of the catalyst using FTIR shown in Figure 3-21.<sup>273,274</sup> The presence of carbonate phase, La<sub>2</sub>O<sub>2</sub>CO<sub>3</sub>, also contributes to the basicity of the catalyst especially the medium basic sites due to more La<sup>3+</sup>-O<sup>2-</sup> pairs present on the surface.<sup>275</sup> Although the decomposition of carbonates occurred above 500°C, the ‘real catalyst’ still preserved the carbonate phase which can be seen on the XRD results above in Figure 3-3 .<sup>101,154,275,276</sup>

As the loading of Cu increased, the amount of desorption of CO<sub>2</sub> decreased for all the basic sites shown in Table 11. This is due to the reduced amount of exposed basic sites. 2.3 wt% Cu/La<sub>2</sub>O<sub>3</sub> has the highest amount of medium basic sites of 263 μmol CO<sub>2</sub> g<sup>-1</sup> (entry 2) followed by 4.6 wt% Cu/La<sub>2</sub>O<sub>3</sub> with medium basic sites of 181 μmol CO<sub>2</sub> g<sup>-1</sup> (entry 3). The amount of medium basic sites for 13.9 wt% Cu/La<sub>2</sub>O<sub>3</sub> is 97 μmol CO<sub>2</sub> g<sup>-1</sup> (entry 6) and it is the lowest amongst all the catalyst which is due to Cu particles covered most of the surface of the catalyst. Therefore the amount of basic sites could contribute to the overall catalytic activity of the reaction.

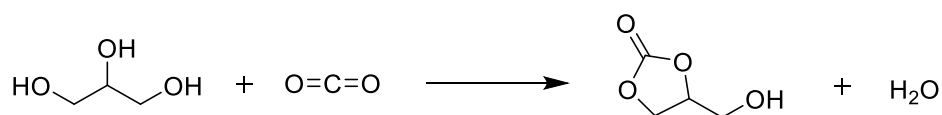


**Table 11: Basic sites distribution calculated on the basis of CO<sub>2</sub>-TPD profiles**

Entry	Catalyst	Basic sites (μmol CO <sub>2</sub> g <sup>-1</sup> )			Total
		Weak	Medium	Strong	
1	La <sub>2</sub> O <sub>3</sub>	7	86	2000	2093
2	2.3 wt% Cu/ La <sub>2</sub> O <sub>3</sub>	14	263	1264	1541
3	4.6 wt% Cu/ La <sub>2</sub> O <sub>3</sub>	6	181	960	1147
4	5.9 wt% Cu/ La <sub>2</sub> O <sub>3</sub>	6	112	337	455
5	6.9 wt% Cu/ La <sub>2</sub> O <sub>3</sub>	6	105	155	266
6	13.9 wt% Cu/ La <sub>2</sub> O <sub>3</sub>	5	97	22	124

### 3.2.2 Catalytic reaction

The direct synthesis of glycerol carbonate from CO<sub>2</sub> and glycerol is highly desirable in terms of sustainability shown in Scheme 3-3 in which two cheap raw materials are converted into useful product with water as the by-product. The reaction is thermodynamically limited due to the presence of water.

**Scheme 3-3: Direct carbonylation of glycerol carbonate from glycerol and CO<sub>2</sub>**

The amount of dehydrating agent for each reaction is always in excess to remove any water formed during the reaction. This is calculated by comparing the number of moles of dehydrating agent with the amount of glycerol used in the reaction.

#### 3.2.2.1 Dehydrating agent-molecular sieves

Molecular sieves 13X (1 g) were tested as the dehydrating agent for the direct carbonylation of glycerol in CO<sub>2</sub> to produce glycerol carbonate. 13X is considered as an inorganic absorbent and it is suggested as an attractive material to producing glycerol carbonate as no by-products are formed, giving 100% selectivity and could be easily regenerated.<sup>158</sup> Attempts have been made previously using molecular sieves, however very low yield of glycerol carbonate was achieved.<sup>135</sup> The reaction requires special and complicated setup.<sup>77</sup> In this reaction, all the reactants were mixed together in a pressurised vessel.

The reaction was heated to 150°C under a pressure of 5.2 MPa for 16 h. After the reaction, the mixture for the carbonylation of glycerol with CO<sub>2</sub> in the presence of molecular sieves as a dehydrating agent was analysed using <sup>1</sup>H NMR and <sup>13</sup>C NMR shown in Figure 3-22 and Figure 3-23 respectively.

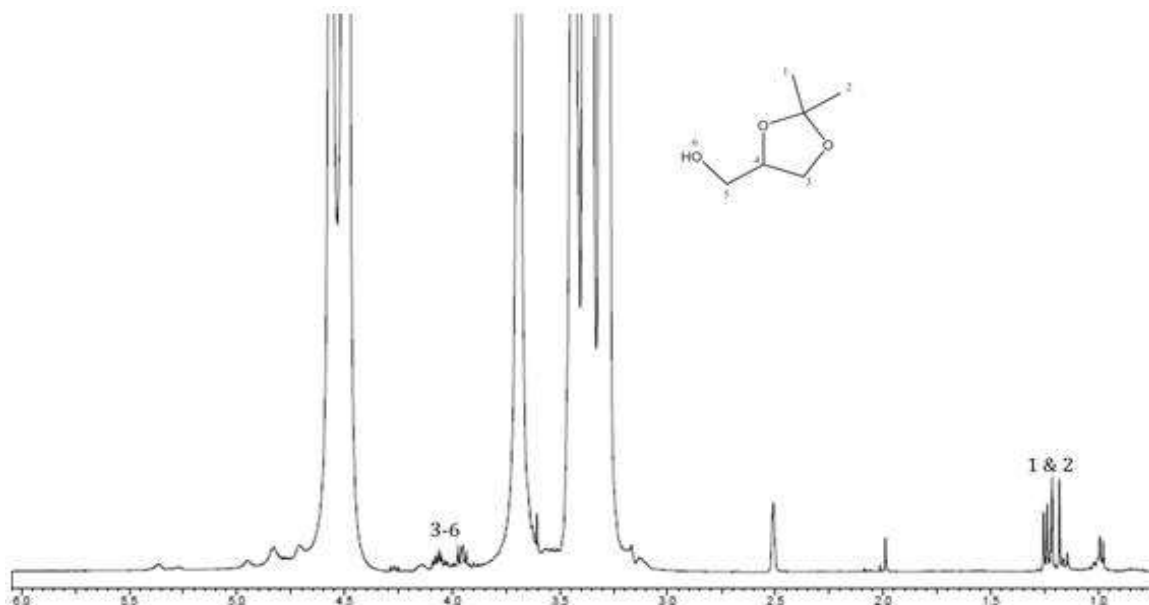


Figure 3-22:  $^1\text{H}$  NMR spectra of the reaction mixture at  $150^\circ\text{C}$  reaction

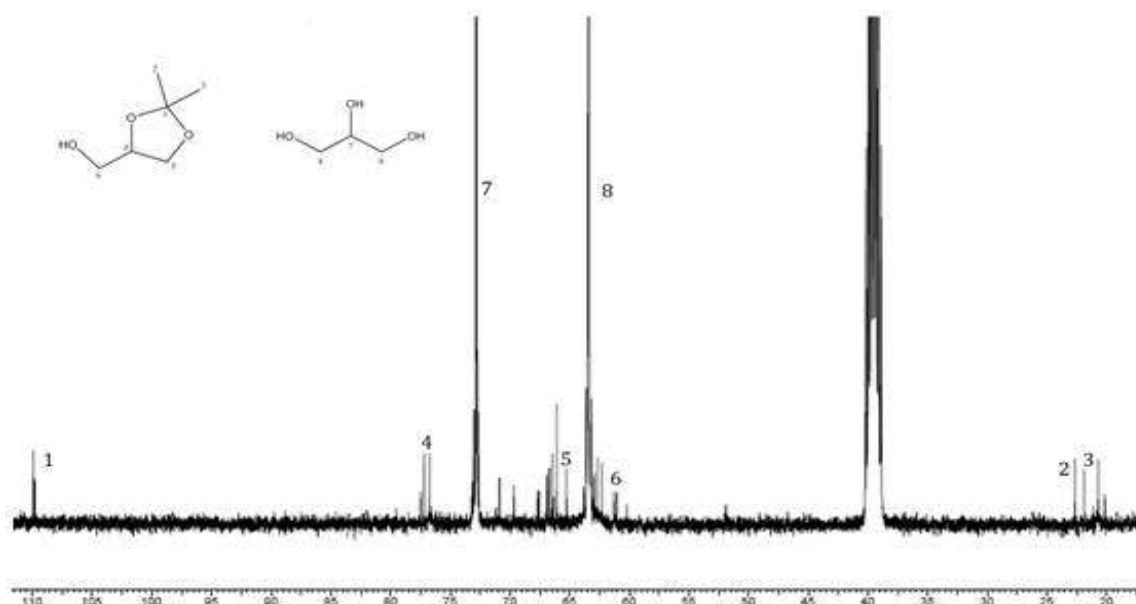


Figure 3-23:  $^{13}\text{C}$  NMR spectra of reaction at  $150^\circ\text{C}$  reaction

From the NMR spectra of the product mixture, the NMR signals correspond to the compound, acetal. In the  $^1\text{H}$  NMR, the signals at 3.8-4.2 ppm can be assigned to the hydrogen of the five-membered ring. The signal at 109 ppm of  $^{13}\text{C}$  NMR corresponds to carbon 1 in Figure 3-23 whereas at 22 ppm and 23 ppm correspond to carbon 2 and carbon 3 respectively. The signal at 63 ppm and 73 ppm can be assigned to carbon 8 and carbon 7 on glycerol respectively. The product can be formed by reaction of glycerol with various aldehydes or ketones yielding five

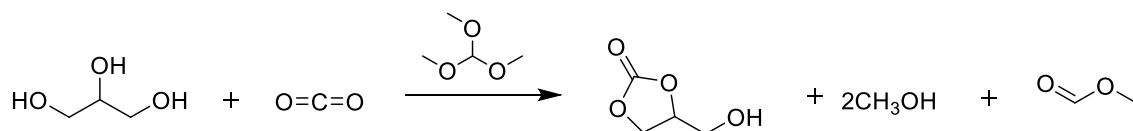
(major) or six-membered ring (minor).<sup>115,277</sup> In this reaction, the source of aldehyde or ketone is acrolein.<sup>277</sup>

Acrolein can be formed by dehydration of glycerol in the presence of the heterogeneous catalyst in the liquid or gas phase for examples zeolites where two molecules of water are being eliminated.<sup>278</sup> The reaction requires higher temperature about 250°C. In this reaction, 16 h reaction at 150°C could produce acrolein as an intermediate.<sup>278</sup>

To perform acetalisation, a catalyst is needed, which is mostly a solid acid catalyst in this case molecular sieves 13X. Therefore the 13X catalyses the acetalisation of glycerol with acrolein forming acetal, in this case solketal or isopropylidene glycerol. Furthermore, zeolites have been reported to catalyse the acetalisation reaction. Glycerol acetals can undergo further side reaction with the remaining hydroxyl group. Therefore in this reaction, molecular sieves are not a suitable dehydrating agent for the direct synthesis of glycerol carbonate from CO<sub>2</sub>.

### 3.2.2.2 Dehydrating agent-Trimethyl orthoformate

Previously, orthoesters have been used as an organic dehydrating agent in the synthesis of dimethyl carbonate from methanol and carbon dioxide.<sup>38</sup> The reaction produced high yields of dimethyl carbonate using the tin complex as the catalyst.<sup>38</sup> Trimethyl orthoformate captures one molecule of water producing two molecules of methanol and one molecule of methyl formate. The formation of dimethyl carbonate from CO<sub>2</sub> and orthoesters is thermodynamically favourable. Therefore trimethyl orthoesters can be used in the carbonylation of glycerol carbonate shown in Scheme 3-4.



**Scheme 3-4: Reaction of glycerol with CO<sub>2</sub> and trimethyl orthoester**

Five sets of reaction times were tested: 1 h, 2 h, 4 h, 6 h and 8 h. The reaction profile in Figure 3-29 indicates that glycerol is being consumed within 2 h during the reaction; products in peak 3 and peak 4 which could not be identified were produced in a great amount which can be seen in the chromatograms, Figure 3-24 and Figure 3-25. As the reaction progressed, reversed reaction seemed to occur, in which glycerol conversion decreases as well as products in peak 3 and peak 4. Glycerol carbonate starts to appear after 2 h in the reaction. Trimethyl orthoformate is being consumed rapidly in the reaction as there is no trace of the dehydrating agent in the GC after 1 h reaction.

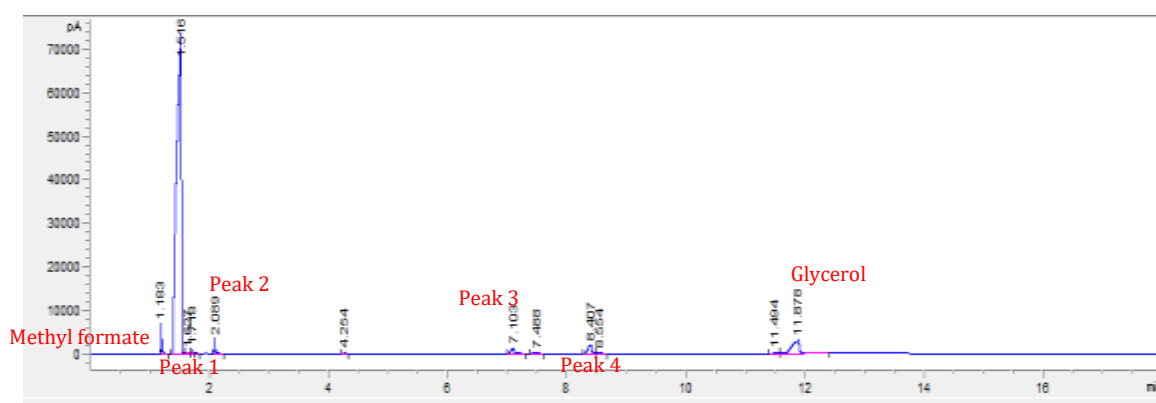


Figure 3-24: GC chromatogram at 1 h during reaction

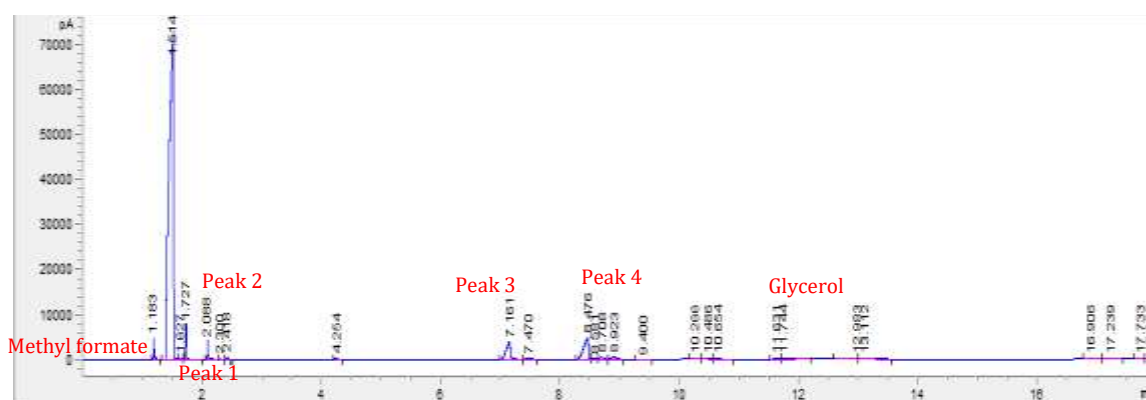


Figure 3-25: GC chromatogram at 2 h during reaction

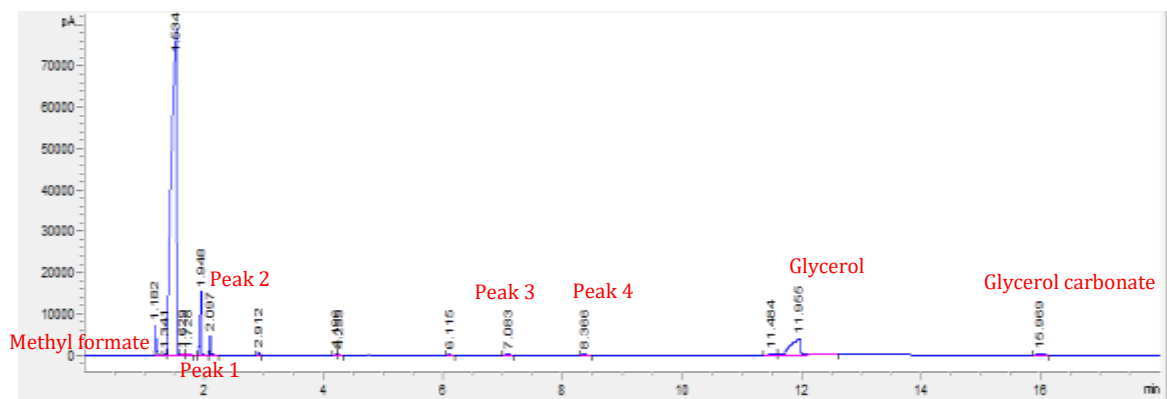


Figure 3-26: GC chromatogram at 4 h during reaction

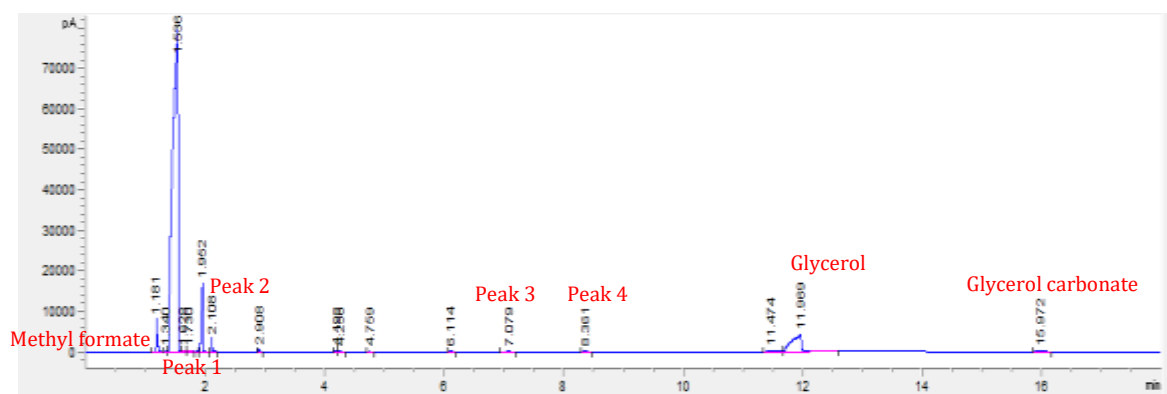


Figure 3-27: GC chromatogram at 6 h during reaction

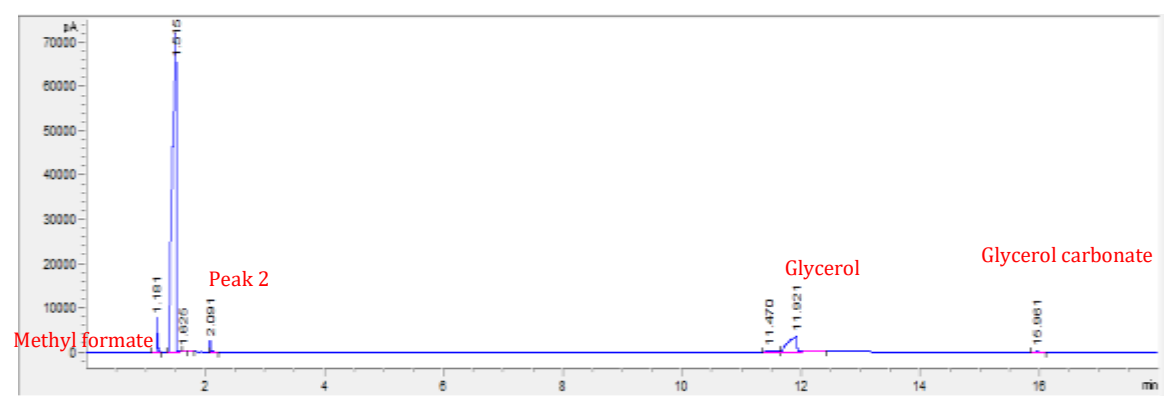
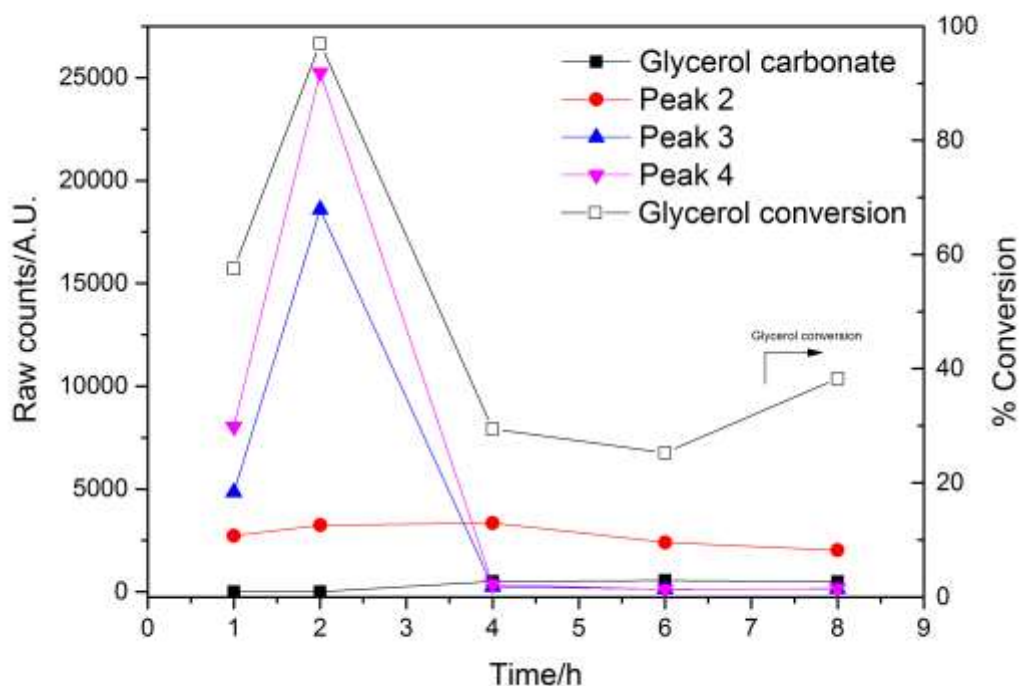


Figure 3-28: GC chromatogram at 8 h during reaction

Table 12 shows the catalytic performance of 2.3 wt% Cu/La<sub>2</sub>O<sub>3</sub> in the synthesis of glycerol carbonate. The conversion of glycerol increased from 58% to 97% after 2 h of reaction. However, no glycerol carbonate had been produced and observed in the GC chromatogram. As the reaction progressed, glycerol conversion decreases from 97% to 38%. Glycerol carbonate appeared during 4 h of the reaction giving a yield of 0.28 mmol, and the yield remained constant after 4 h during the reaction. The mass balances are low in this reaction due to number of unknown products being formed.

**Table 12: Catalytic performance of 2.3 wt% Cu/La<sub>2</sub>O<sub>3</sub> in the synthesis of glycerol carbonate**

Entry	Time/h	Pressure/MPa	Glycerol conversion %	Glycerol Carbonate yield mmol	Mass balance %
1	1	7.3	58	0	42
2	2	7.1	97	0	3
3	4	7.2	29	0.28	71
4	6	7.4	25	0.31	75
5	8	7.4	38	0.28	62
Reaction conditions: 2.3 g glycerol, 5 mL trimethyl orthoformate, 0.11 g catalyst, temperature: 150°C					



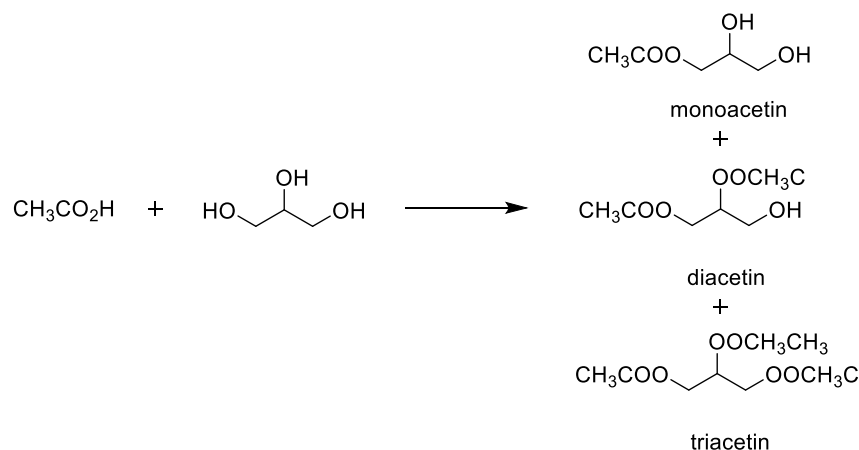
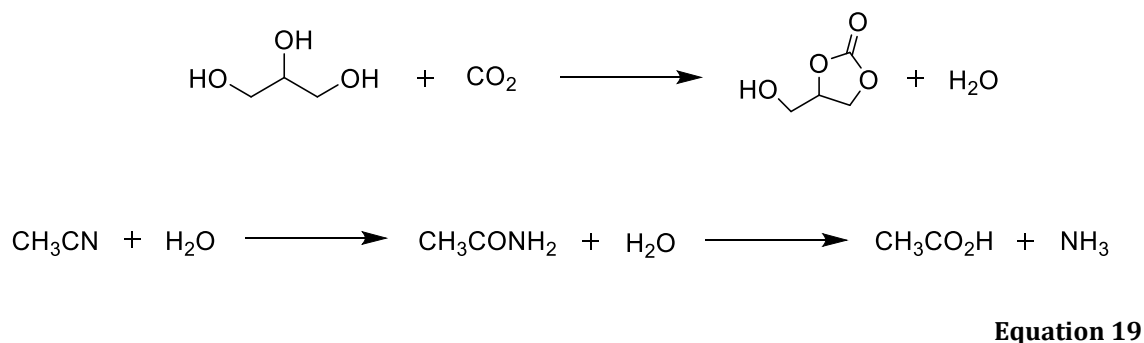
**Figure 3-29: Time online analysis for 2.3 wt% Cu/La<sub>2</sub>O<sub>3</sub> at 150°C, P=7 MPa CO<sub>2</sub>**

The stability of glycerol carbonate was determined in the presence of trimethyl orthoformate and methanol. From the GC analysis, it was observed that glycerol carbonate is being converted back into glycerol. The yield of glycerol carbonate is low in the reaction because glycerol carbonate is not stable in the presence of trimethyl orthoformate and methanol. It is unfortunate that this reaction did not work as expected as the selectivity to glycerol carbonate is 100% judging from the reaction scheme. Therefore trimethyl orthoformate is not a suitable dehydrating agent.

### 3.2.2.3 Dehydrating agent-Acetonitrile

The usage of acetonitrile as dehydrating agent is as attractive way to remove water shown in Equation 19. Acetonitrile is being hydrolysed by water to produce acetamide and further react with water to produce acetic acid and ammonia. The by-products are monoacetin, diacetin and triacetin which are produced from esterification of glycerol and acetic acid shown in Scheme 3-5.





**Scheme 3-5: Reaction between glycerol and acetic acid**

The catalytic performances of Cu/La<sub>2</sub>O<sub>3</sub> for the synthesis of glycerol carbonate at different loadings are tabulated in Table 13. 2.3 wt% Cu/La<sub>2</sub>O<sub>3</sub> gave the best performance amongst all the catalysts tested. 2.3 wt% Cu/La<sub>2</sub>O<sub>3</sub> (entry 2) has achieved 75% conversion of glycerol with 33% glycerol carbonate yield. As the loading of copper increased, the conversion of glycerol reduced significantly. Only 6% glycerol carbonate yield was achieved for 4.6 wt% Cu/La<sub>2</sub>O<sub>3</sub> (entry 3) with 21% glycerol conversion. The conversion and yield are further reduced to 8% and 0.6% respectively when the loading was 13.9 wt% (entry 6). The decrease in catalytic activity can be attributed to the decrease in the amount of basic sites of the catalysts which can be observed in the CO<sub>2</sub>-TPD results.

**Table 13: Catalytic performance of Cu/La<sub>2</sub>O<sub>3</sub> at different loadings in the synthesis of glycerol carbonate from glycerol and CO<sub>2</sub>**

Entry	Catalyst	Selectivity %						Mass Balance %
		Glycerol conversion %	Glycerol carbonate	Monoacetin	Diacetin	Triacetin	Glycerol carbonate yield %	
1	La <sub>2</sub> O <sub>3</sub>	-	-	-	-	-	-	-
2	2.3 wt% Cu/La <sub>2</sub> O <sub>3</sub>	75	33	51	11	5	25	76
3	4.6 wt% Cu/La <sub>2</sub> O <sub>3</sub>	21	25	55	13	7	6	87
4	5.6 wt% Cu/La <sub>2</sub> O <sub>3</sub>	17	21	56	16	7	4	91
5	6.9 wt% Cu/La <sub>2</sub> O <sub>3</sub>	12	14	59	19	8	2	96
6	13.9 wt% Cu/La <sub>2</sub> O <sub>3</sub>	8	8	63	20	8	0.6	93

**Reaction conditions: 2.3 g glycerol, 5 mL acetonitrile, 0.11 g catalyst, temperature: 150°C, pressure: 7.3 MPa, time: 16 h**

In the blank reaction (entry 1), no glycerol carbonate can be observed in the reaction, La<sub>2</sub>O<sub>3</sub> alone could not catalyse the carbonylation of glycerol without the presence of copper. Based on the report by Leitner, transition metal can activate CO<sub>2</sub> molecule by binding to the metal centre with weak interactions.<sup>279</sup> CO<sub>2</sub> will then form a complex with copper and the basic sites of La<sub>2</sub>O<sub>3</sub> forming bend CO<sub>2</sub> ligand.<sup>280</sup> Another report by Li *et al* suggested that CO<sub>2</sub> activation and adsorption can be facilitated by lattice oxygen present on the surface of the catalyst which acts as basic sites.<sup>154</sup> Therefore both of these effects could aid in the catalytic performance.

### 3.2.3 Conclusion

Cu/La<sub>2</sub>O<sub>3</sub> prepared by impregnation method is highly effective heterogeneous catalyst for the direct carbonylation of glycerol to glycerol carbonate. The catalytic activity is largely influenced by the basic sites of the catalyst especially the medium basic sites of the catalyst which has an impact to the conversion and yield of the glycerol carbonate. Different weight loadings of copper on lanthanum oxide catalysts were prepared and 2.3 wt% Cu/La<sub>2</sub>O<sub>3</sub> gives high catalytic performance compared to the other loadings with a glycerol carbonate yield of 25% and conversion 75%. Carbonate phase of the catalyst also has an effect in the overall activity. The choice of dehydrating agent is very crucial to ensure glycerol carbonate is being produced in a higher amount. The presence of acetonitrile shifts the thermodynamic equilibrium by reacting with water and forming acetins by esterification of glycerol and acetic acid.

# **CHAPTER 4**

**ENHANCE ROUTE OF MICROWAVE SYNTHESIS  
OF COPPER SUPPORTED ON LANTHANUM  
OXIDE IN THE DIRECT CARBONYLATION OF  
GLYCEROL CARBONATE FROM CARBON  
DIOXIDE**

## **4 ENHANCE ROUTE OF MICROWAVE SYNTHESIS OF COPPER SUPPORTED ON LANTHANUM OXIDE IN THE DIRECT CARBONYLATION OF GLYCEROL CARBONATE FROM CARBON DIOXIDE**

### **4.1 Introduction**

From chapter 3, 2.3 wt% Cu/La<sub>2</sub>O<sub>3</sub> prepared by impregnation method gives the highest catalytic performance of compare to other loadings achieving 75% conversion and 25% yield of glycerol carbonate at 150°C, 7 MPa for 16 h. However, in the synthesis of the catalyst requires long preparative step especially in the long hydrothermal treatment of 48 h which was reported by Zhang *et al.*<sup>155</sup> Therefore, in this research microwave irradiation is used as a promising technique in the acceleration of lanthanum oxide synthesis. Microwave heating has many benefits such as selective heating at an enhanced rate due to polar molecules absorbing microwave energy. Synthesis times can be dramatically reduced by substituting conventional heating to microwave heating. Synthesis of Cu/La<sub>2</sub>O<sub>3</sub> using microwave irradiation is still a novel field and has a potential to be explored greatly for future reaction.

### **4.2 Results & Discussion**

Hydrothermal methods are generally utilised as they are a straightforward reaction to synthesise mixed oxides. However, the method requires long preparation time. Synthesising mixed oxides using microwave irradiation is a promising new method, which is currently being explored. There is not much literature being reported on the synthesis of lanthanum oxide using the microwave-assisted method. Microwave heating has an advantage in terms of localised heating which allows rapid heating of materials which will lead to rapid precipitation of material.<sup>281</sup> Therefore by replacing the 48 h hydrothermal method with microwave method could reduce the preparation time in addition to impregnating copper at different stages in the synthesis. Table 14 shows the

abbreviations of the catalysts preparation. Figure 4-1 shows the timeline on the synthesis of the catalyst at different preparation methods. The rate limiting step for HT method is the hydrothermal step which can be replaced by microwave method. However drying the catalyst is another rate limiting step for both hydrothermal and microwave method. This can be replaced by early copper incorporation into the catalyst which eliminates impregnation step and drying step.

**Table 14: Abbreviations for catalysts preparation of 2.3 wt% Cu/La<sub>2</sub>O<sub>3</sub>**

<b>Denotation</b>	<b>Preparation method</b>	<b>Total preparation time</b>
<b>HT</b>	Standard hydrothermal (48 h)	125 h~6 days
<b>HT-pre</b>	Standard hydrothermal with early copper incorporation (48 h)	86 h~4 days
<b>MW-16</b>	Standard microwave (16 h)	113 h~5 days
<b>MW-3</b>	Short microwave (3 h)	76 h~3 days
<b>MW-pre</b>	Microwave with 'one-pot' copper incorporation (16 h)	50 h~2 days

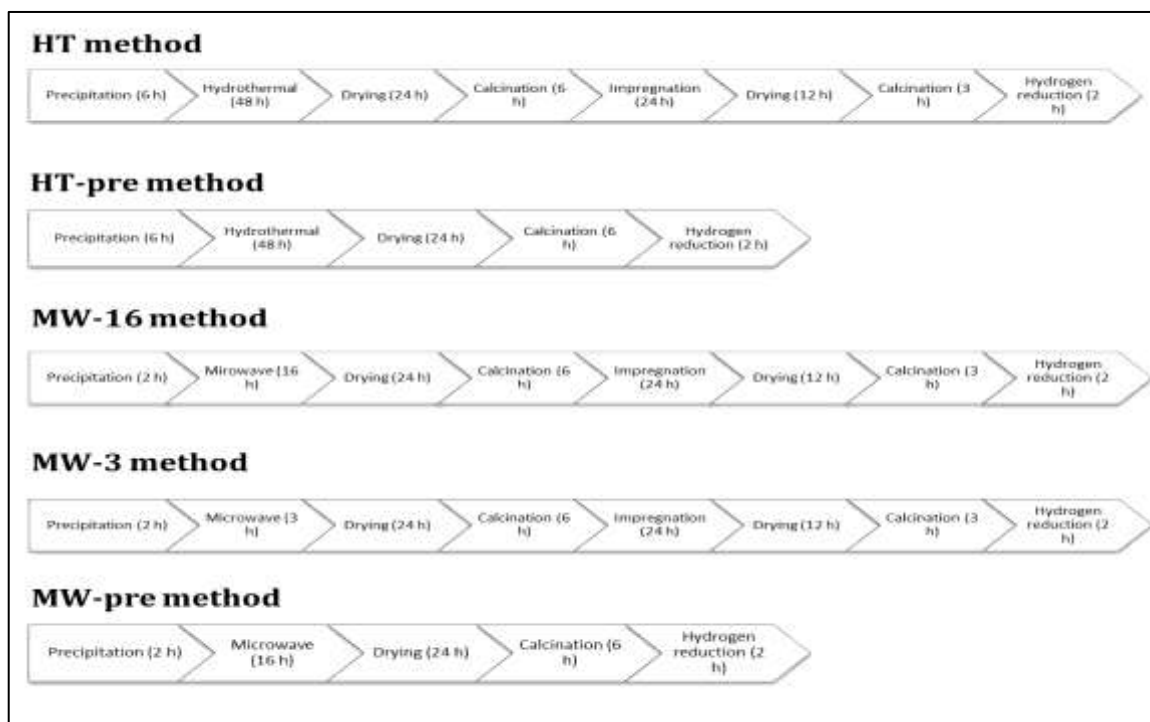


**Figure 4-1: Different preparation methods for copper supported on lanthanum oxide**

## 4.2.1 Catalyst characterisation

### 4.2.1.1 Structural characterisation studies

The samples were characterised by XRD to determine the phase composition as well as the crystallinity of the prepared materials. **Error! Reference source not found.** shows the XRD patterns of  $\text{La}_2\text{O}_3$  prepared by HT and MW-16 method calcined at  $700^\circ\text{C}$ .  $\text{La}_2\text{O}_3$  synthesise using microwave method have similar diffraction peaks with  $\text{La}_2\text{O}_3$  synthesise by hydrothermal method. In MW-16,  $\text{La}_2\text{O}_3$  diffraction peaks at  $26.1^\circ$ ,  $29.1^\circ$ ,  $29.9^\circ$ ,  $39.5^\circ$ ,  $46.0^\circ$ ,  $53.6^\circ$  and  $55.8^\circ$ , which correspond to 100, 022, 011, 012, 110, 200 and 201 planes respectively. The support still maintains its hexagonal crystal phase structure. However,  $\text{La}_2\text{O}_3$  prepared by microwave method shows an amorphous structure, which can be seen from its slightly broad and less intense diffraction peaks. This is due to a shorter aging period for crystallisation. Aging can be defined as the production of ordered crystalline material by spontaneous evolution of a gel structure.<sup>99</sup>

Another reason for low crystallite materials is due to the mechanism of the microwave heating itself. The microwave is recognised for its localised and rapid heating. However, this could be a problem in producing crystallite materials. The rapid and localised heating results in fast nucleation which may inhibit crystal growth thus preventing crystal rearrangement, therefore, producing poor crystallite materials.<sup>282</sup> In some cases ‘impurities’ might be formed due to the isolation of species in the materials caused by rapid heating.<sup>283</sup> Rapid recrystallisation of material produced crystalline particles with small size distribution due to short crystallisation period.<sup>284,285</sup> In contrast to hydrothermal treatment of materials, conventional heating is certainly slower but overtime homogeneous reaction temperature could be achieved which results in slow and steady growth of crystallite materials and in some cases excess crystal growth.<sup>285</sup> Table 15 shows the lattice parameters and particle size of  $\text{La}_2\text{O}_3$  for HT and MW-16 method having particle size of 9.5 nm and 8.4 nm respectively.

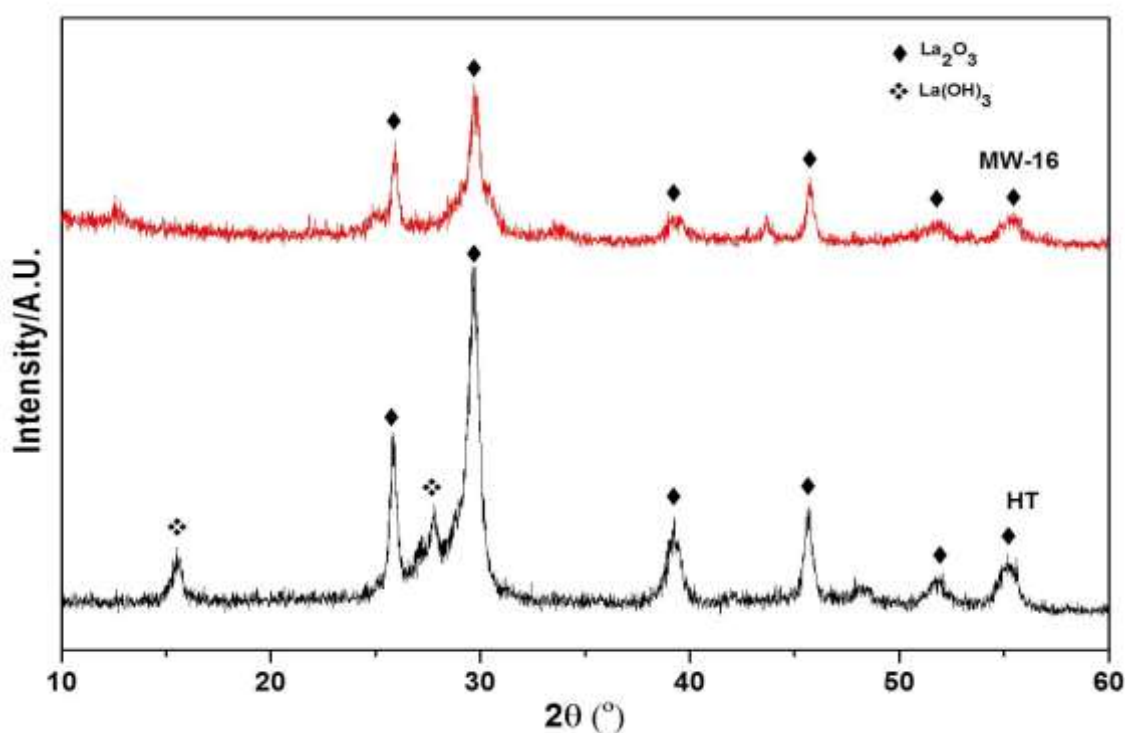


Figure 4-2: XRD patterns of  $\text{La}_2\text{O}_3$  synthesized by HT and MW-16 method

Table 15: Lattice parameters and particle size of  $\text{La}_2\text{O}_3$  for HT and MW-16

Catalyst	Lattice parameters	Particle size
----------	--------------------	---------------



<b>HT</b>	a=4.0 Å	9.5 nm
	b=4.0 Å	
	c=6.0 Å	
<b>MW-16</b>	a=3.9 Å	8.4 nm
	b=3.9 Å	
	c=6.2 Å	

The incorporation of 2.3 wt% Cu into the support in three different preparation methods generate carbonate phase during impregnation step due to interaction with water as mentioned previously shown in Figure 4-3.  $\text{La}_2\text{O}_2\text{CO}_3$  diffraction peaks can be observed at  $10.9^\circ$ ,  $22.2^\circ$ ,  $25.8^\circ$ ,  $30.3^\circ$ ,  $33.6^\circ$  and  $44.5^\circ$  which correspond to 002, 004, 101, 103, 006 and 106 planes respectively for all three preparation methods. The samples also consist of  $\text{La}(\text{OH})_3$  phase having diffraction peaks  $15.6^\circ$ ,  $27.2^\circ$  and  $27.9^\circ$  which corresponds to 100, 110 and 101 planes respectively. The diffraction peaks of MW-3 are broader than MW-16 and HT due to shorter aging period. This evidence was being proved by Bergada *et al* and Méndez *et al* that increasing aging time increases the crystallinity of the materials prepared.<sup>99,286</sup> This shows that the microwave synthesis can be an alternative method to synthesise the same material at a shorter time to be employed in the catalytic reaction.

Another method to reduce the lengthy preparation time in the synthesis of 2.3 wt% Cu/ $\text{La}_2\text{O}_3$  is by incorporating copper at the earlier stage in the synthesis. This reduces the preparation time to 4 days and 2 days for HT-pre and MW-pre respectively. Cu is being incorporated after the preparation of  $\text{La}(\text{OH})_3$  in the HT-pre method. 'One-pot' synthesis method was used for MW-pre in which Cu was incorporated at the start of 16 h microwave treatment shown in Figure 4-3. Carbonate phase would be expected to be the dominant phase after incorporating Cu however the dominant phase for HT-pre is the hydroxyl phase as well as  $\text{La}_2\text{O}_3$  phase. This is because the material was being heat treated up to  $700^\circ\text{C}$  which inhibits the growth of carbonate phase and moreover copper is being incorporated

with  $\text{La}(\text{OH})_3$  instead of  $\text{La}_2\text{O}_3$ . The elimination of impregnation step of Cu to  $\text{La}_2\text{O}_3$  also reduced the amount of  $\text{La}_2\text{O}_2\text{CO}_3$  phase being generated. In the synthesis of MW-pre, the material is very amorphous and the diffraction peaks are not identifiable. One-pot synthesis of copper also eliminates the presence of surface copper on the catalyst. Lattice parameters and particle sizes of 2.3 wt% Cu/ $\text{La}_2\text{O}_3$  at different preparation methods were determined and shown in Table 16. The particle sizes of HT, MW-16, MW-3 and HT-pre were 12.6 nm, 11.5 nm, 10.9 nm and 11.4 nm respectively.

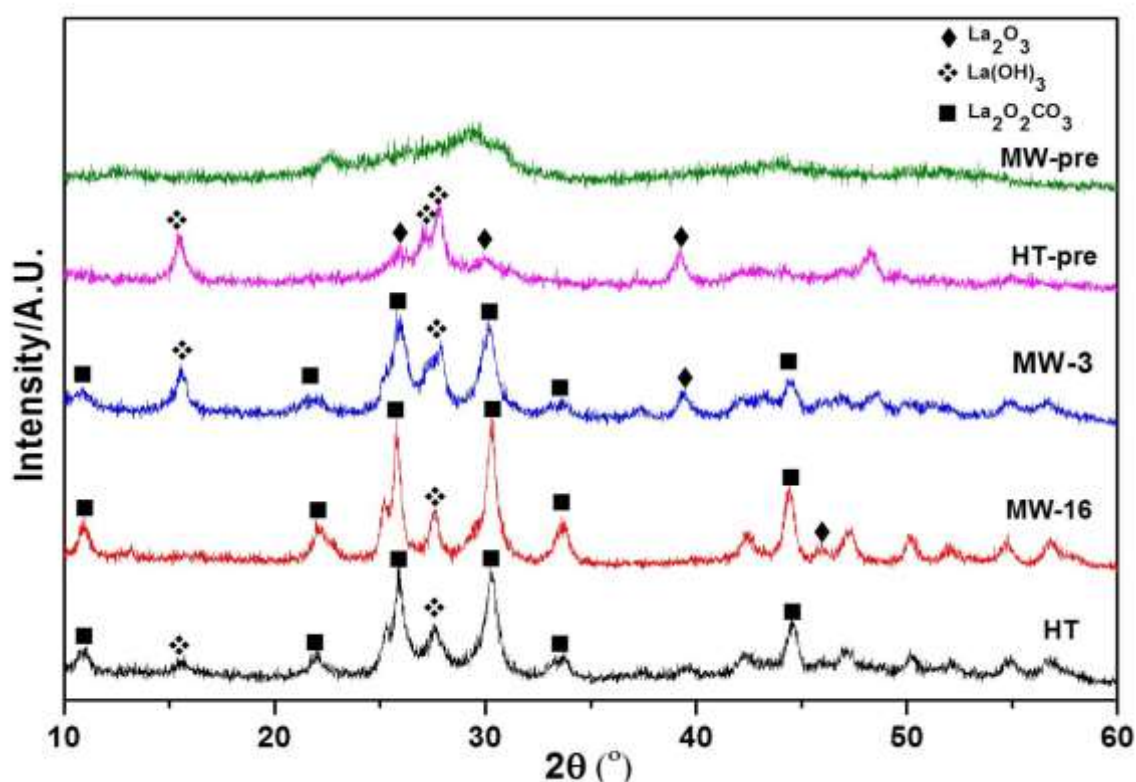


Figure 4-3: XRD patterns of 2.3 wt% Cu/ $\text{La}_2\text{O}_3$  prepared by five different methods: HT, MW-16, MW-3, HT-pre and MW-pre.

Table 16: Lattice parameters and particle size of 2.3 wt% Cu/ $\text{La}_2\text{O}_3$  for different preparation methods

Catalyst	Lattice parameters	Particle size
HT	$a=3.9 \text{ \AA}$	12.6 nm

---

	b=3.9 Å	
	c=16.3 Å	
<b>MW-16</b>	a=4.0 Å	11.5 nm
	b=4.0 Å	
	c=16.2 Å	
<b>MW-3</b>	a=4.0 Å	10.9 nm
	b=4.0 Å	
	c=16.0 Å	
<b>HT-pre</b>	a=4.0 Å	11.4 nm
	b=4.0 Å	
	c=6.1 Å	

---

#### 4.2.1.2 Thermogravimetric analysis (TGA)

TGA analyses were performed on all the samples to investigate the thermal decomposition of lanthanum hydroxide prepared by different methods shown in Figure 4-4.  $\text{La}(\text{OH})_3$  prepared by HT method has approximately three thermal decompositions. The first weight loss can be attributed to the loss of surface water at around 100°C. The next weight loss is due to the formation of  $\text{La}_2\text{O}_2\text{CO}_3$  in which  $\text{La}(\text{OH})_3$  reacts with  $\text{CO}_2$  at about 350°C. Lastly, the thermal decomposition of  $\text{La}(\text{OH})_3$  is at 550°C in which  $\text{La}_2\text{O}_2\text{CO}_3$  transformed into  $\text{La}_2\text{O}_3$  with the release of carbonate. The TGA results agreed with the results from XRD.

HT-pre is when  $\text{Cu}(\text{NO}_3)_2 \cdot 3\text{H}_2\text{O}$  was impregnated to  $\text{La}(\text{OH})_3$  instead of  $\text{La}_2\text{O}_3$ . The thermal decomposition at around 150°C is the decomposition of metal nitrates caused by an intermediate nitrite or through oxide species with variable valence for metal ions.<sup>287</sup> The decomposition above 250°C is due to decomposition of anhydrous nitrates.<sup>287</sup> It is possible that the decomposition of nitrates is favoured than the formation of carbonate species as there is no weight loss at about 350°C.

MW-3 has a similar thermal decomposition as HT. However, the decomposition of  $\text{La}(\text{OH})_3$  prepared by MW-16 appeared to be stable as temperature progressed in which there is no weight loss related to the formation of carbonate phase at around  $350^\circ\text{C}$ . The formation of  $\text{La}_2\text{O}_3$  could not be observed as the TGA method heated the catalysts to just below  $600^\circ\text{C}$ . The difference in decomposition could probably due to the difference in aging time in the microwave. Longer aging time possibly produced 'impurities' during microwave heating as mentioned above which stabilises  $\text{La}(\text{OH})_3$  phase before transforming to the oxide phase.

MW-pre is when copper salts were impregnated at the start of the synthesis. After  $300^\circ\text{C}$ , the material steadily losing weight which indicates that the material is not stable.

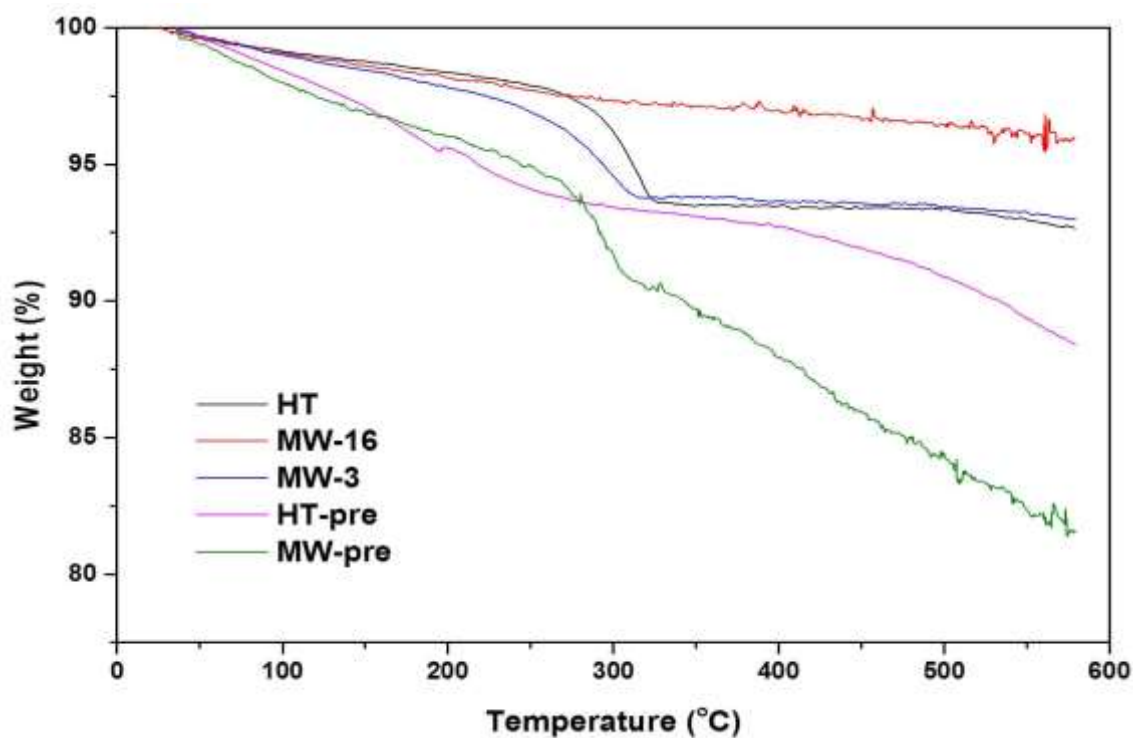


Figure 4-4: Thermogravimetric analysis of synthesized  $\text{La}(\text{OH})_3$  at different preparation methods

#### 4.2.1.3 Reduction profiles characterized by $\text{H}_2$ -TPR

Temperature-programmed reduction provides useful insight on the characteristics of metal reduction and the interaction with the support at different preparation methods. The different preparative methods exhibit different types of Cu species present on the catalyst. The catalyst prepared by HT method shows two distinct reduction peaks around 120°C-180°C and 400°C-550°C. The low-temperature range peak corresponds to highly dispersed CuO species with smaller particle size which was mentioned earlier.<sup>265</sup> The higher temperature region can be attributed to the decomposition of carbonate species.

Catalyst synthesised by MW-16 has similar reduction temperature peak with catalyst synthesised by HT method. Cu salts were impregnated after calcination of the support thus promoting high dispersion of Cu species in an amorphous phase.<sup>288</sup> However the decomposition of carbonate peak for MW-16 is higher than the other carbonate decomposition, which probably corresponds to different preparation methods.

For HT-pre, the incorporation of Cu was done at an earlier stage before the calcination of La(OH)<sub>3</sub> precursor and was heat treated at 700°C. Broad reduction peak can be observed at the range of 200°C-330°C. This could be due to Cu species undergoes sintering during the high heat treatment. The effect would cause dispersed Cu species to agglomerate producing a big bulk of Cu particles.

MW-pre of the catalyst exhibits reduction peak at around 300°C. This is due to the presence of large CuO particles. Motshekga *et al* also reported similar results in which microwave prepared SnO<sub>2</sub> nanoparticles having bigger size compare to the conventional method.<sup>289</sup> The effect is probably attributed to the concentrated amount of solution being used during 'one-pot' synthesis method. The reduced amount of solution prevents the mass transfer of metal salts in the solution.<sup>285,290</sup> Metal salts would be likely to accumulate which would lead to poor dispersion of active species. This agrees with the TPR result in Figure 4-5 in which there is no reduction peak present at around 120°C which corresponds to highly disperse and fine Cu species. There is also a small peak present at around 370°C-440°C which can be attributed to the reduction of highly dispersed Cu clusters having a strong interaction with the support.<sup>291</sup>

Therefore it can be concluded that different types of preparation method significantly affects the dispersion of Cu species and its interaction with the support. Particle size and crystallinity of the catalyst could not be determined in both hydrothermal and microwave method due to low loading of copper at 2.3 wt% which was previously mentioned in Chapter 3.

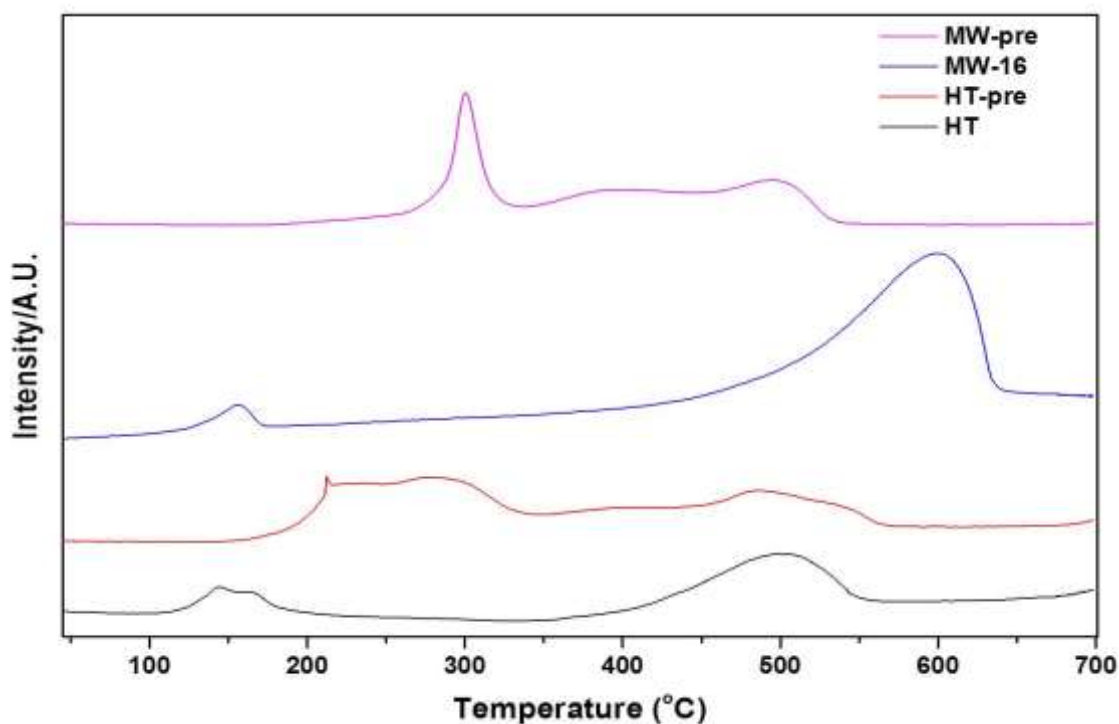


**Figure 4-5: Temperature-programmed reduction profiles of 2.3 wt% Cu/La<sub>2</sub>O<sub>3</sub> prepared by different methods**

#### 4.2.1.4 EDX analysis

**Table 17: Cu wt% analysed by EDX**

Catalyst	Copper wt%
HT	2.65
MW-16	2.92
MW-pre	3.01

The samples were analysed by Energy dispersive X-ray spectroscopy to determine the loading of copper in different preparation method shown in Table 17. HT catalyst has a slightly higher loading of 2.65% instead of 2.3% followed by MW-16 having a weight loading of 2.92%. MW-3 and HT-pre analysis were not being performed.

The highest weight loading is MW-pre having a weight loading of 3.01%. The highest weight loading is expected due to the manner MW-pre was being synthesised. Irregular dispersion of copper and the presence of big copper particles lead to higher weight loading.

#### 4.2.1.5 Basicity measurement by CO<sub>2</sub>-TPD

The CO<sub>2</sub>-TPD determines and measures the strength of basic sites present on the surface of the catalyst and the TPD profiles of 2.3 wt% Cu/La<sub>2</sub>O<sub>3</sub> prepared at different methods are shown in Figure 4-6. The strength of the basic sites can be represented by the temperature in which desorption takes place. The basic sites can be roughly divided into three distinct regions: weak basic sites which occur at around 50°C-150°C, medium basic sites occur between 150°C-550°C and strong basic sites occur above 550°C. The adsorption of weak basic sites is related to -OH groups on the surface of the catalyst. Medium basic sites can be ascribed to bidentate carbonate adsorbed on La-O pairs. Lastly, strong basic sites are caused by the adsorption of unidentate carbonate on isolated O<sup>2-</sup> ions.

The different preparation method produced slightly different desorption peaks. HT has the highest desorption peaks followed by MW-16. In MW-16, the CO<sub>2</sub> desorption peak shift towards low temperatures and there is a reduction in peak area. This could possibly be due to reduce aging time in the microwave synthesis thus producing less crystallisation of samples. In HT-pre, the precursor, La(OH)<sub>3</sub> was impregnated with copper salts before calcination at 700°C and reduction at 450°C. This effect could lead to sintering of copper particles at higher temperature producing a mass of copper particles which will then cover some of the exposed basic sites. Another cause of this effect is during heat treatment of the material, carbonate phases are not observed on the XRD diffraction peaks shown in Figure 4-3. According to Xin *et al* the increase in lattice oxygen (La-O pairs) contributes to the basicity of the catalyst especially medium basic sites due to the presence of

$\text{La}_2\text{O}_2\text{CO}_3$ .<sup>276</sup> In the case of MW-pre, there is, even more, reduction in basic sites due to the method in which the materials were being synthesised. The metal salts would be likely to accumulate due to reducing the amount of solution that prevents the mass transfer of metal salts in the solution.<sup>285,290</sup> This could lead to poor dispersion of active metals in the support thus covering basic sites of the catalyst. Another reason for the low amount of basic sites is due to less aging time.

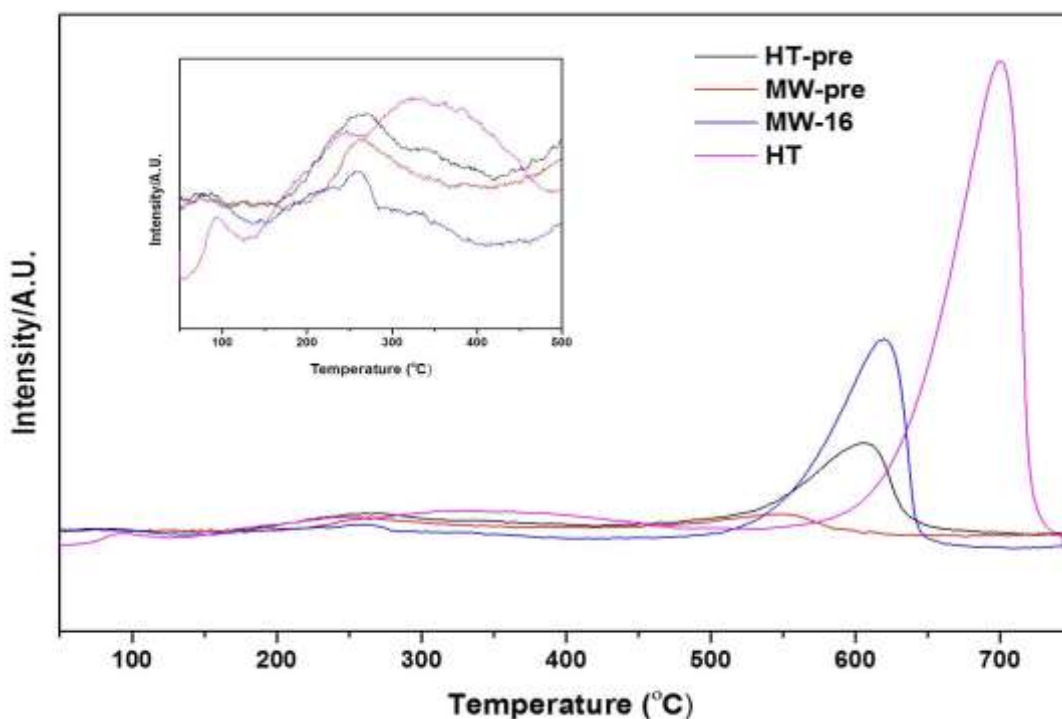


**Figure 4-6: Temperature-programmed desorption profiles of 2.3 wt% Cu/La<sub>2</sub>O<sub>3</sub> at different preparation method**

#### 4.2.2 Catalytic reaction

In this reaction, the catalyst synthesised by hydrothermal method is being compared with other catalyst synthesised by other methods in terms of activity. The experimental section is being described in Chapter 2 in which a general pressure vessel was being used instead of the overhead pressure vessel in Chapter 3.



#### 4.2.2.1 Dehydrating agent-Acetonitrile

The conversions of glycerol are slightly higher for the catalysts prepared by alternative methods than HT catalyst shown in Figure 4-7. The highest conversion of glycerol was achieved by MW-16 with 91.6%, followed by HT-pre with the conversion of 88.5% and MW-pre with the conversion of 87.6%. The decrease in conversion can be related to the decrease amount of basicity. HT catalyst did not follow the trend of basicity although it has a high amount of basicity. The reactions were repeated two times to reduce the error in the reactions. The error for this reaction is 3% and was determined by standard deviation. The high conversion from all the catalyst is due to the long reaction time of 24 h instead of 16 h which is reported in Chapter 3. This leads to over-reaction and this can contribute to the polymerisation of glycerol carbonate. 2.3 wt% Cu/La<sub>2</sub>O<sub>3</sub> synthesised by hydrothermal method (HT) also being subjected to the same reaction conditions.

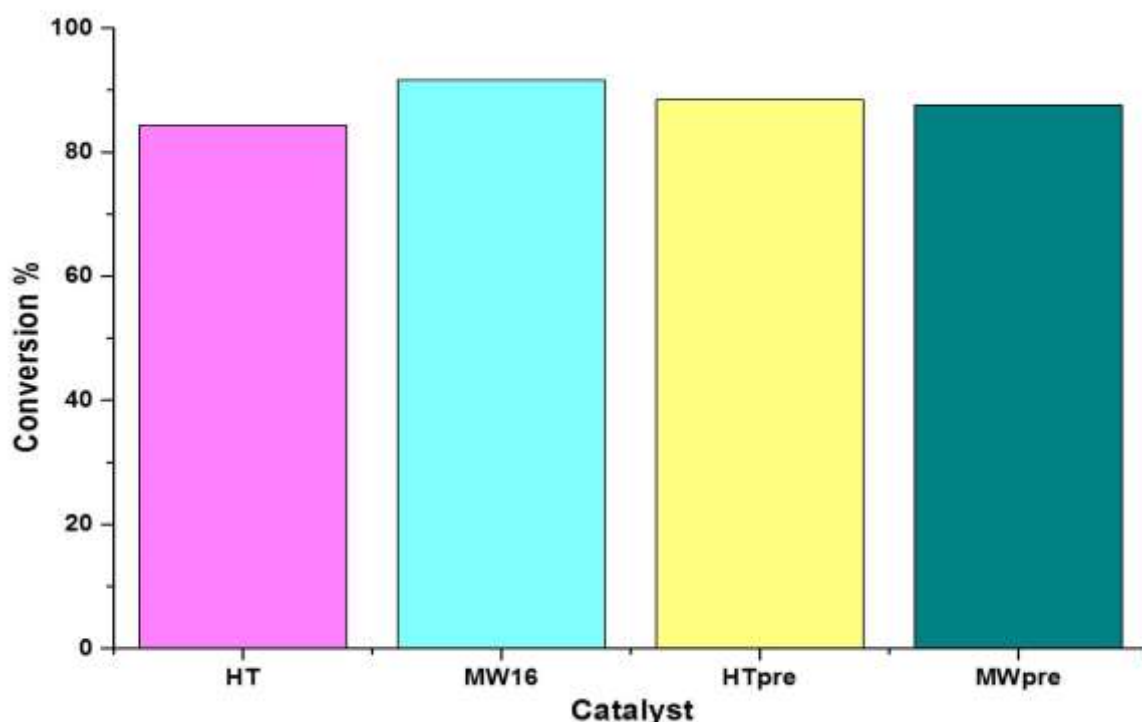
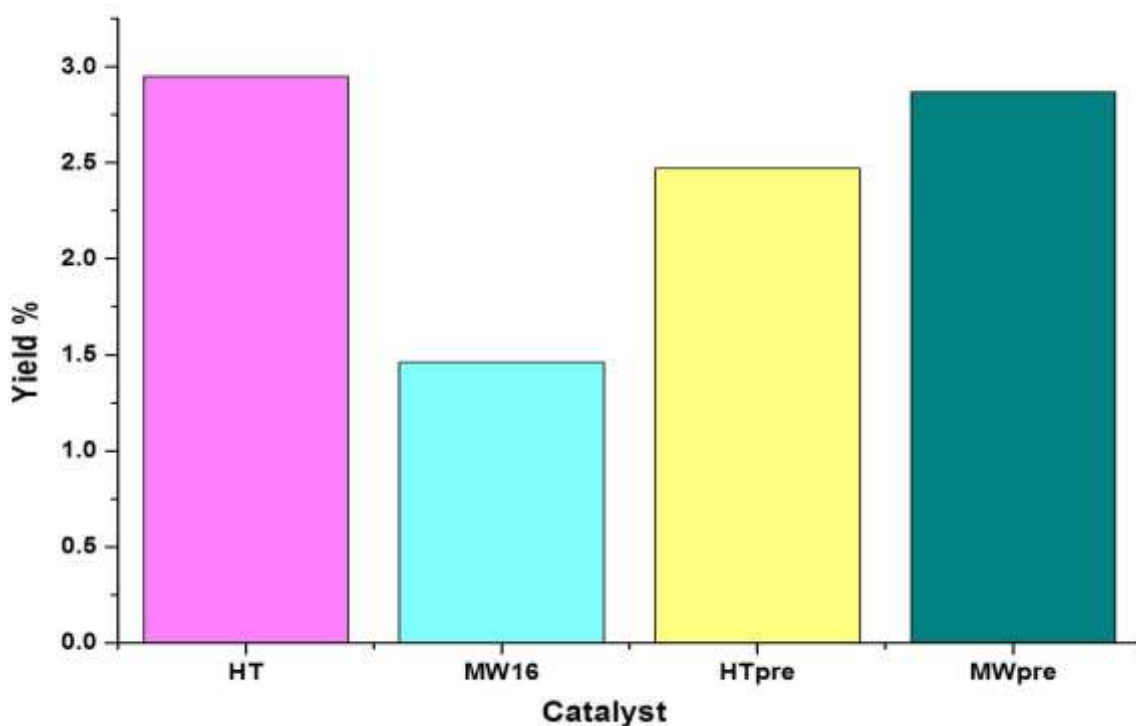


Figure 4-7: Conversion of glycerol for catalysts prepared by different methods. Reaction conditions: 2.3 g glycerol, 5 mL acetonitrile, 0.11 g catalyst, temperature: 150°C, pressure: 6.2 MPa, time: 24 h

Figure 4-8 shows the catalytic performance of the catalysts through yield of glycerol carbonate. HT and MW-pre catalysts have similar performance compare to MW-16 and HT-pre. Although HT and MW-16 have the highest amount of basic sites, the yield of the data for these two catalysts is not comparable. One factor that could contribute to this phenomenon is the dispersion of copper species or what type of copper species that is present on the catalyst in different preparation method which can be analysed using XPS. However, the main focus of this experiment is to reduce the amount preparation time on the synthesis of the catalyst and MW-pre has a similar yield of glycerol carbonate to HT catalyst.

The error for the reaction is 3% determined by standard deviation. Although high conversion of glycerol was obtained and low yield of glycerol carbonate could be linked to longer reaction time which is 24 h. This can be attributed to the polymerisation of glycerol carbonate. The chromatogram produced from the GC had small signals of other products which could not be identified by NMR or GCMS. There is no quantitative measurement of how much glycerol carbonate has reacted on to producing polymers. Therefore there is a need for further investigation on the catalytic reaction where maximum yield of glycerol carbonate can be achieved at less amount of time to avoid polymerisation of products.



**Figure 4-8: Yield of glycerol carbonate for catalysts prepared by different methods. Reaction conditions: 2.3 g glycerol, 5 mL acetonitrile, 0.11 g catalyst, temperature: 150°C, pressure: 6.2 MPa, time: 24 h**

Acetonitrile is being utilised as the dehydrating agent to remove water in the system. Acetonitrile reacts with water forming acetamide which further reacts with water to form acetic acid with the loss of ammonia. Then this will react with glycerol by esterification reaction to form the by-product acetins. However, acetins are produced in low amount in HT-pre and MW-pre and no traces of acetins were found in HT and MW-16 shown in Figure 4-9. Therefore a different mechanism is operating in this reaction. After the reaction, white precipitate residue was recovered on the edges of the reactor. The white precipitate was analysed using XRD and it is ammonium bicarbonate shown in Figure 4-10. Ammonium bicarbonate can be formed by the reaction of ammonia with carbonic acid. Carbonic acid can be produced from water and CO<sub>2</sub>. Scheme 4-1 shows the production of ammonium bicarbonate. Therefore it is possible that the formation of ammonium bicarbonate is an alternative pathway for removing water in the system.

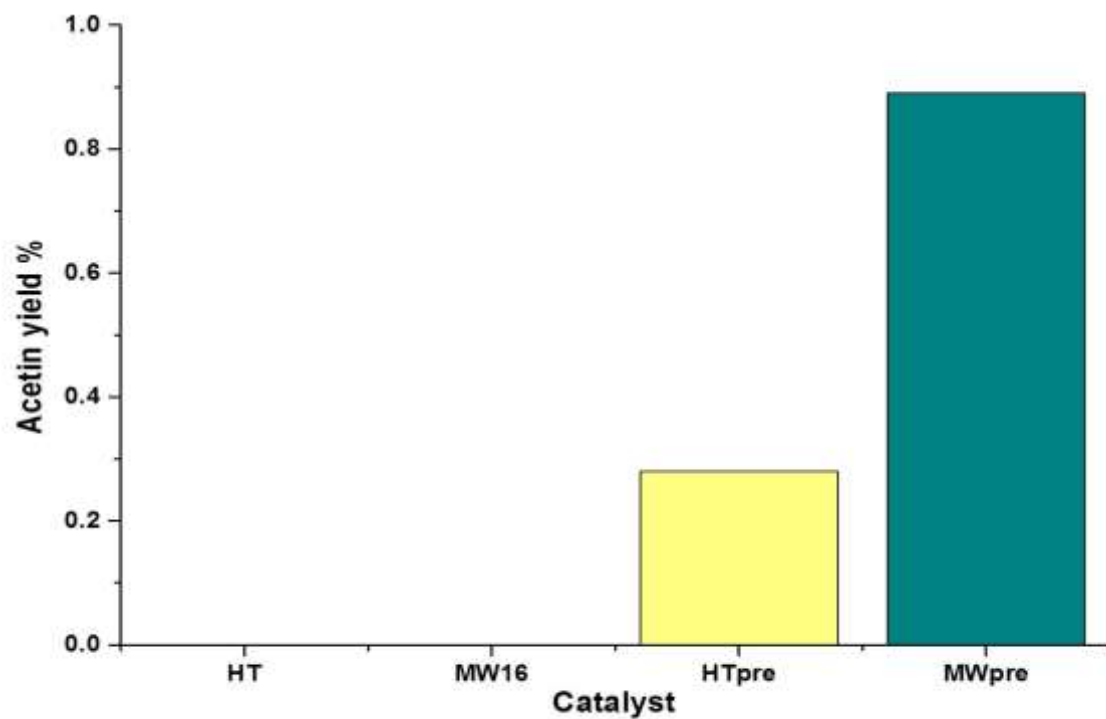


**Figure 4-9: Yield of acetin for catalysts prepared by different methods. Reaction conditions: 2.3 g glycerol, 5 mL acetonitrile, 0.11 g catalyst, temperature: 150°C, pressure: 6.2 MPa, time: 24 h**

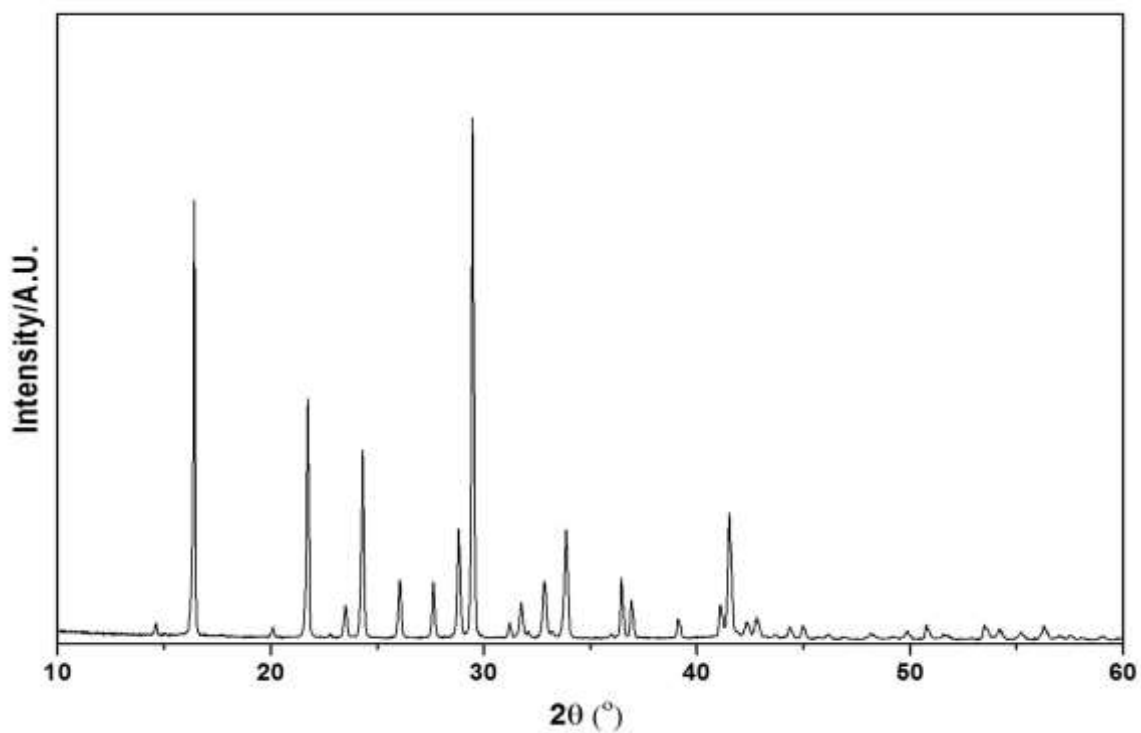
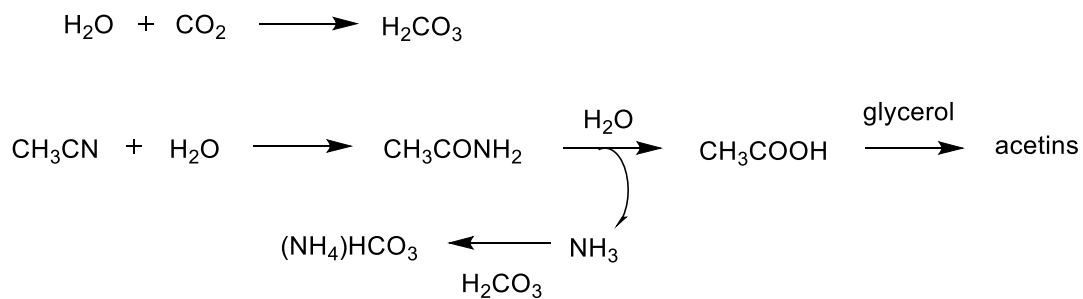


Figure 4-10: XRD patterns of ammonium bicarbonate



Scheme 4-1: Formation of ammonium bicarbonate from ammonia and carbonic acid

### 4.3 Conclusion

In this studies, the effect of different preparative methods used to synthesise 2.3 wt% Cu/La<sub>2</sub>O<sub>3</sub> were investigated. One of the aims of this research is to reduce the long hydrothermal method that Zhang *et al* used in his research by using microwave assisted synthesis of the catalyst. The shorter synthesis of MW-pre is an active catalyst in the synthesis of glycerol carbonate. Zhang *et al* suggested that copper on the surface of the catalyst involves in the activation of CO<sub>2</sub>. However this is not the case, as there is no copper on the surface from the XRD data. MW-pre has a comparable result to the HT method in terms of glycerol carbonate yield. However the glycerol carbonate yield could not be linked to the amount of basic sites. Another effect could contribute to high activity of MW-pre. To understand the reaction mechanism in great detail, short reaction time should be considered to avoid over reaction. Catalytic performance of catalysts from Chapter 3 and Chapter 4 could not be compared due to the differences in the vessel used in the reaction, the reaction time of the reaction and the final pressure achieved in the reaction. All the catalysts including catalyst synthesised by standard hydrothermal method (HT) were subjected to the same reaction condition which was previously discussed in Chapter 2.

# **CHAPTER 5**

## **DIRECT SYNTHESIS OF GLYCEROL CARBONATE FROM GLYCEROL AND CARBON DIOXIDE CATALYSED BY RARE EARTH METAL OXIDES USING 2-CYANOPYRIDINE AS DEHYDRATING AGENT**

## 5 DIRECT SYNTHESIS OF GLYCEROL CARBONATE FROM GLYCEROL AND CARBON DIOXIDE CATALYSE BY RARE EARTH METAL OXIDES USING 2-CYANOPYRIDINE AS DEHYDRATING AGENT

### 5.1 Introduction

In this chapter, rare earth oxides,  $\text{CeO}_2$  and  $\text{La}_2\text{O}_3$  catalytic activities were being investigated in the synthesis of glycerol carbonate using two different catalyst preparation: hydrothermal and microwave methods. Reaction parameters were varied and being examined and discussed in this chapter.

### 5.2 Results & Discussion

#### 5.2.1 Catalyst characterisation

##### 5.2.1.1 Structural characterisation studies

Figure 5-1 shows the XRD patterns of the  $\text{La}_2\text{O}_3$  calcined at two different temperatures: 400°C and 700°C using hydrothermal and microwave method. Both catalysts have hexagonal structure. The carbonate phase can be observed appearing at 400°C but are lost at 700°C. HT  $\text{La}_2\text{O}_3$  400°C diffraction peaks can be observed at 21.9°, 25.7°, 27.5°, 30.5°, 33.1°, 42.0°, 44.3° and 46.1° which correspond to 004, 101, 102, 103, 006, 106, 110 and 107 planes respectively. The diffraction peaks of HT  $\text{La}_2\text{O}_3$  700°C can be observed at 26.1°, 29.1°, 29.9°, 39.5°, 46.0°, 52.1° and 55.9° which correspond to 100, 002, 011, 012, 110, 103 and 201. **Error! Reference source not found.** shows the lattice parameters and particle size of HT  $\text{La}_2\text{O}_3$  at different calcination temperature. The average crystallite of HT  $\text{La}_2\text{O}_3$  400°C and  $\text{La}_2\text{O}_3$  700°C are 2.2 nm and 11.7 nm respectively. The XRD patterns of  $\text{La}_2\text{O}_3$  synthesised by microwave method calcined at two different temperatures are quite difficult to identify as it is too broad indicating the catalyst is quite amorphous.



Figure 5-2 shows the XRD pattern of CeO<sub>2</sub> catalysts prepared at two different calcination temperatures using hydrothermal and microwave method. It can be found that HT CeO<sub>2</sub> has cubic crystal phase (ICCD 34-0394). The diffraction peaks for HT CeO<sub>2</sub> are at 28.5°, 33.0°, 47.5° and 56.1° which correspond to 111, 200, 220 and 311 planes respectively. Table 19 shows the lattice parameters and particle size of CeO<sub>2</sub> synthesised by hydrothermal and microwave method. The average crystallite sizes of HT CeO<sub>2</sub> 400°C and CeO<sub>2</sub> 700°C are 8.6 nm and 19.6 nm respectively. It can be observed that the diffraction peaks are narrowed down with the increase in calcination temperature which indicates sintering forming large particles and increase of crystallite size of HT CeO<sub>2</sub>.

MW CeO<sub>2</sub> diffraction peak can be observed at 28.1°, 32.4°, 47.5° and 55.6° which correspond to 111, 200, 220 and 311 planes respectively. These values are consistent with the literature. However, two unknown peaks at 14.1° and 19.4° appeared in the microwave synthesis. The average crystallite size of MW CeO<sub>2</sub> at 400°C and 700°C are 10.2 nm and 15.6 nm respectively. The broadening of the diffraction peaks suggests that the particles are small and of low crystallinity.

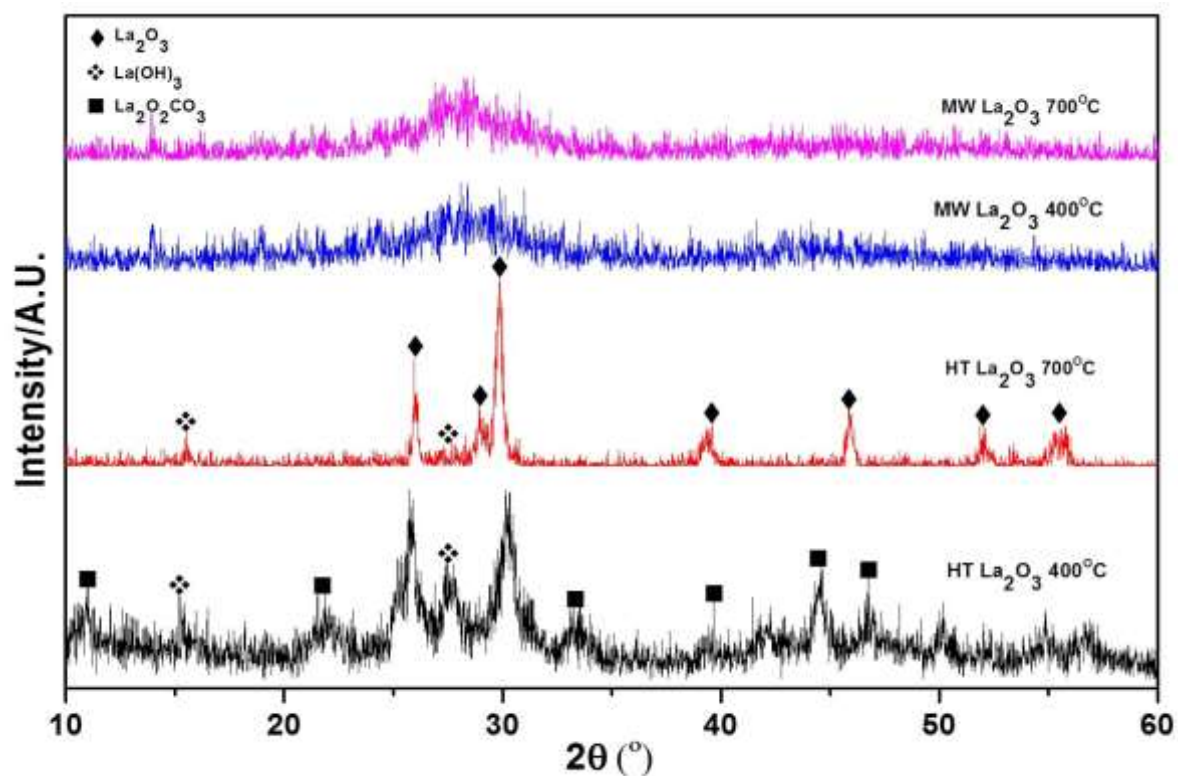


Figure 5-1: XRD patterns of  $\text{La}_2\text{O}_3$  synthesise by hydrothermal and microwave method calcined at two different temperatures

Table 18: Lattice parameters and particle size of  $\text{La}_2\text{O}_3$  synthesised by hydrothermal method at different calcination temperature

Catalyst	Lattice parameters	Particle size
HT $\text{La}_2\text{O}_3$ 400°C	a=4.1 Å b=4.1 Å c=16.2 Å	2.2 nm
HT $\text{La}_2\text{O}_3$ 700°C	a=3.9 Å b=3.9 Å c=6.1 Å	11.7 nm

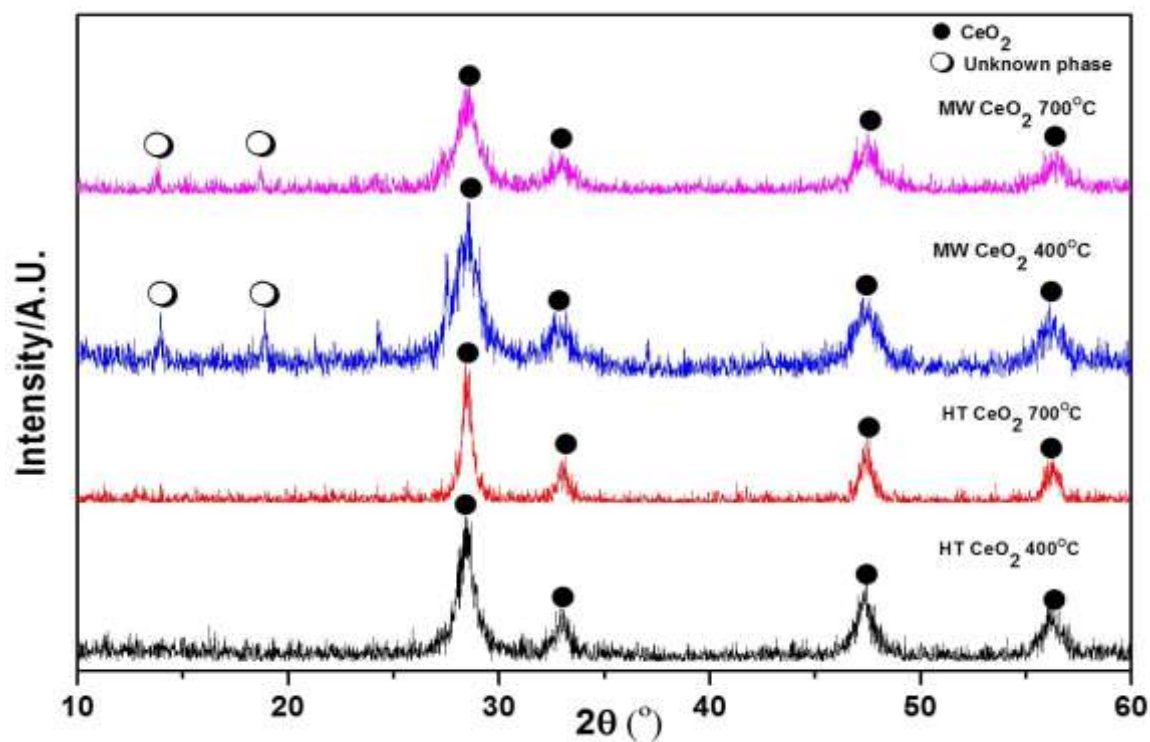


Figure 5-2: XRD patterns of  $\text{CeO}_2$  synthesized by hydrothermal and microwave method calcined at two different temperatures

Table 19: Lattice parameters and particle size of  $\text{CeO}_2$  synthesised by hydrothermal method at different calcination temperature

Catalyst	Lattice parameters	Particle size
HT $\text{CeO}_2$ 400°C	$a=5.4 \text{ \AA}$	8.6 nm
	$b=5.4 \text{ \AA}$	
	$c=5.4 \text{ \AA}$	
HT $\text{CeO}_2$ 700°C	$a=5.4 \text{ \AA}$	19.6 nm
	$b=5.4 \text{ \AA}$	
	$c=5.4 \text{ \AA}$	
MW $\text{CeO}_2$ 400°C	$a=5.4 \text{ \AA}$	10.2 nm
	$b=5.4 \text{ \AA}$	

	c=5.4 Å	
<b>MW CeO<sub>2</sub> 700°C</b>	a=5.4 Å	15.6 nm
	b=5.4 Å	
	c=5.4 Å	

#### 5.2.1.2 Characterisation of N<sub>2</sub> adsorption

BET surface areas and pore volumes of CeO<sub>2</sub> and La<sub>2</sub>O<sub>3</sub> catalysts were analysed to investigate the effect of synthesising catalysts by hydrothermal and microwave method as well as different heat treatments undergone by the catalysts at 400°C and 700°C. The results are summarised in Table 20. The error for BET analysis is 2%.

La<sub>2</sub>O<sub>3</sub> is a stable mixed oxide with a perovskite structure and usually has a low surface area. Typically, commercial La<sub>2</sub>O<sub>3</sub> has a low surface area of 3 m<sup>2</sup> g<sup>-1</sup> whereas La<sub>2</sub>O<sub>3</sub> synthesised by hydrothermal method has a surface area in the range of 30-50 m<sup>2</sup> g<sup>-1</sup>.<sup>292</sup> As expected the surface areas and pore volume decreased as calcination temperature increase. The surface area of HT La<sub>2</sub>O<sub>3</sub> 400°C and HT La<sub>2</sub>O<sub>3</sub> 700°C is 67 m<sup>2</sup> g<sup>-1</sup> (entry 1) and 27 m<sup>2</sup> g<sup>-1</sup> (entry 2) respectively. The pore volume decreases from 0.35 cm<sup>3</sup> g<sup>-1</sup> to 0.06 cm<sup>3</sup> g<sup>-1</sup>. There is not much difference in surface area and pore volume for microwave synthesised La<sub>2</sub>O<sub>3</sub>. MW La<sub>2</sub>O<sub>3</sub> 400°C has a BET surface area of 70 m<sup>2</sup> g<sup>-1</sup> with a pore volume of 0.31 cm<sup>3</sup> g<sup>-1</sup> (entry 3) whereas MW La<sub>2</sub>O<sub>3</sub> 700°C has a BET surface area of 26 m<sup>2</sup> g<sup>-1</sup> with a pore volume of 0.10 cm<sup>3</sup> g<sup>-1</sup> (entry 4). Similar textural properties can be achieved using microwave heating for a shorter period of aging time, 12 h.

The BET surface area and pore volume decreased from 102 m<sup>2</sup> g<sup>-1</sup> (entry 5) to 43 m<sup>2</sup> g<sup>-1</sup> (entry 6) and 0.31 cm<sup>3</sup> g<sup>-1</sup> to 0.18 cm<sup>3</sup> g<sup>-1</sup> with the increase in calcination temperature from 400°C to 700°C for HT CeO<sub>2</sub>. The reduction in surface area is due to the sintering of particles at elevated temperature.<sup>276</sup> MW CeO<sub>2</sub> 400°C has a BET surface area of 67 m<sup>2</sup> g<sup>-1</sup> (entry 7) and did not have similar BET surface area as the catalyst treated hydrothermally. However, the pore volume remained the same. When CeO<sub>2</sub> was treated at 700°C, the BET surface area did not reduce drastically. The BET surface area of MW CeO<sub>2</sub> 700°C is 59 m<sup>2</sup> g<sup>-1</sup> with a pore volume of 0.27

cm<sup>3</sup> g<sup>-1</sup>. This could be due to the presence of unknown phase which can be observed in the XRD patterns above which could possibly prevent bulk sintering of materials at a higher temperature. It should also be noted that there is a difference in crystallite size of microwave materials compare to hydrothermal materials at elevated temperature.

**Table 20: Textural properties of CeO<sub>2</sub> and La<sub>2</sub>O<sub>3</sub>**

Entry	Catalysts	Surface area (m <sup>2</sup> g <sup>-1</sup> )	Pore Volume ( cm <sup>3</sup> g <sup>-1</sup> )
1	HT La <sub>2</sub> O <sub>3</sub> 400°C	67	0.35
2	HT La <sub>2</sub> O <sub>3</sub> 700°C	27	0.06
3	MW La <sub>2</sub> O <sub>3</sub> 400°C	70	0.31
4	MW La <sub>2</sub> O <sub>3</sub> 700°C	26	0.10
5	HT CeO <sub>2</sub> 400°C	102	0.31
6	HT CeO <sub>2</sub> 700°C	43	0.18
7	MW CeO <sub>2</sub> 400°C	67	0.31
8	MW CeO <sub>2</sub> 700°C	59	0.27

#### 5.2.1.3 Basicity measurement by CO<sub>2</sub>-TPD

The CO<sub>2</sub>-TPD profiles of La<sub>2</sub>O<sub>3</sub> synthesised by hydrothermal method are shown in Figure 5-3. For comparison, the CO<sub>2</sub>-TPD profile of standard La<sub>2</sub>O<sub>3</sub> was tested. The CO<sub>2</sub> desorption temperature represents the strength of the basic sites. These can be roughly divided into three distinctive regions: weak basic sites (50°C-150°C), medium basic sites (150°C-550°C) and strong basic sites (above 550°C). According to few reports in the literature, the interaction of CO<sub>2</sub> with OH<sup>-</sup> groups on the surface of the catalyst is related to weak basic sites.<sup>101,293</sup> The medium basic sites can be associated with metal-oxygen pairs and adsorption of CO<sub>2</sub> onto isolated O<sup>2-</sup> anions can be correlated to strong basic sites.<sup>101,293</sup>

Both samples showed intense and broad desorption peaks at around 350°C in the medium basic site region indicating the basic strength is widely distributed.<sup>294</sup> The increase in calcination temperature affects the basicity of the catalyst. The CO<sub>2</sub> desorption peaks shifted slightly to high-temperature region with increasing calcination temperature of the catalyst. The CO<sub>2</sub>-TPD profiles can be deconvoluted and Table 21 shows the amount of CO<sub>2</sub> calculated on the surface of the catalyst. The highest amount of total basic sites is 215 μmol CO<sub>2</sub> g<sup>-1</sup> for HT La<sub>2</sub>O<sub>3</sub> 700°C (entry 2), followed by HT La<sub>2</sub>O<sub>3</sub> 400°C with total basic sites of 164 μmol CO<sub>2</sub> g<sup>-1</sup> (entry 1). However, there is no weak basic site present on the catalyst surface. The CO<sub>2</sub> desorption peaks of microwave materials can be divided into three regions: weak, medium and strong basic sites similar to CO<sub>2</sub> desorption peaks of hydrothermal materials. However, the peaks shifted towards high-temperature region indicating a stronger basic strength of the catalysts. MW La<sub>2</sub>O<sub>3</sub> 400°C has the highest total basic sites of 342 μmol CO<sub>2</sub> g<sup>-1</sup> (entry 3) followed by MW La<sub>2</sub>O<sub>3</sub> 700°C with total basic sites of 287 μmol CO<sub>2</sub> g<sup>-1</sup> (entry 4). The result is quite opposite of the hydrothermal synthesis. Nonetheless, MW La<sub>2</sub>O<sub>3</sub> 700°C has the highest amount of strong basic sites of 50 μmol CO<sub>2</sub> g<sup>-1</sup>.

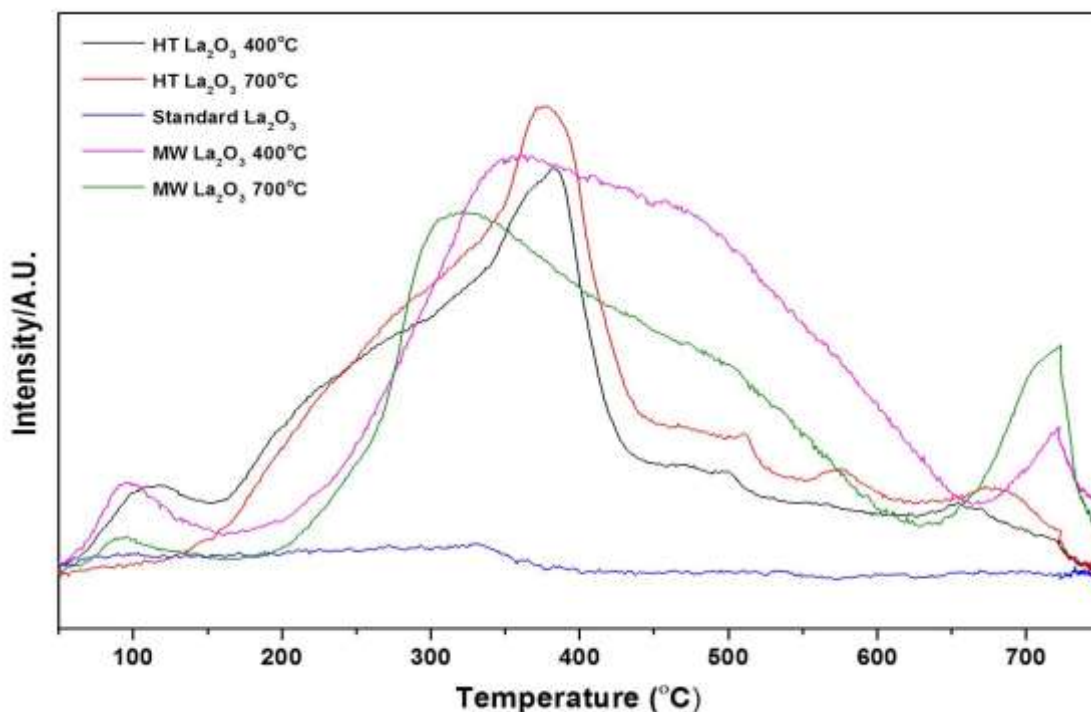


**Figure 5-3: Temperature-programmed desorption profiles of La<sub>2</sub>O<sub>3</sub> prepared by hydrothermal and microwave method calcined at two different temperatures**

**Table 21: Basic sites distribution calculated on the basis of CO<sub>2</sub>-TPD profiles**

Entry	Catalysts	Basic sites ( $\mu\text{mol CO}_2 \text{ g}^{-1}$ )			Total
		Weak	Medium	Strong	
1	HT La <sub>2</sub> O <sub>3</sub> 400°C	7	152	5	164
2	HT La <sub>2</sub> O <sub>3</sub> 700°C	-	205	10	215
3	MW La <sub>2</sub> O <sub>3</sub> 400°C	12	317	13	342
4	MW La <sub>2</sub> O <sub>3</sub> 700°C	4	233	50	287
5	Standard La <sub>2</sub> O <sub>3</sub>	-	1	1	2

The basicity of CeO<sub>2</sub> prepared by hydrothermal and microwave method calcined at two different calcination temperatures were determined by CO<sub>2</sub>-TPD shown in Figure 5-4. Standard CeO<sub>2</sub> obtained from Sigma-Aldrich was also tested as a baseline for the analysis. The amount of desorbed CO<sub>2</sub> from the surface of the catalyst is calculated which relates to the amount of basic sites present on the catalyst. This can be summarised in Table 22.

CO<sub>2</sub> desorption of CeO<sub>2</sub> catalyst can be roughly divided into three regions which are related to the basic strength of the catalyst: weak basic sites (50°C-200°C), medium basic sites (200°C-450°C) and strong basic sites (above 450°C).<sup>215</sup> The basic strengths are related to the adsorption of CO<sub>2</sub> on the surface of the catalyst. FTIR analysis have been performed by Yoshikawa *et al* and they have found that medium basic sites are due to two types of CO<sub>2</sub> adsorption which are monodentate carbonate and bidentate carbonate adsorb on the catalyst surface.<sup>295</sup> Weak basic sites are due to CO<sub>2</sub> desorption of hydrogen carbonate whereas strong basic sites can be attributed to polydentate carbonate species.<sup>295</sup> Figure 5-5 shows the adsorption of CO<sub>2</sub> onto the CeO<sub>2</sub> catalyst surface using FTIR.

The dominant basic sites are the weak basic sites for both catalysts whereas the amount of medium basic sites and strong basic sites are negligible. HT CeO<sub>2</sub> 700°C

has the highest total amount of basic sites of 104  $\mu\text{mol CO}_2 \text{ g}^{-1}$  (entry 2) followed by HT  $\text{CeO}_2$  400°C with basic sites of 94  $\mu\text{mol CO}_2 \text{ g}^{-1}$  (entry 1).

In microwave-assisted heating of  $\text{CeO}_2$ , the  $\text{CO}_2$  desorption peaks shifted slightly towards high temperature indicating the basic strength of MW  $\text{CeO}_2$  is higher than HT  $\text{CeO}_2$ . The peaks for weak basic sites and medium basic sites are slightly overlapped and for the purpose of quantification, the peak is integrated under weak basic sites. As the calcination temperature increases, the amount of basic sites of the catalyst increases. The amount of weak basic sites of microwave materials increased significantly from 112  $\mu\text{mol CO}_2 \text{ g}^{-1}$  (entry 3) to 263  $\mu\text{mol CO}_2 \text{ g}^{-1}$  (entry 4) compare to hydrothermal samples.

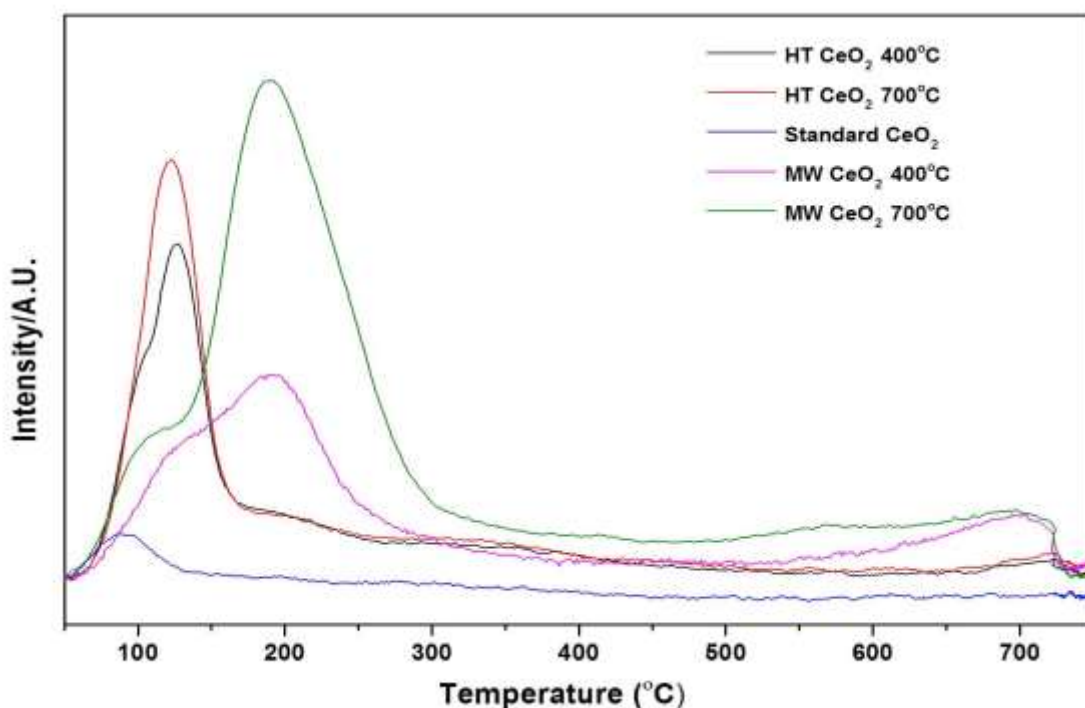


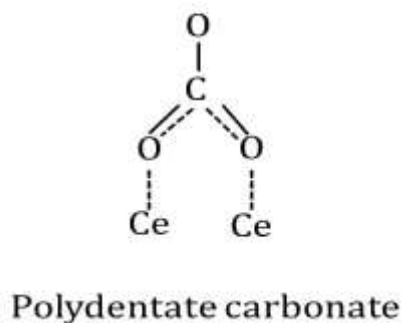
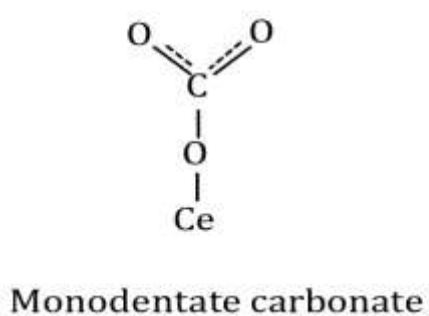
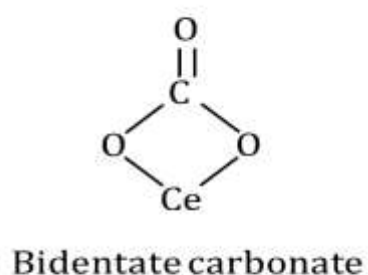
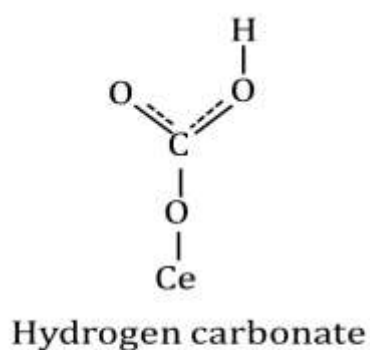
Figure 5-4: Temperature-programmed desorption profiles of  $\text{CeO}_2$  prepared by hydrothermal and microwave method calcined at two different temperatures

Table 22: Basic sites distribution calculated on the basis of  $\text{CO}_2$ -TPD profiles

Basic sites ( $\mu\text{mol CO}_2 \text{ g}^{-1}$ )
---



Entry	Catalysts	Weak	Medium	Strong	Total
1	HT CeO <sub>2</sub> 400°C	87	3	4	94
2	HT CeO <sub>2</sub> 700°C	97	3	3	102
3	MW CeO <sub>2</sub> 400°C	112	-	21	133
4	MW CeO <sub>2</sub> 700°C	229	-	34	263
5	Standard CeO <sub>2</sub>	12	-	3	15



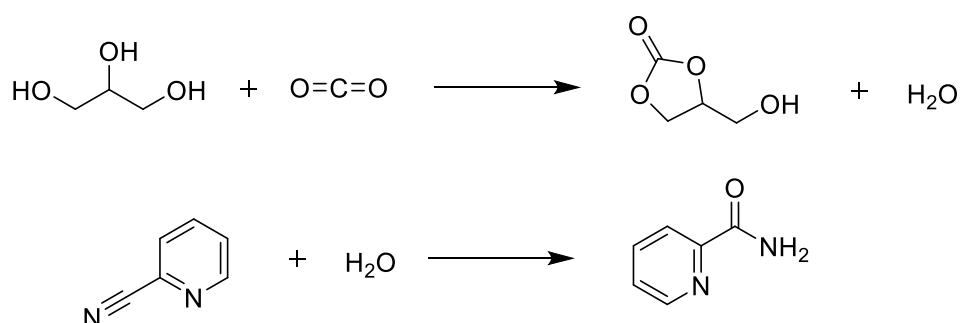
**Figure 5-5: Adsorbed CO<sub>2</sub> on the catalyst surface characterized by FTIR<sup>295</sup>**

The basicity measurement for the catalyst in this chapter is lower than the basicity measurements of the catalyst in Chapter 3 and Chapter 4. This is due to the differences in preparation method for the catalyst which can be found in experimental section, Chapter 2.

## 5.2.2 Catalytic reaction

### 5.2.2.1 Dehydrating agent-2 Cyanopyridine

2-cyanopyridine has been utilised as the dehydrating agent in the synthesis of various cyclic carbonates from CO<sub>2</sub> and diols. Recently Honda *et al* used utilised 2-cyanopyridine in the production of dimethyl carbonate giving a yield of 94%.<sup>163</sup> Therefore 2-cyanopyridine can be used in the synthesis of glycerol carbonate from glycerol and CO<sub>2</sub> as a dehydrating agent to remove water and shift the chemical equilibrium to the product side. Water reacts with 2-cyanopyridine to produce 2-picolinamide. Scheme 5-1 shows the carbonylation of glycerol to glycerol carbonate.



**Scheme 5-1: Reaction of glycerol with CO<sub>2</sub> to produce glycerol carbonate using 2-cyanopyridine as dehydrating agent**

2-cyanopyridine is a stable dehydrating agent compare to acetonitrile. According to Honda *et al*, intermolecular hydrogen bonding forms between N atoms of the

pyridine ring in 2-picolinamide and H atoms in the amide group which then weakens the interaction between the  $\text{NH}_2$  groups and the catalyst for further reaction.<sup>296</sup> Acetonitrile hydration forms an amide which will then further react with water to produce acetic acid. Acetic acid undergoes esterification with glycerol to produce the by-products acetins.<sup>155</sup>

#### 5.2.2.1.1 Effect of pressure

Glycerol carbonate synthesis via direct carbonylation of  $\text{CO}_2$  and glycerol requires high pressure to achieve maximum yield possible.<sup>38</sup> However, this is not the case for the synthesis of glycerol carbonate catalysed by  $\text{CeO}_2$ . Figure 5-6 shows the effect of pressure on the conversion of glycerol and yield of glycerol carbonate. The increase in pressure from 2.8 MPa to 4.2 MPa, the glycerol conversion increases from 6.7% to 12.5%. However, the glycerol conversion starts to decrease to 8.5% with the increase in pressure at 5.4 MPa. The effect of high  $\text{CO}_2$  pressure is due to saturation of  $\text{CO}_2$  on the surface of the catalyst. This could inhibit glycerol and 2-cyanopyridine adsorbing on the catalyst surface. The reaction was repeated four times to reduce error in the reaction. The error for this reaction is 2% using standard deviation method. Plausible reaction mechanism could be proposed which will be discussed later in this chapter.

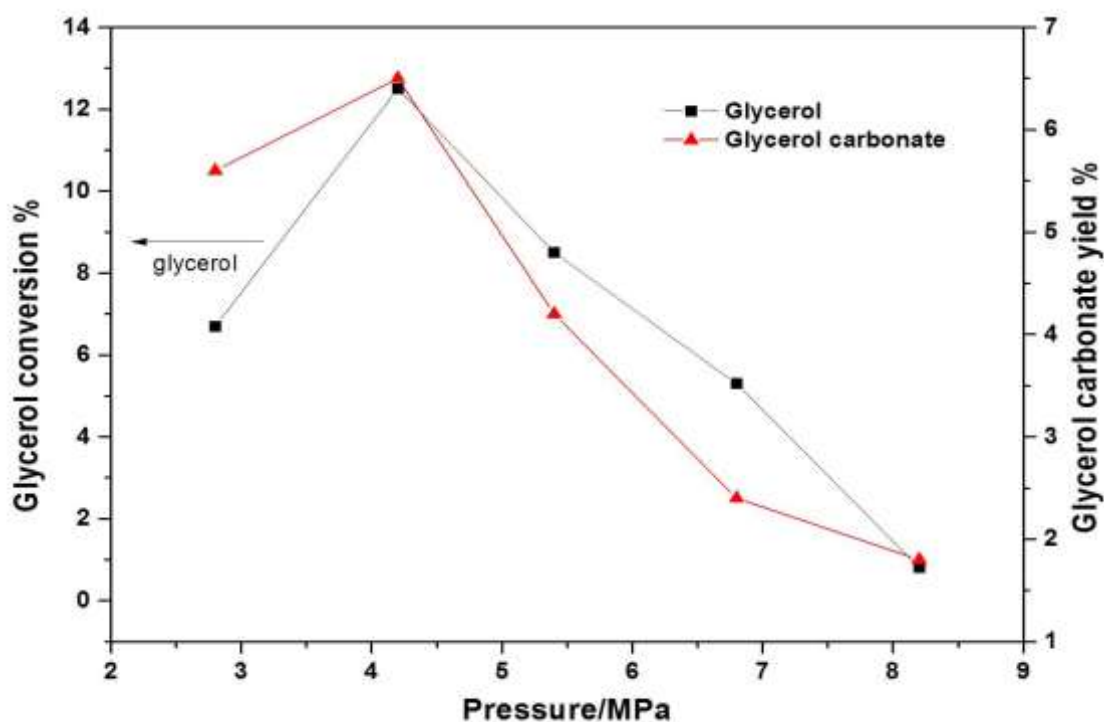


Figure 5-6: Effect of pressure on the carbonylation of glycerol with  $\text{CO}_2$  catalysed by  $\text{CeO}_2$   
 Reaction conditions: 0.92 g glycerol, 3.27 g 2-cyanopyridine, 0.34 g  $\text{CeO}_2$ , temperature: 150°C, time: 5 h

#### 5.2.2.1.2 Effect of reaction time

Figure 5-7 shows the effect reaction time on the reaction of glycerol with  $\text{CO}_2$ . It can be observed that the conversion of glycerol from 12.5% to 26.5% with an increase in reaction time. The yield of glycerol carbonate improved from 6.5% to 11.5% when the reaction time increased from 5 h to 8 h.

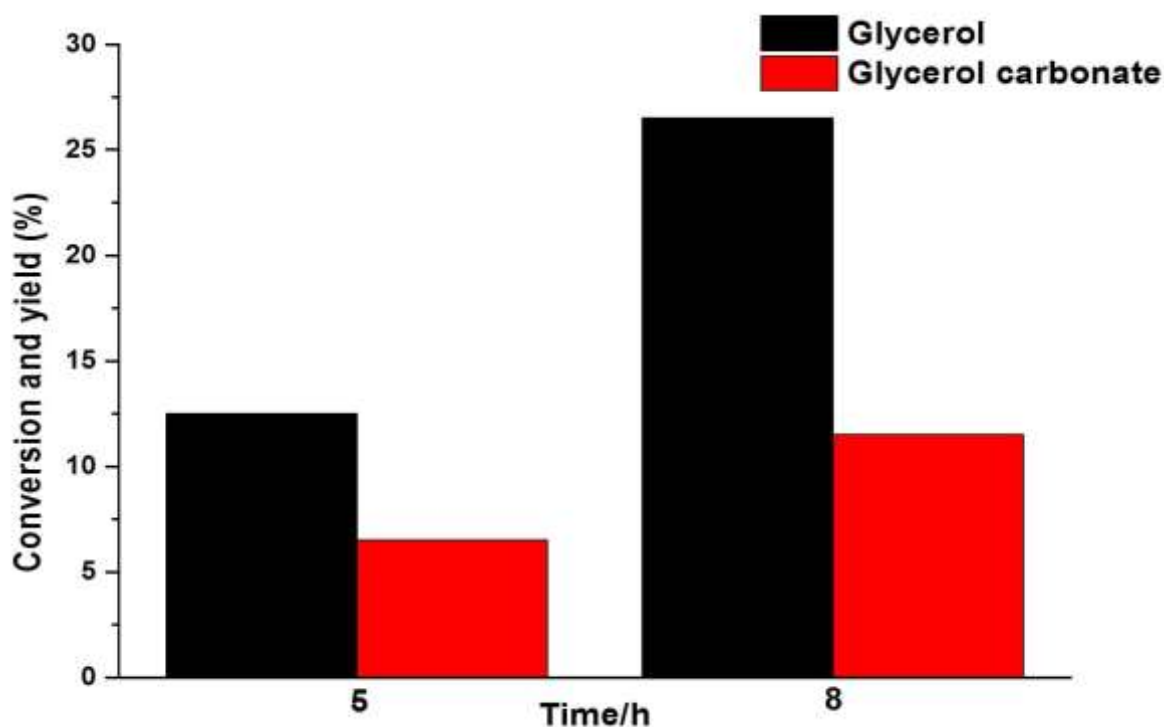


Figure 5-7: Effect of reaction time on the carbonylation of glycerol and CO<sub>2</sub> catalysed by CeO<sub>2</sub>. Reaction conditions: 0.92 g glycerol, 3.27 g 2-cyanopyridine, 0.34 g CeO<sub>2</sub>, temperature: 150°C, pressure: 4.2 MPa

#### 5.2.2.1.3 Effect on the catalyst amount

The amount of catalyst was also examined and can be shown in Figure 5-8. The conversion of glycerol increases from 11.5% to 36.9% with the increase in catalyst amount from 0.34 g to 0.52 g. The glycerol carbonate yield also improved from 9.5% to 17.1%. The order of reaction is first order with the increase in catalyst amount. The increase in stirring speed did not affect the yield of the product therefore mass transport limitation is not a problem in this reaction. The increase in pressure has the same effect as previously mentioned in section 5.2.2.1.1 although the amount of catalyst increases.

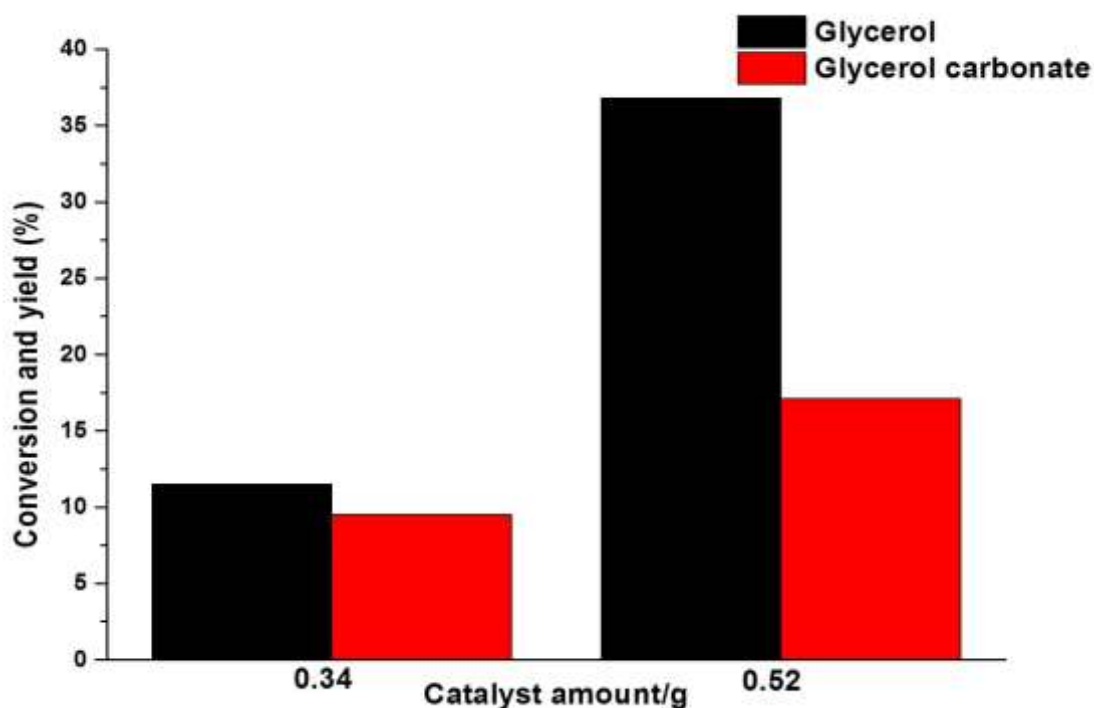
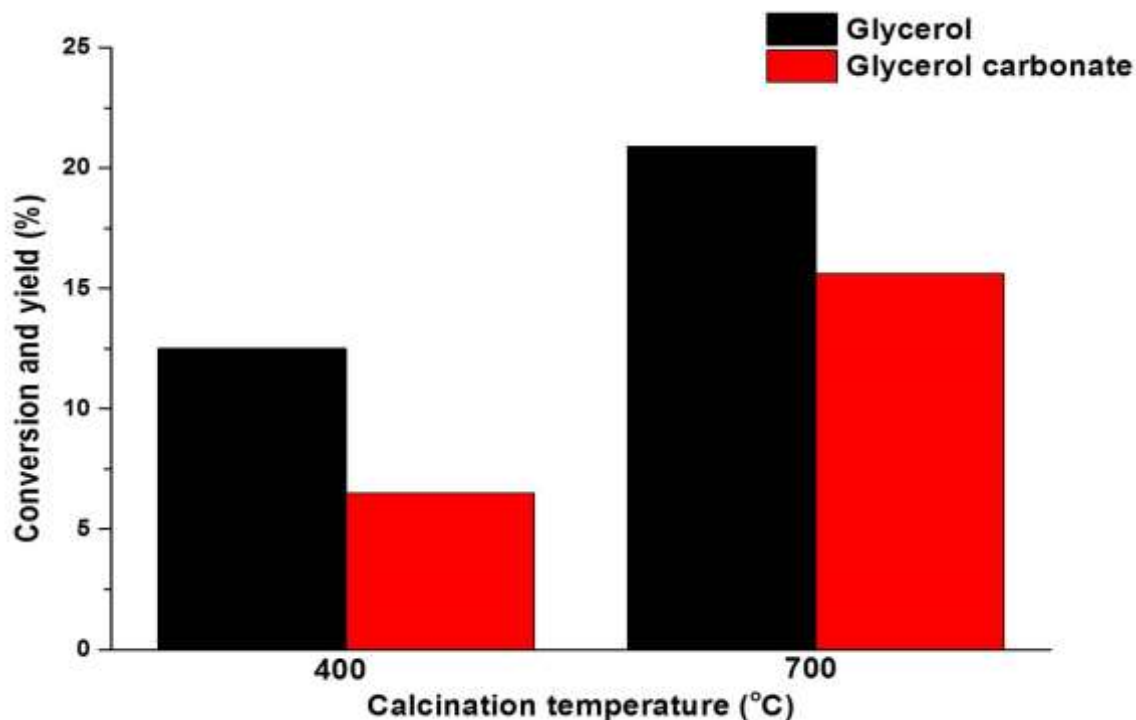


Figure 5-8: Effect of catalyst amount on the carbonylation of glycerol and CO<sub>2</sub>. Reaction conditions: 0.92 g glycerol, 3.27 g 2-cyanopyridine, temperature: 150°C, pressure: 3.1 MPa, time: 8 h

#### 5.2.2.1.4 Effect of calcination temperature of the catalyst

The effect of calcination temperature of CeO<sub>2</sub> has also been investigated on the conversion and yield of glycerol carbonate shown in Figure 5-9. The increase in calcination temperature from 400°C to 700°C caused an increase in glycerol conversion from 12.5% to 20.8%. The yield of glycerol carbonate increases from 6.5% to 15.6%. This is could be associated with the amount of basic sites present on the catalyst especially weak basic sites where the basic sites increase from 87  $\mu\text{mol CO}_2 \text{ g}^{-1}$  to 97  $\mu\text{mol CO}_2 \text{ g}^{-1}$  with the increase in calcination temperature. This is because strong basic sites will tend to adsorb CO<sub>2</sub> more strongly which prevent it from reacting with glycerol.



**Figure 5-9: Effect of calcination temperature of catalyst on the carbonylation of glycerol and CO<sub>2</sub>.** Reaction conditions: 0.92 g glycerol, 3.27 g 2-cyanopyridine, 0.34 g CeO<sub>2</sub>, temperature: 150°C, pressure: 4.2 MPa, time: 5 h

#### 5.2.2.1.5 Effect of preparation method of the catalyst

Hydrothermal synthesis and microwave-assisted heating of the catalyst were investigated and tested in the carbonylation reaction shown in Table 23. For HT CeO<sub>2</sub> 400°C and MW CeO<sub>2</sub> 400°C, the yield of glycerol carbonate were 6.5% (entry 1) and 10.0% (entry 3) respectively. For HT CeO<sub>2</sub> 700°C and MW CeO<sub>2</sub> 700°C, the yield of glycerol carbonate were 15.5% (entry 2) and 18.8% (entry 4) respectively. This shows that the catalyst synthesised by microwave method has a higher catalytic activity for the formation of glycerol carbonate and conversion of glycerol. The result can be correlated to the amount of basic sites present on the MW catalysts in which the weak basic sites of MW CeO<sub>2</sub> 400°C and MW CeO<sub>2</sub> 700°C were 112 μmol CO<sub>2</sub> g<sup>-1</sup> and 229 μmol CO<sub>2</sub> g<sup>-1</sup> respectively.

**Table 23: The effect of preparation method of the catalyst on the carbonylation reaction**

Entry	Catalyst	Calcination temperature °C	Glycerol conversion %	Glycerol carbonate yield%
1	HT CeO <sub>2</sub>	400	12.5	6.5
2	HT CeO <sub>2</sub>	700	20.9	15.5
3	MW CeO <sub>2</sub>	400	25.0	10.1
4	MW CeO <sub>2</sub>	700	30.2	18.8

**Reaction conditions: 0.92 g glycerol, 3.27 g 2-cyanopyridine, 0.34 g CeO<sub>2</sub>, temperature: 150°C, pressure: 4.0 MPa, time: 5 h**

#### **5.2.2.1.6 Effect of catalytic activity of La<sub>2</sub>O<sub>3</sub> and comparison with CeO<sub>2</sub> catalyst**

La<sub>2</sub>O<sub>3</sub> catalysts also being tested in the carbonylation of glycerol with CO<sub>2</sub> to produce glycerol carbonate presented in Table 24. La<sub>2</sub>O<sub>3</sub> synthesised by hydrothermal method shows an increase in glycerol conversion from 22.0% (entry 1) to 25.7% (entry 2) as well glycerol carbonate yield from 8.2% to 12.7% with the increase in calcination temperature of the catalyst. However, the activity of microwave synthesised catalysts shows a decrease in the conversion from 23.2% (entry 3) to 22.2% (entry 4) with the increase in heating treatment of the catalyst. The yield of glycerol carbonate is the same for both MW catalysts. This can be roughly correlated to the amount of basic sites, in this case, is medium basic sites which is dominant in La<sub>2</sub>O<sub>3</sub> catalysts. In MW catalysts, the medium basic sites for La<sub>2</sub>O<sub>3</sub> 400°C is higher than La<sub>2</sub>O<sub>3</sub> 700°C and this shows in the activity of the catalyst. Moreover, the basic sites for MW catalysts are slightly shifted towards high-temperature region.

A comparison of activity between La<sub>2</sub>O<sub>3</sub> and CeO<sub>2</sub> is also investigated. HT CeO<sub>2</sub> (entry 5) shows the highest performance in catalytic activity with 31.4% glycerol conversion and 17.5% glycerol carbonate yield compare to HT La<sub>2</sub>O<sub>3</sub> 700°C (entry 2). The possible reason for this difference in activity is the strength of basic sites.



CeO<sub>2</sub> predominantly have weak basic sites whereas La<sub>2</sub>O<sub>3</sub> have medium basic sites. This will affect the adsorption of reactants on the surface of the catalyst which results in the stronger interaction of reactants in La<sub>2</sub>O<sub>3</sub> thus blocking the active site.

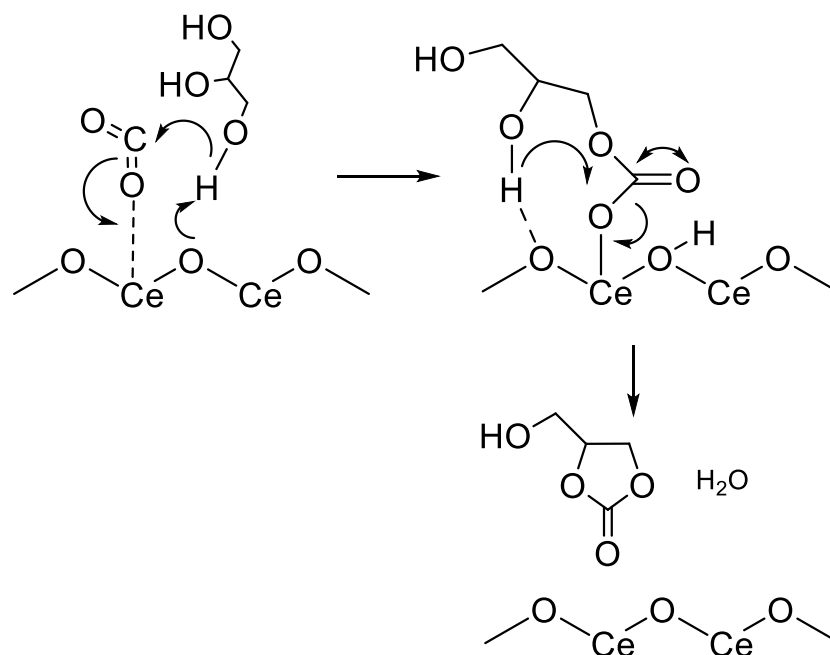
**Table 24: Catalytic activity of prepared catalysts for glycerol carbonylation**

Entry	Catalyst	Calcination temperature °C	Glycerol conversion %	Glycerol carbonate yield %
1	HT La <sub>2</sub> O <sub>3</sub>	400	22	8.2
2	HT La <sub>2</sub> O <sub>3</sub>	700	25.7	12.7
3	MW La <sub>2</sub> O <sub>3</sub>	400	23.2	4.3
4	MW La <sub>2</sub> O <sub>3</sub>	700	22.2	4.3
5	HT CeO <sub>2</sub>	700	31.4	17.5

Reaction conditions: 0.92 g glycerol, 3.27 g 2-cyanopyridine, 2 mmol catalyst, temperature: 150°C, pressure: 3.0 MPa, time: 5 h

#### 5.2.2.1.7 Plausible reaction mechanism

Glycerol is adsorbed onto the catalyst in this case is CeO<sub>2</sub> on the Lewis basic site. The hydrogen of the primary alcohol of glycerol is being abstracted by the basic sites and oxygen will act as a nucleophile. This will then attack CO<sub>2</sub> which was being activated by Lewis acid site shown in Scheme 5-2. Second hydrogen atom on the secondary alcohol of glycerol is adsorbed again on the catalyst, which will then increases nucleophilicity of the oxygen atom. This will then cause intramolecular nucleophilic attack producing glycerol carbonate and water.



**Scheme 5-2: Plausible reaction mechanism of carbonylation of glycerol with CO<sub>2</sub>**

### 5.3 Conclusion

In this reaction, catalytic activity of two catalysts were tested in the direct synthesis of glycerol carbonate from CO<sub>2</sub> using 2-cyanopyridine as a dehydrating agent. CeO<sub>2</sub> synthesised by microwave method showed the highest catalytic activity compare to the catalyst prepared by hydrothermal method. However, the opposite results occurred in La<sub>2</sub>O<sub>3</sub> catalyst in which the hydrothermal method has higher activity compare to the microwave method. The amount of basicity and strength of basic sites have an effect in the overall activity of the catalyst. The selection of dehydrating agent is very important in the CO<sub>2</sub> reactions as high yield of glycerol carbonate can be obtained by using 2-cyanopyridine at a shorter time compare to using acetonitrile. In using acetonitrile as dehydrating agent, there is a tendency of over-reactions due to the production of acetins as by-product of the reaction which was discussed in Chapter 3 and Chapter 4.

# **CHAPTER 6**

## **SYNTHESIS OF GLYCEROL CARBONATE FROM UREA OVER RARE EARTH METAL OXIDES AS A SOLID BASE CATALYST**

## **6 SYNTHESIS OF GLYCEROL CARBONATE FROM UREA OVER RARE EARTH METAL OXIDES AS A SOLID BASE CATALYST**

### **6.1 Introduction**

In this study, two rare earth oxides,  $\text{CeO}_2$  and  $\text{La}_2\text{O}_3$  were tested in the carbonylation of glycerol with urea. The catalysts were prepared by both hydrothermal and microwave method to investigate its activity. The activity of the reaction was also investigated using conventional heating and microwave heating.

Currently, conventional heating is used to synthesise the production of glycerol carbonate via different methods.<sup>118</sup> Teng *et al* have reported using microwave heating in the transesterification of glycerol with dimethyl carbonate giving 93% yield of glycerol carbonate at 65°C in 5 min.<sup>297</sup> Microwave heating is a well-known method to carry out chemical transformations at a shorter period of time with low energy requirement.<sup>298,299</sup> The microwave reaction would be feasible as glycerol has high dielectric properties which could speed up the reaction.<sup>297</sup> The use of microwave as an energy source for the production of glycerol carbonate from urea has not been reported in any literature.

### **6.2 Results and Discussion**

#### **6.2.1 Catalyst characterisation**

The catalyst analysis for this chapter can be found in Chapter 5.

#### 6.2.2.1 Reaction pathways for the reaction between glycerol and urea

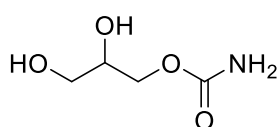


173

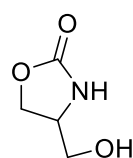
### 6.2.2.2 Comparison on the activity of catalysts

The catalytic behaviour of CeO<sub>2</sub> and La<sub>2</sub>O<sub>3</sub> prepared by two different routes: hydrothermal and microwave method is presented in Table 25. The reactions were carried out at conditions where full glycerol conversion was not achieved, in order to enable a comparison of catalytic activity. Under these conditions, in addition to glycerol carbonate, three other products were detected. There are **SP1**, **SP2** and **SP3**.

**SP1**



**SP2**



**SP3**

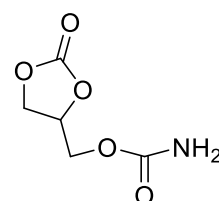


**Table 25: Glycerol carbonate synthesis from urea over various catalyst**

Entry	Catalyst	Calcination temperature °C	Conversion %	Glycerol carbonate	Selectivity %			Glycerol carbonate yield %
					SP1	SP2	SP3	
1	Blank		66	42	22	20	16	28
2	La <sub>2</sub> O <sub>3</sub>	400	94	66	0	21	13	62
3	La <sub>2</sub> O <sub>3</sub>	700	96	71	0	17	12	68
4	MW La <sub>2</sub> O <sub>3</sub>	400	89	56	11	21	12	50
5	MW La <sub>2</sub> O <sub>3</sub>	700	80	56	13	17	14	44
6	CeO <sub>2</sub>	400	71	43	16	26	15	31
7	CeO <sub>2</sub>	700	64	49	14	21	16	32
8	MW CeO <sub>2</sub>	400	70	42	19	23	16	30

<b>9</b>	MW CeO <sub>2</sub>	700	72	48	17	20	16	34
<b>10</b>	Zeolite Y		67	39	24	21	16	26

---

**Reaction conditions: glycerol/urea molar ratio: 1:1.5, temperature 150°C, catalyst: 0.25 g, time: 4 h, under N<sub>2</sub> bubbling.**

In the blank uncatalysed reaction (entry 1), 66% of glycerol was converted in 4 h with 42% selectivity to glycerol carbonate and a 28% glycerol carbonate yield at 150°C. There is no significant effect in reactivity for CeO<sub>2</sub> catalysts prepared by the hydrothermal method. The conversion of glycerol increased to 71% (entry 6) with 43% and 31% selectivity and yield of glycerol carbonate respectively. The selectivity to **SP2** is relatively high for CeO<sub>2</sub>. In the presence of La<sub>2</sub>O<sub>3</sub> (entry 2), both the conversion and selectivity improved significantly. The conversion improved to 94% with the selectivity of 66% to glycerol carbonate and 62% glycerol carbonate yield. There is no trace of **SP1** in the reaction as this is the first product form in the first step of the reaction as the amount of glycerol is near to completion. Although CeO<sub>2</sub> catalysts, in general, have high surface area compare to La<sub>2</sub>O<sub>3</sub>, the catalytic activity cannot be simply correlated to the surface area of the catalysts. By increasing the calcination temperature of La<sub>2</sub>O<sub>3</sub> from 400°C to 700°C, almost all the glycerol had been converted. There is an increase in selectivity to glycerol carbonate from 66% (entry 2) to 71% (entry 3) as well as an increase in glycerol carbonate yield by 6%. There is a reduction in conversion for CeO<sub>2</sub> with the increase in calcination temperature of the catalyst however the selectivity and yield to glycerol carbonate are 49% and 32% (entry 7) respectively. The reactions were repeated four times to improve the results obtained to reduce errors in the experimental data. It was determined by standard deviation method that the error was 2%.

Catalysts prepared by microwave method are also tested in the carbonylation of glycerol with urea. It can be observed that in CeO<sub>2</sub> catalysts (entry 8 and entry 9), there is no significant improvement in conversion and glycerol carbonate yield, the activity is almost similar to the catalysts prepared by hydrothermal method. The interesting result is in MW La<sub>2</sub>O<sub>3</sub> catalysts. These results show that microwave method does not increase the conversion and selectivity of the reaction. The

conversion decreased from 94% (entry 2) to 89% (entry 4) and glycerol carbonate yield reduced to 50% for MW  $\text{La}_2\text{O}_3$  400°C.

The reason for the difference in catalytic activities can be derived from the basic properties of the catalysts measured by  $\text{CO}_2$ -TPD. The performance of  $\text{CeO}_2$  catalysts for both preparation methods showed lower performance as the catalysts have low amounts of medium basic sites which were discussed in Chapter 5. The high catalytic activity of  $\text{La}_2\text{O}_3$  synthesised by the hydrothermal method can be associated with the appropriate amount of medium basic sites of the catalysts which can be seen in Table 21 and Figure 5-3. The increase in activity at higher calcination temperature for  $\text{La}_2\text{O}_3$  is due to the increase in the amount of medium basic sites from 152  $\mu\text{mol CO}_2 \text{ g}^{-1}$  to 205  $\mu\text{mol CO}_2 \text{ g}^{-1}$ . For microwave synthesised catalysts, the opposite happened in which the conversion decreased from 89% (entry 4) to 80% (entry 5) with the increase in calcination temperature. This can be linked to the high amount of medium basic sites present in MW  $\text{La}_2\text{O}_3$  400°C which 317  $\mu\text{mol CO}_2 \text{ g}^{-1}$  compare to MW  $\text{La}_2\text{O}_3$  700°C with 233  $\mu\text{mol CO}_2 \text{ g}^{-1}$  amount of medium basic sites. In general, hydrothermal catalysts of  $\text{La}_2\text{O}_3$  have better performance than microwave catalysts. The low reactivity of microwave catalysts could be due to the strength of medium basic sites which is shifted toward high-temperature region although the amount of medium basic sites is higher than hydrothermal catalysts. Another reason is due to the high amount of strong basic sites which results in strong interaction with the reactants thus blocking the active sites.

Zeolite Y (entry 10) was also being investigated in the carbonylation reaction to compare the activity of the catalyst and the conversion of glycerol is 67% with a selectivity of 39% to glycerol carbonate. Zeolite Y is a well-known acidic catalyst with a high surface area of 700  $\text{m}^2 \text{ g}^{-1}$ . The activity is slightly lower with respect to the uncatalysed reaction. Therefore catalysts containing basic sites have better activity in the synthesis of glycerol carbonate from glycerol and urea.



### 6.2.2.3 Incorporation of metal into the catalyst

Table 26 shows the effect of incorporating copper into the oxides.

**Table 26: Catalytic performance of the catalyst**

Entry	Catalyst	Calcination temperature °C	Conversion %	Selectivity %				
				Glycerol carbonate	SP1	SP2	SP3	Glycerol carbonate yield %
1	CeO <sub>2</sub>	400	71	43	16	26	15	31
2	Cu/CeO <sub>2</sub>	400	77	56	11	21	12	43
3	La <sub>2</sub> O <sub>3</sub>	700	96	71	0	17	12	68
4	Cu/La <sub>2</sub> O <sub>3</sub>	700	98	74	0	14	12	72

**Reaction conditions: glycerol/urea molar ratio: 1:1.5, temperature 150°C, catalyst: 0.25 g, time: 4 h, under N<sub>2</sub> bubbling.**

The introduction of 2.3 wt% copper slightly improves the selectivity and the yield of glycerol carbonate for CeO<sub>2</sub> catalyst. The conversion of glycerol improves from 71% to 77% with the increase of glycerol carbonate yield of 31% (entry 1) to 43% (entry 2). Copper supported in La<sub>2</sub>O<sub>3</sub> also improves the yield of glycerol carbonate to 72% (entry 4) with complete conversion of glycerol after 4 h. Error calculation was made and it was found the experimental error was 1.5%. Although the increase in yield for La<sub>2</sub>O<sub>3</sub> is not as high as CeO<sub>2</sub>, the results are relatively

significant. Cu metal has a higher impact on  $\text{CeO}_2$  than  $\text{La}_2\text{O}_3$  in terms on improvement in yield.

#### 6.2.2.4 Time on line analysis

Time-online reactions have been carried out to compare conversions and selectivity to glycerol carbonate from 0 h to 9 h reaction. For the blank reaction shown in Figure 6-1, 54% glycerol had been converted with 17% yield of glycerol carbonate within 30 min of the reaction and the conversion slowly increases as the reaction progressed. Selectivity to glycerol carbonate also increases slowly with the decrease in **SP1** in which high amounts of **SP1** can be observed at the start of the reaction. This suggests that **SP1** is the first compound formed in the first step. Another indication is that after 7 h reaction, no **SP1** is observed.

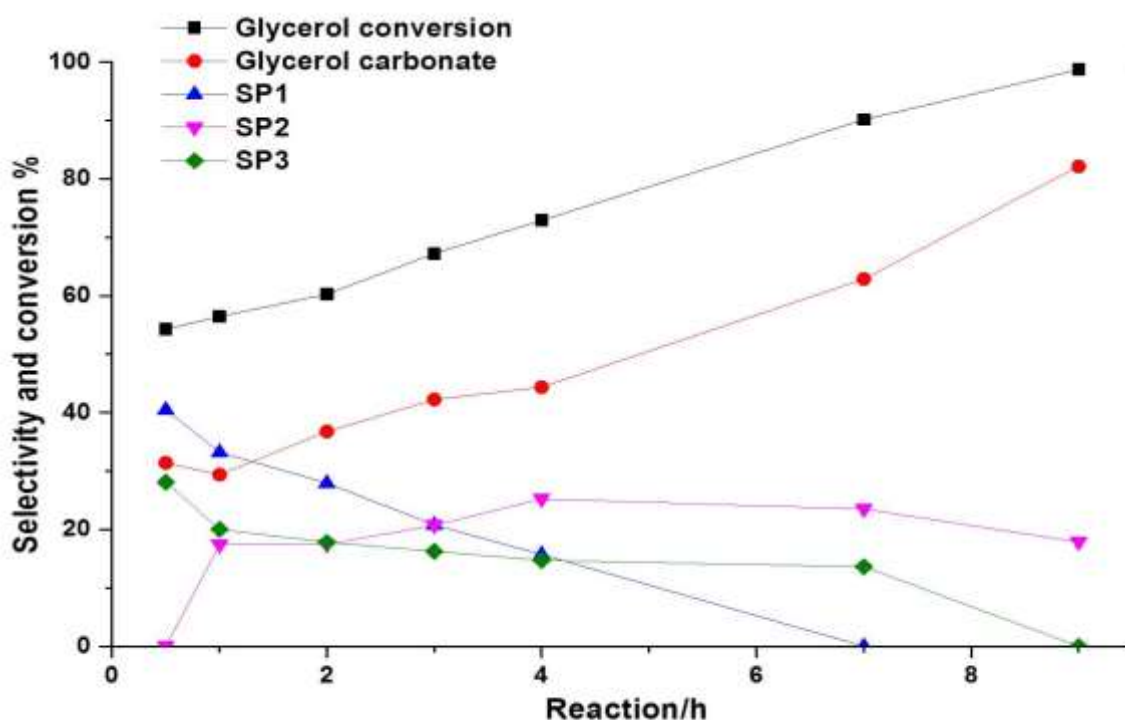


Figure 6-1: Time online analysis for blank reaction. Reaction conditions: glycerol/urea molar ratio: 1:1.5, temperature 150°C, catalyst 0.25 g, time: 4 h, under  $\text{N}_2$  bubbling

Zeolite Y has the worst performance amongst all the catalysts shown in Figure 6-2. Blank reaction surpasses Zeolite Y reaction after 4 h of reaction. 79% of glycerol is being converted during 7 h of reaction with the yield of glycerol carbonate of 34% compare to 57% glycerol carbonate yield of the blank reaction.

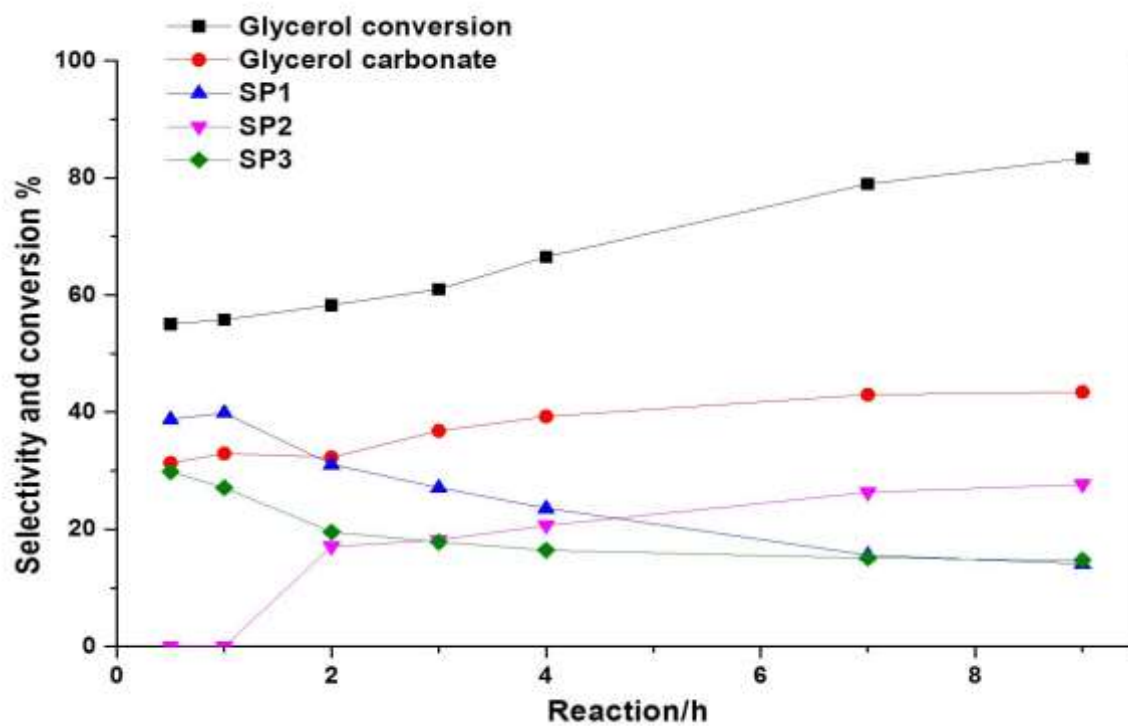


Figure 6-2: Time online analysis for zeolite Y. Reaction conditions: glycerol/urea molar ratio: 1:1.5, temperature 150°C, catalyst 0.25 g, time: 4 h, under N<sub>2</sub> bubbling

The introduction of copper into the catalysts improved the carbonylation reaction slightly especially the selectivity to glycerol carbonate. The conversion increases from 89% (Figure 6-3) to 97% (Figure 6-4) when copper is introduced into CeO<sub>2</sub> catalysts after 7 h of reaction. The selectivity and yield of glycerol carbonate increase from 58% to 69% and from 52% to 67% respectively. The selectivity to **SP2** also decreases from 28% to 18%.

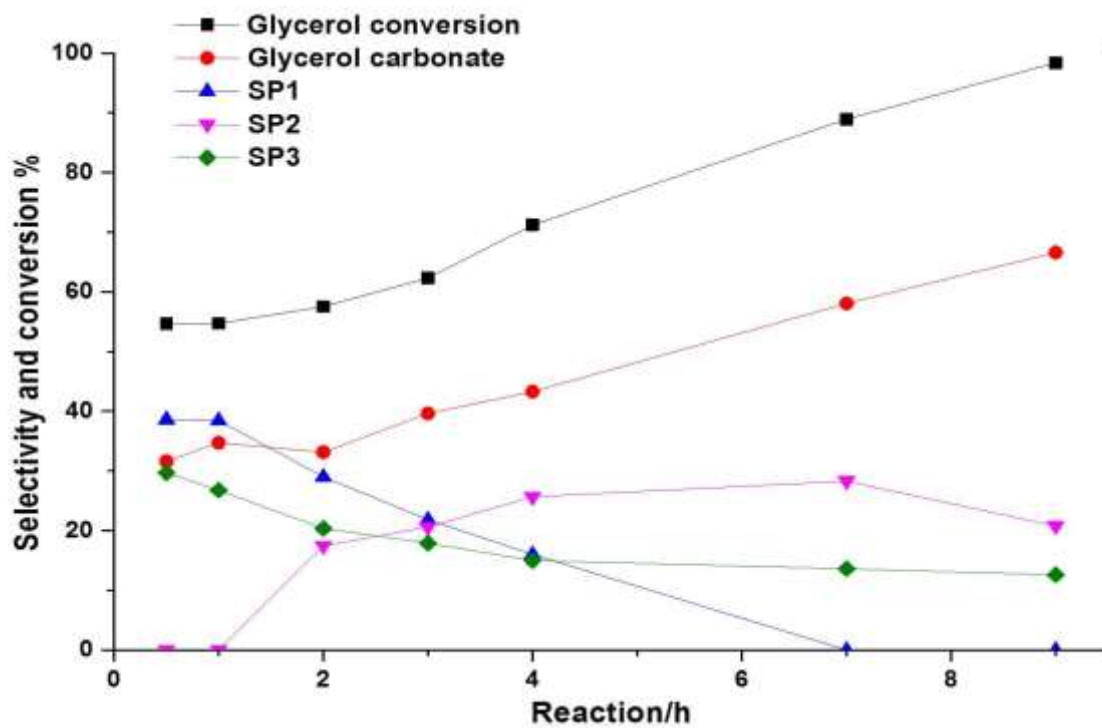


Figure 6-3: Time online analysis for HT CeO<sub>2</sub> 400°C. Reaction conditions: glycerol/urea molar ratio: 1:1.5, temperature 150°C, catalyst 0.25 g, time: 4 h, under N<sub>2</sub> bubbling

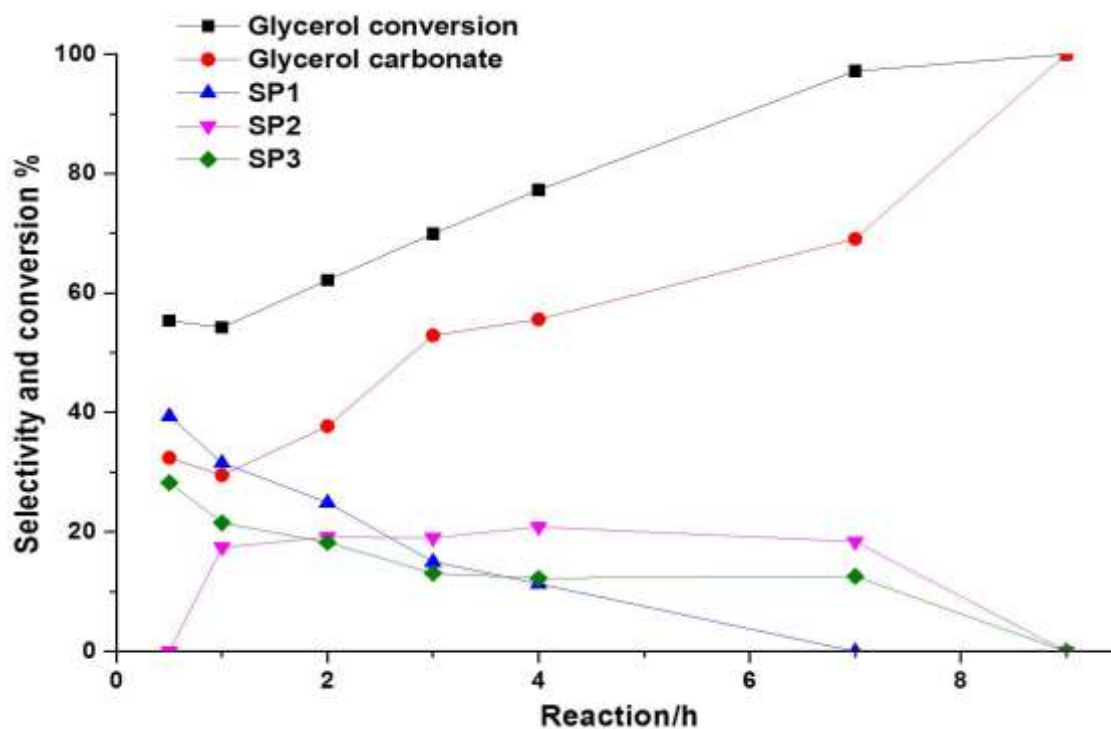


Figure 6-4: Time online analysis for HT CuCeO<sub>2</sub> 400°C. Reaction conditions: glycerol/urea molar ratio: 1:1.5, temperature 150°C, catalyst 0.25 g, time: 4 h, under N<sub>2</sub> bubbling

The reaction profiles for HT La<sub>2</sub>O<sub>3</sub> 700°C (Figure 6-5) and HT CuLa<sub>2</sub>O<sub>3</sub> 700°C (Figure 6-6) showed similar catalytic performances. However, **SP1** is not observed in the reaction for HT CuLa<sub>2</sub>O<sub>3</sub> 700°C at 3 h of reaction whereas there is still **SP1** being detected for HT La<sub>2</sub>O<sub>3</sub> 700°C.

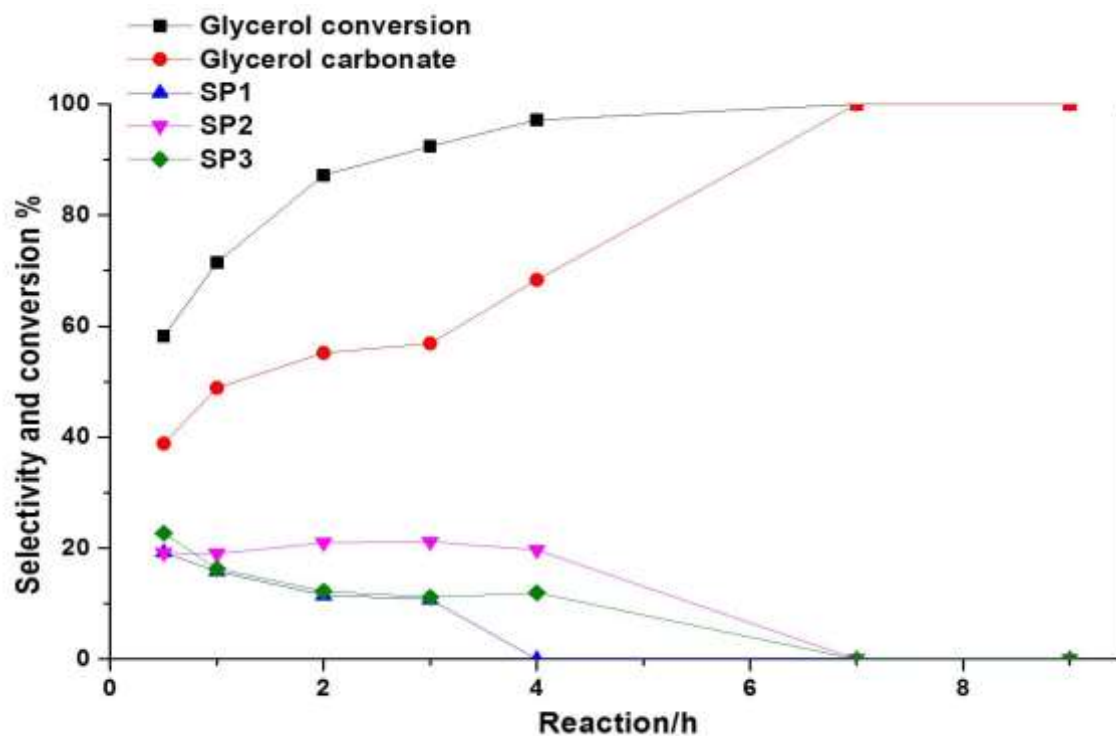


Figure 6-5: Time online analysis for HT La<sub>2</sub>O<sub>3</sub> 700°C. Reaction conditions: glycerol/urea molar ratio: 1:1.5, temperature 150°C, catalyst 0.25 g, time: 4 h, under N<sub>2</sub> bubbling

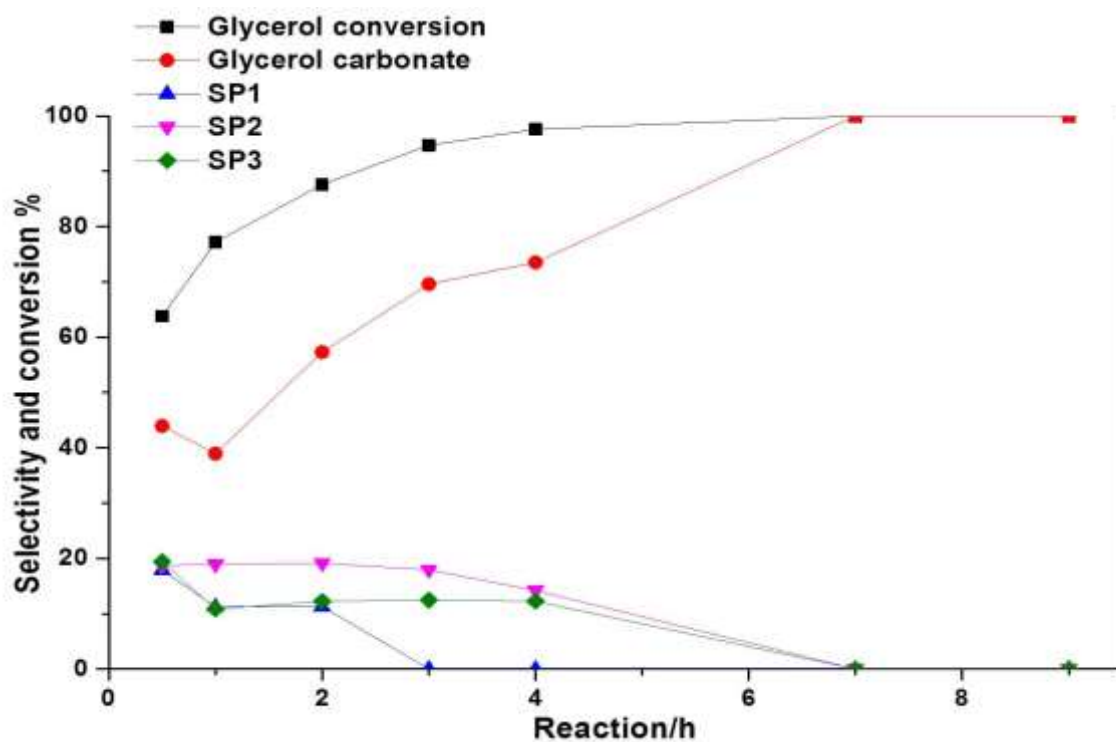


Figure 6-6: Time online analysis for HT CuLa<sub>2</sub>O<sub>3</sub> 700°C. Reaction conditions: glycerol/urea molar ratio: 1:1.5, temperature 150°C, catalyst 0.25 g, time: 4 h, under N<sub>2</sub> bubbling

#### 6.2.2.5 Effect of reaction temperature

The carbonylation of glycerol with urea was carried out at a different temperature to observe the change and results in conversion and selectivity to glycerol carbonate are presented in Table 27.

**Table 27: Catalytic performance for the synthesis of glycerol carbonate at different reaction temperature**

Entry	Catalyst	Rxn temp °C	Time h	Conversion	Selectivity %				
					Glycerol carbonate	SP1	SP2	SP3	Glycerol Carbonate yield %
1	Blank	150	0	0	0	0	0	0	0

			1/2	54	31	39	0	28	17
			1	56	33	40	16	27	18
			2	58	33	31	16	19	19
			3	61	38	26	18	17	22
			4	66	42	22	20	16	28
<b>2</b>	La <sub>2</sub> O <sub>3</sub>	150	0	0	0	0	0	0	0
			1/2	58	39	19	19	23	22
			1	71	49	16	19	16	35
			2	87	55	12	21	12	48
			3	92	57	11	21	11	53
			4	96	71	0	20	12	68
<b>3</b>	La <sub>2</sub> O <sub>3</sub>	170	0	0	0	0	0	0	0
			1/2	73	55	14	16	14	40
			1	84	55	13	20	13	46
			2	96	72	0	16	13	69
<b>4</b>	La <sub>2</sub> O <sub>3</sub>	190	0	0	0	0	0	0	0
			1/2	87	67	0	19	14	59

**Reaction conditions: glycerol/urea molar ratio: 1:1.5, catalyst: 0.25 g, time: 4 h, under N<sub>2</sub> bubbling.**

The conversion of glycerol increased with the increase in reaction temperature. 96% conversion of glycerol (entry 3) was achieved within 2 h of reaction at 170°C with glycerol selectivity of 72% and yield of 69% compare to the reaction conducted at 150°C, in which only 87% glycerol conversion was achieved with



48% glycerol carbonate yield. At 190°C (entry 4), 87% of glycerol was being converted within 30 min of the reaction with no **SP1** was detected.

These studies at higher temperature also indicate that the reaction time can be reduced from 3-4 h typically observed in the literature, to 1-2 h and enhancing the yield to glycerol carbonate.

#### 6.2.2.6 Effect of microwave heating in the carbonylation reaction

The reaction was subjected to two types of heating: conventional and microwave heating. From previous literature, microwave assisted heating was used in the transesterification of glycerol with dimethyl carbonate giving a yield of 93% glycerol carbonate in 5 min reaction.<sup>297</sup> There is no publication in the synthesis of glycerol carbonate from urea using microwave heating and this study is the first of its kind. It is not possible to take samples every hour for time online analysis due to the complicated set-up of the reaction, however, identical reactions were carried out and stopped at the following times: 30 min, 1 h, 2 h, 3 h and 4 h. As in previous experiments, the reactions were performed in the absence of solvent under inert atmosphere by bubbling nitrogen with a molar ratio of 1.5. In this reaction, Cu/La<sub>2</sub>O<sub>3</sub> is selected as it gave the best performance amongst the catalysts tested in previous sections. To have a better comparison, the reaction at T=2 h is being highlighted which can be illustrated in Figure 6-7. Firstly, the blank uncatalysed microwave reaction shows that after 2 h reaction, the conversion of glycerol increases slightly from 58% to 63% with the selectivity to glycerol carbonate increases from 33% to 37% when using microwaves instead of conventional heating. The catalytic performance of Cu/La<sub>2</sub>O<sub>3</sub> catalyst under microwave heating increases from 88% to 97% as well as the increase in glycerol carbonate yield from 50% to 64% compared to CuLa<sub>2</sub>O<sub>3</sub> under conventional heating.

The results obtained are summarised in Table 28 to compare the full-time online reactions on conversion and selectivity to glycerol carbonate from 0 h to 4 h reaction. Changing the mode of heating from conventional heating to microwave heating increases the conversion and yield of glycerol carbonate. The reaction under microwave heating is completed within 3 h of reaction. Under microwave

heating, the selectivity to **SP2** is higher compare to conventional heating which indicates the formation of **SP2** is favourable under microwave heating.

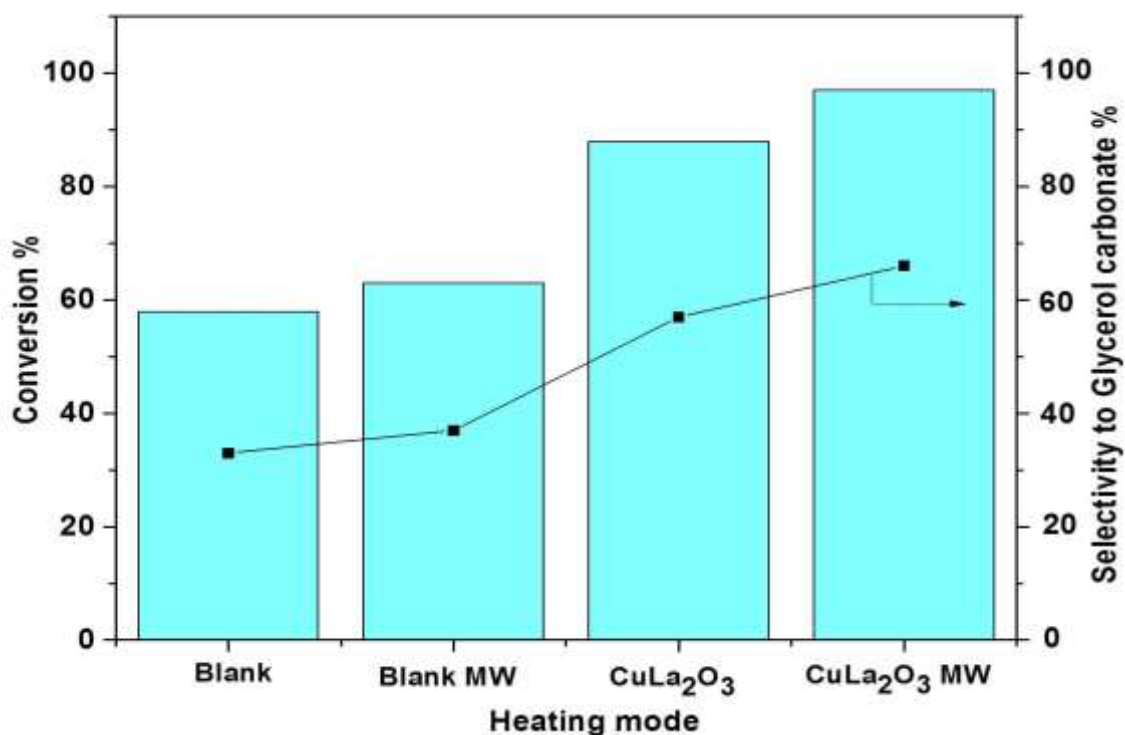


Figure 6-7: Reaction conditions: glycerol/urea molar ratio: 1:1.5, temperature 150°C, catalyst 0.25 g, time: 2 h, under N<sub>2</sub> bubbling, microwave heating (MW)

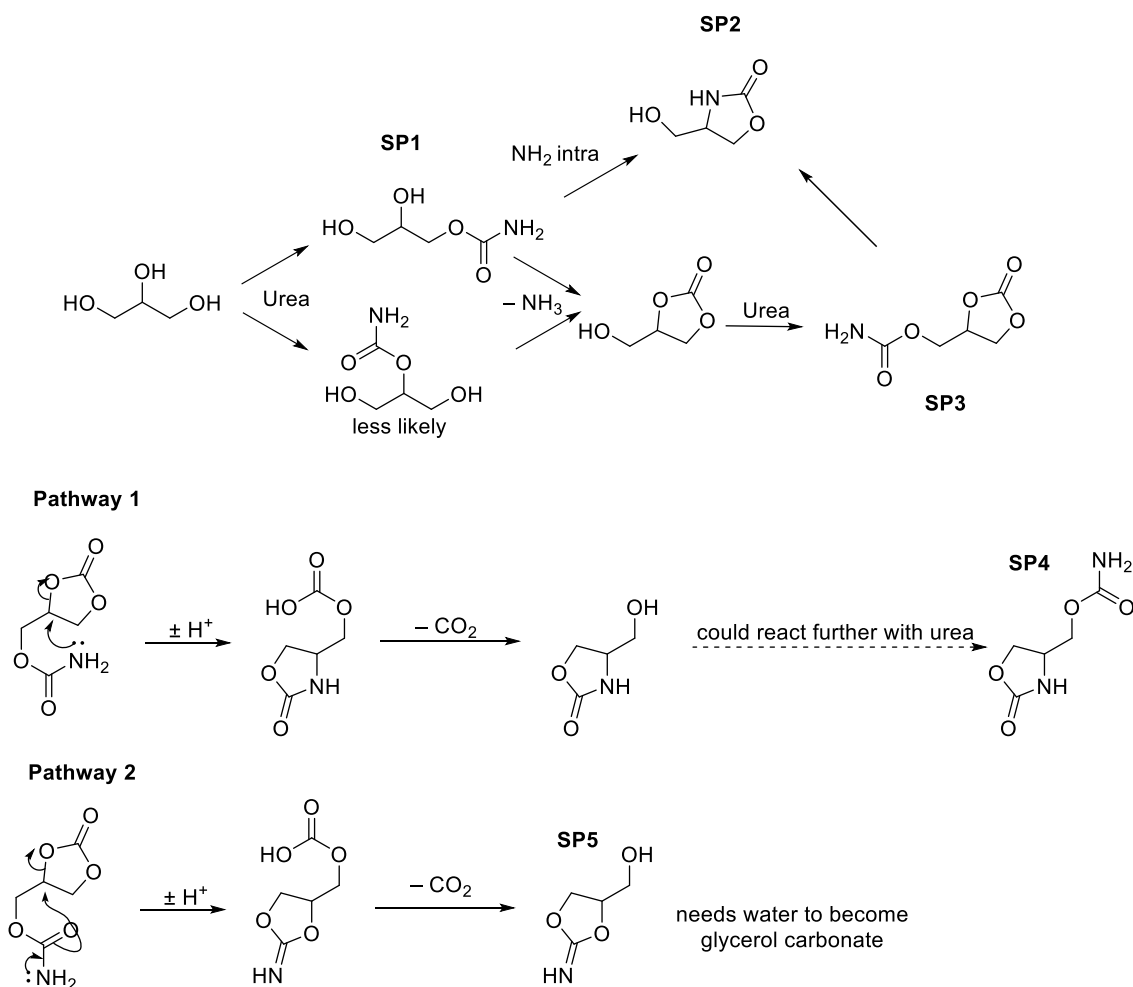
Table 28: Catalytic performance for the synthesis of glycerol carbonate using conventional and microwave heating

				Selectivity				Glycerol carbonate yield %
				%				
Entry	Catalyst	Time h	Conversion	Glycerol carbonate	SP1	SP2	SP3	

<b>1</b>	Blank	0	0	0	0	0	0	0
		1/2	54	31	39	0	28	17
		1	56	33	40	16	27	18
		2	58	33	31	16	19	19
		3	61	38	26	18	17	22
		4	66	42	22	20	16	28
<b>2</b>	Blank MW	0	0	0	0	0	0	0
		1/2	52	33	39	0	28	17
		1	55	30	33	17	20	16
		2	63	37	27	19	17	23
		3	68	40	22	21	16	27
		4	79	44	14	29	14	35
<b>3</b>	Cu/La <sub>2</sub> O <sub>3</sub>	0	0	0	0	0	0	0
		1/2	64	44	18	19	19	28
		1	77	39	11	18	11	40
		2	88	57	11	19	12	50
		3	95	70	0	18	12	66
		4	98	74	0	14	12	72
<b>4</b>	Cu/La <sub>2</sub> O <sub>3</sub> MW	0	0	0	0	0	0	0
		1/2	76	48	15	21	15	37
		1	83	52	14	22	13	43
		2	97	66	0	22	12	64

Reaction conditions: glycerol/urea molar ratio: 1:1.5, catalyst: 0.25 g, time: 4 h, under N<sub>2</sub> bubbling.

### 6.2.2.7 Plausible reaction mechanism



Scheme 6-2: Reaction scheme of glycerol and urea and its possible products.

The reaction between glycerol and urea is shown in Scheme 6-2. The oxygen atom of the primary alcohol on glycerol attacks the carbonyl carbon atom of urea producing 2,3 dihydroxypropyl carbamate (**SP1**) and releasing one ammonia molecule which is removed by vacuum or nitrogen flow. The attack from a secondary hydroxyl group on glycerol is unlikely in this situation and we have

found no evidence in this work. The secondary hydroxyl group of **SP1** attacks the carbonyl carbon atom of **SP1** via an intermolecular attack then releasing ammonia and forming a stable five-membered ring carbonate. Alternatively, the amine group of **SP1** can attack the secondary carbon atom of **SP1** forming 4-(hydroxymethyl) oxazolidin-2-one (**SP2**). The endant hydroxyl group on glycerol carbonate can further react with urea producing (2-oxo-1,3-dioxolan-4-yl)methyl carbamate (**SP3**) which is typically observed at reaction carried out in excess urea. However, **SP3** can undergo an intramolecular attack which can be shown in pathway 1 and 2. In pathway 1, the amine group of **SP3** attacks the carbon of cyclic carbonate forming a five-membered oxazolidone ring, then forming **SP2** by releasing a molecule of carbon dioxide. **SP2** can further react with urea forming, (2-oxooxazolidin-4-yl) methyl carbamate (**SP4**). In pathway 2, carbonyl carbon atom attacks the carbon of cyclic carbonate forming five-membered dioxolane ring then releasing carbon dioxide forming (2-imino-1,3-dioxolan-4-yl)methanol (**SP5**).

### 6.2.3 Conclusion

In conclusion,  $\text{La}_2\text{O}_3$  catalysts synthesised by hydrothermal method have the higher catalytic performance in the synthesis of glycerol carbonate from urea and glycerol with a conversion of 96% and glycerol carbonate yield of 68%. The incorporation of copper into  $\text{La}_2\text{O}_3$  further improves the activity of the catalyst by increasing the yield of glycerol carbonate to 72%. The reaction is further improved by changing the heating mode to microwave heating. The conversion increases from 88% to 97% with an increase in glycerol carbonate yield from 50% to 64% using  $\text{CuLa}_2\text{O}_3$  catalyst under 2 h reaction. In combination with higher reaction temperatures, we were able to reduce typical reaction times shown in the literature to a third without a reduction in glycerol carbonate yield or selectivity.

# **CHAPTER 7**

## **NEW ROUTE FOR THE SYNTHESIS OF SORBITOL CARBONATE VIA TRANSESTERIFICATION OF DMC**

## **7 NEW ROUTE IN THE SYNTHESIS OF SORBITOL CARBONATE**

### **7.1 Introduction**

Sorbitol is one of the 12 platform molecules that have been put together by Werpy and Peterson. Sorbitol has been widely utilised in medical applications as laxative, in food industry as sweetener as well as in cosmetics. There are numerous research have been carried out on conversion of sorbitol into high value added chemicals such as isosorbide, glycols such as ethylene glycol or glycerol, sorbitan and lactic acid shown in Figure 7-1.<sup>300,301,302,35</sup> The synthesis of sorbitol carbonate has not been investigated in great detail. Currently there is one publication published on the synthesis of sorbitol carbonate to produce non-isocyanate polyhydroxyurethane (NIPU) polymer.<sup>208</sup> However the reaction has several steps using additional reagents which are not sustainable. Using the knowledge on the synthesis of glycerol carbonate, similar reactions could be applied to produce sorbitol carbonate. Sorbitol carbonate is relatively new compound and its application has not being explored.

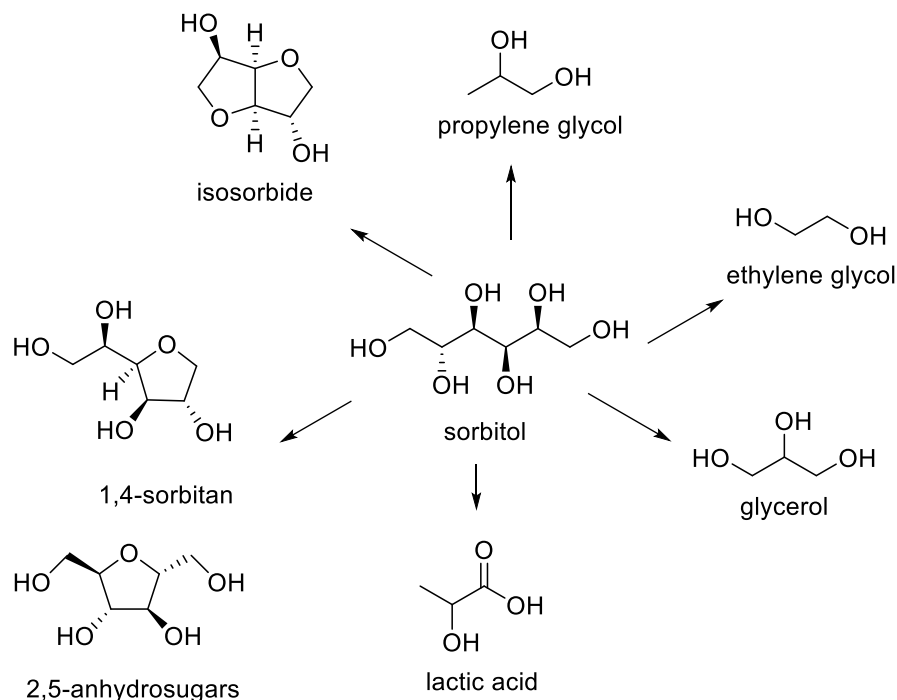
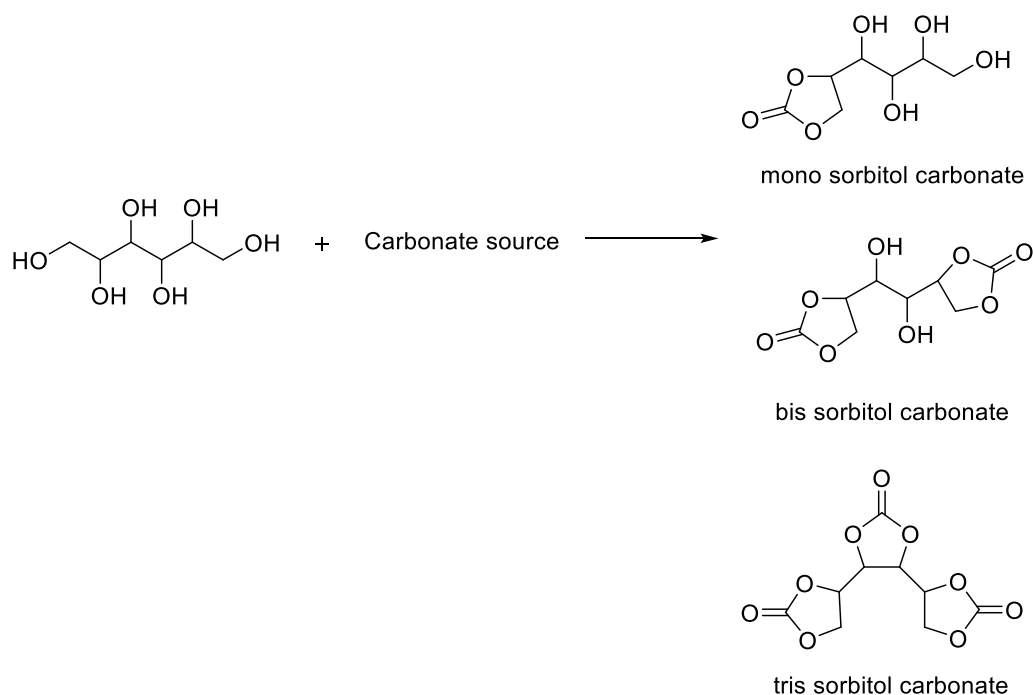


**Figure 7-1: Conversion of sorbitol into high value added products<sup>35</sup>**

In the present study, two types of reaction will be discussed: enzymatic reaction and chemical reaction. First, transesterification reaction of sorbitol and dimethyl carbonate (DMC) using immobilized *Candida Antartica* lipase. The aim for this enzymatic reaction is to achieve selective esterification reaction between sorbitol and DMC. The immobilized enzymes were selected as they reduced leaching out of the enzyme in the reaction media and have the higher chance of being recycled numerous times due to its stability and resistance to thermal shock. The loading of the Lipase B and Novozyme 435 are 2000 u/g and 5000 u/g respectively. Both of these catalysts were commercial catalysts obtained from Sigma-Aldrich. The enzymes can be filtered, however post analysis of the enzymes were not conducted especially leaching test. Second, the reaction of sorbitol with *N,N'*-Carbonyldiimidazole (CDI), these two reagents act as a carbonate source for the chemical reaction. The aim of this reaction is to synthesise tris sorbitol carbonate. In this reaction, qualitative analysis is being performed to identify different types of carbonate in the reaction mixture. Quantitative analysis could not be performed as there is standard for mono, bis and tris sorbitol carbonate.





**Scheme 7-1: Synthesis of sorbitol carbonate**

## 7.2 Results & Discussion

### 7.2.1 Enzymatic reactions of sorbitol carbonate

#### 7.2.1.1 *Candida Antartica* immobilized on Immobead 150 recombinant from yeast named Lipase B

FTIR spectra of samples were taken at the end of reaction are displayed in Figure 7-2. The peak at  $1788\text{ cm}^{-1}$  corresponds to the stretching band of  $\text{C}=\text{O}$  of a five membered cyclic carbonate.<sup>303</sup> The peak that corresponds to DMC at  $1745\text{ cm}^{-1}$  is not observed in the spectra indicating DMC is being consumed in the reaction.<sup>303</sup> The effect of ratio of solvent was investigated for both enzymes. From the figure it can be noted that the intensity of carbonate peaks increase with increase ratio of *t*-BuOH. The band corresponds to OH groups at  $3300\text{ cm}^{-1}$  shows a decrease in intensity with increasing *t*-BuOH. Both of these results show that sorbitol is being converted into sorbitol carbonate. The product formed could be mono sorbitol carbonate of *bis* sorbitol carbonate. The enzymatic reaction under 100% *t*-BuOH

shows a sharp increase in intensity compare to the enzymatic reaction under two different solvent systems.

During a catalytic reaction, enzymes undergo conformational change.<sup>304</sup> Sarda and Densuella have discovered that enzymes have lid which opens that allows the entry of substrate and reacting with the active site inside. Immobilising enzymes to hydrophobic support cause the enzymes to undergo conformational change and are assumed to be held open in an active conformation.<sup>305</sup> Therefore the low activity of the enzymatic reaction could be due to DMSO blocking the active site of the lipase. This confirms that the lipases are inactive in DMSO at higher ratios.

Figure 7-3 shows the presence of new peaks appearing in the region of 4 ppm to 5 ppm which indicates product was forming. However sorbitol peaks are clearly seen in the spectra indicating the low quantity of product being formed. The mass spectrum matches the expected mass of 208 which corresponds to mono-sorbitol carbonate which can be found in the appendix.

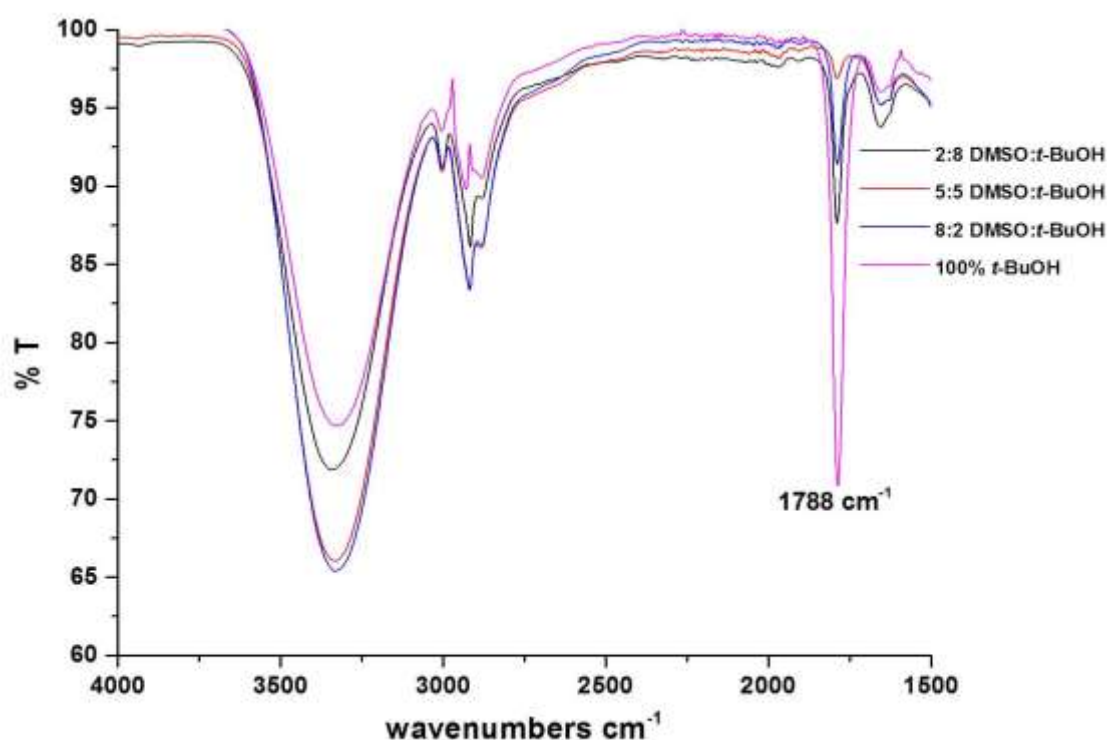


**Figure 7-2: FTIR spectra of reaction samples at different ratio of solvent in the presence of Lipase B**

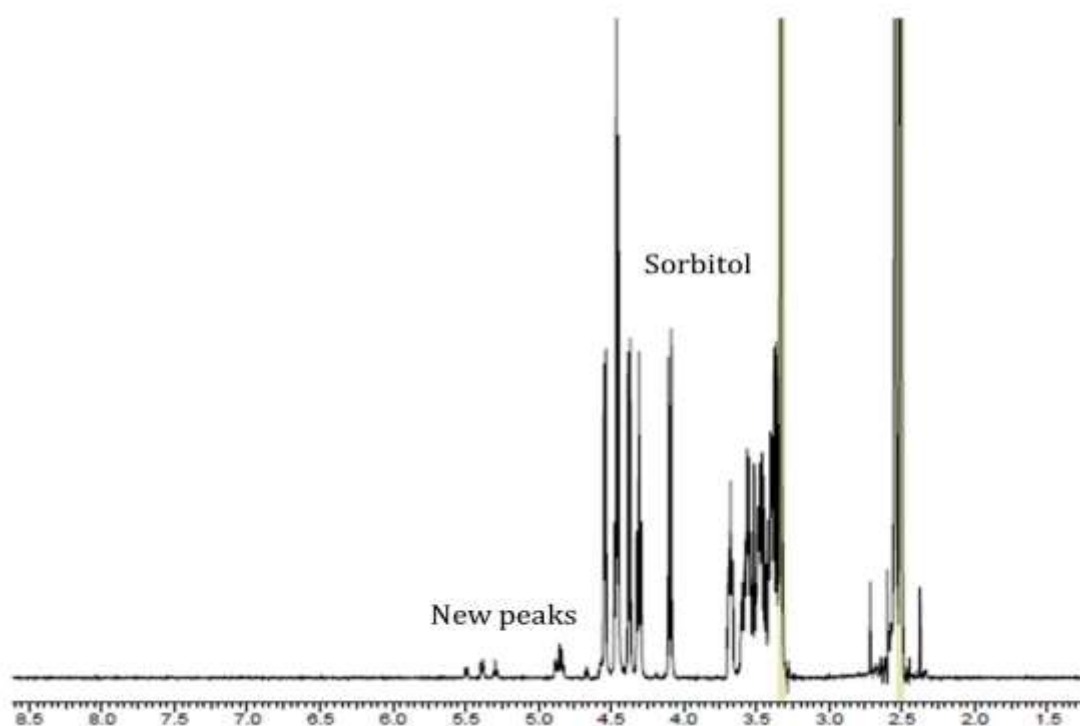


**Figure 7-3: <sup>1</sup>H NMR spectroscopy of the reaction with 20:80 ratio of DMSO:*t*-BuOH after 24 h in the presence of Lipase B**

#### **7.2.1.2 Lipase acrylic resin from *Candida Antartica* (Novozyme 435)**

##### **7.2.1.2.1 The effect of solvent**

The same trend can be observed for the enzyme Novozyme 435 in which the intensity of OH groups on the sorbitol decrease with decrease amount of DMSO which can be observed in Figure 7-4. Reaction under 100% *t*-BuOH shows a significant decrease in bands corresponding to OH stretching band at 3300 cm<sup>-1</sup>, however it can be observed that the band corresponds to carbonate group at 1788 cm<sup>-1</sup> decrease in intensity and appearance of another stretching band at 1739 cm<sup>-1</sup>. This band corresponds to the presence of linear carbonate or six-membered ring cyclic carbonate. There is a possibility of ring opening of five-membered ring carbonate catalysed by Novozyme 435 in the reaction which have been reported in few literatures.<sup>306,307</sup> This is not observed in the reaction catalysed by Lipase B. Novozyme 435 has higher activity of 5000 u/g compare to Lipase B with the activity of 2000 u/g. Another reason for the formation of carbonate peak at 1739 cm<sup>-1</sup> is due to the presence of *t*-BuOH in the reaction. DMSO inhibits sorbitol from fully interacting with the enzymes as intramolecular motions of the enzymes can

be easily affected by the solvent.<sup>186</sup> This was further tested when *t*-BuOH was removed in the reaction mixture with only DMSO acts as a solvent. It was expected that no conversion would be seen in the reaction therefore *t*-BuOH must be present in the reaction mixture in order for the reaction to proceed.

The selection of organic solvents in enzymatic reaction is important as it determines the overall product yield of the reaction. The activity of the enzyme must not be affected by organic solvent as well as its stability and has good solubility with the substrate.<sup>308</sup> *t*-BuOH is a hydrophilic solvent which commonly used in the synthesis of glycerol carbonate with enzymes producing high yield of product as it prevents glycerol from coating on the surface of the enzymes.<sup>186,309</sup> Therefore the solubility of sorbitol in *t*-BuOH and the high activity of Novozyme 435 have an effect in the overall activity of the reaction.

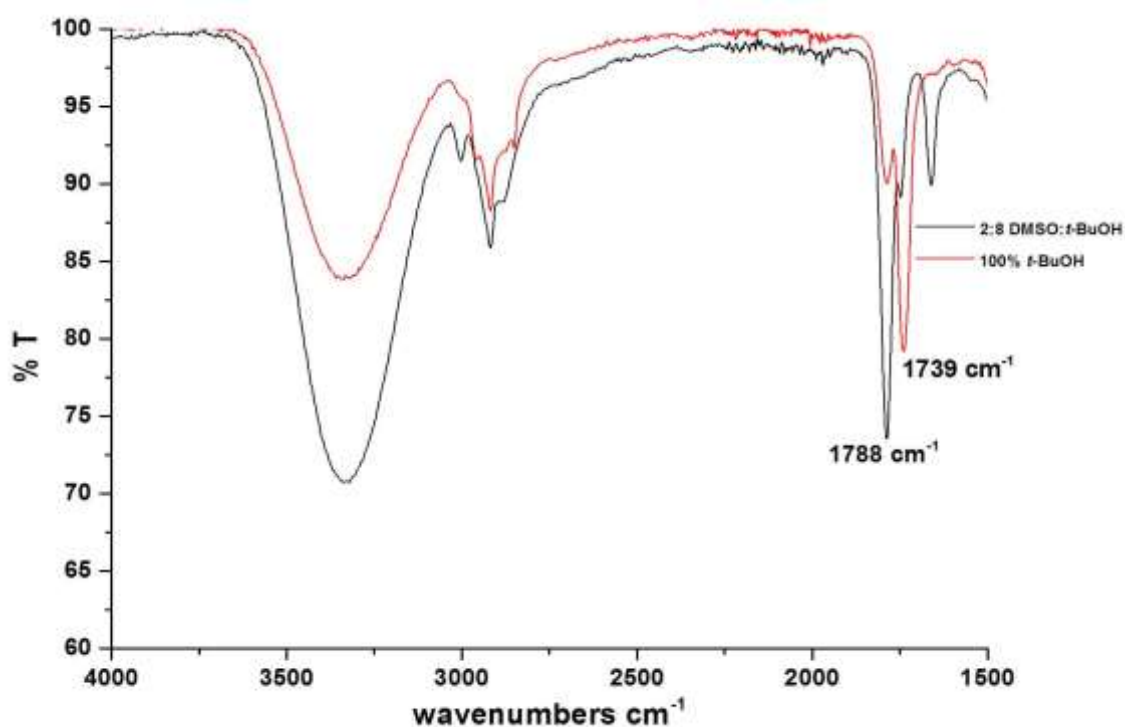
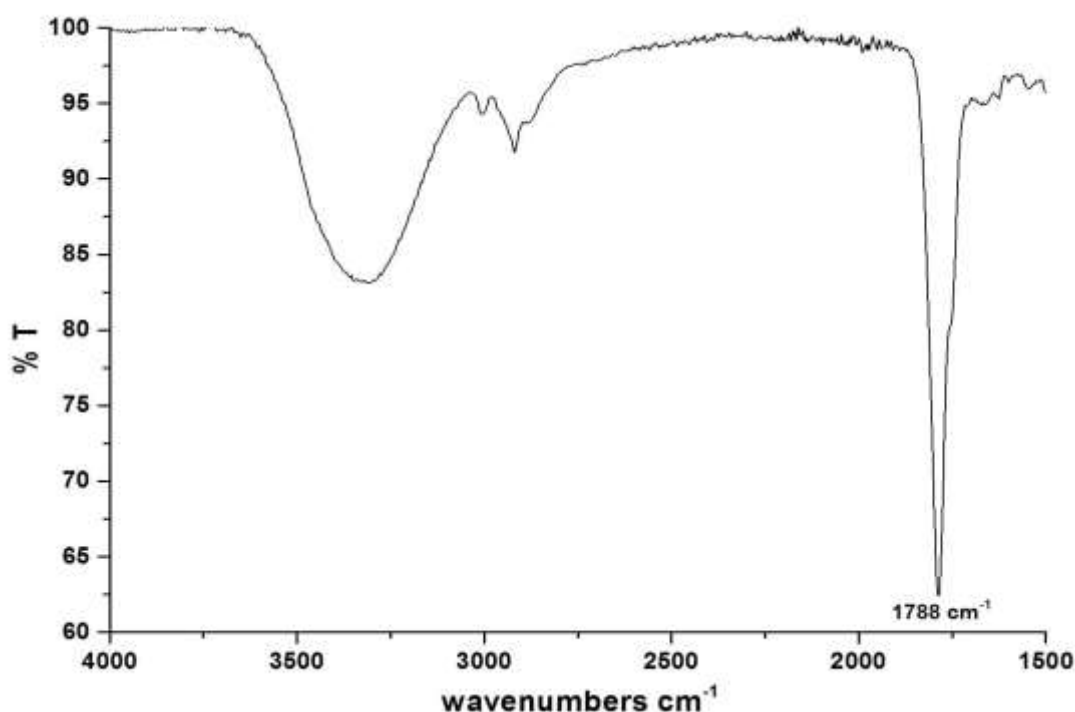


Figure 7-4: FTIR spectra of reaction samples at different ratio of solvent in the presence of Novozyme 435

#### 7.2.1.3 Solvent free reaction of sorbitol and DMC

Another type of reaction was carried out without the use of solvent instead DMC was used as a solvent and was in ten times excess of sorbitol. Solvent free reaction has numerous advantages such as high yield of product, faster reaction with easy separation and purification.<sup>310</sup> A sharp peak at  $1788\text{ cm}^{-1}$  is observed in the FTIR spectra shown in Figure 7-5 and this confirms that the bulk reaction can produce sorbitol carbonate. Q-TOF analysis later confirms that the presence of mono sorbitol carbonate and bis sorbitol carbonate with expected mass of 208 and 234 respectively.



**Figure 7-5: FTIR spectra of reaction sample for solvent free reaction in the presence of Novozyme 435**

#### **7.2.1.4 Solvent free reaction of sorbitol and DMC with silica gel**

Silica gel has been used as a solid support for glycerol in the synthesis of glycerol carbonate and it was found that the conversion of glycerol and yield of glycerol

carbonate increased more than tenfold. Silica does not affect the activity of the enzyme and the glycerol-coated silica gel could be recycled for the next reaction.<sup>310</sup> Sorbitol was heated up to 110°C for 10 min to ensure complete absorption of the substrate onto the support. The intensity of carbonate peak has increased under these conditions shown in Figure 7-6. This agrees with the result Lee *et al* where supporting the substrate increases the conversion. Therefore an excess of DMC can push the reaction towards producing bis sorbitol carbonate although traces of mono sorbitol carbonate can still be observed in the HPLC. Q-TOF has confirmed the presence of bis sorbitol carbonate with a molecular mass of 234 in higher concentrations compare to mono sorbitol carbonate. Longer reaction time could possibly drive the reaction to only producing bis sorbitol carbonate. However tris sorbitol carbonate could not be observed in the chromatogram which indicates that the enzymatic reaction is selective to mono and bis sorbitol carbonate.

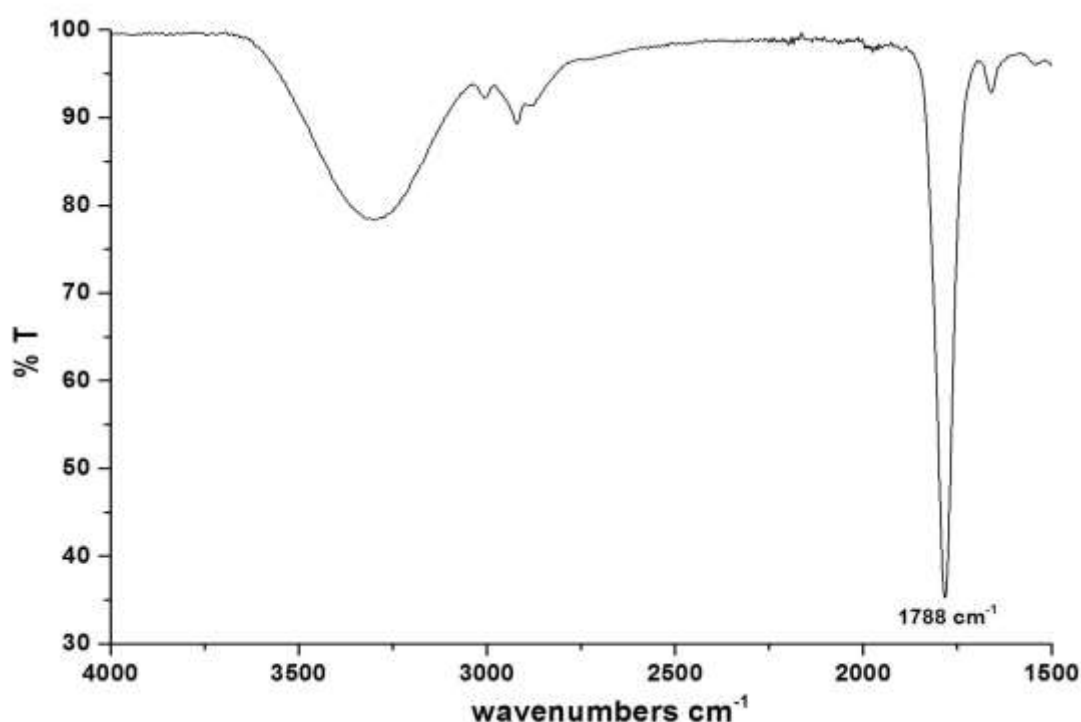


Figure 7-6: FTIR spectra of reaction sample for solvent free reaction with silica gel in the presence of Novozyme 435

## 7.2.2 Chemical reactions of sorbitol carbonate

#### 7.2.2.1 Chemical reactions of sorbitol and CDI

*N,N'*-Carbonyldiimidazole (CDI) was used in the synthesis of sorbitol carbonate to get a better knowledge on the structure of the product formed. CDI is a powerful reagent in the synthesis of amides, esters, acid derivatives and carbamates from alcohol through acyl imidazole intermediates and also it is used to prepare polymers as well as used in peptide coupling.<sup>311,312</sup>

The reagent is also considered 'green' as the wastes that being produced were carbon dioxide and imidazole that is benign and easily separable by-product, which coincide with 12 principles of green chemistry. In addition to that, the reagent is safe to use having mild reaction conditions and produced high yield of products.<sup>312</sup> In the production of organic carbonates, CDI can be considered an alternative to phosgene, due to its low toxicity.<sup>313</sup> There were few literatures being reported that used solvent free synthesis involving CDI as one of the starting reagent producing high yield product. In the case of producing sorbitol carbonate, DMSO was being used as solvent to dissolve both reagents as sorbitol is a polar molecule without affecting CDI. Different substituted sorbitol carbonate could be synthesised using different ratio of CDI. However the reaction is not sustainable in long term and large scale process as CDI is an expensive reagent and the starting materials for making CDI is phosgene with imidazole under anhydrous conditions.<sup>311</sup> It can only be used in small scale process for example in academia.

##### 7.2.2.1.1 Reaction between sorbitol and CDI (1:1) ratio

FTIR spectra shows the presence of carbonyl (C=O) stretching band at 1788 cm<sup>-1</sup> in Figure 7-7 which indicates the presence of carbonyl ring strain of mono sorbitol carbonate. The OH stretch is not clear and there were some peaks around 3000 cm<sup>-1</sup> indicating aromatic C-H which due to imidazole. Purification of product is quite challenging for this reaction as sorbitol only dissolve in polar solvents. Figure 7-8 shows the <sup>1</sup>H NMR spectra of crude mono sorbitol carbonate.

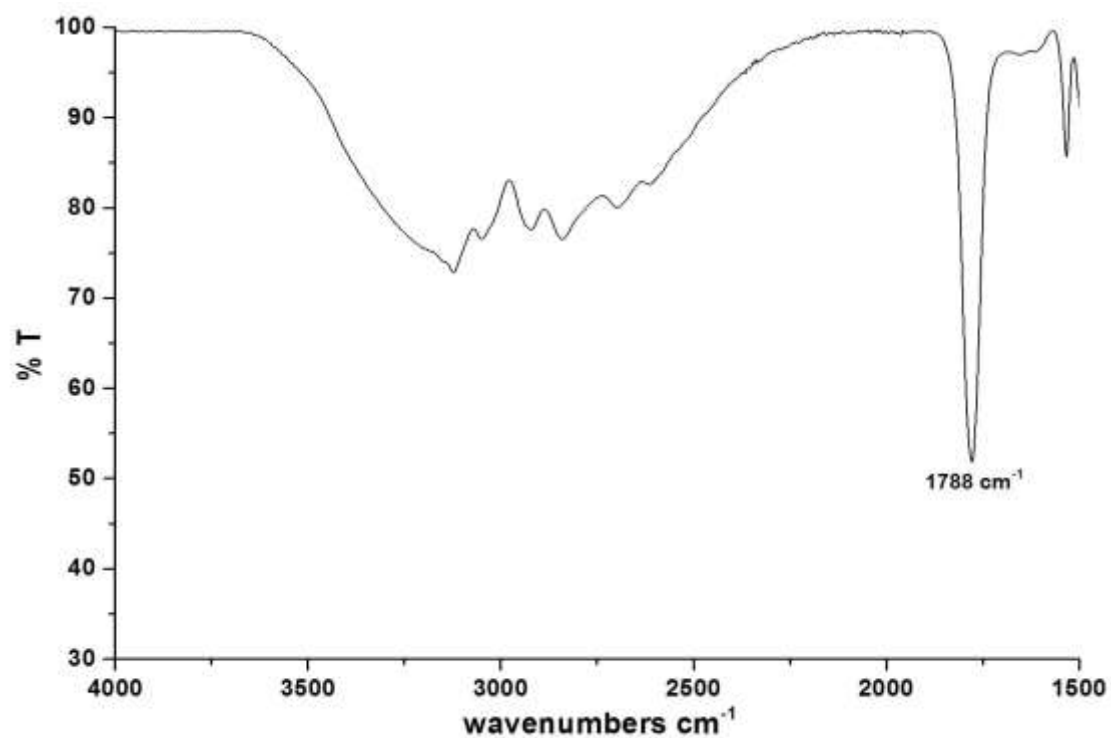


Figure 7-7: FTIR spectra of reaction sample for sorbitol/CDI reaction at 1:1 ratio

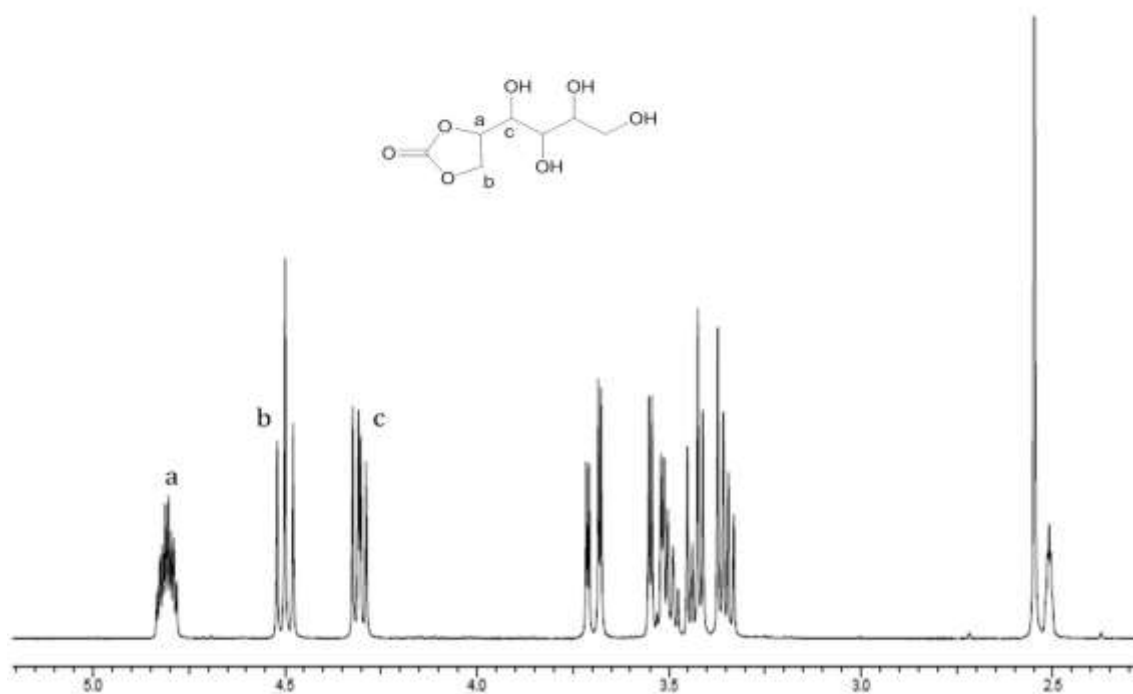


Figure 7-8:  $^1\text{H}$  NMR spectroscopy of the reaction sample for sorbitol/CDI at 1:1 ratio



#### 7.2.2.1.2 Reaction between sorbitol and CDI (1:2) ratio

Bis sorbitol carbonate would be expected to be formed in this reaction and the aim was to isolate this compound. The FTIR spectrum shows similar IR peaks as the 1:1 reaction but with higher intensity of carbonyl peak at 1788  $\text{cm}^{-1}$ .  $^1\text{H}$  NMR spectroscopy shows a mixture of two products present in the reaction mixture: mono sorbitol carbonate and bis sorbitol carbonate.  $^{13}\text{C}$  NMR shows the presence of carbonate peaks at 154 ppm. Several work up steps shows that the impurities were still present. However analysis from the Q-TOF and HPLC show the presence of bis sorbitol carbonate with small traces of mono sorbitol carbonate.

#### 7.2.2.1.3 Reaction between sorbitol and CDI (1:4) ratio

In this reaction, the aim is to synthesise tris sorbitol carbonate. In order to determine the best ratio of CDI and sorbitol to form the targeted tris sorbitol carbonate, 1:4 ratio of sorbitol to CDI was used in excess. The FTIR spectra shows an intense carbonate stretching band at 1788  $\text{cm}^{-1}$  and the presence of OH stretching band at 3300  $\text{cm}^{-1}$  is not observed in the spectra shown in Figure 7-9. This indicates that all the OH groups of sorbitol are being converted. Pure tris sorbitol carbonate can be purified easily by dissolving the reaction mixture in water as tris sorbitol carbonate does not dissolve in water. Imidazole stretching band at around 3000  $\text{cm}^{-1}$  is not observed in the spectra.

The  $^1\text{H}$  NMR and  $^{13}\text{C}$  NMR spectrum confirms the presence of tris sorbitol carbonate shown in Figure 7-10 and Figure 7-11 respectively. In  $^{13}\text{C}$  NMR spectra shows a peak at around 154 ppm which is characteristic of carbonate chemical shift.

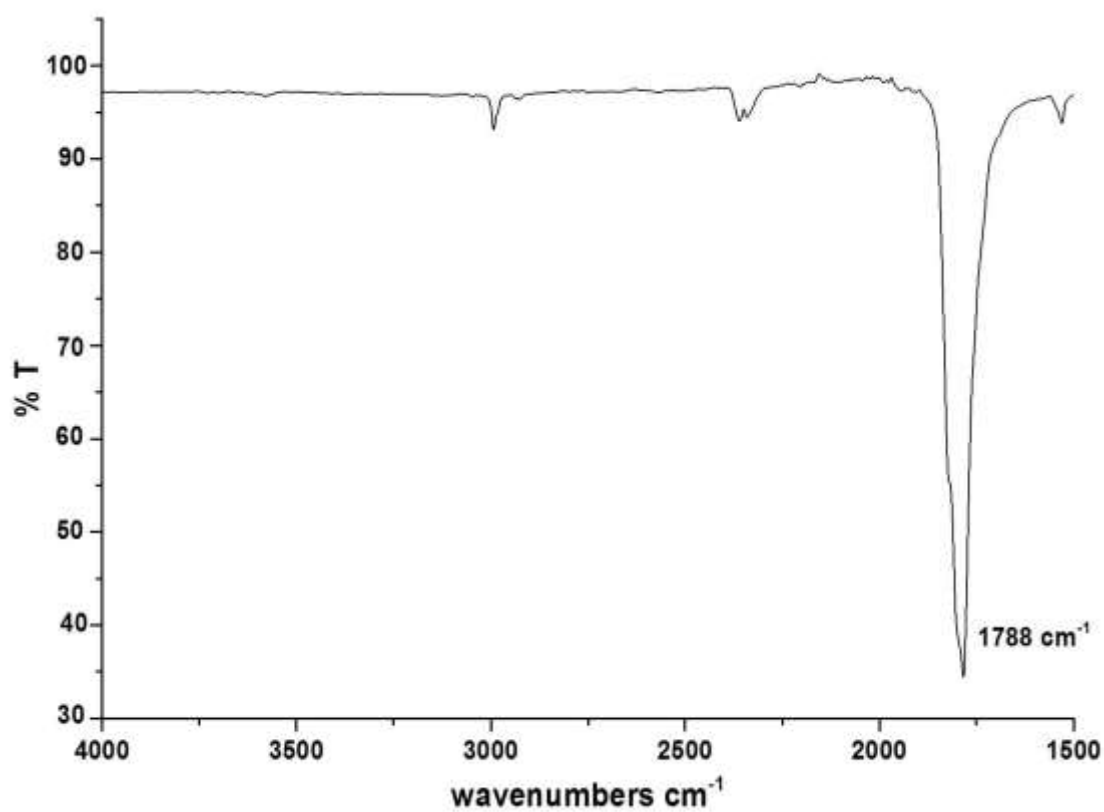


Figure 7-9: FTIR spectra of reaction sample for sorbitol/CDI reaction at 1:4 ratio

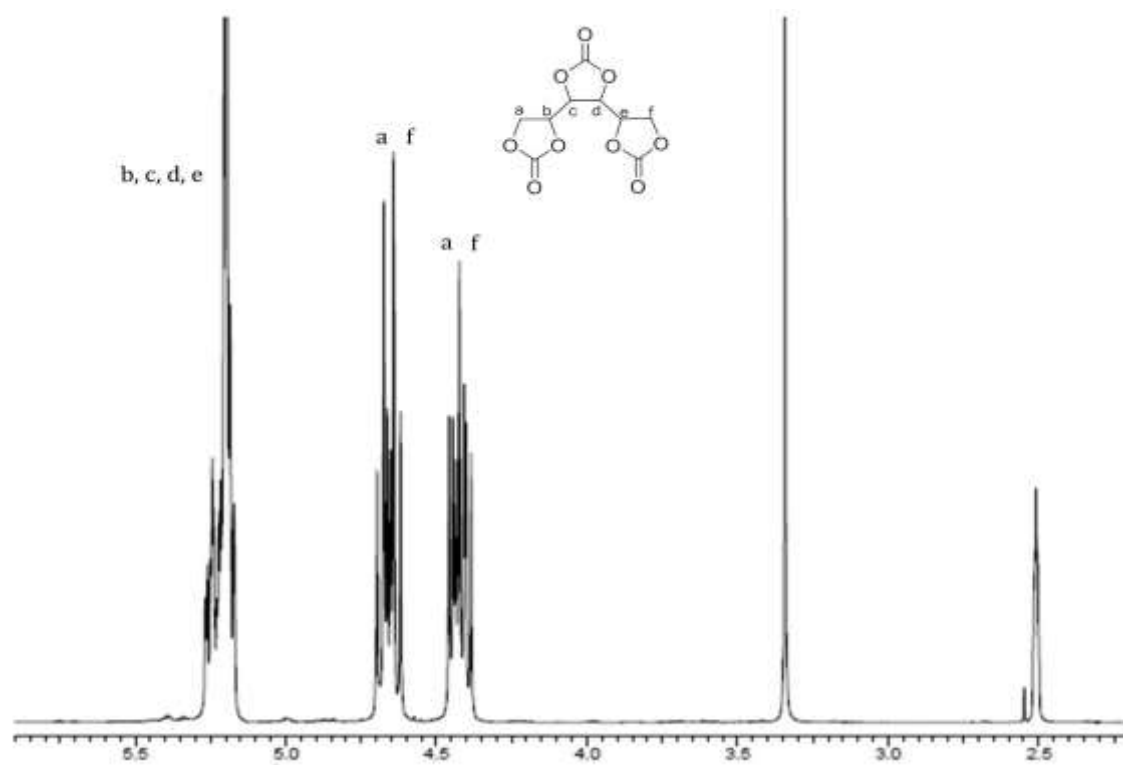


Figure 7-10:  $^1\text{H}$  NMR spectroscopy of the reaction sample for sorbitol/CDI at 1:4 ratio

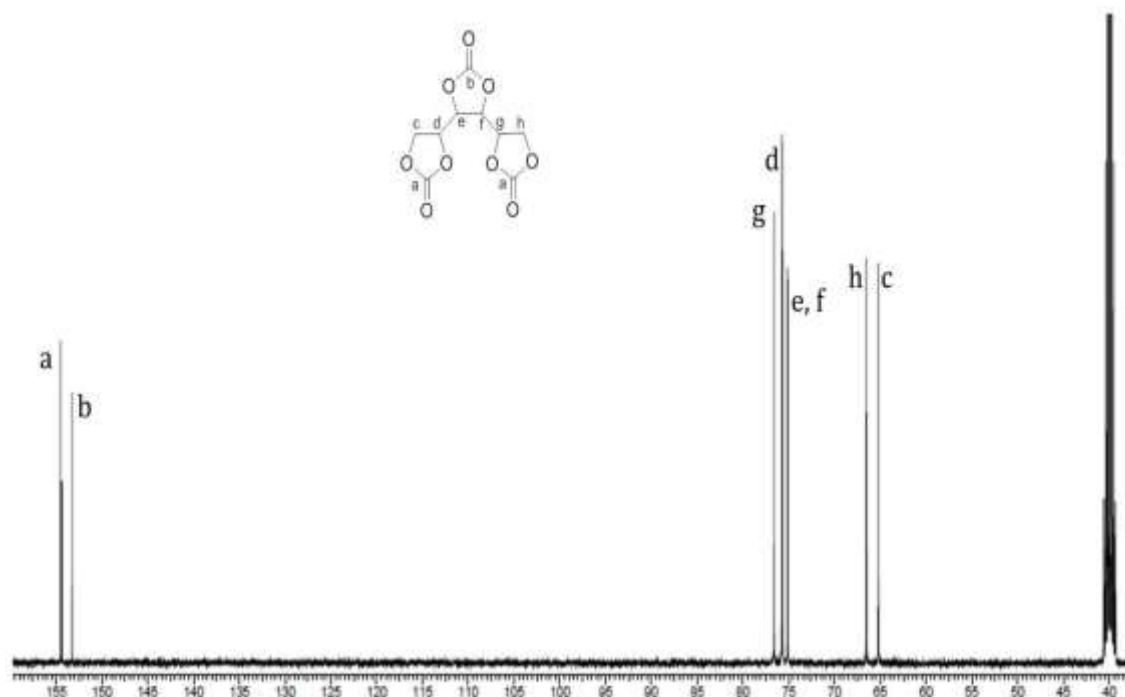


Figure 7-11:  $^{13}\text{C}$  NMR spectroscopy of the reaction sample for sorbitol/CDI at 1:4 ratio

Table 29: C-H-N analysis of the synthesised tris sorbitol carbonate

Elements present	% Calculated	Analysis
<b>C</b>	41.5	41.35
<b>H</b>	3.07	3.24
<b>N</b>	-	-

Table 29 shows the CHN analysis of tris sorbitol carbonate from the chemical reaction. The theoretical elemental formula has the same elemental analysis which indicates that the product formed is tris sorbitol carbonate. After purification of the compound to remove excess imidazole, the yield of the sorbitol carbonate was 63% with a melting point of 132°C-134°C.

#### 7.2.2.1.4 Stability tests of tris sorbitol carbonate

The stability of tris sorbitol carbonate was determined by heating the sample to 100°C for 4 h and 24 h. From the HPLC chromatogram in the appendix, there is

little change from 4 h and 24 h reaction. Tris sorbitol carbonate is stable upon heating to 100°C. Impurities of bis sorbitol carbonate can be seen appearing in the spectra which is not due to heating however the amount of bis sorbitol carbonate reduced after heating for 24 h. The mixture of CDI and tris sorbitol carbonate was also tested to determine the stability of the carbonate. HPLC chromatogram shows tris sorbitol carbonate is stable and there is no breakdown of the carbonate and only CDI decomposing into imidazole.

### **7.3 Conclusion**

The production of sorbitol carbonate directly from sorbitol is the first ever reported synthesis. The presence of organic solvents has an effect in the production of the carbonates in which DMSO inhibits the formation of carbonates. Solvent-free reaction is an attractive method to synthesise the carbonates giving high amount of carbonates. Bis sorbitol carbonate can only be achieved by enzymatic reaction. In chemical reaction, tris sorbitol carbonate has been successfully synthesised.

# **CHAPTER 8**

## **CONCLUSION AND FUTURE WORK**

## 8 CONCLUSION AND FUTURE WORK

Two different routes in the synthesis of glycerol carbonate were being investigated: direct carbonylation of glycerol carbonate from CO<sub>2</sub> and synthesis of glycerol carbonate from urea.

The synthesis of glycerol carbonate from CO<sub>2</sub> is the most attractive route in valorisation of glycerol as it utilised two cheap raw materials in which the atom economy of the reaction is 87%. In the direct carbonylation of glycerol carbonate from CO<sub>2</sub>, different dehydrating agents were tested and acetonitrile gave the best yield of glycerol carbonate. The reaction was catalysed by copper supported on lanthanum oxide and different loadings of copper were investigated in chapter 3 and the catalysts were synthesised by hydrothermal method. The yield of glycerol carbonate decreases with increasing copper loading. 2.3 wt% of Cu/La<sub>2</sub>O<sub>3</sub> gave the highest yield of glycerol carbonate of 25% with 75% conversion of glycerol with the selectivity of 33% to glycerol carbonate for 16 h reaction. The performance of the catalyst can be correlated to the amount of basic sites and 2.3 wt% Cu/La<sub>2</sub>O<sub>3</sub> has the highest basic sites amongst the other catalysts. For future work, lower loadings of copper could be tested in the synthesis of glycerol carbonate.

Then the synthesis of 2.3 wt% Cu/La<sub>2</sub>O<sub>3</sub> was modified due to its long hydrothermal method. In chapter 4, the aim is to decrease preparation time of the catalysts by replacing the hydrothermal method to microwave synthesis. The research is primarily for catalyst development. In this reaction, the experiments were run for 24 h instead of 16 h reaction. MW-pre has higher activity compare to other catalyst being synthesised. 87.6% of glycerol conversion was achieved with glycerol carbonate yield of 2.8%. The MW-pre catalyst has similar performance with HT catalyst. Ammonium bicarbonate was discovered in after the reaction and it is possible that the formation of ammonium bicarbonate provides an alternative pathway for water removal. For future work, shorter reaction time should be conducted to prevent over reaction and possibility of polymerisation of the products overtime. Time online studies is not an option in this reaction due to high

pressure CO<sub>2</sub> as well as depressurisation of the gas, however, individual reaction should be repeated at a range of different time in the future.

In chapter 5, we have found that 2-cyanopyridine is a better better dehydrating agent compare to using acetonitrile. Different reaction conditions were tested in the reaction. The conversion of glycerol increases from 6.7% to 12.5% with an increase in pressure from 2.8 MPa to 4.2 MPa. However, the conversion decreases with increasing pressure due to saturation of CO<sub>2</sub> on the surface of the catalyst. In this study, cerium oxide and lanthanum oxide were tested in the synthesis of glycerol carbonate from CO<sub>2</sub>. It was found that cerium oxide is a superior catalyst compare to lanthanum oxide in which the conversion of glycerol was 31.4% with glycerol carbonate yield of 17.5% compare to La<sub>2</sub>O<sub>3</sub> in which the conversion of glycerol was 25.7% with glycerol carbonate yield of 12.7%. Cerium oxide synthesised by microwave method has achieved 30% conversion of glycerol and 18.8% glycerol carbonate yield at 150°C, 4.0 MPa for 5 h compare to using cerium oxide synthesised by hydrothermal method. Therefore microwave method can be used to synthesise catalyst at shorter time with better performance.

Urea is being used as a carbonate source in the synthesis of glycerol carbonate which having an atom economy of 78% which was discussed in chapter 6. Two rare earth metal oxides were tested in the reaction and lanthanum oxide gave the best activity in producing glycerol carbonate. The introduction of copper into lanthanum oxide increases the activity further. The glycerol conversion increases from 96% to 98% when using Cu/La<sub>2</sub>O<sub>3</sub> and the glycerol carbonate yield increases from 68% to 72% in 4 h reaction. The reaction is further improved by switching the mode of heating to microwave heating. The reaction achieved 97% conversion of glycerol and 64% glycerol carbonate yield catalysed by Cu/La<sub>2</sub>O<sub>3</sub> in 2 h reaction. For future work, time on line analysis should be attempted instead of individual reactions during microwave reaction. The use of vacuum is an alternative way to remove ammonia instead of using flow of nitrogen and to compare the reaction performance.

The synthesis of sorbitol carbonate was discussed in chapter 7 using two methods: enzymatic method and chemical method. This is first ever reported synthesis of sorbitol carbonate directly from sorbitol. Quantitative analysis is not possible as there is no standard for the products. However, in this reaction qualitative

methods were used to identify the products. Mono sorbitol carbonate and bis sorbitol carbonate were found in enzymatic reaction. In chemical reaction, tris sorbitol carbonate was successfully synthesised using 1:4 ratio. For future work, separation of mono and bis sorbitol carbonate using prep column as it is difficult to separate the two products. Optimisation of enzymatic reaction to ensure selectivity to only one type sorbitol carbonate in this case is bis sorbitol carbonate. With the successful production of tris sorbitol carbonate, the attention can be shifted towards using different methods in synthesising the carbonates. The reaction with CO<sub>2</sub> is highly desirable due to the number of OH groups that could be carbonated therefore capturing and sequester more carbon dioxide.

We have demonstrated the production of cyclic organic carbonates using glycerol and sorbitol. Therefore there is a potential to expand this research further in utilising renewable polyols that can be further carbonated.



# **CHAPTER 9**

## **APPENDIX**

## 9 APPENDIX

### 9.1 CHAPTER 3

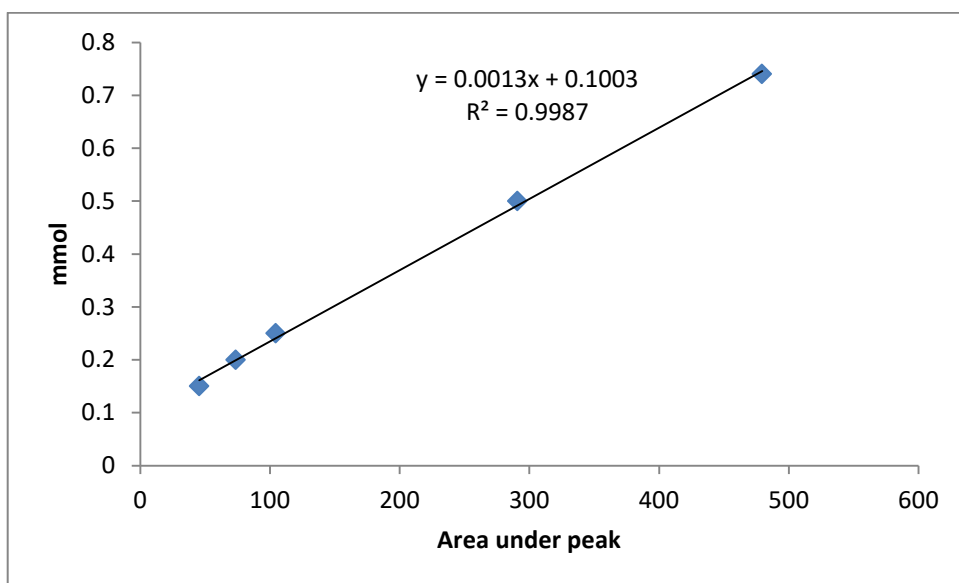


Figure 9-1: Calibration of glycerol

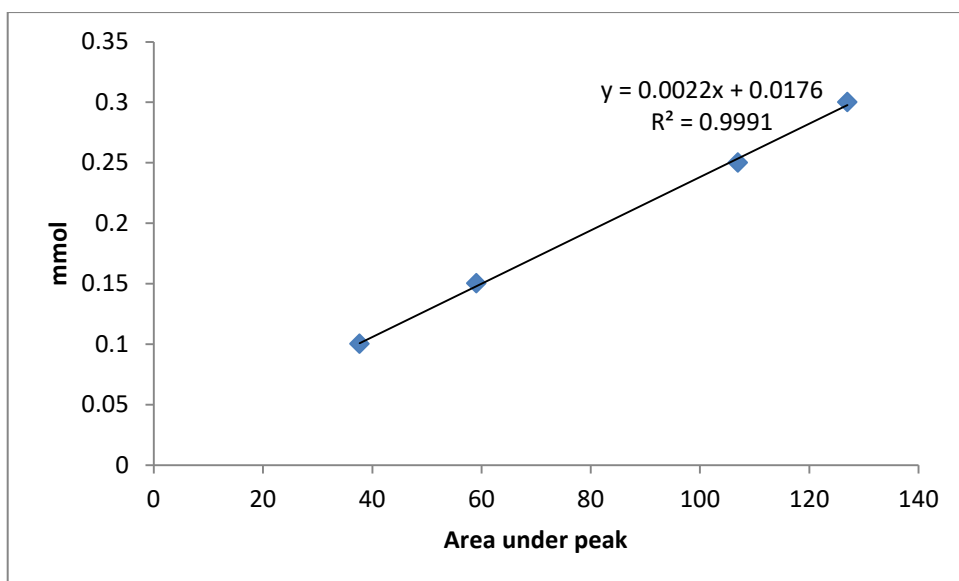


Figure 9-2: Calibration of glycerol carbonate

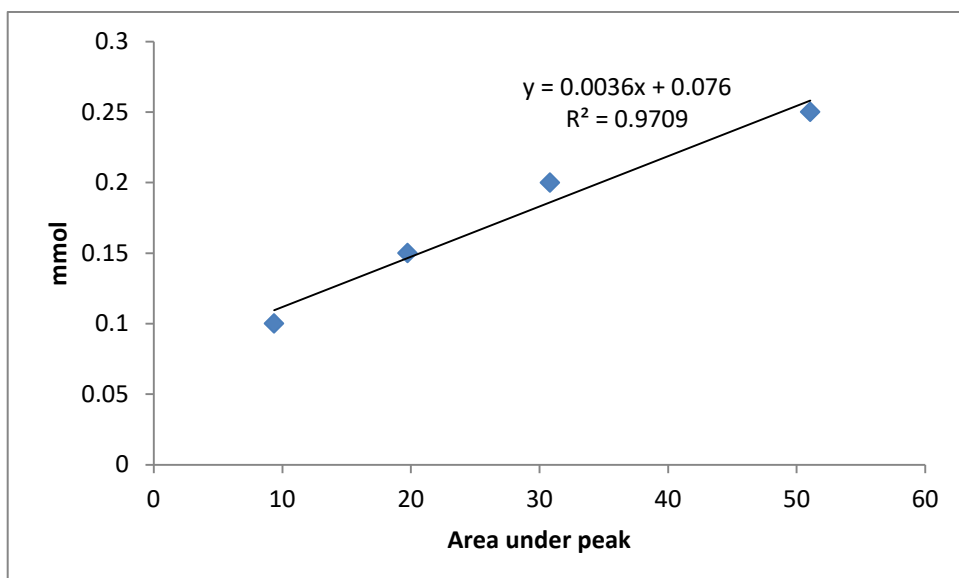


Figure 9-3: Calibration curve of monoacetin

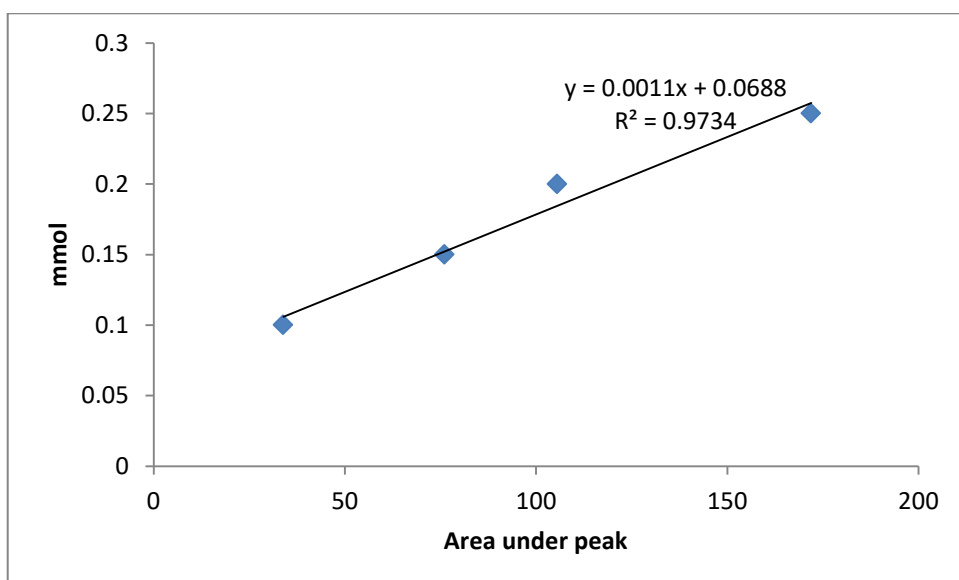


Figure 9-4: Calibration curve of diacetin

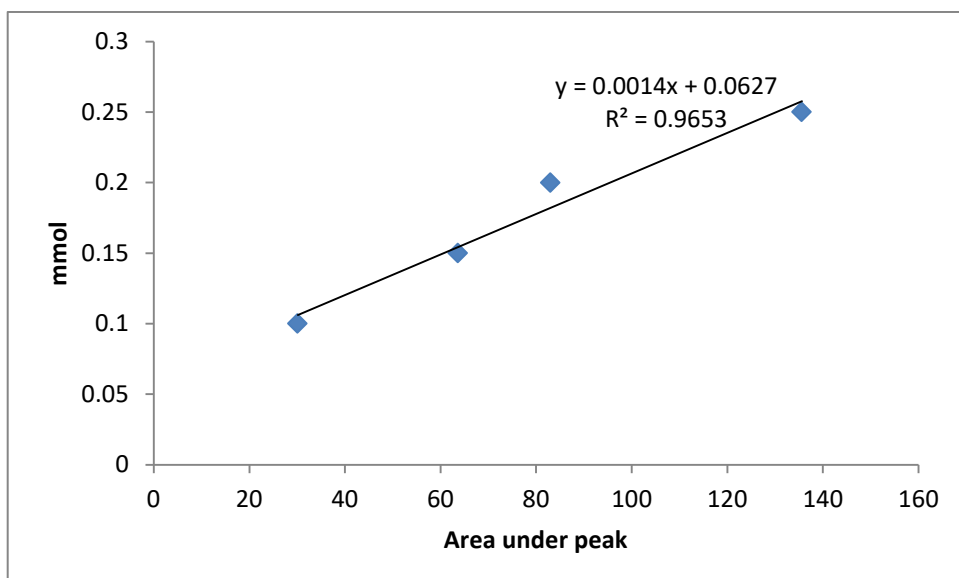


Figure 9-5: Calibration curve of triacetin

## 9.2 CHAPTER 5

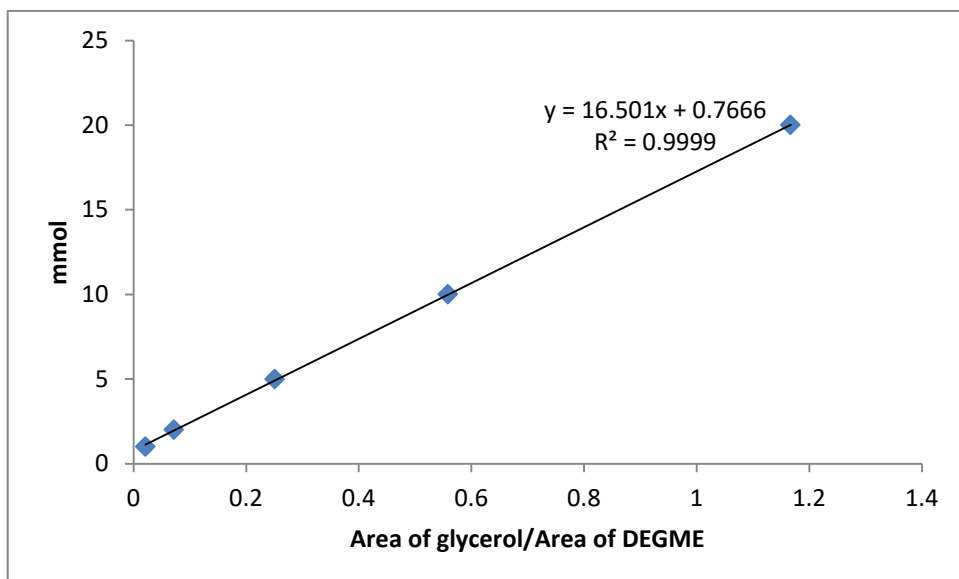


Figure 9-6: Calibration curve of glycerol

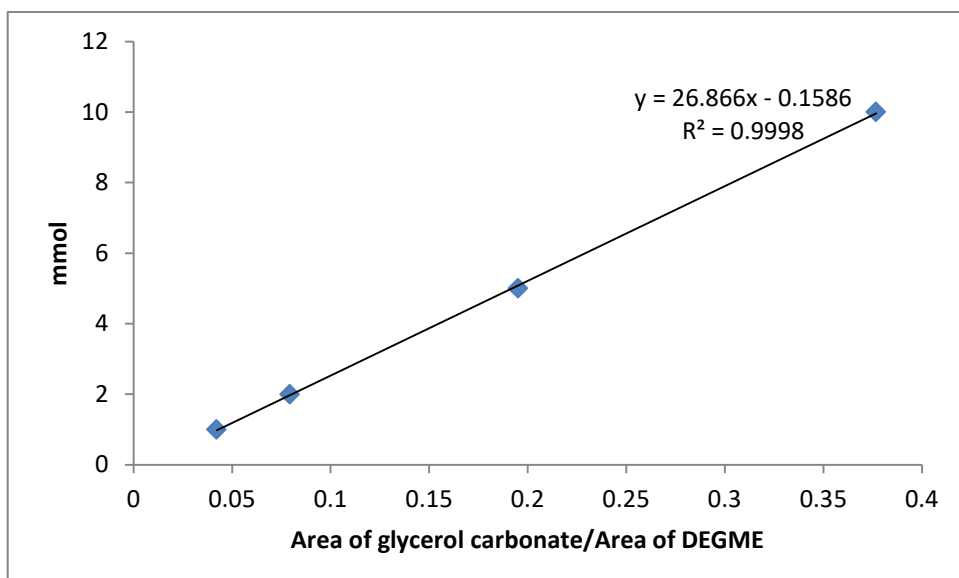


Figure 9-7: Calibration curve of glycerol carbonate

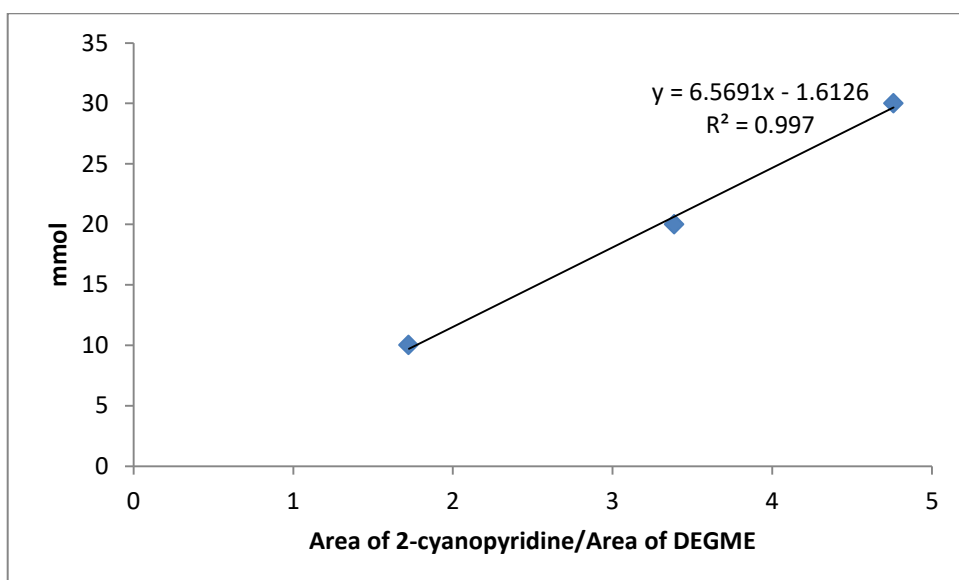


Figure 9-8: Calibration curve of 2-cyanopyridine

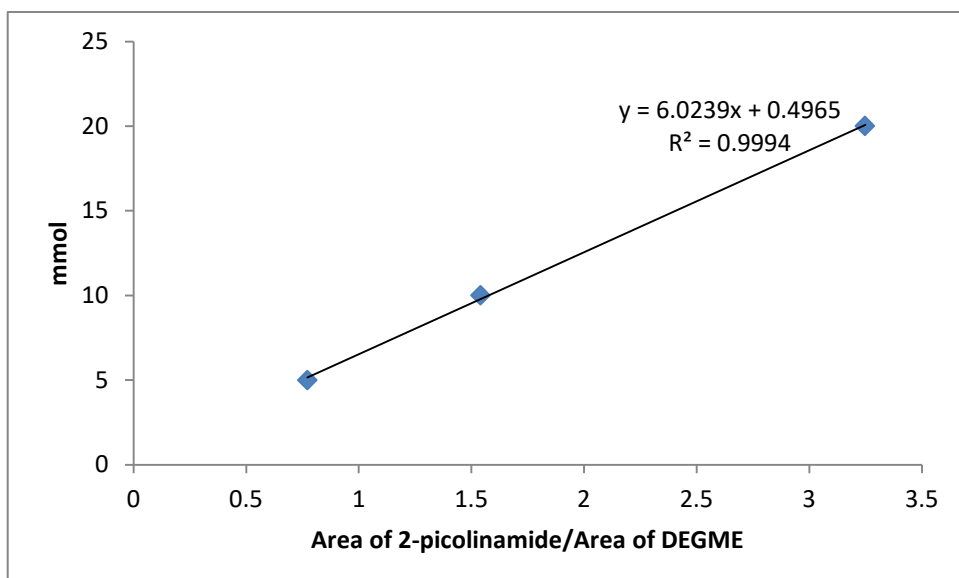


Figure 9-9: Calibration curve of 2-picolinamide

### 9.3 CHAPTER 6

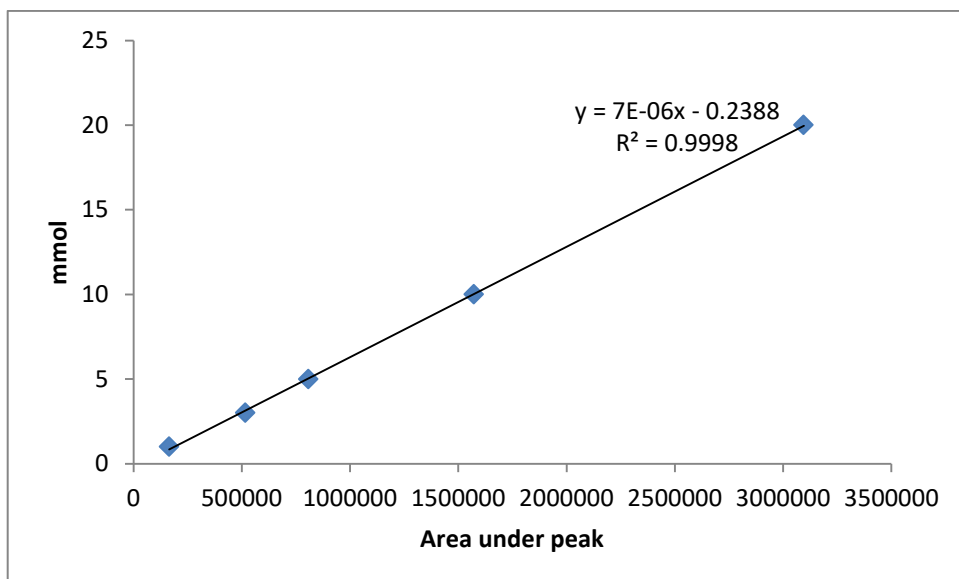


Figure 9-10: Calibration curve of glycerol

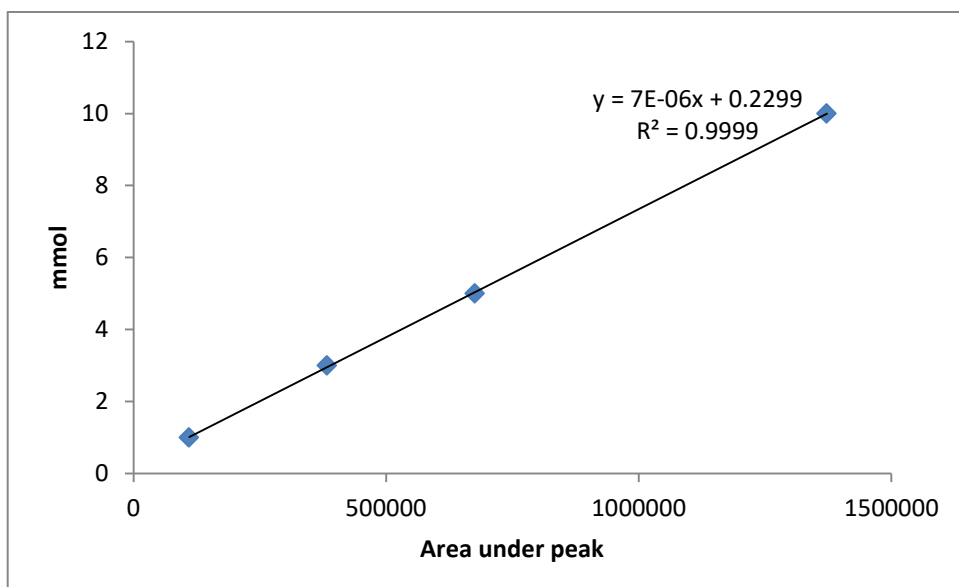


Figure 9-11: Calibration curve of glycerol carbonate

#### 9.4 CHAPTER 7

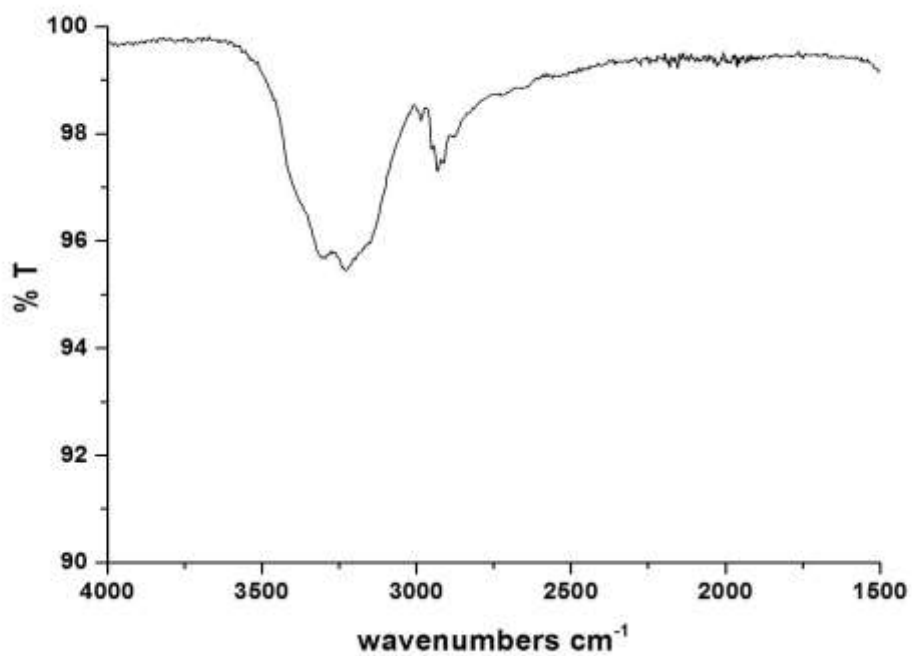


Figure 9-12: IR of sorbitol

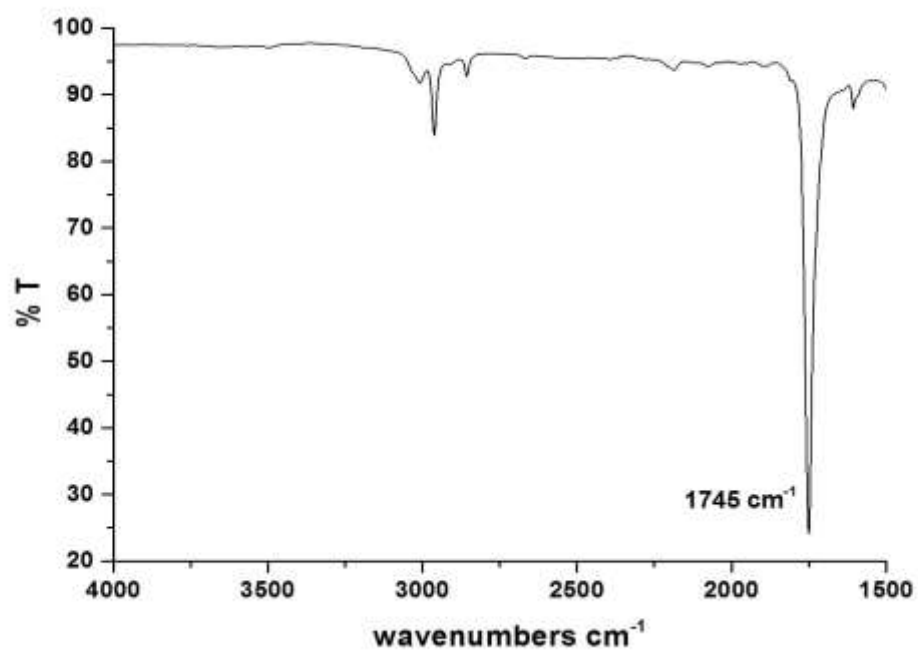


Figure 9-13: IR of DMC

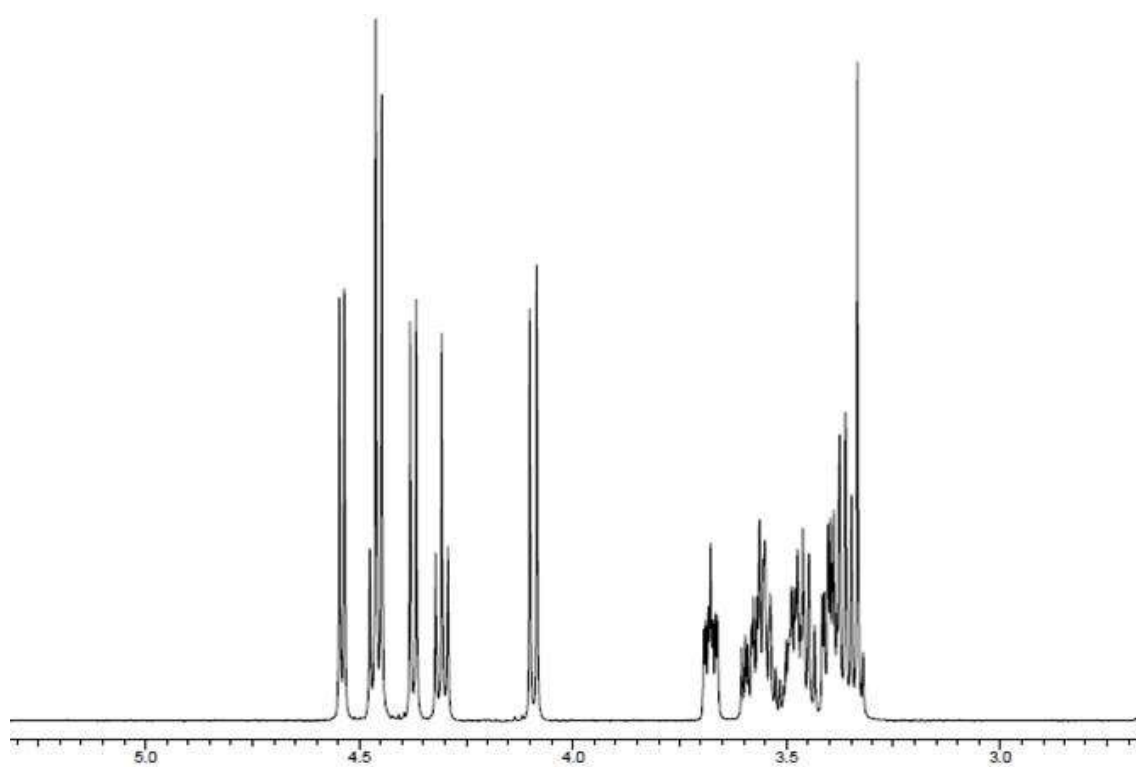
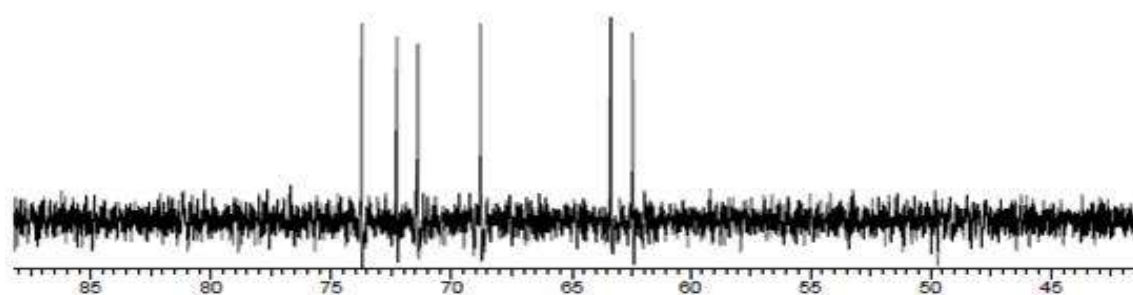


Figure 9-14: <sup>1</sup>H NMR of sorbitol





**Figure 9-15:**  $^{13}\text{C}$  NMR of sorbitol

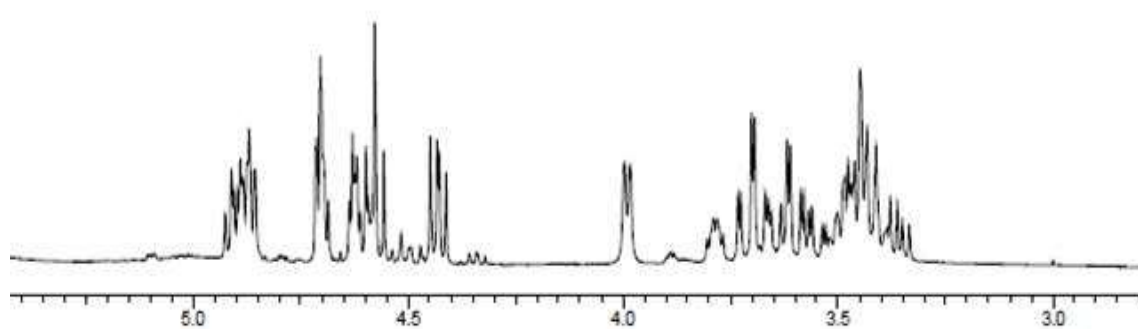


Figure 9-16:  $^1\text{H}$  NMR of sorbitol/CDI at 1:2 ratio

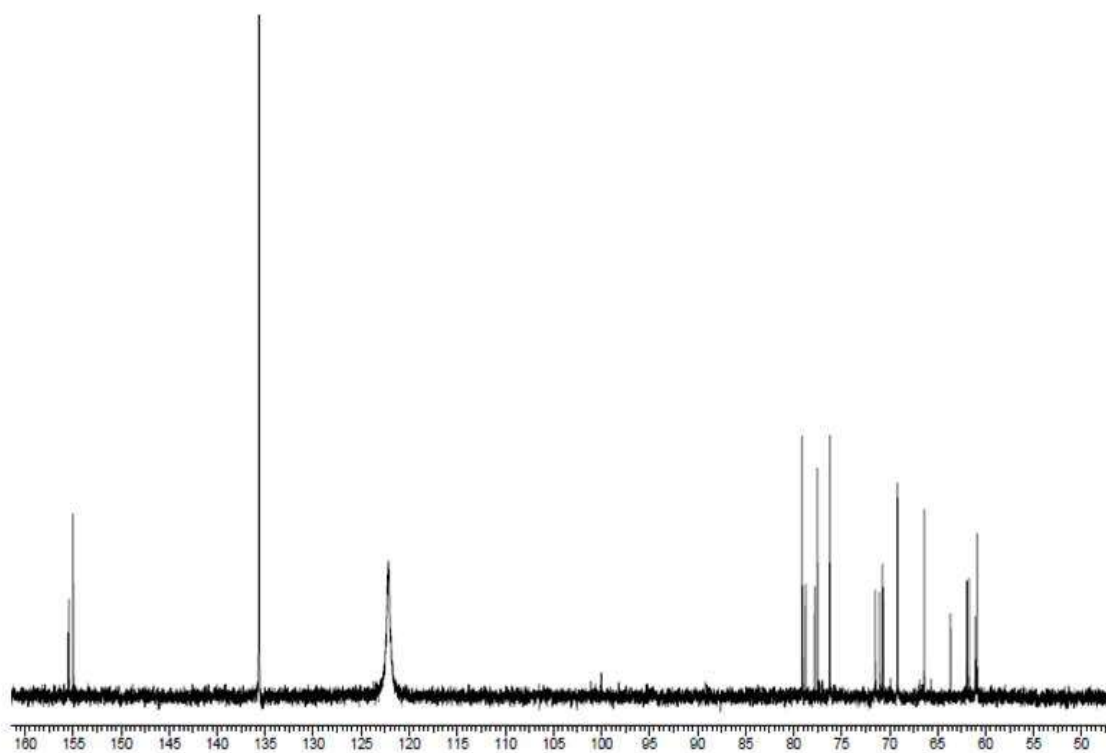


Figure 9-17:  $^{13}\text{C}$  NMR of sorbitol/ CDI at 1:2 ratio

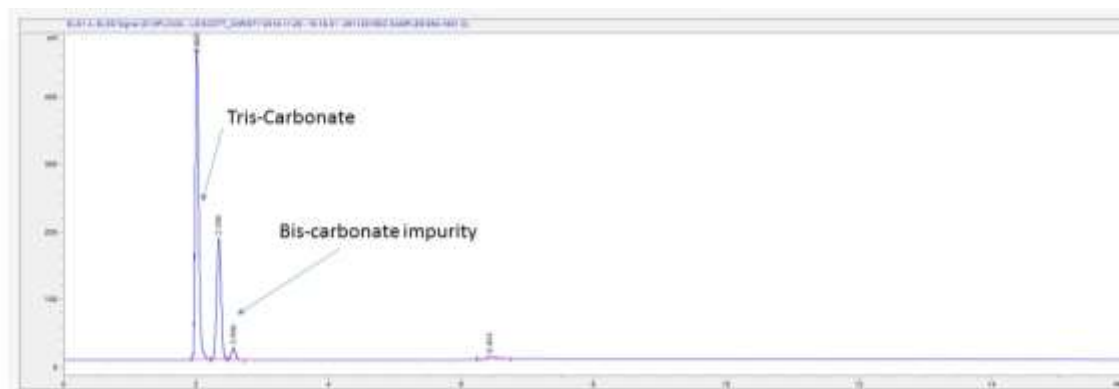


Figure 9-18: The HPLC chromatogram of tris sorbitol carbonate heated at 100°C for 4 h

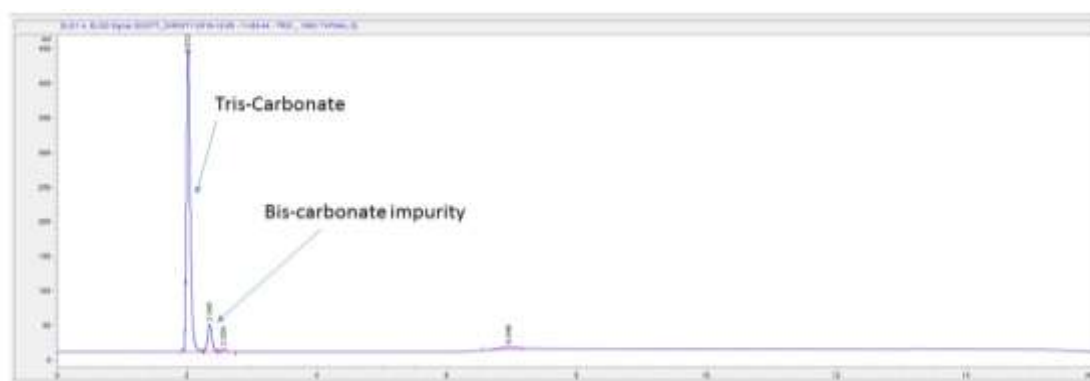


Figure 9-19: The HPLC chromatogram of tris sorbitol carbonate heated at 100°C for 24 h

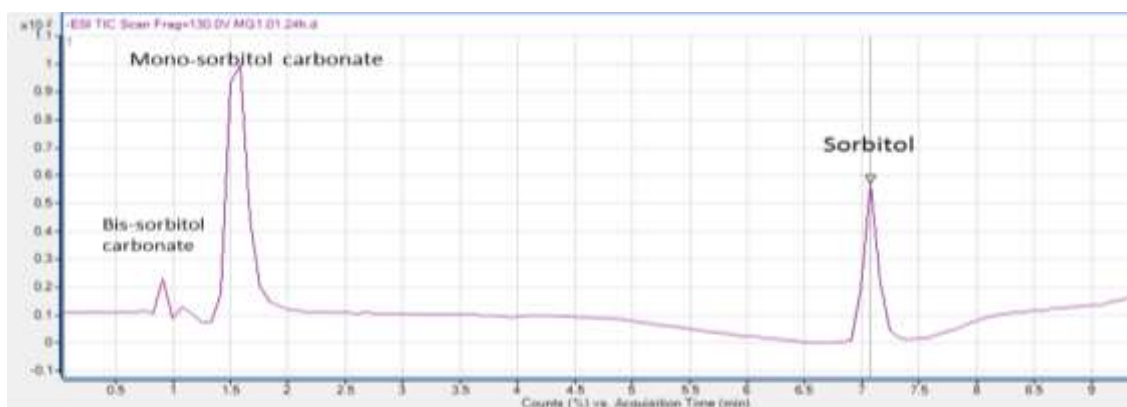
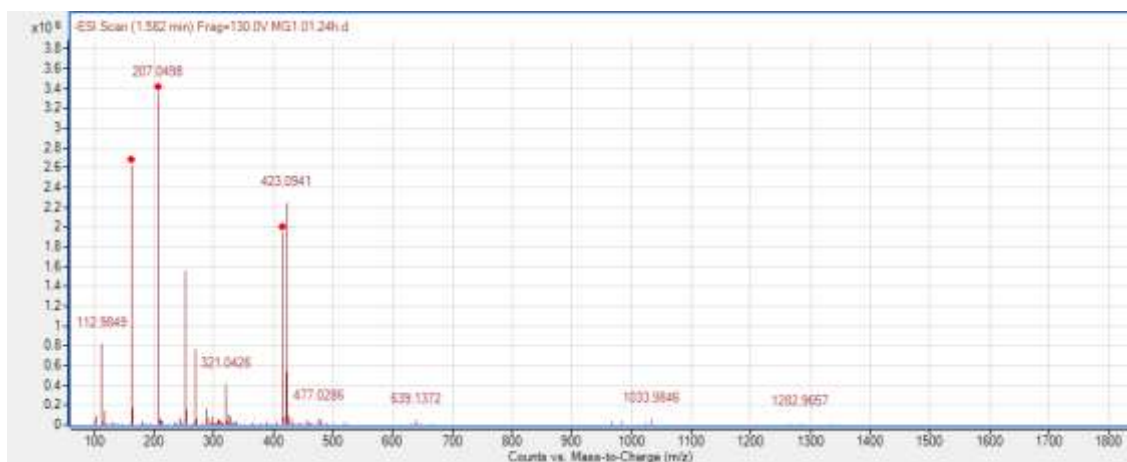


Figure 9-20: TIC chromatogram in negative mode using HILIC column



**Figure 9-21: Mass spectrum [M-1] at t=1.45 min for mono sorbitol carbonate from Figure 9-20**

## 10 References

1. Ben-Eli, M. U. Sustainability: The Five Core Principles - A New Framework. 1–12 (2006).
2. Mihelcic, J. R. *et al.* Sustainability science and engineering: the emergence of a new metadiscipline. *Environ. Sci. Technol.* **37**, 5314–5324 (2003).
3. Hjeresen, D. L., Kirchhoff, M. M. & Lankey, R. L. Green Chemistry: Environment, Economics, and Competitiveness. *Corp. Environ. Strateg.* **9**, 259–266 (2002).
4. Sauv , S. & Desrosiers, M. A review of what is an emerging contaminant. *Chem. Cent. J.* **8**, 15 (2014).
5. Anastas, P. T. & Warner, J. C. *Green Chemistry: Theory and Practice*. Oxford University press (1998).
6. Trost, B. M. Atom Economy—A Challenge for Organic Synthesis: Homogeneous Catalysis Leads the Way. *Angew. Chemie Int. Ed. English* **34**, 259–281 (1995).
7. Sheldon, R. a. The E Factor: fifteen years on. *Green Chem.* **9**, 1273 (2007).
8. Kirchhoff, M. M. Promoting sustainability through green chemistry. *Resour.*

*Conserv. Recycl.* **44**, 237–243 (2005).

9. Mehrara, M. Energy consumption and economic growth: The case of oil exporting countries. *Energy Policy* **35**, 2939–2945 (2007).
10. Olah, G. A., Goepfert, A. & Prakash, G. K. S. *Beyond Oil and Gas: The Methanol Economy: Second Edition. Beyond Oil and Gas: The Methanol Economy: Second Edition* (2009). doi:10.1002/9783527627806
11. International Council on Clean Transportation. An Introduction To Petroleum Refining and the Production of Ultra Low Sulfur Gasoline. 1–33 (2011).
12. Jukić A. Petroleum Refining and Petrochemical Processes Crude oil: composition, classification; Coal; Oil Shale; Tar Sand; Gas Hydrates. 14–20 (2013).
13. Ahuja, D. & Tatsutani, M. Sustainable energy for developing countries. *S.a.P.I.En.S* **2**, 1–16 (2009).
14. WEC. World Energy Resources. *World Energy Counc. Rep.* **1**, 4 (2016).
15. Huang, Y. F., Huang, G. H., Hu, Z. Y., Maqsood, I. & Chakma, A. Development of an expert system for tackling the public's perception to climate-change impacts on petroleum industry. *Expert Syst. Appl.* **29**, 817–829 (2005).
16. Wang, H. L. *et al.* Characterization and assessment of volatile organic compounds (VOCs) emissions from typical industries. *Chinese Sci. Bull.* **58**, 724–730 (2013).
17. Cetin, E., Odabasi, M. & Seyfioglu, R. Ambient volatile organic compound (VOC) concentrations around a petrochemical complex and a petroleum refinery. *Sci. Total Environ.* **312**, 103–112 (2003).
18. WHO. Health Aspects of Air Pollution with Particulate Matter , Ozone and Nitrogen Dioxide. *Rep. a WHO Work. Gr. Bonn, Ger. 13–15 January 2003* 98 (2003). doi:10.2105/AJPH.48.7.913
19. Welton, T. Solvents and sustainable chemistry. *Proc. R. Soc. A* **471**, 1–26 (2015).

20. Rana, K. K. & Rana, S. Fundamentals , Representative Applications and Future Perspectives of Green Chemistry : A Short Review. 1–16 (2014).  
doi:10.4236/oalib.1100748
21. Xie, X. & Tang, Y. Efficient synthesis of simvastatin by use of whole-cell biocatalysis. *Appl. Environ. Microbiol.* **73**, 2054–2060 (2007).
22. Enache, D. I. *et al.* Solvent-Free Oxidation of Primary Alcohols to Aldehydes Using. *Science (80-. ).* **311**, 362–366 (2006).
23. United Nations. *World Economic and Social Survey 2013. New York: Department for Economic and Social Affairs* (2013).  
doi:10.1016/j.compind.2010.10.001
24. Edenhofer, O. *et al.* *IPCC, 2011: Summary for Policymakers. In: IPCC Special Report on Renewable Energy Sources and Climate Change Mitigation. Cambridge University Press* (2011). doi:10.5860/CHOICE.49-6309
25. EREC. Renewable Energy Technology Roadmap 20% by 2020. *Renew. Energy* (2008).
26. Vandaele, N. & Porter, W. Renewable Energy in Developing and Developed Nations: Outlooks to 2040. *J. Undergrad. Res.* **15**, 1–7 (2015).
27. Baskar, C., Baskar, S. & Dhillon, R. S. *Biomass conversion: The interface of biotechnology, chemistry and materials science. Biomass Conversion: The Interface of Biotechnology, Chemistry and Materials Science* (2012).  
doi:10.1007/978-3-642-28418-2
28. From, B. & What, P. Current biofuel.
29. Power, C. & Right, I. H. Clean Power and Fuel — If Handled Right. 1–12 (2010).
30. UK Parliamentary Office of Science and Technology. Postnote Number 293: Transport biofuels. *Transp. Policy* **14**, 533–543 (2007).
31. Mesa, L. *et al.* Comparison of process configurations for ethanol production from two-step pretreated sugarcane bagasse. *Chem. Eng. J.* **175**, 185–191 (2011).

32. Begum, S., Rasul, M. G. & Akbar, D. An Investigation on Thermo Chemical Conversions of Solid Waste for Energy Recovery. **6**, 624–630 (2012).
33. Naik, S. N., Goud, V. V., Rout, P. K. & Dalai, A. K. Production of first and second generation biofuels: A comprehensive review. *Renew. Sustain. Energy Rev.* **14**, 578–597 (2010).
34. Clark, J. & Deswarte, F. *Introduction to Chemicals from Biomass: Second Edition. Introduction to Chemicals from Biomass: Second Edition* (2015). doi:10.1002/9781118714478
35. Werpy, T. and Petersen, G., Werpy, T. & Petersen, G. Top Value Added Chemicals from Biomass Volume I — Results of Screening for Potential Candidates from Sugars and Synthesis Gas Top Value Added Chemicals From Biomass Volume I : Results of Screening for Potential Candidates. *Other Inf. PBD 1 Aug 2004* Medium: ED; Size: 76 pp. pages (2004). doi:10.2172/15008859
36. Shaikh, A.-A. G. & Sivaram, S. Organic Carbonates. *Chem. Rev.* **96**, 951–976 (1996).
37. Schäffner, B., Schäffner, F., Verevkin, S. P. & Börner, A. Organic Carbonates as Solvents in Synthesis and Catalysis. *Chem. Rev.* **110**, 4554–4581 (2010).
38. Sakakura, T. & Kohno, K. The synthesis of organic carbonates from carbon dioxide. *Chem Commun* 1312–1330 (2009). doi:10.1039/b819997c
39. Lee, J.-C. & Litt, M. H. Ring-Opening Polymerization of Ethylene Carbonate and Depolymerization of Poly(ethylene oxide-co-ethylene carbonate). *Macromolecules* **33**, 1618–1627 (2000).
40. Tobishima, S., Arakawa, M., Hirai, T. & Yamaki, J. Ethylene carbonate-based electrolytes for rechargeable lithium batteries. *J. Power Sources* **26**, 449–454 (1989).
41. <Cyclic organic carbonates serve as solvents and reactive diluents.pdf>.
42. Schaffner, B., Holz, J., Verevkin, S. P. & Borner, A. Organic carbonates as alternative solvents for palladium-catalyzed substitution reactions.

*ChemSusChem* **1**, 249–253 (2008).

43. Xu, K. Nonaqueous Liquid Electrolytes for Lithium-Based Rechargeable Batteries. *Chem. Rev.* **104**, 4303–4418 (2004).
44. <Catalysis in biodiesel production by transesterification processes-An insight.pdf>.
45. Pacheco, M. A. & Marshall, C. L. Review of Dimethyl Carbonate (DMC) Manufacture and Its Characteristics as a Fuel Additive. *Energy & Fuels* **11**, 2–29 (1997).
46. Tundo, P. & Perosa, A. Green organic syntheses: organic carbonates as methylating agents. *Chem Rec* **2**, 13–23 (2002).
47. Tundo, P. & Selva, M. The Chemistry of Dimethyl Carbonate. *Acc. Chem. Res.* **35**, 706–716 (2002).
48. Buysch, H.-J. in *Ullmann's Encyclopedia of Industrial Chemistry* (Wiley-VCH Verlag GmbH & Co. KGaA, 2000). doi:10.1002/14356007.a05\_197
49. Keller, T., Holtbruegge, J., Niesbach, A. & Górak, A. Transesterification of Dimethyl Carbonate with Ethanol To Form Ethyl Methyl Carbonate and Diethyl Carbonate: A Comprehensive Study on Chemical Equilibrium and Reaction Kinetics. *Ind. Eng. Chem. Res.* **50**, 11073–11086 (2011).
50. Wang, M., Zhao, N., Wei & Sun, Y. Synthesis of Dimethyl Carbonate from Urea and Methanol over ZnO. *Ind. Eng. Chem. Res.* **44**, 7596–7599 (2005).
51. Wang, D., Yang, B., Zhai, X. & Zhou, L. Synthesis of diethyl carbonate by catalytic alcoholysis of urea. *Fuel Process. Technol.* **88**, 807–812 (2007).
52. Nash, T. THE ABSORPTION OF PHOSGENE BY AQUEOUS SOLUTIONS AND ITS RELATION TO TOXICITY. **14**, 227–233 (1971).
53. Warner, J. C., Cannon, A. S. & Dye, K. M. Green chemistry. *Environ. Impact Assess. Rev.* **24**, 775–799 (2004).
54. Wu, X. F., Neumann, H. & Beller, M. Palladium-catalyzed oxidative carbonylation reactions. *ChemSusChem* **6**, 229–241 (2013).



55. Gabriele, B. *et al.* A general and expedient synthesis of 5- and 6-membered cyclic carbonates by palladium-catalyzed oxidative carbonylation of 1,2- and 1,3-diols. *ChemSusChem* **4**, 1778–1786 (2011).
56. Romano, U., Tesel, R., Mauri, M. M. & Rebora, P. Synthesis of Dimethyl Carbonate from Methanol, Carbon Monoxide, and Oxygen Catalyzed by Copper Compounds. *Ind. Eng. Chem. Prod. Res. Dev.* **19**, 396–403 (1980).
57. Bhanage, B. M., Fujita, S. I., Ikushima, Y. & Arai, M. Synthesis of dimethyl carbonate and glycols from carbon dioxide, epoxides, and methanol using heterogeneous basic metal oxide catalysts with high activity and selectivity. *Appl. Catal. A Gen.* **219**, 259–266 (2001).
58. Zielinska-Nadolska, I., Warmuzinski, K. & Richter, J. Zeolite and other heterogeneous catalysts for the transesterification reaction of dimethyl carbonate with ethanol. *Catal. Today* **114**, 226–230 (2006).
59. Su, D. S. & Thomas, A. Nanochemical concepts for a sustainable energy supply. *ChemSusChem* **3**, 120 (2010).
60. Dasari, M. A., Kiatsimkul, P. P., Sutterlin, W. R. & Suppes, G. J. Low-pressure hydrogenolysis of glycerol to propylene glycol. *Appl. Catal. A Gen.* **281**, 225–231 (2005).
61. Dorskocil, E. J., Bordawekar, S. V., Kaye, B. G. & Davis, R. J. UV-vis spectroscopy of iodine adsorbed on alkali-metal-modified zeolite catalysts for addition of carbon dioxide to ethylene oxide. *J. Phys. Chem. B* **103**, 6277–6282 (1999).
62. Choudary, B. M. *et al.* Mg-Al-O-t-Bu hydrotalcite: A new and efficient heterogeneous catalyst for transesterification. *J. Mol. Catal. A Chem.* **159**, 411–416 (2000).
63. Harmer, M. A. & Sun, Q. Solid acid catalysis using ion-exchange resins. *Appl. Catal. a-General* **221**, 45–62 (2001).
64. Wang, S. *et al.* Transesterification of dimethyl oxalate with phenol under SnO<sub>2</sub>/SiO<sub>2</sub> catalysts. *Ind. Eng. Chem. Res.* **43**, 4027–4030 (2004).
65. Meyer, U. & Hoelderich, W. F. Transesterification of methyl benzoate and

- dimethyl terephthalate with ethylene glycol over superbases. *Appl. Catal. A Gen.* **179**, 131–137 (1999).
66. Gao, Z. W., Wang, S. F. & Xia, C. G. Synthesis of propylene carbonate from urea and 1,2-propanediol. *Chinese Chem. Lett.* **20**, 131–135 (2009).
  67. Li, Q., Zhang, W., Zhao, N., Wei, W. & Sun, Y. Synthesis of cyclic carbonates from urea and diols over metal oxides. *Catal. Today* **115**, 111–116 (2006).
  68. Joe, W. *et al.* Synthesis of dimethyl carbonate from urea and methanol over ZnO(X)–CeO<sub>2</sub>(1–X) catalysts prepared by a sol–gel method. *J. Ind. Eng. Chem.* **18**, 1018–1022 (2012).
  69. Li, Q., Zhao, N., Wei, W. & Sun, Y. Catalytic performance of metal oxides for the synthesis of propylene carbonate from urea and 1,2-propanediol. *J. Mol. Catal. A Chem.* **270**, 44–49 (2007).
  70. Sheldon, R. a. R. R. a. *et al.* Green Chemistry and Catalysis. *WILEY-VCH Verlag GmbH Co* (2007).
  71. Langanke, J. *et al.* Carbon dioxide (CO<sub>2</sub>) as sustainable feedstock for polyurethane production. *Green Chem.* 1865–1870 (2014). doi:10.1039/C3GC41788C
  72. Sakakura, T., Choi, J. C. & Yasuda, H. Transformation of carbon dioxide. *Chemical Reviews* **107**, 2365–2387 (2007).
  73. Mikkelsen, M., Jørgensen, M. & Krebs, F. C. The Teraton Challenge. A Review of Fixation and Transformation of Carbon Dioxide. *Energy Environ. Sci.* **3**, 43–81 (2010).
  74. Bruneau, C. & Dixneuf, P. H. Catalytic incorporation of CO<sub>2</sub> into organic substrates: Synthesis of unsaturated carbamates, carbonates and ureas. *J. Mol. Catal.* **74**, 97–107 (1992).
  75. Aresta, M. *Carbon Dioxide as Chemical Feedstock. Carbon Dioxide as Chemical Feedstock* (2010). doi:10.1002/9783527629916
  76. Arbeláez, O., Orrego, A., Bustamante, F. & Villa, A. L. Direct Synthesis of Diethyl Carbonate from CO<sub>2</sub> and CH<sub>3</sub>CH<sub>2</sub>OH Over Cu–Ni/AC Catalyst. *Top.*

*Catal.* **55**, 668–672 (2012).

77. Choi, J.-C., He, L.-N., Yasuda, H. & Sakakura, T. Selective and high yield synthesis of dimethyl carbonate directly from carbon dioxide and methanol. *Green Chem.* **4**, 230–234 (2002).
78. Zevenhoven, R., Eloneva, S. & Teir, S. Chemical fixation of CO<sub>2</sub> in carbonates: Routes to valuable products and long-term storage. *Catal. Today* **115**, 73–79 (2006).
79. Li, J. & Wang, T. Chemical equilibrium of glycerol carbonate synthesis from glycerol. *J. Chem. Thermodyn.* **43**, 731–736 (2011).
80. Wang, J.-Q. *et al.* Synthesis of dimethyl carbonate from CO<sub>2</sub> and ethylene oxide catalyzed by K<sub>2</sub>CO<sub>3</sub>-based binary salts in the presence of H<sub>2</sub>O. *Green Chem.* **13**, 3213 (2011).
81. Miao, C. X., Wang, J. Q., Wu, Y., Du, Y. & He, L. N. Bifunctional metal-salen complexes as efficient catalysts for the fixation of CO<sub>2</sub> with epoxides under solvent-free conditions. *ChemSusChem* **1**, 236–241 (2008).
82. Liu, Q., Wu, L., Jackstell, R. & Beller, M. Using carbon dioxide as a building block in organic synthesis. *Nat. Commun.* **6**, 5933 (2015).
83. Zalomaeva, O. V *et al.* Cyclic carbonates synthesis from epoxides and CO<sub>2</sub> over metal–organic framework Cr-MIL-101. *J. Catal.* **298**, 179–185 (2013).
84. Eta, V. *et al.* Synthesis of dimethyl carbonate from methanol and carbon dioxide: Circumventing thermodynamic limitations. *Ind. Eng. Chem. Res.* **49**, 9609–9617 (2010).
85. van Santen, R. Future perspectives in catalysis. *NRSC-Catalysis* 82 (2009).
86. Deutschmann, O., Knüzinger, H., Kochloefl, K. & Turek, T. *Heterogeneous Catalysis and Solid Catalysts. Ullmann's Encyclopedia of Industrial Chemistry* (2000). doi:10.1002/14356007.a05\_313.pub2
87. Haupt, C. *et al.* Transient enzyme - Substrate recognition monitored by real-time NMR. *J. Am. Chem. Soc.* **133**, 11154–11162 (2011).

88. Chorkendorff, I. & Niemantsverdriet, J. W. Catalyst Characterization. *Concepts Mod. Catal. Kinet.* 129–166 (2005). doi:10.1002/3527602658.ch4
89. Davis, M. E. & Davis, R. J. Heterogeneous Catalysis. *Fundam. Chem. React. Eng.* **4**, 133–183 (2012).
90. Cavani, F. & Trifiró, F. Classification of industrial catalysts and catalysis for the petrochemical industry. *Catal. Today* **34**, 269–279 (1997).
91. Dąbrowski, A. Adsorption - From theory to practice. *Adv. Colloid Interface Sci.* **93**, 135–224 (2001).
92. Ross, J. R. H. Surfaces and Adsorption. *Heterog. Catal.* 17–45 (2012). doi:10.1016/B978-0-444-53363-0.10002-7
93. Bowker, M. Surface science: The going rate for catalysts. *Nat. Mater.* **1**, 205–206 (2002).
94. Xie, F., Zhang, T. A., Dreisinger, D. & Doyle, F. A critical review on solvent extraction of rare earths from aqueous solutions. *Miner. Eng.* **56**, 10–28 (2014).
95. Kopia, A., Kowalski, K., Chmielowska, M. & Leroux, C. Electron microscopy and spectroscopy investigations of CuO<sub>x</sub>-CeO<sub>2</sub>-δ/Si thin films. *Surf. Sci.* **602**, 1313–1321 (2008).
96. Corradi, A. B., Bondioli, F., Ferrari, A. M. & Manfredini, T. Synthesis and characterization of nanosized ceria powders by microwave-hydrothermal method. *Mater. Res. Bull.* **41**, 38–44 (2006).
97. Lair, V., Ringuedé, A., Vermaut, P. & Griveau, S. Synthesis and characterization of cerium oxide by electrochemical methods. *Phys. status solidi* **5**, 3492–3495 (2008).
98. Kale, S. S., Jadhav, K. R., Patil, P. S., Gujar, T. P. & Lokhande, C. D. Characterizations of spray-deposited lanthanum oxide (La<sub>2</sub>O<sub>3</sub>) thin films. *Mater. Lett.* **59**, 3007–3009 (2005).
99. Méndez, M. *et al.* Effect of the La(OH)<sub>3</sub> preparation method on the surface and rehydroxylation properties of resulting La<sub>2</sub>O<sub>3</sub> nanoparticles. *J.*

*Nanoparticle Res.* **15**, 1479 (2013).

100. Méndez, M. *et al.* Effect of Thermal Annealing on the Kinetics of Rehydroxylation of Eu<sup>3+</sup>:La<sub>2</sub>O<sub>3</sub> Nanocrystals. *Inorg. Chem.* **51**, 6139–6146 (2012).
101. Wang, L., Ma, Y., Wang, Y., Liu, S. & Deng, Y. Efficient synthesis of glycerol carbonate from glycerol and urea with lanthanum oxide as a solid base catalyst. *Catal. Commun.* **12**, 1458–1462 (2011).
102. Liu, Z., Zheng, D., Su, Y., Liu, Z. & Tong, Y. Facile and Efficient Electrochemical Synthesis of Lanthanum Hydroxide Nanospindles and Nanorods. *Electrochem. Solid-State Lett.* **13**, E15 (2010).
103. Wu, Z., Jin, R., Liu, Y. & Wang, H. Ceria modified MnO<sub>x</sub>/TiO<sub>2</sub> as a superior catalyst for NO reduction with NH<sub>3</sub> at low-temperature. *Catal. Commun.* **9**, 2217–2220 (2008).
104. Juárez, R., Corma, A. & García, H. Gold nanoparticles promote the catalytic activity of ceria for the transalkylation of propylene carbonate to dimethyl carbonate. *Green Chem.* **11**, 949 (2009).
105. Zhang, P. *et al.* Promoting effects of lanthanum on the catalytic activity of Au/TiO<sub>2</sub> nanotubes for CO oxidation. *RSC Adv.* **5**, 11989–11995 (2015).
106. Tan, H. W., Abdul Aziz, A. R. & Aroua, M. K. Glycerol production and its applications as a raw material: A review. *Renew. Sustain. Energy Rev.* **27**, 118–127 (2013).
107. Hammond, G. P., Kallu, S. & McManus, M. C. Development of biofuels for the UK automotive market. *Appl. Energy* **85**, 506–515 (2008).
108. Ehsan, M. & Chowdhury, M. T. H. Production of Biodiesel Using Alkaline Based Catalysts From Waste Cooking Oil: A Case Study. *Procedia Eng.* **105**, 638–645 (2015).
109. Commodity chemicals derived from glycerol, an important biorefinery feedstock. *Chem Rev* **110**, 1807 (2010).
110. Johnson, D. T. & Taconi, K. A. The glycerin glut: Options for the value-added

- conversion of crude glycerol resulting from biodiesel production. *Environ. Prog.* **26**, 338–348 (2007).
111. Ott, L., Bicker, M. & Vogel, H. Catalytic dehydration of glycerol in sub- and supercritical water: a new chemical process for acrolein production. *Green Chem.* **8**, 214 (2006).
  112. Bell, B. M. *et al.* Glycerin as a Renewable Feedstock for Epichlorohydrin Production. The GTE Process. *CLEAN - Soil, Air, Water* **36**, 657–661 (2008).
  113. Santacesaria, E., Tesser, R., Serio, M. Di, Casale, L. & Verde, D. New process for producing epichlorohydrin via glycerol chlorination. in *Industrial and Engineering Chemistry Research* **49**, 964–970 (2010).
  114. <Recent Inventions in Glycerol Transformations and Processing.pdf>.
  115. Behr, A., Eilting, J., Irawadi, K., Leschinski, J. & Lindner, F. Improved utilization of renewable resources: New important derivatives of glycerol. *Green Chem.* **10**, 13–30 (2008).
  116. Pagliaro, M., Ciriminna, R., Kimura, H., Rossi, M. & Della Pina, C. From glycerol to value-added products. *Angew Chem Int Ed Engl* **46**, 4434–4440 (2007).
  117. Nguyen, N. T. & Demirel, Y. A Novel Biodiesel and Glycerol Carbonate Production Plant. *Int. J. Chem. React. Eng.* **9**, 5–7 (2011).
  118. Ochoa-Gómez, J. R., Gómez-Jiménez-Aberasturi, O., Ramírez-López, C. & Belsué, M. A Brief Review on Industrial Alternatives for the Manufacturing of Glycerol Carbonate, a Green Chemical. *Org. Process Res. Dev.* **16**, 389–399 (2012).
  119. Nguyen, N. & Demirel, Y. Economic Analysis of Biodiesel and Glycerol Carbonate Production Plant by Glycerolysis. *J. Sustain. Bioenergy Syst.* **3**, 209–216 (2013).
  120. Hu, J. *et al.* Oxidative carbonylation of glycerol to glycerol carbonate catalyzed by PdCl<sub>2</sub>(phen)/KI. *Appl. Catal. A Gen.* **386**, 188–193 (2010).
  121. Singh, D., Reddy, B., Ganesh, A. & Mahajani, S. Zinc/Lanthanum Mixed-Oxide Catalyst for the Synthesis of Glycerol Carbonate by Transesterification of

Glycerol. *Ind. Eng. Chem. Res.* 140605140950009 (2014).

doi:10.1021/ie5011564

122. Kumar, P., With, P., Srivastava, V. C., Gläser, R. & Mishra, I. M. Glycerol Carbonate Synthesis by Hierarchically Structured Catalysts: Catalytic Activity and Characterization. *Ind. Eng. Chem. Res.* **54**, 12543–12552 (2015).
123. Ishak, Z. I., Sairi, N. A., Alias, Y., Aroua, M. K. T. & Yusoff, R. Production of glycerol carbonate from glycerol with aid of ionic liquid as catalyst. *Chem. Eng. J.* **297**, 128–138 (2016).
124. Tudorache, M., Negoï, A. & Parvulescu, V. I. Enhancement of the valorization of renewable glycerol: The effects of the surfactant-enzyme interaction on the biocatalytic synthesis of glycerol carbonate. *Catal. Today* (2015). doi:10.1016/j.cattod.2016.02.038
125. Ochoa-Gomez, J. R., Gomez-Jimenez-Aberasturi, O., Ramirez-Lopez, C. & Maestro-Madurga, B. Synthesis of glycerol 1,2-carbonate by transesterification of glycerol with dimethyl carbonate using triethylamine as a facile separable homogeneous catalyst. *Green Chem.* **14**, 3368–3376 (2012).
126. Chiappe, C. & Rajamani, S. Synthesis of glycerol carbonate from glycerol and dimethyl carbonate in basic ionic liquids. *Pure Appl. Chem.* **84**, 755–762 (2011).
127. Tempelaar, S., Mespouille, L., Coulembier, O., Dubois, P. & Dove, A. P. Synthesis and post-polymerisation modifications of aliphatic poly(carbonate)s prepared by ring-opening polymerisation. *Chem. Soc. Rev.* **42**, 1312–36 (2013).
128. Zhang, Z., Rackemann, D. W., Doherty, W. O. S. & O'Hara, I. M. Glycerol carbonate as green solvent for pretreatment of sugarcane bagasse. *Biotechnol. Biofuels* **6**, 153 (2013).
129. Selva, M., Perosa, A., Guidi, S. & Cattelan, L. Ionic liquids as transesterification catalysts: applications for the synthesis of linear and cyclic organic carbonates. *Beilstein J. Org. Chem.* **12**, 1911–1924 (2016).

130. Díaz-Álvarez, A. E., Francos, J., Lastra-Barreira, B., Crochet, P. & Cadierno, V. Glycerol and derived solvents: new sustainable reaction media for organic synthesis. *Chem. Commun. (Camb)*. **47**, 6208–6227 (2011).
131. Clements, J. H. Reactive Applications of Cyclic Alkylene Carbonates. *Ind. Eng. Chem. Res.* **42**, 663–674 (2003).
132. Dibenedetto, A. *et al.* Converting wastes into added value products: from glycerol to glycerol carbonate, glycidol and epichlorohydrin using environmentally friendly synthetic routes. *Tetrahedron* **67**, 1308–1313 (2011).
133. <Synthesis of 1,2-glycerol carbonate from carbon dioxide The role of methanol in fluid phase equilibrium.pdf>.
134. Ochoa-Gómez, J. R. *et al.* Synthesis of glycerol carbonate from glycerol and dimethyl carbonate by transesterification: Catalyst screening and reaction optimization. *Appl. Catal. A Gen.* **366**, 315–324 (2009).
135. Aresta, M., Dibenedetto, A., Nocito, F. & Pastore, C. A study on the carboxylation of glycerol to glycerol carbonate with carbon dioxide: The role of the catalyst, solvent and reaction conditions. *J. Mol. Catal. A Chem.* **257**, 149–153 (2006).
136. Sonnati, M. O. *et al.* Glycerol carbonate as a versatile building block for tomorrow: synthesis, reactivity, properties and applications. *Green Chem.* **15**, 283 (2013).
137. Teng, W. K., Ngoh, G. C., Yusoff, R. & Aroua, M. K. A review on the performance of glycerol carbonate production via catalytic transesterification: Effects of influencing parameters. *Energy Convers. Manag.* **88**, 484–497 (2014).
138. Simanjuntak, F. S. H. *et al.* CaO-catalyzed synthesis of glycerol carbonate from glycerol and dimethyl carbonate: Isolation and characterization of an active Ca species. *Appl. Catal. A Gen.* **401**, 220–225 (2011).
139. Li, J. & Wang, T. On the deactivation of alkali solid catalysts for the synthesis of glycerol carbonate from glycerol and dimethyl carbonate. *React. Kinet.*



*Mech. Catal.* **102**, 113–126 (2011).

140. Climent, M. J. *et al.* Chemicals from biomass: Synthesis of glycerol carbonate by transesterification and carbonylation with urea with hydrotalcite catalysts. The role of acid–base pairs. *J. Catal.* **269**, 140–149 (2010).
141. Ceri Hammond, Jose A. Lopez-Sanchez, Mohd Hasbi Ab Rahim, Nikolaos Dimitratos, Robert L. Jenkins, Albert F. Carley, Qian He, Christopher J. Kiely, D. W. K. and G. J. H. Synthesis of glycerol carbonate from glycerol and urea with gold-based catalysts. *Dalt. Trans.* **40**, 3927–3937 (2011).
142. Meessen, J. H. & Petersen, H. in *Ullmann's Encyclopedia of Industrial Chemistry* (Wiley-VCH Verlag GmbH & Co. KGaA, 2000).  
doi:10.1002/14356007.a27\_333
143. Yoo, J.-W. & Mouloungui, Z. in *Nanotechnology in Mesosstructured Materials Proceedings of the 3rd International Materials Symposium* (eds. Sang-Eon Park Ryong Ryoo, W.-S. A. C. W. L. & Chang, J.-S.) **146**, 757–760 (Elsevier, 2003).
144. Rubio-Marcos, F., Calvino-Casilda, V., Ba??ares, M. A. & Fernandez, J. F. Novel hierarchical Co<sub>3</sub>O<sub>4</sub>/ZnO mixtures by dry nanodispersion and their catalytic application in the carbonylation of glycerol. *J. Catal.* **275**, 288–293 (2010).
145. Wang, D. & Zhang, X. Synthesis of glycerol carbonate from glycerol and urea over lanthanum compounds. *React. Kinet. Mech. Catal.* 597–609 (2015).  
doi:10.1007/s11144-015-0858-8
146. Zhang, J. & He, D. Lanthanum-based mixed oxides for the synthesis of glycerol carbonate from glycerol and urea. *React. Kinet. Mech. Catal.* **113**, 375–392 (2014).
147. Hasbi Ab Rahim, M. *et al.* Gold{ } palladium and gold-palladium supported nanoparticles for the synthesis of glycerol carbonate from glycerol and urea. *Catal. Sci. Technol.* **2**, 1914–1924 (2012).
148. Kondawar, S. E., Potdar, A. S. & Rode, C. V. Solvent-free carbonylation of glycerol with urea using metal loaded MCM-41 catalysts. *RSC Adv.* **5**, 16452–16460 (2015).

149. Jagadeeswaraiah, K., Ramesh Kumar, C., Rajashekar, A., Srivani, A. & Lingaiah, N. The Role of Tungsten Oxide Species Supported on Titania Catalysts for the Synthesis of Glycerol Carbonate from Glycerol and Urea. *Catal. Letters* **146**, 692–700 (2016).
150. Aresta, M., Dibenedetto, A., Nocito, F. & Ferragina, C. Valorization of bio-glycerol: New catalytic materials for the synthesis of glycerol carbonate via glycerolysis of urea. *J. Catal.* **268**, 106–114 (2009).
151. Vieville, C., Yoo, J. W., Pelet, S. & Mouloungui, Z. Synthesis of glycerol carbonate by direct carbonatation of glycerol in supercritical CO<sub>2</sub> in the presence of zeolites and ion exchange resins. *Catal. Letters* **56**, 245–247 (1998).
152. George, J., Patel, Y., Pillai, S. M. & Munshi, P. Methanol assisted selective formation of 1,2-glycerol carbonate from glycerol and carbon dioxide using nBu<sub>2</sub>SnO as a catalyst. *J. Mol. Catal. A Chem.* **304**, 1–7 (2009).
153. Ochoa-Gómez, J. R. *et al.* Synthesis of glycerol carbonate from 3-chloro-1,2-propanediol and carbon dioxide using triethylamine as both solvent and CO<sub>2</sub> fixation–activation agent. *Chem. Eng. J.* **175**, 505–511 (2011).
154. Li, H. *et al.* The synthesis of glycerol carbonate from glycerol and CO<sub>2</sub> over La<sub>2</sub>O<sub>2</sub>CO<sub>3</sub>–ZnO catalysts. *Catal. Sci. Technol.* **3**, 2801 (2013).
155. Zhang, J. & He, D. Surface properties of Cu/La<sub>2</sub>O<sub>3</sub> and its catalytic performance in the synthesis of glycerol carbonate and monoacetin from glycerol and carbon dioxide. *J. Colloid Interface Sci.* **419**, 31–8 (2014).
156. Li, H. *et al.* Direct carbonylation of glycerol with CO<sub>2</sub> to glycerol carbonate over Zn/Al/La/X (X=F, Cl, Br) catalysts: The influence of the interlayer anion. *J. Mol. Catal. A Chem.* **402**, 71–78 (2015).
157. Park, J. H. *et al.* Isolation and characterization of intermediate catalytic species in the Zn-catalyzed glycerolysis of urea. *Appl. Catal. A Gen.* **433–434**, 35–40 (2012).
158. Honda, M., Tamura, M., Nakagawa, Y. & Tomishige, K. Catalytic CO<sub>2</sub> conversion to organic carbonates with alcohols in combination with

- dehydration system. *Catal. Sci. Technol.* **4**, 2830 (2014).
159. Johnson, W. S. *et al.* Simple stereoselective version of the Claisen rearrangement leading to trans-trisubstituted olefinic bonds. Synthesis of squalene. *J. Am. Chem. Soc.* **92**, 741–743 (1970).
  160. Giner, J. L. DMOBO: An improvement on the OBO orthoester protecting group. *Org. Lett.* **7**, 499–501 (2005).
  161. Sakakura, T., Saito, Y., Okano, M., Choi, J.-C. & Sako, T. Selective Conversion of Carbon Dioxide to Dimethyl Carbonate by Molecular Catalysis. *J. Org. Chem.* **63**, 7095–7096 (1998).
  162. Honda, M. *et al.* Tandem carboxylation-hydration reaction system from methanol, CO<sub>2</sub> and benzonitrile to dimethyl carbonate and benzamide catalyzed by CeO<sub>2</sub>. *ChemCatChem* **3**, 365–370 (2011).
  163. Honda, M. *et al.* Ceria-catalyzed conversion of carbon dioxide into dimethyl carbonate with 2-cyanopyridine. *ChemSusChem* **6**, 1341–1344 (2013).
  164. Alberts, B. *et al.* *Molecular Biology of the Cell. 4th Edition*, New York (2002).
  165. Copeland, R. A. *ENZYMES A Practical Introduction to Structure, Mechanism and Data Analysis. Wiley-VCH* (2000). doi:10.1021/jm020467f
  166. Berg, J. M., Tymoczko, J. L. & Stryer, L. in *Biochemistry textbook* 1026 (2010).
  167. Petsko, G. a. *et al.* Chapter 2 From Structure to Function. *Protein Struct. Funct.* **14**, 200–4 (2004).
  168. Biochemistry, S. & Site, A. Structural Biochemistry / Enzyme / Active Site.
  169. Apal, E. *et al.* Enzyme Specificity. *Enzyme* 1–4 doi:10.1016/0022-5193(65)90108-6
  170. Corporation, W. B. Introduction to Enzymes. *Eff. pH* 1 (2015). doi:doi:10.1201/9781420094343-c1
  171. Cleland, W. Enzyme kinetics 1. *Wiley Encycl. Chem. Biol.* **6**, 1–11 (1967).
  172. Keller, M. A., Piedrafita, G. & Ralser, M. The widespread role of non-

- enzymatic reactions in cellular metabolism. *Current Opinion in Biotechnology* **34**, 153–161 (2015).
173. Sharma, S. & Kanwar, S. S. Organic Solvent Tolerant Lipases and Applications. **2014**, (2014).
  174. Kumar, A., Dhar, K., Kanwar, S. S. & Arora, P. K. Lipase catalysis in organic solvents: advantages and applications. *Biol. Proced. Online* **18**, 2 (2016).
  175. Shah, S., Solanki, K. & Gupta, M. N. Enhancement of lipase activity in non-aqueous media upon immobilization on multi-walled carbon nanotubes. *Chem. Cent. J.* **1**, 30 (2007).
  176. Homaei, A. A., Sariri, R., Vianello, F. & Stevanato, R. Enzyme immobilization: An update. *Journal of Chemical Biology* **6**, 185–205 (2013).
  177. Stergiou, P. Y. *et al.* Advances in lipase-catalyzed esterification reactions. *Biotechnol. Adv.* **31**, 1846–1859 (2013).
  178. Adlercreutz, P. Immobilisation and application of lipases in organic media. *Chem. Soc. Rev.* **42**, 6406–36 (2013).
  179. Stepankova, V. *et al.* Strategies for stabilization of enzymes in organic solvents. *ACS Catalysis* **3**, 2823–2836 (2013).
  180. Cao, S. G., Feng, Y., Liu, Z. B., Ding, Z. T. & Cheng, Y. H. Lipase catalysis in organic solvents. *Appl. Biochem. Biotechnol.* **32**, 7–13 (1992).
  181. Klibanov, A. M. Improving enzymes by using them in organic solvents. *Nature* **409**, 241–246 (2001).
  182. Kumar, A. & Kanwar, S. S. Catalytic Potential of a Nitrocellulose Membrane-Immobilized Lipase in Aqueous and Organic Media. (2011). doi:10.1002/app
  183. Gupta, S., Bhattacharya, A. & Murthy, C. N. Biocatalysis and Agricultural Biotechnology Tune to immobilize lipases on polymer membranes : Techniques , factors and prospects. *Biocatal. Agric. Biotechnol.* **2**, 171–190 (2013).
  184. Kim, S. C., Kim, Y. H., Lee, H., Yoon, D. Y. & Song, B. K. Lipase-catalyzed

- synthesis of glycerol carbonate from renewable glycerol and dimethyl carbonate through transesterification. *J. Mol. Catal. B Enzym.* **49**, 75–78 (2007).
185. Waghmare, G. V, Vetal, M. D. & Rathod, V. K. Ultrasonics Sonochemistry Ultrasound assisted enzyme catalyzed synthesis of glycerol carbonate from glycerol and dimethyl carbonate. *Ultrason. - Sonochemistry* **22**, 311–316 (2015).
  186. Jung, H. *et al.* Enzyme and Microbial Technology Enzymatic production of glycerol carbonate from by-product after biodiesel manufacturing process. *Enzyme Microb. Technol.* **51**, 143–147 (2012).
  187. Fowles, J. *et al.* A review of the toxicological and environmental hazards and risks of tetrahydrofuran. *Crit. Rev. Toxicol.* **43**, 811–828 (2013).
  188. Hwa, K. & Park, L. C. Biosynthesis of glycerol carbonate from glycerol by lipase in dimethyl carbonate as the solvent. 1059–1065 (2010).  
doi:10.1007/s00449-010-0431-9
  189. Cave, G. W. V, Raston, L. & Scott, J. L. synthesis with remarkable versatility. (2001). doi:10.1039/b106677n
  190. Tundo, P., Aricò, F., Rosamilia, A. E., Grego, S. & Rossi, L. in *Green Chemical Reactions* (eds. Tundo, P. & Esposito, V.) 213–232 (Springer Netherlands, 2008). doi:10.1007/978-1-4020-8457-7\_10
  191. Tudorache, M., Negoii, A., Tudora, B. & Parvulescu, V. I. Environmental-friendly strategy for biocatalytic conversion of waste glycerol to glycerol carbonate. *Appl. Catal. B Environ.* **146**, 274–278 (2014).
  192. Bolívar-Díaz, C. L., Calvino-Casilda, V., Rubio-Marcos, F., Fernández, J. F. & Bañares, M. A. New concepts for process intensification in the conversion of glycerol carbonate to glycidol. *Appl. Catal. B Environ.* **129**, 575–579 (2013).
  193. Mogilaiah, K., Jagadeeshwar, K. & Prasad, R. S. Microwave Irradiation. **48**, 1466–1469 (2009).
  194. Kappe, C. O. Controlled Microwave Heating in Modern Organic. *Angew.*

*Chemie-International Ed.* **43**, 6250–6284 (2004).

195. Gude, V. G., Patil, P., Martinez-Guerra, E., Deng, S. & Nirmalakhandan, N. Microwave energy potential for biodiesel production. *Sustain. Chem. Process.* **1**, 5 (2013).
196. Galema, S. a. Microwave chemistry. *Chem. Soc. Rev.* **26**, 233 (1997).
197. Horikoshi, S. & Serpone, N. Preparation of Heterogeneous Catalysts by a Microwave Selective Heating Method. *Microwaves Catal.* 77–108 (2015). doi:10.1002/9783527688111.ch5
198. Gawande, M. B., Shelke, S. N., Zboril, R. & Varma, R. S. Microwave-assisted chemistry: Synthetic applications for rapid assembly of nanomaterials and organics. *Acc. Chem. Res.* **47**, 1338–1348 (2014).
199. Huang, Y.-F., Chiueh, P.-T. & Lo, S.-L. A review on microwave pyrolysis of lignocellulosic biomass. *Sustain. Environ. Res.* **26**, 103–109 (2016).
200. Romano, P. N. *et al.* Microwave-Assisted Selective Hydrogenation of Furfural to Furfuryl Alcohol Employing a Green and Noble Metal-Free Copper Catalyst. *ChemSusChem* **9**, 3387–3392 (2016).
201. Kusserow, B., Schimpf, S. & Claus, P. C.-10. 1002/Adsc. 20039002. Hydrogenation of Glucose to Sorbitol over Nickel and Ruthenium Catalysts. *Adv. Synth. Catal.* **345**, 289–299 (2003).
202. Shrotri, A., Tanksale, A., Beltramini, J. N., Gurav, H. & Chilukuri, S. V. Conversion of cellulose to polyols over promoted nickel catalysts. *Catal. Sci. Technol.* **2**, 1852 (2012).
203. Almeida, J. M. A. R. *et al.* Screening of mono- and bi-functional catalysts for the one-pot conversion of cellobiose into sorbitol. *Catal. Today* **279**, Part, 187–193 (2017).
204. Wells, J. G. *et al.* Laboratory investigation of hemorrhagic colitis outbreaks associated with a rare Escherichia coli serotype. *J. Clin. Microbiol.* **18**, 512–520 (1983).
205. Ruppert, A. M., Weinberg, K. & Palkovits, R. Hydrogenolysis goes bio: from

- carbohydrates and sugar alcohols to platform chemicals. *Angew Chem Int Ed Engl* **51**, 2564–2601 (2012).
206. Metzger, J. O. Production of liquid hydrocarbons from biomass. *Angew Chem Int Ed Engl* **45**, 696–698 (2006).
  207. Vilcocq, L. *et al.* New bifunctional catalytic systems for sorbitol transformation into biofuels. *Appl. Catal. B Environ.* **148–149**, 499–508 (2014).
  208. Schmidt, S., Ritter, B. S., Kratzert, D., Bruchmann, B. & Mülhaupt, R. Isocyanate-Free Route to Poly(carbohydrate–urethane) Thermosets and 100% Bio-Based Coatings Derived from Glycerol Feedstock. *Macromolecules* **49**, 7268–7276 (2016).
  209. Yadav, G. D., Sharma, R. V & Katole, S. O. Selective Dehydration of Glycerol to Acrolein: Development of Efficient and Robust Solid Acid Catalyst MUICaT-5. *Ind. Eng. Chem. Res.* **52**, 10133–10144 (2013).
  210. Hayashi, H. & Hakuta, Y. Hydrothermal Synthesis of metal oxide nanoparticles in supercritical water. *Materials (Basel)*. **3**, 3794–3817 (2010).
  211. Machmudah, S. *et al.* Preparation of Ceria-Zirconia Mixed Oxide by Hydrothermal Synthesis. *Mod. Appl. Sci.* **9**, 134–139 (2015).
  212. Rabenau, A. Role of Hydrothermal Synthesis in Preparative Chemistry. *Angew. Chemie - Int. Ed. English* **24**, 1026–1040 (1985).
  213. Yoshida, K. *et al.* Effect of microwave irradiation on the electronic structure of ZnO. *J. Phys. Chem. Solids* **83**, 47–51 (2015).
  214. Mehta, S. K., Kumar, S., Chaudhary, S. & Bhasin, K. K. Effect of Cationic Surfactant Head Groups on Synthesis, Growth and Agglomeration Behavior of ZnS Nanoparticles. *Nanoscale Res. Lett.* **4**, 1197 (2009).
  215. Liu, J., Li, Y., Zhang, J. & He, D. Glycerol carbonylation with CO<sub>2</sub> to glycerol carbonate over CeO<sub>2</sub> catalyst and the influence of CeO<sub>2</sub> preparation methods and reaction parameters. *Appl. Catal. A Gen.* **513**, 9–18 (2016).
  216. Waseda, Y., Matsubara, E. & Shinoda, K. *X-Ray Diffraction Crystallography*.

*Zhurnal Eksperimental'noi i Teoreticheskoi Fiziki* (2011). doi:10.1007/978-3-642-16635-8

217. Krumeick, F. Properties of electrons, their interactions with matter and applications in electron microscopy. *Www.Microscopy.Ethz.Ch* 1–23 (2011). doi:10.1007/s00339-002-2060-x
218. Bagheri, S., Muhd Julkapli, N. & Bee Abd Hamid, S. Titanium dioxide as a catalyst support in heterogeneous catalysis. *ScientificWorldJournal* **2014**, 727496 (2014).
219. Thomas, J. M. & Thomas, W. J. *Principles and practice of heterogeneous catalysis. Journal of Catalysis* **171**, (1997).
220. Cox, D. M. Chapter 4 High Surface Area Materials. 1–18 (1993).
221. Zdravkov, B. D., Čermák, J. J., Šefara, M. & Janků, J. Pore classification in the characterization of porous materials: A perspective. *Cent. Eur. J. Chem.* **5**, 1158–1158 (2007).
222. Lüth, H. *Surfaces and Interfaces of Solid Materials. Springer Study Edition* (1995).
223. Keller, J. U. & Staudt, R. *Gas adsorption equilibria: Experimental methods and adsorptive isotherms. Gas Adsorption Equilibria: Experimental Methods and Adsorptive Isotherms* (2005). doi:10.1007/b102056
224. Weidenthaler, C. Pitfalls in the characterization of nanoporous and nanosized materials. *Nanoscale* **3**, 792–810 (2011).
225. Mahle, J. J. An adsorption equilibrium model for Type 5 isotherms. *Carbon N. Y.* **40**, 2753–2759 (2002).
226. Fagerlund, G. Determination of specific surface by the BET method. *Matériaux Constr.* **6**, 239–245 (1973).
227. Joshi, M., Bhattacharyya, A. & Ali, S. W. Characterization techniques for nanotechnology applications in textiles. *Indian J. Fibre Text. Res.* **33**, 304–317 (2008).



228. Egerton, R. F. *Physical principles of electron microscopy. Materials Today* **8**, (2005).
229. Williams, D. B. & Carter, C. B. *Transmission Electron Microscopy: A Textbook for Materials Science. Materials Science* **1–4**, (2009).
230. Corma, a. Inorganic Solid Acids and Their Use in Acid-Catalyzed Hydrocarbon Reactions. *Chem. Rev. (Washington, D C )* **95**, 559–614 (1995).
231. Fadoni, M. & Lucarelli, L. Temperature programmed desorption , reduction , oxidation and flow chemisorption for the characterisation of heterogeneous catalysts . Theoretical aspects , instrumentation and applications. *Stud. Surf. Sci. Catal.* **120**, 177–225 (1999).
232. Hemmann, F., Jaeger, C. & Kemnitz, E. Comparison of acidic site quantification methods for a series of nanoscopic aluminum hydroxide fluorides. *RSC Adv.* **4**, 56900–56909 (2014).
233. Hakim, A. *et al.* Studies on CO<sub>2</sub> Adsorption and Desorption Properties from Various Types of Iron Oxides (FeO, Fe<sub>2</sub>O<sub>3</sub>, and Fe<sub>3</sub>O<sub>4</sub>). *Ind. Eng. Chem. Res.* **55**, 7888–7897 (2016).
234. Chou, C. W. *et al.* Temperature-programmed reduction study on calcination of nano-palladium. *J. Phys. Chem. B* **105**, 9113–9117 (2001).
235. Subramanian, B. S. Temperature -Programmed Reduction of Platinum Group Metals Catalysts. *Pmr* **36-98** 98–103 (1992).
236. González-Rovira, L. *et al.* Formation and characterization of nanotubes of La(OH)(3) obtained using porous alumina membranes. *Nanotechnology* **19**, 495305 (2008).
237. Klingenberg, B. & Vannice, M. A. Influence of Pretreatment on Lanthanum Nitrate, Carbonate, and Oxide Powders. *Chem. Mater.* **8**, 2755–2768 (1996).
238. Füglein, E. *et al.* THERMAL BEHAVIOUR OF LANTHANUM HYDROXIDE IN DEPENDENCY OF PRESSURE Ekkehard Füglein and Dirk Walter. 95100 (2006).
239. Fleming, P., Farrell, R. A., Holmes, J. D. & Morris, M. A. The Rapid Formation of

- La(OH)<sub>3</sub> from La<sub>2</sub>O<sub>3</sub> Powders on Exposure to Water Vapor. *J. Am. Ceram. Soc.* **93**, 1187–1194 (2010).
240. Wang, X., Wang, M., Song, H. & Ding, B. A simple sol–gel technique for preparing lanthanum oxide nanopowders. *Mater. Lett.* **60**, 2261–2265 (2006).
  241. Irusta, S., Cornaglia, L. M. & Lombardo, E. A. Effects of rhodium and platinum on the reactivity of lanthanum phases. *Mater. Chem. Phys.* **86**, 440–447 (2004).
  242. Füglein, E. & Walter, D. Thermal analysis of lanthanum hydroxide. *J. Therm. Anal. Calorim.* **110**, 199–202 (2012).
  243. Bernal, S., Botana, F. J., Garcia, R., Ramirez, F. & Rodríguez-Izquierdo, J. M. Solid state chemistry of the preparation of lanthana-supported metal catalysts --- study of the impregnation step. *J. Mater. Sci.* **22**, 3793–3800 (1987).
  244. Bernal, S. *et al.* Preparation of some rare earth oxide supported rhodium catalysts: Study of the supports. *Mater. Chem. Phys.* **17**, 433–443 (1987).
  245. Kim, S. J., Han, W. K., Kang, S. G., Han, M. S. & Cheong, Y. H. Formation of Lanthanum Hydroxide and Oxide via Precipitation. *Solid State Phenom.* **135**, 23–26 (2008).
  246. Ozawa, M., Onoe, R. & Kato, H. Formation and decomposition of some rare earth (RE = La, Ce, Pr) hydroxides and oxides by homogeneous precipitation. in *Journal of Alloys and Compounds* **408–412**, 556–559 (2006).
  247. Zhu, J., Gui, Z. & Ding, Y. A simple route to lanthanum hydroxide nanorods. *Mater. Lett.* **62**, 2373–2376 (2008).
  248. Shirsat, A. N., Ali, M., Kaimal, K. N. G., Bharadwaj, S. R. & Das, D. Thermochemistry of La<sub>2</sub>O<sub>2</sub>CO<sub>3</sub> decomposition. *Thermochim. Acta* **399**, 167–170 (2003).
  249. Nandi, M., Sarkar, K., Seikh, M. & Bhaumik, A. Mesoporous lanthanum-manganese oxides with nanoscale periodicity, high surface area and

- ferromagnetic property. *Microporous Mesoporous Mater.* **143**, 392–397 (2011).
250. Sashkina, K. a., Semeikina, V. S., Labko, V. S., Rudina, N. a. & Parkhomchuk, E. V. Template method for the synthesis of a heterogeneous fenton catalyst based on the hierarchical zeolite FeZSM-5. *Kinet. Catal.* **54**, 638–643 (2013).
  251. Mu, Q. & Wang, Y. Synthesis, characterization, shape-preserved transformation, and optical properties of La(OH)<sub>3</sub>, La<sub>2</sub>O<sub>2</sub>CO<sub>3</sub>, and La<sub>2</sub>O<sub>3</sub> nanorods. *J. Alloys Compd.* **509**, 396–401 (2011).
  252. Shi, R. *et al.* A highly efficient Cu/La<sub>2</sub>O<sub>3</sub> catalyst for transfer dehydrogenation of primary aliphatic alcohols. *Green Chem.* **12**, 108 (2010).
  253. Wang, X. & Li, Y. Synthesis and characterization of lanthanide hydroxide single-crystal nanowires. *Angew. Chemie - Int. Ed.* **41**, 4790–4793 (2002).
  254. Zhang, M. *et al.* A low-temperature route for the synthesis of nanocrystalline LaB<sub>6</sub>. *J. Solid State Chem.* **181**, 294–297 (2008).
  255. Salavati-Niasari, M., Hosseinzadeh, G. & Amiri, O. Synthesis of Monodisperse Lanthanum Hydroxide Nanoparticles and Nanorods by Sonochemical Method. *J. Clust. Sci.* **23**, 459–468 (2012).
  256. Ma, X., Zhang, H., Ji, Y., Xu, J. & Yang, D. Synthesis of ultrafine lanthanum hydroxide nanorods by a simple hydrothermal process. *Mater. Lett.* **58**, 1180–1182 (2004).
  257. Mazloumi, M. *et al.* 3D bundles of self-assembled lanthanum hydroxide nanorods via a rapid microwave-assisted route. *J. Alloys Compd.* **473**, 283–287 (2009).
  258. Deng, J., Zhang, L., Au, C. T. & Dai, H. Template-free synthesis of high surface area single-crystalline lanthanum hydroxide nanorods via a low-temperature solution route. *Mater. Lett.* **63**, 632–634 (2009).
  259. Hou, B., Xu, Y., Wu, D. & Sun, Y. Synthesis and characterization of ultralong lanthanum hydroxide nanorods via solvothermal method. *J. Mater. Sci.* **42**, 1397–1400 (2007).

260. Choudhary, V. R., Uphade, B. S., Pataskar, S. G. & Keshavaraja, A. Low-Temperature Complete Combustion of Methane over Mn-, Co-, and Fe-Stabilized ZrO<sub>2</sub>. *Angew. Chemie Int. Ed. English* **35**, 2393–2395 (1996).
261. Liu, W. & Flytzanistephanopoulos, M. Total Oxidation of Carbon Monoxide and Methane over Transition Metal Fluorite Oxide Composite Catalysts: I. Catalyst Composition and Activity. *J. Catal.* **153**, 304–316 (1995).
262. Kundakovic, L. & Flytzani-Stephanopoulos, M. Reduction characteristics of copper oxide in cerium and zirconium oxide systems. *Appl. Catal. A Gen.* **171**, 13–29 (1998).
263. Konsolakis, M. & Ioakeimidis, Z. Surface/structure functionalization of copper-based catalysts by metal-support and/or metal-metal interactions. *Appl. Surf. Sci.* **320**, 244–255 (2014).
264. Yang, R., Li, X., Wu, J., Zhang, X. & Zhang, Z. Promotion Effects of Copper and Lanthanum Oxides on Nickel/Gamma-Alumina Catalyst in the Hydrotreating of Crude 2-Ethylhexanol. *J. Phys. Chem. C* **113**, 17787–17794 (2009).
265. Huang, Z., Cui, F., Kang, H. & Chen, J. Highly dispersed silica-supported copper nanoparticles prepared by precipitation–gel method: a simple but efficient and stable catalyst for glycerol hydrogenolysis. *Chem. ...* 5090–5099 (2008). doi:doi: 10.1021/cm8006233
266. Chang, F. W., Kuo, W. Y. & Lee, K. C. Dehydrogenation of ethanol over copper catalysts on rice husk ash prepared by incipient wetness impregnation. *Appl. Catal. A Gen.* **246**, 253–264 (2003).
267. Chary, K. V. R., Seela, K. K., Sagar, G. V & Sreedhar, B. Characterization and reactivity of niobia supported copper oxide catalysts. *J. Phys. Chem. B* **108**, 658–663 (2004).
268. Marchi, a. J., Fierro, J. L. G., Santamaría, J. & Monzón, a. Dehydrogenation of isopropyl alcohol on a Cu/SiO<sub>2</sub> catalyst: A study of the activity evolution and reactivation of the catalyst. *Appl. Catal. A Gen.* **142**, 375–386 (1996).
269. Yu, H. & Zhai, Q. Z. Preparation and characterization of (SBA-15)-La<sub>2</sub>O<sub>3</sub> host-guest composite materials. *J. Solid State Chem.* **181**, 2424–2432 (2008).

270. Sheng, X., Zhou, Y., Duan, Y., Zhang, Y. & Xue, M. Effect of different lanthanum source and preparation method on the lanthanum-doped mesoporous SBA-15 synthesis. *J. Porous Mater.* **18**, 677–683 (2011).
271. Pestryakov, A. N. *et al.* Study of copper nanoparticles formation on supports of different nature by UV–Vis diffuse reflectance spectroscopy. *Chem. Phys. Lett.* **385**, 173–176 (2004).
272. Wu, G., Wang, X., Wei, W. & Sun, Y. Fluorine-modified Mg–Al mixed oxides: A solid base with variable basic sites and tunable basicity. *Appl. Catal. A Gen.* **377**, 107–113 (2010).
273. Di Cosimo, J. I., Díez, V. K., Xu, M., Iglesia, E. & Apesteguía, C. R. Structure and Surface and Catalytic Properties of Mg–Al Basic Oxides. *J. Catal.* **178**, 499–510 (1998).
274. Shen, S. C., Chen, X. & Kawi, S. CO<sub>2</sub> adsorption over Si–MCM-41 materials having basic sites created by postmodification with La<sub>2</sub>O<sub>3</sub>. *Langmuir* **20**, 9130–9137 (2004).
275. Wang, F. *et al.* Highly Efficient Dehydrogenation of Primary Aliphatic Alcohols Catalyzed by Cu Nanoparticles Dispersed on Rod-Shaped La<sub>2</sub>O<sub>2</sub>CO<sub>3</sub>. *ACS Catal.* **3**, 890–894 (2013).
276. Xin, S., Wang, L., Li, H., Huang, K. & Li, F. Synthesis of diethyl carbonate from urea and ethanol over lanthanum oxide as a heterogeneous basic catalyst. *Fuel Process. Technol.* **126**, 453–459 (2014).
277. Manjunathan, P., Maradur, S. P., Halgeri, A. B. & Shanbhag, G. V. Room temperature synthesis of solketal from acetalization of glycerol with acetone: Effect of crystallite size and the role of acidity of beta zeolite. *J. Mol. Catal. A Chem.* **396**, 47–54 (2015).
278. Jia, C.-J., Liu, Y., Schmidt, W., Lu, A.-H. & Schüth, F. Small-sized HZSM-5 zeolite as highly active catalyst for gas phase dehydration of glycerol to acrolein. *J. Catal.* **269**, 71–79 (2010).
279. Leitner, W. The coordination chemistry of carbon dioxide and its relevance for catalysis: A critical survey. *Coord. Chem. Rev.* **153**, 257–284 (1996).

280. Gibson, D. H. & Gibson, D. H. Carbon dioxide coordination chemistry: metal complexes and surface-bound species. What relationships? *Coord. Chem. Rev.* **186**, 335–355 (1999).
281. Komarneni, S., Rajha, R. K. & Katsuki, H. Microwave-hydrothermal processing of titanium dioxide. *Mater. Chem. Phys.* **61**, 50–54 (1999).
282. Tatlier, M., Bariş Cigizoglu, K., Tokay, B. & Erdem-Şenatalar, A. Microwave vs. conventional synthesis of analcime from clear solutions. *J. Cryst. Growth* **306**, 146–151 (2007).
283. Bonaccorsi, L. & Proverbio, E. Microwave assisted crystallization of zeolite A from dense gels. *J. Cryst. Growth* **247**, 555–562 (2003).
284. Wilson, G. J., Matijasevich, A. S., Mitchell, D. R. G., Schulz, J. C. & Will, G. D. Modification of TiO<sub>2</sub> for enhanced surface properties: Finite ostwald ripening by a microwave hydrothermal process. *Langmuir* **22**, 2016–2027 (2006).
285. Wang, H. *et al.* Deposition of {WO<sub>3</sub>} on Al<sub>2</sub>O<sub>3</sub> via a microwave hydrothermal method to prepare highly dispersed W/Al<sub>2</sub>O<sub>3</sub> hydrodesulfurization catalyst. *Fuel* **136**, 185–193 (2014).
286. Bergadà, O. *et al.* Microwave effect during aging on the porosity and basic properties of hydrotalcites. *Microporous Mesoporous Mater.* **101**, 363–373 (2007).
287. Yuvaraj, S., Fan-Yuan, L., Tsong-Huei, C. & Chuin-Tih, Y. Thermal Decomposition of Metal Nitrates in Air and Hydrogen Environments. *J. Phys. Chem. B* **107**, 1044–1047 (2003).
288. Avgouropoulos, G., Ioannides, T. & Matralis, H. Influence of the preparation method on the performance of CuO–CeO<sub>2</sub> catalysts for the selective oxidation of CO. *Appl. Catal. B Environ.* **56**, 87–93 (2005).
289. Motshekga, S., Pillai, S. K. & Ray, S. S. Conventional wet impregnation versus microwave-assisted synthesis of SnO<sub>2</sub>/CNT composites. *J. Nanoparticle Res.* **13**, 1093–1099 (2011).

290. Villegas, L., Masset, F. & Guilhaume, N. Wet impregnation of alumina-washcoated monoliths: Effect of the drying procedure on Ni distribution and on autothermal reforming activity. *Appl. Catal. A Gen.* **320**, 43–55 (2007).
291. Vidya Sagar, G., Venkat, P., Rao, R., Srikanth, C. S. & Chary, K. V. R. Dispersion and Reactivity of Copper Catalysts Supported on Al<sub>2</sub>O<sub>3</sub> -ZrO<sub>2</sub>. *J. Phys. Chem. B* **110**, 13881–13888 (2006).
292. Zhou, Q. *et al.* Nano La<sub>2</sub>O<sub>3</sub> as a heterogeneous catalyst for biodiesel synthesis by transesterification of *Jatropha curcas* L. oil. *J. Ind. Eng. Chem.* **31**, 385–392 (2015).
293. Cannilla, C., Bonura, G., Rombi, E., Arena, F. & Frusteri, F. Highly effective MnCeO<sub>x</sub> catalysts for biodiesel production by transesterification of vegetable oils with methanol. *Appl. Catal. A Gen.* **382**, 158–166 (2010).
294. Jagadeeswaraiah, K., Kumar, C. R., Prasad, P. S. S., Loridant, S. & Lingaiah, N. Synthesis of glycerol carbonate from glycerol and urea over tin-tungsten mixed oxide catalysts. *Appl. Catal. A Gen.* **469**, 165–172 (2014).
295. Yoshikawa, K., Sato, H., Kaneeda, M. & Kondo, J. N. Synthesis and analysis of {CO<sub>2</sub>} adsorbents based on cerium oxide. *J. {CO<sub>2</sub>} Util.* **8**, 34–38 (2014).
296. Honda, M. *et al.* Organic carbonate synthesis from {CO<sub>2</sub>} and alcohol over CeO<sub>2</sub> with 2-cyanopyridine: Scope and mechanistic studies. *J. Catal.* **318**, 95–107 (2014).
297. Teng, W. K., Ngoh, G. C., Yusoff, R. & Aroua, M. K. Microwave-assisted transesterification of industrial grade crude glycerol for the production of glycerol carbonate. *Chem. Eng. J.* **284**, 469–477 (2016).
298. Pawar, R. R., Jadhav, S. V & Bajaj, H. C. Microwave-assisted rapid valorization of glycerol towards acetals and ketals. *Chem. Eng. J.* **235**, 61–66 (2014).
299. Liu, J. *et al.* Microwave-assisted pretreatment of recalcitrant softwood in aqueous glycerol. *Bioresour. Technol.* **101**, 9355–9360 (2010).
300. Ahmed, I. *et al.* Liquid-phase dehydration of sorbitol to isosorbide using sulfated titania as a solid acid catalyst. *Chem. Eng. Sci.* **93**, 91–95 (2013).

301. Guo, X. *et al.* Conversion of biomass-derived sorbitol to glycols over carbon-materials supported Ru-based catalysts. *Sci. Rep.* **5**, 16451 (2015).
302. Ramírez-López, C. A., Ochoa-Gómez, J. R., Gil-Río, S., Gómez-Jiménez-Aberasturi, O. & Torrecilla-Soria, J. Chemicals from biomass: synthesis of lactic acid by alkaline hydrothermal conversion of sorbitol. *J. Chem. Technol. Biotechnol.* **86**, 867–874 (2011).
303. Rokicki, G., Rakoczy, P., Parzuchowski, P. & Sobiecki, M. Hyperbranched aliphatic polyethers obtained from environmentally benign monomer: glycerol carbonate. *Green Chem.* **7**, 529 (2005).
304. Ferrario, V. *et al.* Conformational Changes of Lipases in Aqueous Media: A Comparative Computational Study and Experimental Implications. *Adv. Synth. Catal.* **353**, 2466–2480 (2011).
305. Hanefeld, U., Gardossi, L. & Magner, E. Understanding enzyme immobilisation. *Chem. Soc. Rev.* **38**, 453–468 (2009).
306. Kobayashi, S. Lipase-catalyzed polyester synthesis – A green polymer chemistry. *Proc. Jpn. Acad. Ser. B. Phys. Biol. Sci.* **86**, 338–365 (2010).
307. Feng, J., Zhuo, R., He, F. & Wang, X. Synthesis of functional polycarbonates by lipase-catalyzed ring-opening polymerization. *Macromol. Symp.* **195**, 237–240 (2003).
308. Laane, C., Boeren, S., Vos, K. & Veeger, C. Rules for Optimization of Biocatalysis in Organic Solvents. *Biotechnol. Bioeng.* **102**, 1–8 (2009).
309. Seong, P.-J. *et al.* Enzymatic coproduction of biodiesel and glycerol carbonate from soybean oil and dimethyl carbonate. *Enzyme Microb. Technol.* **48**, 505–509 (2011).
310. Lee, K. H., Park, C.-H. & Lee, E. Y. Biosynthesis of glycerol carbonate from glycerol by lipase in dimethyl carbonate as the solvent. *Bioprocess Biosyst. Eng.* **33**, 1059–1065 (2010).
311. Staab, H. A. New Methods of Preparative Organic Chemistry IV. Syntheses Using Heterocyclic Amides (Azolides). *Angew. Chemie Int. Ed. English* **1**, 351–



367 (1962).

312. Verma, S. K., Ghorpade, R., Pratap, A. & Kaushik, M. P. Solvent free, N,N'-carbonyldiimidazole (CDI) mediated amidation. *Tetrahedron Lett.* **53**, 2373–2376 (2012).
313. Rannard, S. P. & Davis, N. J. Controlled Synthesis of Asymmetric Dialkyl and Cyclic Carbonates Using the Highly Selective Reactions of Imidazole Carboxylic Esters. *Org. Lett.* **1**, 933–936 (1999).